An Entangled Bayesian Gestalt: Mean-field, Monte-Carlo and Quantum Inference in Hierarchical Perception

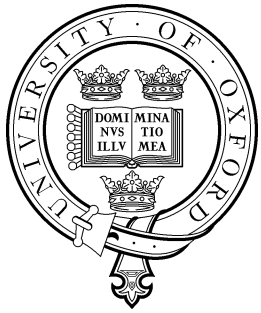

Charles Fox

Christ Church

University of Oxford

A thesis submitted for the degree of

Doctor of Philosophy

Trinity 2008

Jenny,
this one's for you

Acknowledgements

With thanks to:

My adviser Prof. Stephen Roberts for allowing me total academic freedom to pursue my own ideas,

Examiners Prof. Sir Mike Brady and Prof. Kathryn Laskey,

My family – all of you – for unfailing support over the years.

Anuj Dawar for spending many hours teaching me Quantum Computing in Borders coffee shop. David Deutsch for his valuable time listening to and helping with the quantum Gibbs sampler. John Quinn for help with particle filters and the meaning of Bayes. Amos Storkey for wondering if quantum Gibbs does work after all. Matthew Dovey for help with blackboards and introducing me to the London computer music scene. Penny Probert Smith for help with low-level methods. Neil Girdhar for talking too much. Chris Raphael for access to and in-depth voyages through his Music++ code. Iead Rezek and John Winn for help understanding variational methods. Stuart Hameroff and Roger Penrose for discussions about their quantum ideas. Stephen N.P. Smith for inspiring me to become an Engineer. Josh Tenenbaum, Nick Chater and Alan Yuille for ideas about the 'Bayesian Brain'. Douglas Hofstadter, Eric Nichols, Chris Honey and FARG for detailed discussions about Copycat, music, philosophy and everything. Mark Taylor and Hiu-Wan Yu for moral and logistical support. Tony Prescott and the Adaptive Behaviour Research Group in Sheffield for a stimulating part-time working environment. Housemen Chris Aycock, Akshay Mangla, Jason Lotay, Dan Koch and Raphael Espinoza; and local tabs Andy Bower, Rob Fellows and Chris Ramshaw; for collectively keeping it real.

Abstract

Scene perception is the general task of constructing an interpretation of low-level sense data in terms of high-level objects, whose number is not known in advance. This task is examined from a Bayesian perspective. Simple examples from musical Machine Listening are provided, but this thesis is intended as a general view of scene perception.

After reviewing relevant mathematics and low-level pre-processing methods, the psychologically inspired concepts of priming and pruning are introduced, first in a novel extension to low-level particle filters, then in a mid-level segmentation step, and finally in the high-level hierarchical perception setting. Inference in the mid- and high-level networks is intractable so two approximate methods – mean-field and Monte Carlo – are examined. A novel mean-field Machine Listening application is presented, and is extended to handle multiple objects using priming and pruning ideas from classical Artificial Intelligence. A novel priming and pruning Monte Carlo sampler is developed, which is specialised for high-level perception, and provides new Bayesian semantics for classical blackboard systems. Extensions to learning and action selection are discussed. The previously unexplored field of Bayesian inference with quantum computing is examined in the scene perception context, showing how a new algorithm on quantum hardware can generalise both mean-field and Monte-Carlo approaches to obtain a free quadratic speedup using only local operators.

Contents

Chapter 1

Introduction

1.1 Scene perception

This thesis is about scene perception. *Scene perception* is the general task of constructing a unitary, coherent and useful interpretation of low-level sense data, in terms of almost-known high-level objects whose numerosity is not known in advance. *Unitary* means there is a single unambiguous interpretation, in contrast to a fuzzy or probabilistic set of possible interpretations. *Coherent* means that the parts of the scene are mutually non-contradictory. *Useful* means as close to optimal as computationally possible, with respect to some task. *Almost-known* means that we have approximate a priori models of the high-level objects, but some of their details may be inaccurate and occasionally whole models may be missing and need to be learned.

Fig. 1.1 shows some examples of particular domains of scene perception. Visual scene perception (a) is perhaps the best-known example. In vision, the low-level data consists of coloured pixels, and the known high-level objects are physical three-dimensional structures such as *HOUSE*, *PERSON* and *SKY*. Vision tasks are typically characterised as atemporal: the task is to interpret a static image offline[1]. A simpler scene perception domain is tactile scene perception. (b) shows a simulation of a whiskered robot, whose task is to construct a high-level interpretation of its three-dimensional environment from the low-level bending data from its whiskers as they make contact with objects of different shapes and textures. Unlike the typical visual task, the scene here is a map of the whole spatial environment around the robot, rather than a sub-region of this space defined by the view of some camera. Another difference is that with whiskers, the sense data arrive over time, even though the scene itself may not be changing over time. This temporal element leads to the notion of 'attention': the robot can choose where to place its whiskers to gather data and

[1] though recent work has begun to consider video scene perception

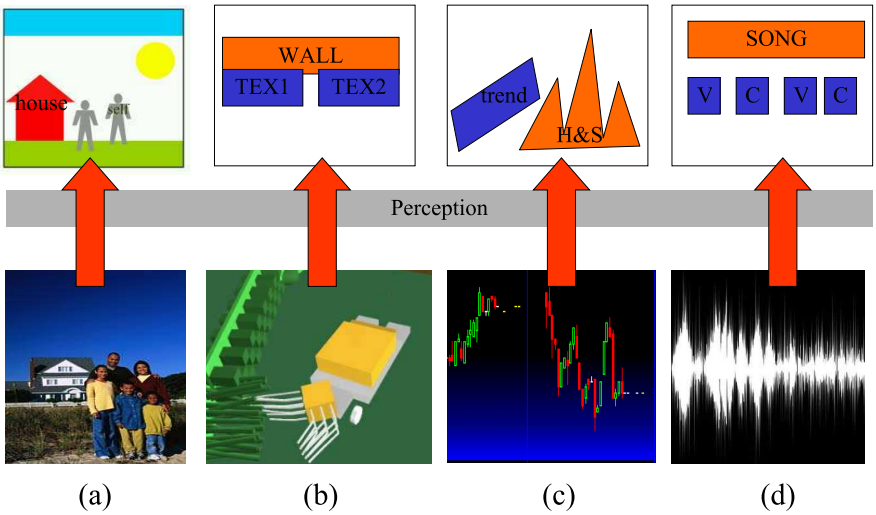

Figure 1.1: Examples of scene perception domains. (a) Visual scene perception from images. (b) Tactile scene perception by a simulated whiskered robot. (c) Financial time series perceived as large-scale patterns. (d) Semi-improved musical scene perception.

perform computations on that data. Attention can be used in vision but its presence is less obvious in static image interpretation tasks than in the whisker task where the robot must physically move over time to gather information. Both the visual and tactile tasks considered above aim to construct static models of spatial three-dimensional scenes. Other particular types of scene perception may seek to construct interpretations of *temporal* structures. 'Chartist' financial traders attempt to interpret the low-level time series data of asset prices in terms of high-level objects such as the 'head-and-shoulders' pattern and 'trend lines' shown in (c). As in tactile scene perception, attention is important but is now less controllable than in the tactile case. The trader may focus his *computations* on any point of the time series seen so far, but the arrival of new data is now beyond his control – unlike the tactile robot which can choose where in the world to collect data. The finance example especially emphasises the role of utility in perception. Traders do not passively construct interpretations of price series for fun: they do it for profit. This means they will try to perceive the scene in terms of structures that are not just a good fit to the data, but also have some (supposed) power to make money via their 'filling in' of the unobserved parts of the scene – in the temporal case, their predictions of the future.[2] Speech scene perception has similar attributes to this type of financial scene perception. Again, low-level data – this time audio samples – arrives over time, and the perceiver

[2]Similarly, fortune-tellers look for structures in tea-leaves which allow them to make a profit rather than structures which merely fit the low-level tea-leaf data.

may focus computational but not data-collection attention. Speech perception has perhaps the best-developed theory of *hierarchies* of percepts. In vision, a *HOUSE* may be made of subcomponents, *WINDOW*, *DOOR*, *WALL* and *ROOF*, and the *WINDOW* may be made of several glass *PANE*s. In speech, intricate theories of grammar describe how similarly, a *SENTENCE* may be made of *NOUN-PHRASE*s and *VERB-PHRASE*s which in turn are made of various other parts of speech in highly specific orderings. Musical scene perception (d) will be used as the running particular example in this thesis. Musical scenes are auditory performances by one or more musicians, and like language, include detailed structure at many levels. As in language and finance, data arrive over time, and the scene exists over time rather than space. The structures are simpler than natural language and vision – both of which have grown huge research areas around their minutiae – but are just complex enough to capture most of the *general* features of the *general* scene perception task. Unlike finance, they are predictable enough to allow realistic building and testing of simple models. Like speech, low-level data arrives as audio samples. A hierarchy of musical percepts can be constructed, beginning with events such as onsets of drum hits, progressing through musical bars and chords, and up to large-scale structures such as verses and choruses.

1.1.1 Simplified scene perception

Artificial Intelligence (AI) research has commonly used two simplifications of general scene perception: microdomains and deterministic scenes. *Microdomains* [81] are artificial scenes constructed specifically to illustrate particular aspects of scene perception whilst keeping the tasks as computationally simple as possible. *Deterministic scenes* drop the requirement that the scene content is unknown in advance. For example, in musical scenes, we may often assume that we possess a known musical score of what notes will be played; or in certain constrained vision problems such as production line automation or medical image analysis [109] we may assume that the scene will contain exactly one object of a known type. In these cases, the overall structure is known, though the parameters of the models (such as musical tempo or visual object position and configuration) are unknown.

Classical AI (i.e. pre-1990s, non-probabilistic and predominantly symbol-based; e.g. [144]) often took microdomain approaches in order to demonstrate general concepts using very limited computational resources. Whilst this laid the conceptual foundation for much present work, three particular problems were later found to have recurred in this approach. First, the microdomain approach by definition limits

testing to computationally feasible data sets. This meant that computationally intractable tasks (in the sense of NP-hardness, discussed in chapter 2) could be scaled down and appeared to be easily solvable. But of course such methods do not scale up to real world problems on account of their intractability. The classical microdomain approach ignored computational complexity. Second, classical AI's use of symbols often lead to a problem of modularity, in which the really hard parts of tasks were performed (sometimes unknowingly) by humans in their pre-processing of the raw data into symbols for use by the program. The SME and BACON projects were classical examples of this problem, as discussed in [23]. Third, the brittleness of classical logic is of little use in real-world noisy data. To its credit however, non-microdomain classical AI researched scalable heuristics for tractable model construction, such as those of the 'blackboard systems' reviewed in chapter 5.

In contrast, the more recent Machine Learning approach to AI (e.g. [11]) has preferred the deterministic scene simplification. Where classical AI drew on mathematical logic as its basis, Machine Learning begins with Statistics – in particular subjective Bayesian probability theory as reviewed in chapter 2. Statistical thought throughout the twentieth century has had much in common with the aims of AI, seeking to infer explanations of low-level data in terms of models, and to make optimal actions based on those explanations. However much of its focus has been on finding analytical solution and efficient approximation algorithms for particular models, rather than on automating the initial selection of models. R.A. Fisher held the opinion that 'initial choice of candidate models is more an art than a science' [25], and most modern Statistics texts focus on inference methods within models and on model comparison rather than on the selection of initial hypotheses. For example, in most branches of science, complex hypotheses are constructed by scientists using their creativity and knowledge of their field. Data are then collected, and the methods of Statistics are used to test hypotheses. In scene perception however, hypothesis selection is key, as we do not in advance what objects are in the scene and thus what models to use. We cannot usually evaluate *all* known models (such as models of pink elephants at every possible location in the room) at every moment in time. But neither can we ask a human domain expert to use her knowledge and creativity to conjecture an appropriate hypothesis set at every moment, if we wish to construct autonomous agents. Scene perception systems need to automate this task as well as making inferences and comparing models.

1.1.2 Minidomain approach

This thesis examines the general task of scene perception, using a musical *minidomain* as a recurring example. Like a microdomain, a minidomain is chosen specifically to illustrate general concepts, but in a simplified task chosen to fit computational and research restrictions (in this case, a desktop PC and a three year doctoral thesis). Unlike a microdomain, a minidomain has some practical use in the real world rather than being the simplest possible 'toy' exemplar. In the case of music, microdomains could for example include the perception of three-note melodies chosen to illustrate perception of rising and falling melodies [122]. In contrast, the minidomain described in chapter 3 – semi-improvised musical perception – while being 'mini' enough to be feasible under our constraints, is a real-world practical problem with immediate useful applications such as in components of automated musical accompaniment systems. The requirement for real-world activity also removes the classic temptations to move the hard problems into human pre-processing. If the algorithms are to run online, there will be no time to repeatedly ask human experts to suggest models – the algorithms must be responsible for this part of perception too. This leads to the idea of implementing a 'whole iguana' [18], that is, a complete vertical stack of perception components which begin by processing the raw lowest level data (in this case, audio samples) and increase in abstraction up to the highest level of objects in the world (in this case, large musical structures such as verses and choruses). The minidomain approach aims to implement a whole though small iguana: emphasis is given to a complete vertical stack in a small domain. In contrast, much of the Machine Learning approach focuses on detailed implementation of some single layer in a rich domain (for example it is not uncommon for vision theses to spend three years researching a slight improvement to some low-level feature detector); and classic microdomain-based AI built a limited number of layers for a limited domain.

The musical minidomain is described fully in chapter 3, but briefly it is that of perceiving simple semi-improvised, almost-known musical performances. *Semi-improvised* is the type of compositional and improvisational structure found in forms of Western jazz and popular music as well as non-Western art musics such as Indian raga, in which a 'composition' is fluid and open to interpretation by the performers at the level of notes, rhythm, chords and large-scale structures, though bound together by a set of strong prior conventions. Conventions may be written, such as the suggested chords and melodies found in jazz and pop arrangements, or may be the product of aural tradition, such as the motifs that are associated with particular ragas or particular jazz pieces; and 'standard' chord substitutions, rhythmic devices,

and structural changes (such as inserting extra choruses on the fly if the audience is enjoying the piece and wants more). Relative semi-improvised perception also arises when a performance is deterministic but the listener only has a vague prior upon it, as occurs when an unfamiliar listener perceives a performance of a notated, deterministic symphony. We restrict the minidomain to a series of sub-tasks, chosen specifically to represent general scene perception tasks across all vertical layers of perception. In particular, the concepts of feature-based priming, 'almost-known'-ness and the presence of global probability factors are characteristic of the general problem and we ensure they are retained in the minidomain. The minidomain and the sub-tasks within it are slightly artificial, being restricted to feasible complexities on a modern desktop PC, and restricted in development time by the requirements of a doctoral thesis. We emphasise that the software implementations discussed here are used to illustrate and demonstrate the ideas about scene perception of the thesis: they are not yet intended to be practical tools (although we hope that development of the research presented here could later produce such tools).

1.1.3 Engineering vs. biology

The purpose of the thesis is to present a unified view of what the perceptual process for scenes could be, all the way up from raw data to high-level concepts, but presented in a minidomain to allow it to be feasible. 'The perceptual process' is left as a deliberately ambiguous phrase, which can refer to both the human (or animal) biological perception system, or to a constructed, engineered method for performing perception by machine. There is a continuum of research approaches between hard engineering AI (which only cares about producing solutions to tasks) and computational neuroscience (which only cares about explaining what biological neurons do). The present work is close to the engineering side of this continuum, but with some weight given to biological ideas. In particular we intend the architectures to inform computational neuroscientists' high-levels models of what perception is, and perhaps provide inspiration for future biological theories that implement the engineering ideas. A point of strong agreement between the engineering and neuroscience views is the need for parallel distributed processing (PDP) architectures, developed for completely different reasons. Neuroscience studies the distributed system that is the brain, which – as far as is known – appears to lack any central executive unit (except possibly during very high-level conscious decision making), instead using a multitude of parallel structures to process information. Machine Learning, on the other hand, has independently discovered the utility of parallel distributed message-passing algorithms as

a means of making efficient inferences, and all the algorithms used in this thesis have this character. Such algorithms will become especially useful as processor technology moves towards multi-cores. We have chosen to use such algorithms mostly for engineering efficiency reasons, but also as a weak biological constraint, to prevent the architectures from being neurally implausible on the grounds of central planning requirements.

1.1.4 Speeding up scene perception

A fundamental difficultly with general scene perception is that it is computationally intractable, because inference – even approximate inference – is known to be NP-hard [32]. This would appear to invalidate the whole project of scaling up to real-world systems, if not for the fact that an existing computational device – the brain – is known to be capable of performing it very well indeed. The brain's general mechanism for scene perception is not currently known (though research such as the present work aims to provide candidate mechanisms to model and test). Scaling up from microdomains to minidomains can quickly reach the threshold of intractability for exact inference. Several methods have been proposed to speed up inference to get closer to real time execution. An essential view, taken here as in all non-trivial Machine Learning, is the need for approximations. Rather than compute exact probability distributions and functions of those distributions, we work with related but simplified versions of those distributions. The variational and sampling approaches are reviewed and used throughout this thesis. However it is known [148] that even approximate inference is still NP-hard in the sense of reaching an arbitrary degree of accuracy, and the approximate inference algorithms used in the minidomain tasks still require greater than real time to run on a desktop PC to produce reasonable results. A key point is the introduction of *heuristics* in the sense of classical AI: algorithms which make ad-hoc but empirically-useful simplifications to the task to improve its performance. We will draw on the classical AI ideas of blackboards, priming and pruning, but use them as heuristics in Bayesian networks. However even with good heuristics, inference can be very slow (slower than real-time).

More radical solutions to the slowness of perception have been suggested. One possibility is that the real brain is an extremely large parallel processor, using brute force parallel computation to solve NP-hard problems up to some size. However, such parallelism can only achieve a constant factor speedup, given by the number of parallel units, which is not even counted by standard computational complexity theory. So it appears that we are left with a desperate problem: how can any computing device,

including the brain, possibly solve real-world sized scene perception problems when we know them to be NP-hard?

One radical suggestion based on cutting-edge computer science is that *quantum computing* – the new underlying theory of all computation, which generalises classical Turing machines [42] – may be able to give a greater speedup than brute-force parallelism. While quantum computing has not yet entered the commercial mainstream, its theory [119] has been well-developed since the mid 1980s, and proof-of-concept hardware has been constructed and successfully demonstrated standard algorithms in practice by IBM, MIT and others [157]. Outside the peer-reviewed literature, commercial enterprises claim to have successfully implemented non-general forms of quantum computing, adiabatic [113] and secure cryptography [92], the latter in the context of a real financial transfer between investment banks. Both theory and practice have showed greater than constant factor speedups in a variety of tasks, including a quadratic speedup for unstructured database search [71]. Though extremely unconventional, this is of interest with regard to the scene perception task, as it provides a speedup far greater than the constant factor gain from brute force parallelism. Quantum methods have also been gaining currency in biology over the last 30 years [102], [41] as increased computation power allows more accurate Schrödinger-equation modelling of biological and pharmaceutical molecules. Given the large computational speedups of theoretical quantum computing, it seems unlikely that biology should *not* use such computations *if physically convenient*. This thesis has nothing to say about the biological plausibility of quantum computing except to note that the current quadratic speedup for database search relies on the use of large coherent global operators, which would seem to be especially difficult to implement biologically. Out of sheer desperation at the slowness of all known Bayesian approximation methods – even with good heuristics – the final part of this thesis considers how future quantum hardware could speed up general scene perception. Unlike the previous unstructured database search method, we continue to respect the weak biological constraint that algorithms should be comprised of parallel, local messages only, rather than large global operators, and derive a novel quantum computational form of the Gibbs sampler which achieves a quadratic speedup using only local operators.

1.2 Minidomain subtasks: a slice of iguana

The minidomain under consideration is semi-improvised musical scene perception. Fig. 3.1 (in chapter 3) shows an example application of this domain in automated accompaniment. The laptop attached to the drum kit runs a perception system

which listens to the musicians (and perhaps also received direct control signals from the drummer) and schedules MIDI accompaniment notes to play along with them. For example, this could be used if the bass player is absent from the rehearsal, to fill in the bass part automatically – even if the players make semi-improvised structural, rhythmic and tonal changes on the fly.

As our use of the minidomain is to illustrate a general view of scene perception across all *vertical* layers, we will focus only on particular subtasks of such an accompaniment system which are relevant to achieving this goal. We will not consider the generation of accompaniment, or perception of individual notes or melodies. These are all fascinating areas within the accompaniment problem, but are not required for our more theoretical goal. Rather, we pick a minimum set of subtasks from the architecture shown in fig. 3.26 to use as illustrations of all vertical layers. The architecture shown in the figure begins with human performers generating sound waves. Some form of pre-processing is performed (which we refer to as 'hash-classifiers' for reasons that will become apparent in chapter 2), which occupies a similar architectural position to the pre-thalamic nuclei of the biological system. In chapter 4 we use information from the drummer's signals in a program, *RhythmKitten*, to infer a single segmentation of time into musical bars, which form the basic 'grid' of the high-level blackboard system on which larger structures will be extended in chapter 6. We will use only *chord* information from a single instrument to illustrate these structures, which will include riffs, verses, choruses and songs. The blackboard – implemented in a program called *ThomCat* – will handle rivalry, priming and pruning of hypotheses.

We do not aim to implement a complete computer music system, but to give enough illustrations of all levels of perception to demonstrate a 'whole iguana' view of scene perception. We have trimmed the minidomain into a series of implemented subtasks: pre-processing, rhythm recognition, blackboard construction and blackboard inference, which together form a whole 'vertical slice of iguana'.

While it is not currently possible to obtain desktop quantum computing to illustrate high-level quantum scene perception speedups, chapter 7 will give theory and proof-of-concepts simulations showing how inference in ThomCat-like domains may be improved using quantum hardware, and gesture towards a hypothetical *ErwinCat* program at the highest level of the vertical slice.

1.3 Positions-in-time and attention

Music is inherently temporal, unlike other forms of scene perception such as vision, and provides a useful minidomain to emphasise this often overlooked aspect of scene

perception. Two broad classes of temporal representation have been used in Machine Learning and classic AI. *Dynamic-state* models maintain beliefs over the state at a point or points in time. *Position-in-time* models maintain beliefs over the time at which an event or events occur. The latter are a better fit with subjective notions of perception, and are a good fit with blackboard concepts and heuristics. Though both approaches have similar computational powers we work mostly with position-in-time architectures. Classically, blackboard systems were often discussed using the language of logic, for example statements of the form `isAtLocation(object,location)`, giving rise to apparently mathematical-looking descriptions. We take the view that modern object oriented languages have largely removed the need for such representation, as the languages *themselves* are rich enough to express such information. For example, the instruction `object.setLocation(location)` expresses exactly the same state of the world as the classical logical form (though as a constructive command rather than a descriptive statement). Such constructive statements appear throughout our code implementations but are mostly described in simple English in the dissertation text. (In contrast, the Bayesian *inference* methods that run on these constructions are best described using continuous mathematics notation.)

A key distinction is between *represented* and *representing* time. The former is the domain of the blackboard in which the scene is constructed, and which behaves much like space in visual scenes. The latter is the real processor time in which computation about these structures is performed. Confusion between the two has led to great philosophical debates [40], and we hope that our implemented models show concretely how to resolve them. Again this issue is not as apparent in other scene perception domains such as vision. The notion of *attention* involves these two concepts of time, as we may focus our inferences onto distant past represented times (i.e. when thinking about the past) but these computations are always performed at the present representing time.

All the algorithms here – from low-level particle filters through variational rhythm trackers to hierarchical Gibbs blackboards and quantum Gibbs sampler – are built on the same concept of the *annealing cycle* in representing time. They maintain a set of beliefs about the content of represented time, but during representing time the attended beliefs are 'heated', 'cooled' and 'collapsed' regularly to update them. We postulate this 'blowtorch of attention' as a basic mechanism for scene perception.

1.4 Contributions to knowledge

- A novel 'priming' particle filter algorithm for musical score following (published in Proceedings of the International Computer Music Conference 2007, [60]).
- A novel application of variational message passing to simultaneous beat tracking and rhythm recognition (published in Proceedings of the International Computer Music Conference 2007, [62]).
- A re-appraisal and re-construction of classical blackboard system ideas – in particular the Copycat architecture – in a modern Machine Learning framework.
- Practical Bayesian blackboard methods for high-level musical scene perception, illustrating the above ideas. (Published in Proceedings of the AAAI International Florida Artificial Intelligence Research Society Conference 2008, [58]).
- An open-source quantum computing simulation library for Matlab, called QCF (published as Oxford University Technical Report PARG-03-02, [55]; and as SourceForge code downloaded by more than 70 users from June 2007 to June 2008).
- A new local-only quantum computing algorithm which generalises the Gibbs sampler and achieves a quadratic speedup (Published in the Second AAAI Symposium on Quantum Interaction, 2008, [63]).
- Clarification of the role of heuristic 'hash-classifiers' in inference and action selection (published in part in Proceedings of the AAAI International Florida Artificial Intelligence Research Society Conference 2008, [59]).
- An illustration of the 'vertical iguana slice' minidomain methodology for AI.
- Steps towards computational definitions of psychological concepts such as priming, attention, and rivalry, which may help to clarify discussion.

Chapter 2

Inference

2.1 Bayesian theory

In Statistics, we are generally given a parametric model for data, but are uncertain about its parameters and wish to make inferences about them from data. Given a model M with parameters θ generating data D with $P(D|M,\theta)$, we use Bayes' theorem to invert the model:

$$P(\theta|D,M) = \frac{P(D|\theta,M)P(\theta|M)}{P(D|M)}$$

The term on the left is called the *posterior*. The three terms on the right are called the *likelihood*, the *prior*, and the *evidence*. The evidence can be obtained using the integrating out theorem over θ.

The posterior can be utilised in various ways: ideally, the whole distribution is preserved and future inferences involving θ are made by integrating over it. If we seek a single statistic to describe the value of θ, we may quote the value with the maximum probability, the *maximum a posteriori (MAP)* value: $\theta_{MAP} = \arg\max_\theta P(\theta|D,M)$, or we may choose to quote the mean or the median of the posterior. The choice here depends on what we want to do with the result: if we are interested in the average height of a population, the mean or median is appropriate; however if we want to know the best place in a piece of music to provide accompaniment, the MAP may be more appropriate. The standard deviation of the posterior can be used as an indication of uncertainty in these statistics. Sometimes we will be interested in the joint distribution of particular subsets of variables, and in these cases we can choose to quote values such as the MAP solution for the subset's joint.

The evidence term $P(D|M)$ is independent of θ so does not need to be computed for the parameter-fitting task. However it becomes useful if we are given two or more competing models to fit the data. Then the $P(D|M_i)$ give us likelihoods that

each model generated the data. These may be combined with prior beliefs about the presence of the models to give posteriors for the models, to compare them:

$$P(M_i|D) = \frac{1}{Z}P(D|M_i)P(M_i)$$

where evidence Z is a normalising coefficient, in this case summing over all candidate models M_j,

$$Z = P(D) = \sum_j P(D|M_j)P(M_j)$$

Models with large numbers of parameters are automatically penalised for over-fitting the data by this system – giving a mathematical clarification of 'Occam's razor'.

When a prediction of a random variable f is required, we can choose to work with only the most probable model $\hat{M}$ and predict using $P(f|\hat{M})$; or if resources allow, we may go 'fully-Bayesian' by keeping all the models and integrating over them:

$$P(f|D) = \sum_j P(f|M_j)P(M_j|D)$$

The latter is the optimal strategy for a rational agent with infinitely large and fast computational resources. But for real-world agents it is often considerably time-consuming to compute. Time consumption often carries its own utility penalties so the strategy may not be optimal for such agents.

2.1.1 Conjugacy and the exponential family

When making inferences using Bayes theorem, a prior distribution $P(\theta)$ is updated on observation of a variable x to become the posterior $P(\theta|x)$ by

$$P(\theta|x) \propto P(\theta)P(x|\theta)$$

It is computationally convenient if the posterior has the same parametric form as the prior, in which case the result of the inference may be represented simply by updating these parameters. For a given parametric likelihood form, a prior/posterior form is said to be *conjugate* to the likelihood form if it has this property.

A large class of likelihood-prior conjugates is the *exponential family* of distributions, which are defined by

$$P(x|\theta) = \exp\{\langle u(x)|\phi(\theta)\rangle + f(x) + g(\phi)\}$$

where $u(x)$ is a vector of *sufficient statistics*, $\phi(\theta)$ is a vector of multi-linear *natural parameters*, $\langle|\rangle$ is the inner product operation, and g is a multi-linear function and f is

a normalising function. We will make heavy use of conjugate-exponential distributions in variational inference due to their simplified computational properties. A problem with their use is that they assume our subjective priors to have particular parametric forms, which may not exactly match our actual beliefs. However in practice many beliefs are unimodal and approximately exponential – generally with Gaussian or Gaussian-like shapes defined on various domains.

2.2 Bayesian networks

The configuration space of a model grows exponentially in its number of variables. So in general, representing and computing with the full posterior requires exponential space and time respectively. However many models exhibit *conditional independence* relationships between variables which may be exploited to reduce space and time requirements. Variables X and Y are conditionally independent on variable Z if $P(X, Y|Z) = P(X|Z)P(Y|Z)$. The minimal set of variables Z separating X from all other variables Y in the model is called the *Markov blanket* of X, or $mb(X)$.

Bayesian networks (BNs) [124] are directed acyclic graphs (DAGs) which represent conditional independence relationships intuitively for models of the form

$$P(X_1, X_2, ...X_N) = \prod_{i=1}^{N} P(X_i|par(X_i))$$

with the parent function *par* satisfying, $par(X_i) \subset \{X_j|j < i\}$. The DAG represents each variable X_i by a node, and contains a directed edge from each parent of X_i to X_i. Each node is associated with a function $P(X_i|par(X_i))$. The DAG structure is utilised by many algorithms for performing efficient inference.

Pearl [124] showed that for DAGs which are also polytrees, with discrete-valued variables, there is a polynomial-time algorithm for making inferences about variable marginals. The following update equations are computed repeatedly for each possible value x_i of each node X_i until they converge:

$$
\begin{aligned}
Bel(x_i) &\leftarrow \alpha\lambda(x_i)\pi(x_i) \\
\lambda(x_i) &\leftarrow \prod_j \lambda_{Y_j}(x_i) \\
\pi(x_i) &\leftarrow \sum_{u_1 \ldots u_n} P(x : u_1, ..., u_n) \prod_i \pi_X(u_i) \\
\lambda_X(u_i) &\leftarrow \sum_{x_i} \lambda(x_i) \sum_{u_k : k \neq i} P(x_i : u_1, ...u_n) \prod_{k \neq i} \pi_X(u_k) \\
\pi_{Y_j}(x_i) &\leftarrow \alpha(\prod_{k \neq j} \lambda_{Y_k}(x_i)) \sum_{u_1, ...u_n} P(x_i : u_1, ...u_n) \prod_i \pi_X(u_i)
\end{aligned}
$$

where U_i are the parents of X and Y_i are the children of X. *Bel* becomes the posterior marginal belief in a node's state; π the prior; and λ the likelihood. $\lambda_X(u_i)$ are likelihood messages sent by X to its parents and $\pi_{Y_j}(x_i)$ are prior messages sent to its children.

If we wish to make a decision based on the value of a single node, then we should use its marginal *Bel* distribution. However for some tasks we are instead interested in the configuration of a *collection* of nodes. In scene perception we want to know the single most likely interpretation of the whole musical environment so that we can make accompaniment actions based on it. [30] gives an alternative message-passing algorithm called *max-propagation* which enables this form of inference on polytrees.

Bayesian networks are intended [124] to model causality rather than merely passive correlation. For causal modelling, the network is provided with a set of operators $do(X_i = x_i)$ which when applied to nodes X_i, set $pa(X_i) = \emptyset$ and $P(X_i) = \delta(X_i; x_i)$. δ is a Kronecker or Dirac Delta function for discrete or continuous nodes respectively. The *do* operators correspond [125] to the effects of performing an intervention on the system being modelled.

Fig. 2.1 shows a visualisation of a Bayesian Network structure being used by Pearl's algorithm. The task, described in full in [124], is to compute the posterior probability of a burglary, given an observation of the alarm sounding and evidence of a radio report that there has been an earthquake (which may also explain the alarm activation). Similar visualisations will be used in the next chapter.

Similar networks and update equations can be constructed for certain classes of continuous state networks, namely those which nodes have conjugate priors as neighbours [124]. For such variables, there exist simple equations to update the posterior parameters as a function of the prior and likelihood parameters. A particularly simple case occurs with collections of Gaussian-valued nodes, parametrised by (μ, σ). Such nodes are self-conjugate as the sum of any number of Gaussian variables is also

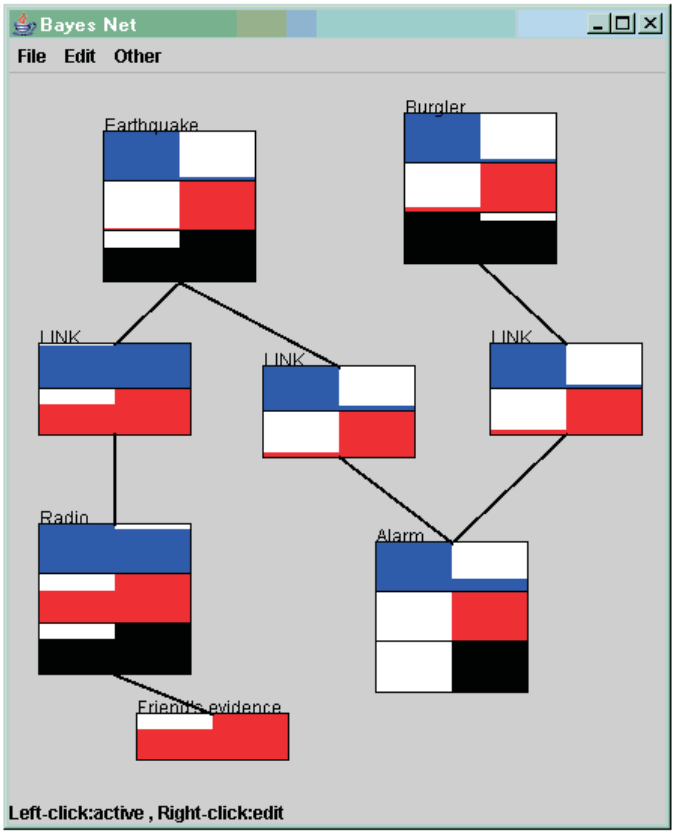

Figure 2.1: A Bayesian network program running Pearl's classic 'Earthquake' example. Each node contains three binary discrete pdfs: the prior, likelihood and belief (from top to bottom). Similarly, two messages – prior and likelihood pdfs – are shown on each of the links. The distributions are over the binary states True (left) and False (right). The Earthquake and Burglar were initialised to have a high prior on being False. Likelihood evidence was attached to the Radio event giving a high likelihood of that event having occurred. The belief pdfs show that Earthquake is more probable than Burglar. (All graphical pdfs are normalised in this figure so that the height of the largest one equals the height of the box.)

Gaussian. In the general case, we may create Bayesian networks with arbitrary mixtures of parameter types. However in such cases are unlikely to yield tractable exact message passing algorithms. Various methods for approximate inference are reviewed in section 2.2.2.

Graphical models (GMs) generalise BNs by dropping the BN requirements that the network be directed and causal. Models used in physics such as Ising models [19] and Boltzmann machines [1] are examples of GMs that are not Bayesian networks. In GMs, undirected pairwise specify pairwise probability *factors*, which are functions of the connected nodes' values and multiply into the joint posterior. Models having only pairwise undirected links are called *Markov random fields* (MRFs) and generalise the Ising Model (which is restricted to having identical factors on all links). MRFs are also known as 'structural equation models' in some fields. Any graphical model can be converted into an equivalent MRF form [117], though this discards causal semantics and usually adds nodes.

2.2.1 Dynamic Bayesian networks

A *Hidden Markov Model* (HMM) [129] is a special case of a Bayesian network, having all discrete-valued nodes, a particular structure, and particular set of observations. A set of hidden variables X_t are conditioned in a sequence such $P(X_t) = f(X_{t-1})$ (this is the *Markov property*) where f is the *transition* function. A set of observation nodes Y_t are conditioned on the hidden variables, $P(Y_t) = g(X_t)$. t is often (though not necessarily) used to represent time. When the nodes are continuous and f and g are Gaussians, the resulting model is called a *Kalman filter*.

2.2.1.1 Dynamic time warping

Dynamic time warping (DTW) [130] is a pre-Bayesian approach to sequence alignment, using standard dynamic programming to perform a similar task to HMMs. Given two sequences of symbols – the template and the observation – we wish to map each member of the observation to a member of the template. DTW assumes that there exists a distance measure on pairs of sequence elements. DTW creates a local distance matrix L with elements L_{it} which are the distances between the ith member of the input sequence and the tth member of a template sequence. Dynamic programming is then used to find the shortest path through the matrix subject to specified constraints on the form of paths. A second 'total distance' matrix keeps track of the shortest distance from the start to each column t of row i. The algorithm is independent of path histories, so is of order $O(T)$ at each point in time, where T

is the length of the template sequence. For path constraints which allow only steps from row i to row $i+1$, DTW is equivalent to a HMM with a flat transition prior over the allowable future states.

2.2.2 Loopy graphs and approximate inference

The Pearl update equations are valid only for polytrees, which is a severe limitation. We will often have some data D which can be accounted for by two different models M_1 and M_2. To allow these models to compete, we need a parent node N which controls the joint probabilities of M_1 and/or M_2. So we have probabilities $P(M_1, M_2|N), P(D|M_1), P(D|M_2)$ which form an acyclic *loop* as shown in fig. 2.2. (A *cycle*, in contrast, is a *directed* loop, such as $a \to b \to a$.) With the Pearl equations invalid, we must use alternative algorithms.

2.2.2.1 Brute force inference

For small BNs, it is possible to compute the complete posterior by tracing all possible paths through the network and keeping track of their probabilities. General inference may then be done by cropping and re-normalising this posterior to condition on evidence. Such brute-force computation would be intractable $O(\prod_{i=1}^{i=N} d_i)$ where there are N nodes having discrete state sizes d_i, and would be uncomputable for general continuous nodes.

2.2.2.2 Clustering and junction trees

If the cycles are 'small' it may be possible to manually group nodes together that are involved in loops, into larger nodes with more complex states (i.e. tensor products of the loopy nodes).

The junction tree or J-tree algorithm automates the manual clustering process. The DAG is converted algorithmically into an undirected graph, some extra edges added (via a process known as *moralisation*, or 'marrying parents'), and cliques found (which is itself an NP-hard problem). Then a new undirected graph is constructed where each of these cliques becomes a node. Joint PDFs are computed for each clique, and messages are sent between cliques to normalise them [86]. This requires 'compiling' the network into the 'junction tree' form every time an inference is required, so is unlikely to be useful for realtime systems when the network structure is changing.

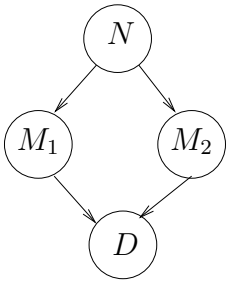

Figure 2.2: Loops arise when rival models are considered to explain data D.

2.2.2.3 Loopy belief propagation

Simply applying the polytree Pearl equations to loopy graphs without modification achieves reasonable approximations to the node marginals in useful cases [116, 65]. [162] explains this by showing that the computed marginals do not correspond to marginals of any actual joint, but are obtained by replacing the true entropy of the joint with a 'Bethe entropy' simplification which assumes the joint is factorisable as in a polytree. Approximation accuracy may be improved at the expense of extra computation by performing Bethe-like message passing on clusters rather than nodes, as in the J-tree algorithm: this approach is known as the Kikuchi approximation due to its connection to a statistical mechanics method of the same name [162].

As the Pearl equations compute individual node marginals, the Bethe approximation computes approximate node marginals. For many applications, such as scene perception, we prefer a single estimate of the MAP of the joint, as found by the max-propagation equations in the polytree case. The loopy message passing scheme can be converted into an MAP-joint estimator by introducing a temperature parameter T [164], and replacing $P(x|par(x))$ by $P(x|par(x))^{1/T}$. As $T \to 0$, the joint tends to a *Delta spike*[1] at the MAP. As a Delta spike is equal to the product of its marginals, the Bethe node marginals may be interpreted as factors in the approximate joint MAP. Temperature must be reduced slowly to avoid becoming trapped in local minima; and even the global MAP estimate if found is still a Bethe approximation, not the true MAP. This scheme is called *deterministic annealing*.

2.2.2.4 Monte Carlo sampling

The previous methods (with the exception of deterministic annealing) are all to compute or estimate the individual node marginals. However in scene perception tasks we want to approximate the MAP of the joint $P(x_{i=1:N})$, not the individual nodes

[1] i.e. the product $\prod_i \delta(x_i; X_i)$ of Kronecker and/or Delta distributions on node variables X_i, according to their discreteness or continuousness.

$\{P_i(x_i)\}_{i=1:N}$. We will discuss two classes of methods that do this, and one speculative method. The fundamental problem with joint distributions is that they are exponential in size: even just writing them down would require exponential space and hence exponential computing time (to visit each location and write its value). The first approximate method – Monte Carlo sampling – uses the N nodes in a network over exponential time: at each time-step, a sample from the joint is displayed on the network, so the set of states of the network *over exponential time* represents the joint. The second method – mean-fields – does not represent the true joint at all, but aims to find a factorisable distribution $Q(x_{i=1:N}) = \prod_{i=1}^{N} Q_i(x_i)$ that is 'similar' to it. By being factorisable into node marginals, the N nodes of the network can represent the whole approximate joint by storing marginals as in the Pearl/Bethe scheme. Sampling represents the exponential complexity of the joint over exponential time; mean-field discards the exponential complexity and represents a tractable approximation with tractable resources at a single point in time. In chapter 7, we will show how future quantum hardware could resolve this tradeoff by representing the exponential-sized joint with the tractable N nodes at a single time, making use of physical entanglement to represent the correlations.

Monte Carlo (MC) sampling produces a series of samples drawn from the joint, which taken together over time represent the joint. To achieve an arbitrary error in quantities computed from the samples, an exponential number of samples is needed: however MC can be converted into a tractable approximation method by taking fewer samples in tractable time and allowing higher approximation errors. Drawing samples from a high-dimensional distribution is a hard problem: the naive approach of compiling a cumulative table then looking up values from a uniform distribution would require the whole joint to be computed in advance by brute force: which is what we are trying to avoid! A second naive method is to draw samples from a uniform distribution over the same domain as the joint, $U(x_{i=1:N})$, evaluate the probability of each under P, and re-normalise them to appear as if they came from P. However in high dimensional space, the uniform distribution is unlikely to produce *any* 'good' samples from peaks in P [44]. Methods are needed that draw samples from good areas of P instead. For simple P we may be able to construct an approximate $Q \approx P$ from which we can sample easily (e.g. a high dimensional, moment-matched Gaussian) then apply the same re-weighting scheme as in the uniform case: this is called *importance sampling*. Alternatively, *rejection sampling* [44] uses a criterion to keep or reject the Q samples such that the kept samples form a sample from P without re-weighting. For large networks, as we will use, it is not usually possible to find a single suitable Q to use these methods.

An alternative is to use *Markov Chain Monte Carlo* (MCMC) methods [44] which construct a different $Q(x'|x)$ at each step, conditioned on the current sample x. The idea is to approximate and move within only the local area of the joint around the current sample, in a similar manner to gradient descent style optimisation methods which assume some local knowledge of the landscape. Applying the rejection sampling method in this context gives rise to *Metropolis-Hastings* (MH) sampling. *Gibbs sampling* is a special case of MH in which the Q is chosen to be the exact conditional $Q(x'_i|x) = P(x'_i|\{x_{j\neq i}\})$ holding all $x_{j\neq i}$ constant, and proposals are always accepted. Due to graphical models' use of local probability factors this is a particularly simple form of MCMC to implement in inference problems. It is implemented by holding the state of all nodes constant except for one (randomly chosen) node; computing the conditional distribution for the node; and sampling from it to give that node's value in the next network state.

Gibbs sampling is not usually the most efficient MH method. In general, MH is faster when prior structural and domain knowledge about P allows more accurate and extensive $Q(x'|x) \approx P(x'|x)$ to be designed. For particular problems, a custom Q can be designed using this knowledge: the art here is to design a Q that is easy to sample from and is also similar to the local P according to domain knowledge. In visual image perception a MH method found to be useful is cluster sampling [5] which proposes and accepts flips of state in clusters of locally-connected nodes (rather than individual nodes as used in Gibbs). In low-level harmonic music scene perception, custom kernels which model explicit moves between numbers of notes and their pitches was useful in offline transcription [68]. As with model design, inventing MH kernels is a creative process based upon domain knowledge and trial-and-error.

For real-time temporal networks, we may use a form of multi-sample MH for approximate inference of dynamic-state slice marginals as in the DTW, HMM and Kalman filter models, to limit the number of hypotheses under consideration. The *particle filter* [45] (also known as 'sequential importance resampler') maintains a population of samples at each slice, used to propose samples for the next slice; and the acceptance probability P then involves the next likelihood from the temporal data.

Like Bethe propagation, Monte Carlo methods are easily converted from joint-approximators into MAP optimisers by introducing and reducing a temperature parameter, i.e. replacing all P with $P^{1/T}$. This was first performed on a Gibbs sampler, and annealed MH sampling has come to be known as *simulated annealing* [91], although we emphasise that annealing can be applied to all the joint-approximating methods considered here in the same way. Finding useful annealing *schedules* – i.e. the sequence of temperatures to use at each step – is something of a black art and

is usually done by trial-and-error in practice. Too fast, and annealing gets stuck in local minima; too slow and annealing may take impractical lengths of time to run.[2] Chapter 6 will apply annealed Gibbs to hierarchical scene perception. Simulated *tempering* [104] adapts the temperature in response to the current network state, heating it when it appears to have reached a minimum energy to escape from local minima and encourage further exploration.

2.2.2.5 Variational Bayesian inference

The size of a joint over N variables is exponential in N, so representing it exactly generally requires exponential space, and exponential time to compute. An alternative strategy is to replace the exact joint $P(x)$ with some approximate joint $Q(x)$ having simpler computational properties which allow it to be represented in a smaller space (and require less time to compute). This approach is called *Variational Bayes (VB)* and is applied in chapter 4. In particular, we will assume $Q(x) = \prod_i Q_i(x_i)$ to be factorisable into the product of individual variable factors $Q_i(x_i)$. Under this assumption, we may then represent $Q(x)$ by the state of a graphical model at a *single* point in time, by arranging for the nodes to contain these factors. This form of Q is called a *mean-field* approximation (a particular form of variational Bayes), and assumes that the nodes are uncorrelated with one another: it is precisely factors involving pairs and groups of variables that have been excluded from the parametric form. So the approximation is likely to be good for problems having weak correlation structures, and bad for heavily combinatorial-type problems with strong correlations.

Once a parametric form for $Q(x;\theta)$ is specified, some algorithm may be used to find the best θ to make Q as 'close' to the true P as possible. 'Close' may be defined in various ways, but using the KL divergence,

$$KL[Q(x)||P(x|D)] = \int dx.Q(x) \ln \frac{Q(x)}{P(x|D)}$$

can lead to particularly efficient algorithms in cases where the network is conjugate exponential (or approximated by conjugate exponentials). It can be shown [2] that defining $L[Q(x)]$ as

$$\ln P(D) = KL[Q(x|D)||P(x)] - L[Q(x)]$$

transforms the task of minimising the KL divergence into that of maximising

$$L[Q(x)] = -KL[Q_i(x_i)||Q^*(x_i)] + H[Q_i(\bar{x}_i)] + \ln Z$$

[2]The 'Robbins-Munroe criteria' provide theoretical conditions for exact convergence, but are of limited practical use as they require an infinite number of steps.

where x_i is any hidden node, $\bar{x}_i$ is the set of hidden nodes excluding x_i, H is the Shannon entropy, $Q_i^*(x_i) = \frac{1}{Z} \exp\langle \ln P(x, D) \rangle_{Q(\bar{x}_i)}$ and Z normalises $Q_i^*(x_i)$. A node-updating algorithm similar to Pearl's may be constructed to find (under certain conditions) local maxima. This algorithm optimises the above in a greedy sense, by altering one node's $Q_i(x_i)$ at a time (with nodes chosen in any order). As only the KL term is dependent on x_i, L is maximised with respect to Q_i by setting $Q_i \leftarrow Q_i^*$, thus achieving the lowest possible value, zero, for the KL term. Making use of the Markov blanket we can write the updates as

$$Q(x_i) \leftarrow \frac{1}{Z} \exp\langle \ln P(x_i, \bar{x}_i, D \rangle_{Q(\bar{x}_i)}$$

which makes the update for a node a function of the distributions of only its local, Markov blanket nodes. For conjugate exponential networks the updates have particularly simple forms due the presence of analytic expectations [12, 160].

The model log likelihood, $\log P(d|M)$, has a tractable lower bound which is useful for approximate model comparison:

$$\sum_{i=1}^{N} \left[\langle \log P(x_i | par(x_i)) \rangle_Q - \langle \log Q_i(x_i) \rangle_Q \right].$$

2.3 Towards a quantum generalisation

Sampling methods require intractable, exponential time to represent a complete joint over N variables, as they must generally visit each network configuration at least once to make an exact representation. Variational methods – including Bethe and mean-field approximations – drop correlation information and compute an approximate joint, which can be expressed in terms of local node factors only. Neither of these schemes is ideal for scene perception, in which we will see that nodes can be highly correlated due to 'rivalry' links, but also in which inference often must run in real-time if it is to assist in performing actions. Chapter 7 will investigate how future hardware could combine aspects of both sampling and variational methods, to give a joint that is factored into single-node potentials (as in VB) but which still is able to represent global correlations (as in sampling) – and which runs using local message passing (as with all the Bayesian methods reviewed here). Such a representation is impossible using conventional Turing machine hardware, but recent theoretical work (and practical proof-of-concept demonstrations) suggest that quantum computers may be capable of storing global correlations locally by exploiting physical 'entanglement'. The need for representation of exponential-sized joints is the Achilles heel of practical Bayesian

inference[3], and quantum computing theory might allow such full representations to exist in linear-sized space! Little work has been done on the links between quantum computing and Bayesian inference. Chapter 7 will present novel work which makes these connections and provides an algorithm for constructing such representations.

The difficulty in quantum algorithms lies in the limited and counter-intuitive allowable forms of interaction during computation, and in reading out the results. Few useful quantum algorithms are known, though Grover's algorithm [71] shows that unstructured search over N elements is possible in $O(\sqrt{N})$ time. However Grover's algorithm requires the use of a single, monolithic physical operator acting on the whole computational state, which is difficult to achieve in practice. An exciting question is whether a similar speedup can be obtained for Bayesian networks in the localised 'message-passing' manner of the other algorithms we have seen: that is, using only small local operators acting on nodes and their neighbours. Chapter 7 will show that this is indeed possible, and that scene perception networks can obtain a quadratic speedup (over a classical Gibbs sampler) using only local quantum operators.

2.4 Temporal hierarchies

We have already seen two temporal models: DTW and the HMM, both of which make a perception *of* a score time *at* each real time. However they are limited to perceiving a single position in a linear, predetermined musical score. More generally, we will be interested in scores that are generated from hierarchical grammars and other probabilistic factors. Our grammatical models will be based upon *stochastic context-free grammars* (SCFGs). A SCFG is a set G of rules r of the form

$$(A \to B_1, B_2, B_3), p_r$$

where

$$\forall a \sum_{\{r \in G : A_r = a\}} p_r = 1$$

The symbol B_i of rule r may appear as the LHS term of other rules, in which case B_i is called *nonterminal*; otherwise it is a *terminal*. The grammar describes a set of term rewriting rules, having probability p_r of rewriting. The probability of a parse of a string of terminals is given by the product of the probabilities of the rewrites used to make the parse. Though general scene perception is not context-free, the SCFG model can form a base for context-sensitive extensions. For example, in the music

[3]Hence the classical statisticians' joke: How many Bayesians does it take to change a light bulb? Only N but it takes them exponential time.

domain, we might maintain a global musical key which influences low-level percepts in addition to the rest of the grammar. For this reason we review two standard methods for parsing SCFGs. We will restrict our SCFGs to non-recursive grammars, i.e. we do not allow grammars which have possible infinite rewriting derivations.

2.4.0.6 Hidden semi-Markov models (HSMMs)

The Markov property of HMMs means that once the system is in a state i, there is a constant transition probability of it moving to the next state j. The probability is independent of the amount of time spent in state i. For domains where we know a prior on the expected duration in each state, this is not a very appropriate model. For example, if we choose to model each note of a musical score by a state, then we would very much like to be able to specify expected durations of these notes. A naive attempt at such a specification is to choose transition probabilities so that the mean time spent in the state matches our expectation. Consider a simple model with two states, A and B, with $p = P(B|A)$, $q = P(A|A)$. Assume that once the system is in state B it stays there. Let A represent a note which we expect to last for 4 frames. We could then set $p = 1/4$. So the average number of frames spent in state A is 4. Chapter 3 will show why this naive attempt fails due to a 'sandboxing' effect.

To make the transitions depend on the time spent in the state, we must relax the Markov assumption. One model which does this is the *hidden semi-Markov model (HSMM)* [115]. In the HSMM, each state has an explicit duration PDF associated with it. On entering a new state, a duration is drawn from this PDF, specifying how many observations to generate from the state. When those observations are generated, we proceed to draw the next state from the transition matrix. Inference can be performed with a slight modification of the Viterbi algorithm [115]. As with the regular HMM Viterbi method, this gives the most likely path through the system, not the most likely individual states. HSMMs can be generalised to hierarchical hidden Markov models (HHMMs) having states at multiple levels, each of which has a duration and generates low-level states during its presence [115]. This is equivalent to performing parsing of SCFGs with a fixed height of hierarchy.

2.4.1 Inside-outside algorithm

HSMM and HHMMs are dynamic-state models. Chapter 5 will review blackboard systems which are position-in-time, but we here discuss the standard *inside-outside* parsing algorithm (IO) which is also of this category. We give a novel Bayesian

network formulation with a modified Pearl likelihood message (based on insights from the more complex formulation of [108]).

IO instantiates $L \times L \times M$ nodes where L is the length of the terminal string to be parsed and M is the number of rules in the grammar. Each node represents a rule instantiated with a start time and and end time. A node for a a rule r instance is regarded as a generator of its RHS sub-component instances with probability p_r, and these form causal links in the network. Messages are passed which are similar to the Pearl equations, but with the single important difference of ignoring explaining-away effects in the likelihood messages. That is, the likelihood message is

$$\lambda_X(u_j) = \sum_{x_i} \lambda(x_i) P(x_i : u_j)$$

instead of Pearl's

$$\lambda_X(u_j) = \sum_{x_i} \lambda(x_i) \sum_{u_k : k \neq j} P(x_i : u_1, ...u_n) \prod_{k \neq j} \pi_X(u_k)$$

These messages give exact marginal probabilities of rule instances existing at each location, in polynomial time. This is interesting within the Bayesian network framework, because tractable inference has apparently been performed on a highly loopy graph – and by using a strange, simplified Pearl message! The reason for this is that IO exploits the context-specific independence of the parsing problem. The modified Pearl rule has deliberately excluded all explaining-away information: parent u_i simply assumes that all competing parents are off when computing its own probability of being on. This works because we have domain knowledge that a successful parse will never include two 'on' rival explanations of the same child: that is part of the meaning of a parse. So these conditions are simply excluded from consideration: in the terminology of [108], they are not part of the 'feasible set'.

IO is a surprisingly efficient algorithm for the highly loopy but specific problem of parsing SCFGs, due to this assumption that no pairs of parents are ever simultaneously active, and there is therefore complete context-specific independence. However this delicate property is destroyed by any context-sensitive factors in the generating distribution. For example, IO breaks down for natural language grammars which allow for a global context such as the environment that utterances are made in (which will encourage groups of words related to the same environment over words from different environments, even when they appear at distant places in a sentence). This property is found in most forms of scene perception – there is usually some global context which affects percepts in this way, and renders the IO algorithm useless. In

the musical scene minidomain, the global 'key' is one such factor, and for this reason we cannot use the IO algorithm. This is an important point, because if IO was possible for general scene perception, then it would provide a tractable exact algorithm and the task would be considerably less interesting! We will, however, draw on IO's key observation that rival parents are never active together, and reuse it to construct speedups for other, more general algorithms.

IO is effectively a version of the Pearl equations, which compute marginal rather than joint probabilities. Analogous to the conversion from Pearl messages to max-propagation, and from forward-backward to Viterbi algorithms, IO may also be converted to a MAP joint algorithm, known as the CYK algorithm [163].

2.5 Statistics and hash-classifiers

There are often situations where we do not have enough knowledge or time to work with full generative models as described so far in this chapter. Such models postulate a set of causal relationships between objects, and use algorithms derived from Bayes' theorem to invert the causal probabilities and infer the causes from the data. As we have seen, this requires a generative model and intensive computation. An alternative heuristic method is to postulate some arbitrary parametric function mapping directly from the data to likelihoods of high-level causes (possibly many links away in the generative model) and 'train' the parameters to approximate the generative inferences as well as possible, where training means searching for the best parameter settings. (The 'correct' solutions used for training may be found by detailed offline generative inference of the causes of the data, or the causes may simply be observed along with the data, eliminating the need for generative modelling.) In Statistics, this method of cause selection is called a 'discriminative classifier'; in Computer Science, an approximate fast mapping from large data to a set of labels is called a 'hash function'. We will use these terms interchangeably, and sometimes '*hash-classifier*' to emphasise their unity. Hash-classifiers are often made of two stages: one which maps the data to some lower-dimensional feature space, then a classifier-proper which maps this space to model likelihoods.

The first mapping is sometimes called a *feature* or a *statistic*. The role of statistics in Bayesian inference is rather awkward. *Sufficient* statistics have a well-defined Bayesian meaning[4], but general statistics (defined as 'a function of the data') do not, other than that they have been found useful empirically in some hash-classifier.

[4] A statistic $S(D)$ of data D is defined as sufficient for a generating model parameter θ if knowing D tells us no more about θ than knowing $S(D)$.

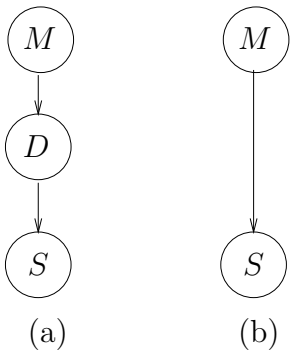

Figure 2.3: (a) True generative model: values of statistics S are caused by data D. (b) Hash-classifier assumption: statistics are caused directly by model M.

Statistics should not be confused with the results of full Bayesian inference, which are posterior probabilities of model parameters giving a model and the data.

Statistics are arbitrarily chosen functions of the data, and are therefore completely caused by the data: $M \rightarrow D \rightarrow S$ (fig. 2.3(a)). It is clear from the structure of this graph that we cannot generally make inferences about M from knowing only S and ignoring D. But this is exactly what features are used for in approximate models. We assume a simplified model, $M \rightarrow S$ (fig. 2.3(b)), where S is often a set of independent children of M, and use the best-fitting transition $P(S|M)$ that we can find. In the exact model $M \rightarrow D \rightarrow S$, the two transitions $P(D|M)$ and $P(S|D)$ are exact and are determined by the model and by the statistic definitions respectively. But in the approximate model $M \rightarrow S$ the transition is

$$P(S|M) = \int P(S|D)P(D|M)dD$$

which is generally intractable to evaluate. So as a further approximation – the classifier-proper – it is common to choose an approximate function $Q(S|M) \approx P(S|M)$. This function could be learned from data or set by hand, in both cases using domain knowledge to guess useful parametric forms.

We will use hash-classifiers for two purposes. First, at the lowest levels of perception, there is usually a large amount of data arriving from the physical world in each short time interval. For example, in music, factors such as the size of the room, the weather, and the performer's temperament all affect the data. We cannot model all such factors in real-time, so it is useful to use a hash-classifier to reduce the data to simpler features, such as pitch and volume, and assume that our generative model generates these features under a computationally simple (e.g. linear) classifier-proper likelihood function. Second, all levels of hierarchical perception face the problem of model *recall*: given limited computational resources, we cannot test all possible known

explanations of the data, but must quickly and heuristically select useful models to try. Hash-classifiers can be used to quickly map the data to a set of likely candidates – a form of priming – which can then be used in full generative inference.

Chapter 3

Low-level audio inference in the music minidomain

The focus of this thesis is on general mechanisms of high-level perception, but all non-trivial high-level systems must be driven by some preprocessed low-level data. We have chosen the minidomain of musical audio perception to illustrate high-level cognitive processes. One of the reasons for this choice is that its low-level prepossessing requirements are relatively simple (compared with 2D or 3D vision for example). That said, investigation of low-level musical audio methods is still an active research area. While it is not our intention to re-implement or extend the state of the art in low-level audio processing, it is important to review existing techniques to gain an understanding of what preprocessed inputs are currently available for input to high-level systems. It is also important to see what tasks can be performed using low-level methods alone in order to justify the use of higher-level methods.

Studying low-level methods also provides a first opportunity to see example applications of the Bayesian techniques reviewed in the previous chapter. While it is not our focus to extend the state of the art, we will in passing note how a standard particle filter may be extended to use novel bottom-up priming to improve current score-followers. This will serve as a first introduction to the notion of priming which will form a general theme of this thesis.

This chapter begins by introducing the music minidomain and gives example practical applications to motivate it. It then reviews basic concepts from audio signal processing and musical structures, and useful hash-classifiers. Next, the established musical perception field of score-following is reviewed, tested and extended by introducing the notion of priming. We show that score-free detection and classification of onsets is possible, which is a requirement for the rhythm segmentation model of chapter 4. Existing approaches to rhythm recognition are reviewed then an overall architecture for the minidomain task is introduced.

3.1 The music minidomain

The minidomain of *musical scene perception* has been chosen as a running example to work with in this thesis. Briefly, this is the task of listening to an input musical signal, with some incomplete prior knowledge of the musical score being performed, and outputting a belief in the current structure, location and speed of the performance. This output could be used, for example, to drive electronic accompaniment parts alongside the live performers. At its simplest, systems currently exist that provide a backing track to follow a karaoke performer or concerto soloist performing a known sequence of notes. (Note that the task is to *follow* the performer, we must understand what she is doing in order to follow her own choice of timing – it is not good enough to provide a pre-recorded accompaniment at a fixed tempo. This is itself a very difficult problem.) At its most complex, jazz musicians report that to understand and perform in a group of improvising musicians is one of the most creative and intelligent activities they undertake as humans, involving levels of pattern recognition from low-level melody and rhythm fragments, large-scale song structures, and masses of 'cultural prior' knowledge about standard forms, acceptable chord sequences, and historical performances. Great jazz performers can make musical references to their peers, which can be recognised and appreciated as such by those with the appropriate prior knowledge. We will aim for the middle-ground in the scope of this thesis: we will try to follow various types of simple 'semi-improvised music'. This task has been chosen as a minidomain example in which to study general perceptual processes: in particular it is a sufficiently rich task to allow ideas about time and action to be incorporated; its low-level pre-processing is relatively simple to allow us to quickly move on to focus on the high-level aspects; data is easy to gather and systems can be tested on useful tasks in real time. Finally at its highest level, we will see NP-hardness emerge in perception which will lead into a discussion of novel physical devices for faster pattern recognition.

Semi-improvised music consists largely of recognisable 'chunks' or patterns, at various levels of hierarchy. Such patterns can be thought of as cultural priors that a listener or accompanist needs to be aware of to understand the structure of the music. For example, four-beat drum rhythms are often used to mark out low-level bar structure. Once this structure is established, chord patterns such as the twelve-bar blues mark out larger structures. Over these structures are known melodies, or perhaps improvisations which – despite being composed on the spot – are still usually constructed from a known vocabulary of melodic motifs. To accompany this type of music, the accompanist must share (or learn) this knowledge. Each structure is a

model of what can happen in the music; somehow these models must be primed and 'brought to mind'; then tested to see if they fit; and the best interpretation decided upon – where 'best' means relative to the goal of providing an accompaniment that the performers like (and ultimately generating the maximum amount of reward from audiences).

3.1.1 Practical applications

Computers are becoming ubiquitous in music performance. It is notable how many laptops are presently appearing in classical, pop, jazz and theatre performances, and new styles of music are emerging that fuse electronic and acoustic sounds. Much of this music is produced offline in studios and is difficult to perform live due to the problem of synchronising the electronics to the live performers. When playing live, even major bands must give the drummer a pair of headphones with a click track, forcing the band to play at a predetermined speed along with the recordings. Performers could have much more room for expression if they were in control of the tempo instead of having to follow a predetermined tempo. Pattern analysis systems are needed to to understand what the players are doing, and provide the electronic accompaniment parts in response to their actions. An example drummer's-eye-view montage is shown in fig. 3.1. Sitting at an electronic drum kit, and performing with two other musicians, the drummer can watch the system running on a laptop by his side. (As the drummer is the primary time-keeper it makes sense for him to look after the system too.) Other uses for such systems could include:

- An amateur pop band writes a song using a PC which features sampled sounds during each chorus. At present they need an extra band member to sit by a laptop until the chorus then press the sample trigger. This member could be freed up to play something more interesting if the triggers were automatic.

- Large amateur groups such as swing bands often suffer from player absenteeism, which is detrimental if those absent are from the rhythm section (piano, bass, guitar). These groups may be controlled by human leaders who make structural as well as tempo changes on the fly, such as deciding to insert extra solos. The missing parts could be filled in by a MIDI device.

- New styles of music such as *jazz-n-bass* [150] are emerging which can only currently be created offline. These genres could be made live on stage with this technology. For example, jazz-n-bass features vastly complex drum patterns

which would require about six arms (or three drummers) to play. The technology could listen to a more basic but live drum part then fill in the rest of the predetermined patterns.

- Modern performances often require lighting effects to be synchronised to the music. At present this involves employing an engineer to listen to the music and activate the text. This could be automated.

This thesis is about the general task of scene perception. While the above applications are interesting and motivational, this thesis does not aim to implement a complete perception or accompaniment system, but provides a theoretical framework and small proof-of-concept implementations for various aspects of the general scene perception task. Semi-improvised musical scene perception is used as an example purely because it is a nice minidomain in which to work.

3.2 Review of musical audio structures

The focus of this thesis is on high-level structures but we must first understand foundational lower-level structures. The windowed Discrete Fourier Transform is a useful aid to this and is described here.

The complex exponentials, $\{e^{jwt}\}_\omega$ form a complete basis for the space of functions $x(t) : \mathbb{R} \to \mathbb{R}$, where $j = \sqrt{-1}$. $x(t)$ can be represented by the projections $X(\omega)$:

$$X(\omega) = \int_{-\infty}^{\infty} x(t) e^{-j\omega t} dt$$

$x(t)$ can be recovered by the inverse:

$$x(t) = \frac{1}{2\pi} \int_{-\infty}^{\infty} X(\omega) e^{j\omega t} d\omega$$

This can be used to transform a time-domain signal such as an audio signal into the frequency domain. Following from the Schwarz inequality, the Uncertainty Principle is the mathematical bound,

$$\sigma_\omega \sigma_t \geq \frac{1}{2}$$

where

$$\sigma_t^2 = \int (t - \bar{t}) |x(t)|^2 dt$$

$$\sigma_w^2 = \frac{1}{2\pi} \int (\omega - \bar{\omega}) |X(\omega)|^2 dt$$

Figure 3.1: Montage showing an example application of musical scene perception: guitar, vocals, keyboards and a MIDI drumkit send data to a laptop running a scene perception and accompaniment system. The system constructs an interpretation of what the players are doing, and schedules additional electronic sounds into the mix.

This shows an inherent tradeoff between the spread of energy in a signal over time and spread of energy over frequency in its transform. Thus by applying window functions [103] which localise a signal in time, we degrade resolution in the frequency domain. The finite discrete version, the *discrete Fourier transform* (DFT) is given by:

$$X[k] = \sum_{n=-M/2}^{M/2-1} x[t] e^{(-2\pi k t j)/M} \tag{3.1}$$

$$x[t] = \frac{1}{M} \sum_{k=-M/2}^{M/2-1} X[k] e^{(-2\pi k t j)/M} \tag{3.2}$$

The short-time power DFT, or *spectrogram* is simply the series of squared absolute values of DFTs computed at consecutive (and possibly overlapping) windows of the audio wave. Visually it gives a quick and useful picture of useful aspects of musical signals, which will be used in the next section. The spectrogram is a potentially useful feature for hash-classifiers.[1]

3.2.1 Musical audio signals

Here we examine and discuss sample spectrograms from various instruments, to gain an understanding of raw musical audio data.

Human hearing responds to the energy and pitch of sounds. Energy roughly correlates with subjective 'loudness'. Pitch is more complex: many sounds, including all musical instruments except some percussion, are generated by vibrating sources having several simultaneous harmonic modes, $\omega_i = i\omega_0, i \in \mathbb{N}$. In general we do not perceive harmonic components separately but perceive a single 'pitch' corresponding to ω_o along with a vaguer notion of 'timbre' corresponding to the shape of the amplitude curve of the harmonics. (See [16] for highly detailed psychological investigations into human pitch and timbre groupings.)

The guitar, piano and drums are percussive instruments: they involve hitting an object then allowing it to sustain vibration before decaying away (either naturally or with the aid of a controllable damping device). For these instruments, we expect to see a strong *attack* in the waveform – i.e. a sudden increase in energy at the onset of the note – which then dies away. These instruments may show *transient* harmonics, which are essentially random high frequency components at the brief moment the object is struck. This behaviour is shown in fig. 3.2(e) which shows the large-scale

[1] Interestingly, a related statistic, the periodogram, has a generative interpretation under strong assumptions about the source, see [17].

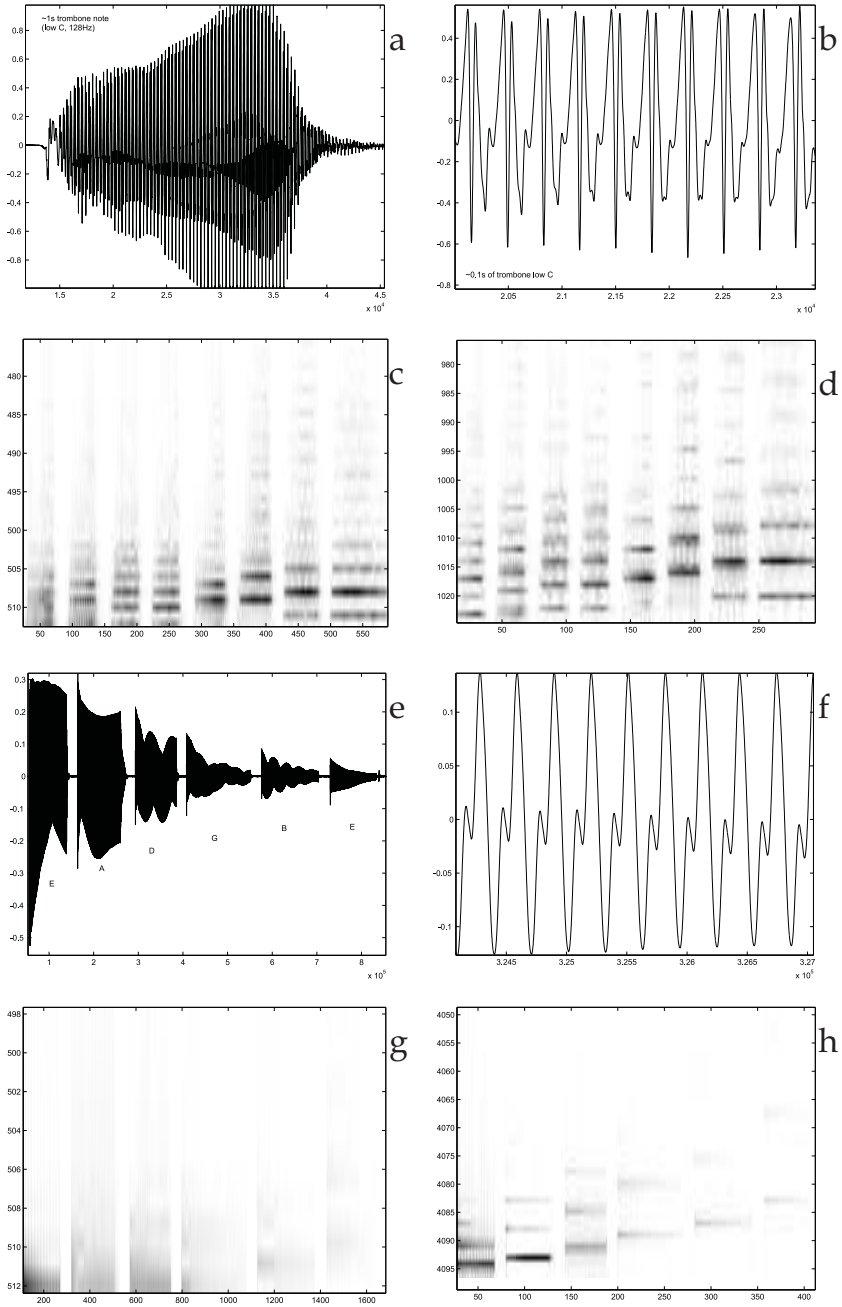

Figure 3.2: (a) Large-scale time-domain view of a single 1s trombone note. (b) Close up of trombone waveform. (c) Spectrogram of trombone scale (the previous figures showed the first note of this scale). Sampling was at 8192Hz, windows were 512 samples. Resolution is poor for the low harmonics. (d) Spectrogram of same trombone scale, but linearly interpolated to 16384Hz and windowed at 1024 samples, improving resolution of the low harmonics at the expense of processing power. (e) Large scale waveform of the six open guitar strings, each played for about 1s. (f) Close up of guitar waveform, for single open D string note (g) 512-point spectrogram of 8192Hz-sampled guitar open strings. Resolution is poor. (h) 4096-point spectrogram of 16384Hz-resampled guitar open strings. This improves the resolution.

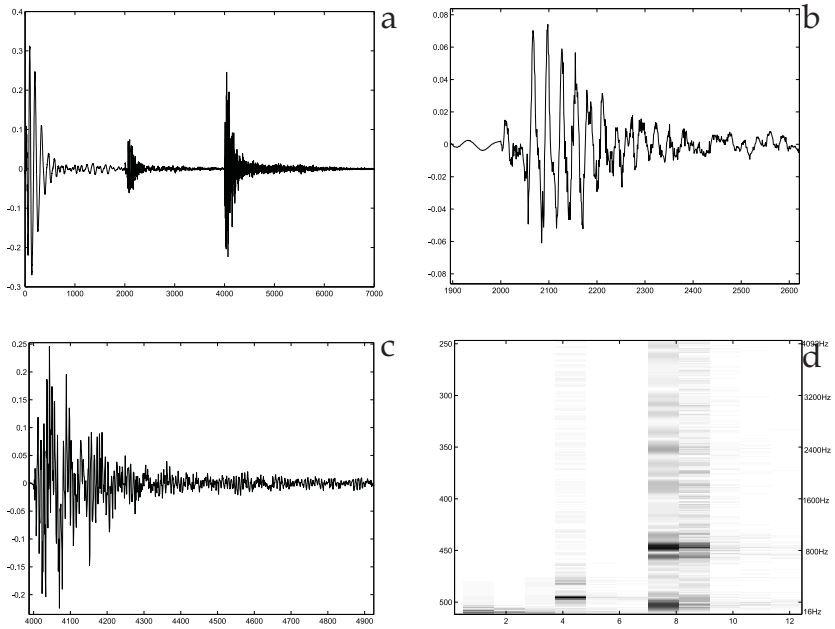

Figure 3.3: (a) Large scale time-domain waveform of simple 2s drum pattern: (bass, hihat, snare). (b) Close up of hihat waveform. (c) Close up of snare waveform. (d) 512-point spectrogram of drum pattern. Increasing the window size has little effect on the resolution as the sounds are not harmonic.

waveform produced by playing the six open strings of a guitar in sequence, and in fig. 3.3(a) which shows drum hits on the bass, hihat, and snare.

In contrast, instruments such as the trombone, clarinet, voice and some synthesisers allow the energy flow to be controlled *throughout* the duration of the note. Fig. 3.2(b) shows the waveform of a single trombone note: its energy is seen to increase over time as the player's breath power increases.

Fig. 3.2(d) shows spectrograms of a scale played on the trombone. Its harmonic series can be seen clearly, and is roughly exponentially decaying with higher harmonics.[2] In contrast, the guitar spectra for the open string series in fig. 3.2(h) is less structured, perhaps due to guitarists' higher level of manipulation over the harmonics.

Percussive instruments are likely to have more easily recognisable onsets than wind instruments, but wind instruments have more recognisable harmonic series once the notes have started. (Players of the instruments see high variability as an advantageous expressive feature, whereas for scene perception it becomes a 'nuisance'!)

[2]Interestingly, the fundamental is quieter than the first harmonic. This may be due to the shape of the trombone bell creating a higher impedance for the very low frequencies. We will not be concerned with such details in this thesis, but they may become important in industrial systems.

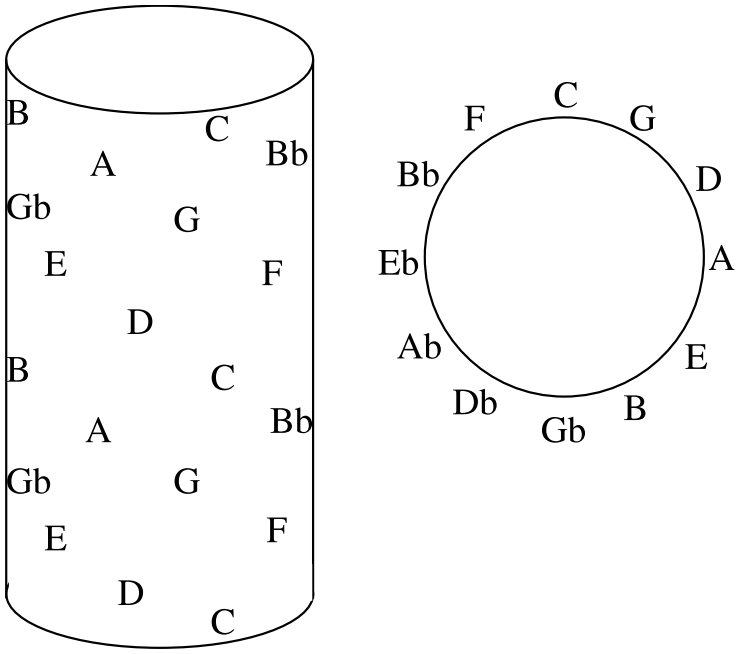

Figure 3.4: *Left*: Helmholtz space spiral representation. *Right*: viewed from above it shows the circle of fifths.

3.2.2 Pitch

Perception of the Western pitch system may be visualised as a three-dimensional cylinder surface as in fig. 3.4, sometimes known as 'Helmholtz space'[3]. Here the circle of fifths is mapped around the circumference of the cylinder, while the frequency is mapped vertically. Many musical concepts become intuitive in this representation: notes that sound pleasant together are close; the pentatonic scale is found within a tight band of the circumference, and the major and minor scales are found roughly as any set of notes that is visible from one side of the cylinder.[4] Melodies generally have a 'home' note on which they begin and end. In terms of the Helmholtz cylinder above, many melodies can be viewed as journeys away from the home note, taking paths mostly of small steps around the cylinder and occasional large leaps (c.f. [121]).

3.2.3 Chords

Chords are sets of notes played together. The major and minor chords are defined as the sets of the first, third and fifth of the major and minor scales respectively, and are

[3]The structure has been described by many authors, but [158] reports some of the earliest steps towards it, in the 1885 appendix by Ellis.

[4]It is an interesting an open question whether some auditory neural structure exists that is isomorphic to this phenomenal model.

the most common chords. We will notate major chords by the lower case letter corresponding to their first (e.g. *c,f,g♭*), and minor chords with the same lower case letter suffixed with 'm' for 'minor' (e.g. *cm,fm,g♭m*).[5] Modifiers can be applied by adding additional notes to these chords. Chords form patterns on the Helmholtz surface, and pleasant-sounding sequences of chords generally make slow gradual movements around the surface. Like melody paths, these produce feelings of tension as they move away from their home location, and resolution when they arrive back.

Importantly, there is more to the perception of a chord than the existence of the note frequencies that comprise it. Chords are usually (especially in pop and jazz) perceived as a 'field' covering a whole bar or half-bar of music. So even if the actual notes are only present for a small part of the bar, and not necessarily played together, perception of the chord 'field' still occurs. For example, monophonic instruments often produce perception of chordality by playing arpeggios (i.e. sequences of chord notes). So it is unlikely that chordality can be determined locally in a signal – the structure and priors also play a role.

The chords derived from a major scale can be notated by Roman numerals, for example II is the chord formed using the second note of the scale as its root note. For a major scale this will be a minor chord, written IIm. As with melodic fragments, there are many well-known chord sequence fragments which are often reused. For example the 12-bar blues, (I,I,I,I,VI,VI,I,I,V,VI,I,V) and Pachelbel's Cannon, (I,V,VIm,IIm,III,VI,V) occur in countless compositions. Such sequences – even if their presence was not determined in advance – are still recognisable by improvising musicians, and provide strong hierarchical priors on what to expect next.

Human perception of chords tends to take place without perception of the individual notes that comprise them (see [73] for a brief empirical study). This poses a problem for generative model theories of perception, of the form $CHORD \rightarrow NOTES \rightarrow DATA$, which would suggest that notes must be inferred from the data before chords. Speculatively, this can be viewed as an example of human hash-classifiers as shortcuts in inference: it is possible to compute statistics of the data which correlate well with the chord (such as the 'CDV' statistic of section 3.3.5) and classify chord likelihoods approximately from these statistics, using the simplified model $CHORD \rightarrow CDV(DATA)$. The information about chords can *then* be used to constrain the inference over possible note combinations, and perhaps avoid some of the combinatorial explosion from possible note combinations.

[5] This is because chords will be used in chapter 6 as grammar terminals, which are conventionally notated by lower-case symbols.

3.2.4 Keys

The subjective experience of key is important in Western music. As with all subjective higher-level musical concepts it is difficult to define exactly, but a workable (though debatable) definition is as a tuple (θ, n_h) comprising an angle θ around the circle of fifths and Helmholtz cylinder, and a home note n_h. Visually, imagine the Helmholtz cylinder rotated so that θ is facing the viewer. Then, the Western major and Aeolean scales correspond to the set of notes on the visible side of the cylinder, under certain choices of home notes. The key effectively provides a prior, preferring notes which are visible, and especially those near the home note. Key is not directly observable by the listener but is inferred from the *global* distribution of notes and chords, whose percepts are themselves affected by the prior from the key. Section 6.2.1 will show that this is an important source of graph loopiness and global probability factors for high-level inference. Music often changes key for middle sections (often called 'middle 8's in popular music) to provide variety. This is like temporarily rotating the cylinder. The simplified models in this thesis will assume that key does not change and is thus a global variable.

3.2.5 Rhythm

Rhythm perception is one of the most primitive human instincts, yet it is still hard to capture its definition. Roughly, our music domain is assumed to consist of *bars* each containing a small number of *beats*. Beats occur at regular score intervals throughout the whole piece (though the speed or *tempo* at which the score is played may change). Beats are positions in the music that human listener would tap along to – or change the direction of their body movement as they dance (see [156] for a theory of beat perception as resonance of a physical dancer due to rhythmic impulses). Typically there are four beats in a bar. Two, three and six are less common. Other numbers are uncommon. A bar is thus a perceptual unit of analysis: musicians break up the sequence of beats into bars according to recognisable rhythm patterns. Whilst we perceive four regular beats, it is often the case that the actual positions of rhythmic events of the bar do not correspond to those beats. Fig. 3.5 shows three bars of rhythm: the first has all the notes on the beats; the second has off-beat notes at the end of the bar; and the third is highly off-beat (it could be used by a drummer for special effect, to mark the end of a large-scale structure for example). So there is a difference between the event times and the unobservable underlying beat. The notes in the figure are drum notes; however we will see in section 3.8 that we can also extract similar rhythmic features from other instruments. For example, guitar

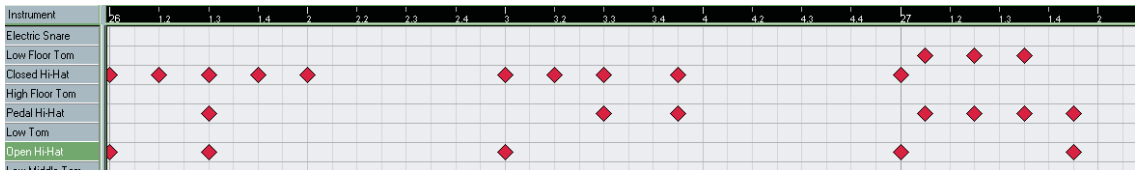

Figure 3.5: On-beat, partially off-beat, and heavily syncopated rhythms. The rows are hihat, snare and bass drum.

players often strike the strings at three distinctive velocities, corresponding to the hihat, bass and snare rhythm events. Orchestral composers use similar devices to mark the rhythm, though are usually spread over the whole orchestra rather than a single instrument.

Perception of beats and bars is difficult because there is scope for much ambiguity. Fig. 3.6(a) shows an example of *between-bar* ambiguity: a listener familiar with military bands would probably chunk this into 'marching' bars beginning at the points marked '*', but a listener more accustomed to electronic dance music might chunk it into classic 'two-step' drum'n'bass bars beginning at the '†' points. *Within-bar* ambiguity is illustrated in the two bars of fig. 3.6(b): here the rows represent different onset types; the first bar is a standard four-beat pattern with the snare on beat 3. The second bar is similar but the snare hit occurs later. This could be interpreted in at least three ways: (1) the pattern could be the same standard four-beat pattern as in bar one, but with an onset-detection error giving rise to the snare being perceived as late; (2) the pattern may be the same standard four-beat pattern but the player made a (possibly deliberate) mistake of playing the snare late; (3) it may be a new pattern with the snare on beat 3.5. The difference between (2) and (3) is subtle and even debatable: if the player makes the same 'error' of (2) several times then we begin to perceive it as a new pattern as in (3). Skilled composers and performers can exploit both kinds of ambiguity, for example by stressing certain beats to increase their importance in our perception, and even to the extent of making music appear to flip back and forth between rival percepts. (Famous examples include the perceived ambiguous shift of beat position in Tchaikovsky's *Symphony Number 4* and electronic dance music tracks 'dropping' the beat at unexpected locations; [76] gives a drummer's guide to creating many such 'rhythmic illusions'.)

3.2.6 High-level structures

Beyond the level of bars, perception of music becomes much more subjective and there is less agreement (both between listeners and scholars) about how it 'should' be

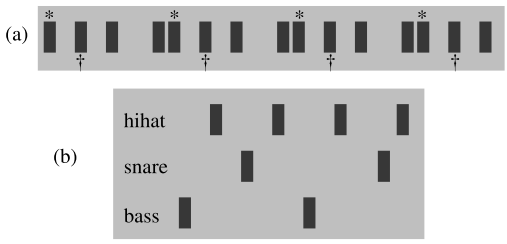

Figure 3.6: (a) Between-bar and (b) within-bar ambiguity.

perceived. One useful way to think of larger structures is as forming a grammatical hierarchy. For example, many songs share an identical top-level structure (or simple variants of it):

$$SONG \rightarrow \{INTRO, VERSE, CHORUS, VERSE, CHORUS,$$
$$MIDDLE8, CHORUS, OUTRO\}$$

whose components may be further decomposed, for example:

$$VERSE \rightarrow \{RIFF1, RIFF2, RIFF1, RIFF2\}$$

A riff might be broken down into parts for different instruments (played simultaneously, not sequentially; we notate this here using square brackets instead of braces):

$$RIFF \rightarrow [VOCAL\text{-}MELODY, BASS\text{-}RIFF, GUITAR\text{-}CHORDS]$$

The guitar chords structure might comprise a sequence of bars containing chords:

$$GUITAR\text{-}CHORDS \rightarrow \{c, c, f, g\}$$

Similarly, melodies could decompose into notes within a bar, and rhythms could be written as types of percussive hit within a bar (possibly played in conjunction with a chord in the case of tonal rhythmic instruments such as the rhythm guitar.) Chapter 6 will consider perception of such high-level structures in a probabilistic framework.

3.3 A menagerie of musical hash-classifiers

As discussed in section 2.5, the fullest Bayesian view of signal processing would be to consider the set of all possible generative models $\{M_i\}$ for the whole signal D, and compute posterior beliefs $P(D|M_i)P(M_i)$ in each of them in turn. For example, if we know a priori that the signal consists of notes from a piano with at most r notes played simultaneously, we could construct all possible combinations of notes at all possible

times as the model set, assign a prior to each based on our knowledge of the music, and compute their likelihoods. For the general musical scene perception problem this requires an intractable number of hypotheses. For offline musical transcription, this type of fully Bayesian inference has been approximated using sampling on powerful computers running for long periods of time (e.g. several days) [68]. However it is not appropriate for real-time applications. A simplification is to use hash-classifiers. We split the audio signal into short frames that can be analysed separately, then compute useful statistics (features) of the frames and assume some simple classifier-proper to map from statistics to model likelihoods as described in section 2.5. This is a common and useful approach to take, so we here review a few statistics and classifiers-proper (making little distinction between the two concepts) that will be used later in this chapter. Many others can be found used in computational music contest reports such as MIREX [47]. Each mapping is given an acronym for future reference.

3.3.1 Normalised power DFT (NPDFT)

$$NPDFT[t] = \frac{1}{Z_t}|DFT(Hann(x[t - M + 1 : t]))|^2$$

This vector-valued, temporal feature, where $|\cdot|$ and the squaring operator are performed point-wise, is useful in measuring pitch. It is invariant to amplitude as it is normalised by a normalising coefficient Z_t. It has some theoretical basis in that the square of the spectral values measures the physical energy carried in their frequency bands. The Hann (or other) window is used in practice to reduce wrap-around errors.

3.3.2 Radial basis functions (RBF)

Radial basis function [11] neural networks are simply Gaussian likelihood detectors. An RBF neuron takes a vector y as input, and output a Gaussian value $N(\mu - y, \Sigma)$ which may be interpreted as a likelihood that the input y was an instance of the multivariate Gaussian model with mean μ and covariance Σ. An RBF neuron can be thought of as giving the strength of pattern-matching between the input and a template model μ.

3.3.3 Normalised dot product (NDP)

This is a 'second-layer' statistic which is applied on top of an existing statistic f. It is a distance measure between a vector of input statistic values $f(y)$ and a vector of target statistics $f(s)$.

$$NDP = \frac{\langle f(y)|f(s)\rangle}{\sqrt{|f(y)||f(s)|}} \tag{3.3}$$

Musical examples of NDP include comparing current spectra to those of a set of candidate score locations.

3.3.4 Chroma vectors (CHV)

DFT and similar features are good for making explicit the individual harmonic components in a frame. However we saw that perceptual notes are made of harmonic series of components, and typical instruments produce series with roughly exponentially decaying amplitudes. Thus a chromatic scale of prototypical notes $\{n_i\}_i$ can be modelled as having DFT spectra:

$$n_i[\omega] = \frac{1}{Z}\sum_{k=1}^{10} \exp(-k) N(\omega; 2^{\frac{i}{12}} k\omega_0, \sigma^2)$$

as shown in fig. 3.7, where $N(\omega; \mu, \sigma^2)$ is the Gaussian PDF, ω_0 is the fundamental frequency of the lowest considered pitch, and σ is chosen by hand to give a reasonable spread but without interfering with neighbouring frequencies. (Ideally σ would be derived from acoustic theory or fit to data.) Heuristically, 10 harmonics are used.

Taking the NDP of an input audio frame with a pre-compiled bank of note models (e.g. one model for each note in a three-octave range) produces a statistic which can be assumed to approximate the likelihoods of the notes occurring in the frame. It is useful to sum over the note models from all octaves to produce an octave-independent 12-note *chroma vector*,

$$CHV[i] = \sum_k \langle n_{i+12k}|X[t]\rangle$$

3.3.5 Chordality vectors (CDV)

As we constructed the CHV from a sum of harmonic templates, so we may continue and construct templates for whole chords as sums of their constituent chroma templates. As with CHV, chordality templates may then be used with NDP on input audio to approximate the likelihoods $P(frame|chord)$.

Figure 3.7: Note template as an exponential harmonic series blurred by a Gaussian.

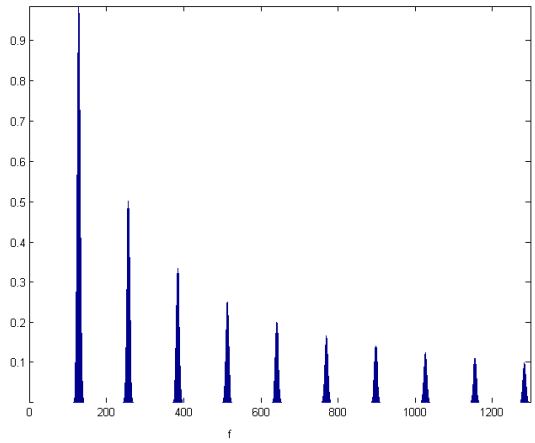

3.3.6 Energy feature (E1)

$$E1[t] = \sum_{m=0}^{M+1} x^2[t-m]$$

measures the total physical energy in M-sample frames, and is useful [131] for distinguishing between notes and rests. If suitably normalised it can be useful for distinguishing between loud and quiet notes or parts of notes – normalisation is typically needed because external factors such as the players distance from the microphone and mixer settings can alter the global level, even within a performance.

3.3.7 Novelty (NOV)

Novelty is a second-level feature, over an existing temporal feature f:

$$NOV(f)[t] = \frac{f[t] - \mu_{j=t-L:t}(f[j])}{\sigma_{j=t-L:t}(f[j])}$$

It measures how many standard deviations the present value is from a running windowed mean μ. It is useful for detecting musical onsets which produce sudden large (e.g. 10σ) jumps in energy features.

3.3.8 Raphael burstiness (RB)

$$RB[t] = \frac{1}{E1[t]} \left(\sum_{t=0}^{M/3} x^2[t] - 2 \sum_{t=M/3+1}^{2M/3} x^2[t] + \sum_{t=2M/3+1}^{M-1} x^2[t] \right)$$

This convolves the energy signal with a hard edge detector, looking for short bursts of energy. It is similar to many on-centre/off-surround neural receptive fields, and was found [131] to provide useful information about note onsets.

3.3.9 Raphael generative spectra (RGS)

Another pitch-based feature [131]. Let $n_i[\omega]$ be note DFT models as used in the CHV derivation. We then treat each note n_i as a candidate generative model for the FFT frequency bins $X[\omega]$ observed in the data – this assumption leads to

$$P(X|n_i) \propto RGS[i] = \prod_{\omega} n_i[\omega]^{X[\omega]} = \exp \sum_{\omega} X[\omega] \log n_i[\omega]$$

3.4 Overview of existing research areas

Throughout our discussions we will make two key distinctions about automated accompaniment tasks. First, *deterministic* music is that which is written in a score in advance and performed with little or no deviation from that score. In contrast, *improvised* music is composed during the performance and is not known in advance. *Semi-improvised* music will be described in detail later, but roughly is music which has predetermined elements that are combined in an improved way during the performance. Second, *monophonic* music has only one note present at each point in time; *polyphonic* music may have many.

Research into *score following* has been active for about 20 years. This is the task of following a deterministic musical score. The only commercial score-follower is Dannenberg's *SmartMusic* module in the *Finale* music software package, which follows a monophonic, deterministic score. Academic research has focused mostly on contemporary classical performance (being largely funded by IRCAM, the French contemporary music institute), and has also been mostly monophonic and deterministic. A typical application would be a live clarinetist playing a concerto from sheet music, with a computer following and providing the accompaniment. The leading academic system is Raphael's *Music++*, which performed this task live at the NIPS[6] 2001 conference [134]. Score following is reviewed in detail later. However, the scenarios discussed in section 3.1.1 require more advanced inference than these existing systems as they involve *semi-improvised* music.

The recognition of audio notes and chords is itself a difficult problem, and commercial music *transcription* software is notoriously unreliable. Auditory psychologists

[6] Advances in Neural Information Processing Systems

such as [43] have reached identical conclusions to their visual counterparts (e.g. [79]) – that we do not perceive low-level sense data directly, but instead perceive high-level models, such as tones and melodies in the auditory case. [43] shows many cases where music transcription software would fail because the tones we perceive do not even exist in the data, they exist only in our models and in the context that we hear them. This is where a Bayesian approach will be useful as we may represent uncertainties in the low-level description of the audio streams, and apply higher level models to finding their best interpretation. The transcription task may be seen as complementary to deterministic score following: In score following, perception is relatively easy as the music is deterministic, but real-time and action selection is important. Transcription focuses on hard non-deterministic perception, may run offline, and requires no action selection. Transcription will be reviewed in more detail in chapter 5 when we discuss high-level perception. The present chapter focuses on low-level methods, which naturally may provide input to the higher-level systems discussed later.

A sub-task of transcription which is especially relevant in real-time systems is *beat-tracking*. This research assumes that the problem of finding the beat positions can be tackled independently from the rest of transcription, for example using only energy statistics from the audio signal and ignoring pitch. Beat-tracking aims to provide the temporal grid for the rest of perception in which to to take place. The semi-improvised domain may be thought of as real-time transcription of small highly-constrained chunks, so beat-tracking can be used to find the locations of the chunks, whose contents can then be passed to higher levels for analysis.

3.5 Score following: review and preliminary tests

As the deterministic problem is the starting point for our semi-improvised task, we now review score following in detail. As it is difficult to obtain running code from score-following authors, aspects of leading systems were reimplemented during this review to gain a more detailed understanding of their strengths and weaknesses. The examples and illustrations are drawn from these reimplementations.

3.5.1 Dynamic time warping

Dannenberg [33], [34], [36], [72], [35] published the first paper on score following in 1984, using DTW to follow deterministic monophonic MIDI performances and accompany them with MIDI. The task was simply to align a known sequence of MIDI events with their observations. DTW allowed for occasional insertion and omission of notes, or notes played in the wrong order. Three possible DTW moves

were considered for each state in the path matrix: horizontally forwards; straight down; and diagonally forwards and down; rather than performing exact inference. In real-time, the best path is noted at each new input, and the search on the next row is constrained to nearby elements within an arbitrary window of this path. For DTWs that can be written as HMMs, this constraint is equivalent to using a single particle in particle filter inference. Dannenberg's later papers extended the DTW algorithm to run on audio data, using NDP on DFT features to follow polyphonic scores and ensembles of players. The following section replicates some of his early experiments to test the performance of DTW.

3.5.1.1 DTW experiments

DTW was coded as a Matlab function taking template and observation input vectors as inputs, along with a distance measure on these vectors, and outputting an optimal time warp map between them. Following Dannenberg, a parameterisable maximum jump size was used, and only forward transitions were allowed. Fig. 3.8 shows a simple example of the DTW component in action on a non-musical template (score) sequence $(1, 2, 3, 4, 5)$ and observation sequence (1,3,2,2,3,4,2,5,5,1). The simple distance measure $1 - \delta_{ij}$ is used (i.e. the distance is 0 between two identical numeric symbols; and 1 between two different symbols) and the maximum jump size was 4. In score-following, the numbers could represent musical pitches; the template would then be the score as a sequence of ordered pitches, and the observation would be an input stream of pitches. (DTW has no notion of note length under this interpretation.) The cumulative distance is shown by the gray-scale, and the optimal path is plotted. The optimal path assigns score states (1,1,2,2,3,4,5,5,5,5,5) to the observations.

A first DTW experiment used symbolic real-time MIDI data with no maximum jump size. Again, the delta distance measure was used on the symbols. Incoming MIDI events were streamed in real-time into Matlab and matched to a template score. As expected, this produced good real-time alignment for small scores, and was resilient to small errors of insertion, omission and incorrect notes (e.g. resilient to about 6 mistakes in a 20 note score). This emulates Dannenberg's early MIDI score followers of the 1980s. As expected, DTW could not deal with large jumps in the score, and could not deal with backwards jumps at all. The alignment algorithm only runs when a new note event occurs, and is thus incapable of providing accompaniment events at times between notes. It can provide such events *on* new notes, but even then there is some latency between the note occurring and the event being scheduled and played. We would prefer a more intelligent scheduler, capable of predicting when notes will occur and scheduling events in advance.

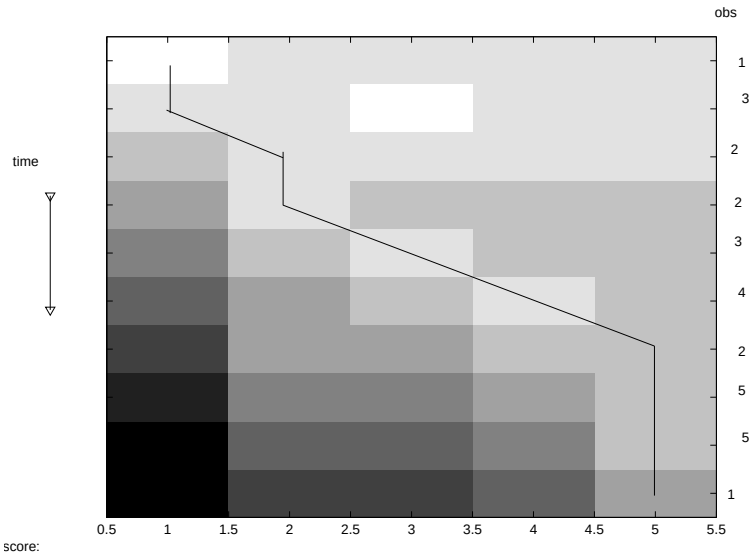

Figure 3.8: Simple example of DTW algorithm. The template states are on the horizontal; the observations over time are vertical. Darker shades are greater cumulative distances.

Figure 3.9: Score used in Bach performances. (Asterisks indicate accompaniment points.) From *Cello Suite 2, BWV 1008: Prelude.*

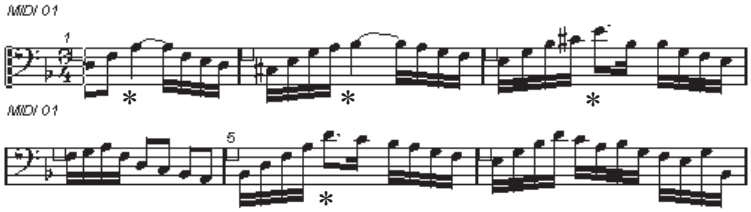

A second experiment tested audio DTW in an offline setting. Eleven recordings were made of an eight-bar Bach excerpt played on the trombone (fig. 3.9). Each recording was played in a different style, involving stretching tempos, emphasising different phrases, and expressing different musical feelings. Deliberate mis-pitched notes were included. The first recording was used as the template, and the others aligned to it. The NDP on NPDFT feature was used as the distance measure. Sampling was at 16kHz and 25% overlapping frames of 512 samples were used, resulting in about 450 frames per recording. Exact DTW (i.e. using no maximum jump size and considering all possible positions at each step) was slower than real-time. Examples of local and total distances using exact DTW are shown in figure 3.10 with the optimal warp path overlaid on the total distance image. The alignment was approximately correct (as judged by the performer) on 8 of the 10 exact DTW runs.

To regain real-time execution for the audio case, the maximum jump was set to 4 frames, and the single particle assumption was used. The real-time system was

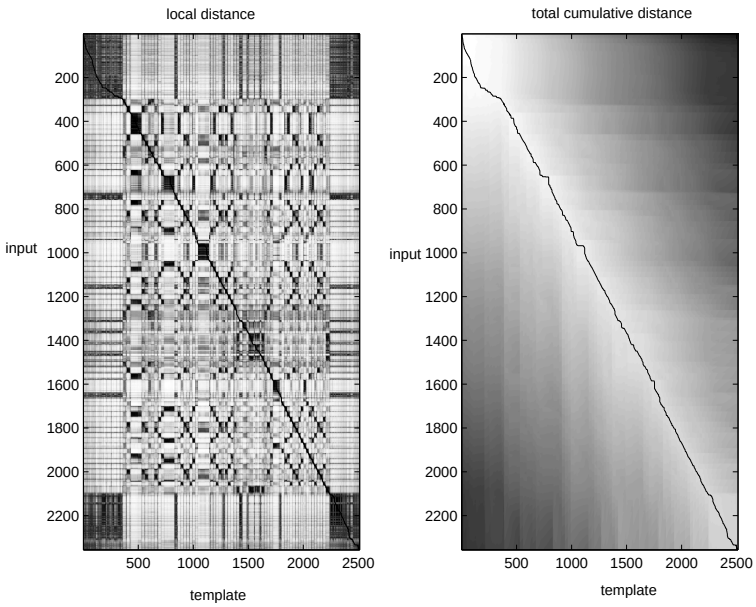

Figure 3.10: DTW on 2 Bach performances. The horizontal axis is the template recording; the vertical axis is the input. Left: local distances of FFT spectra. Right: best cumulative distances. The optimal DTW path is also shown.

tested by a live trombone player, with MIDI accompaniment notes being output at the asterisk points of fig. 3.9. It is difficult to quantify performance objectively, as it varies with the style and expression of the player, but it was possible to make the accompaniment correct about 90% of the time by deliberately playing with little variation or expression, and about 70% of the time when playing normally. The accompaniment notes occurred in roughly the correct locations but were often missing and were almost always out of time with the beat. There was a noticeable latency of accompaniment.

3.5.1.2 DTW limitations

The fundamental limitation of DTW is that is had no notion of tempo, only of discrete changes of score position. In the MIDI case this means the accompaniment events can only be played at performance event points, and they are always a little late because they happen just *after* the performed notes. The problem is reduced in the audio case as there are as many states as frames of audio, however DTW still fails during long held notes as it is unable to distinguish their substates. Dannenberg used heuristic methods to estimate the tempo from recent observed events, but a more accurate method is to assign priors on state transitions and maintain probabilistic beliefs over state. This is achieved by hidden Markov models, examined in the next

Figure 3.11: C major scale played in note classification test

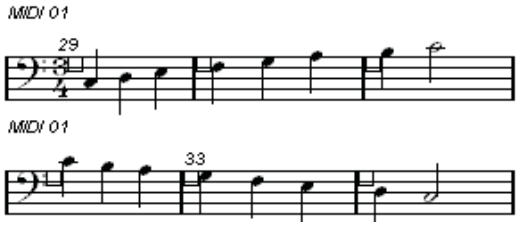

section. Importantly, another problem – to which practical HMMs are equally prone – is that when particle-based tracking becomes lost it is unlikely ever to return.

3.5.2 Hidden Markov models

In real-time, DTW algorithms typically consider only a fixed window (of perhaps 100 audio frames) about the previous best point. For DTWs which constrain the path so that each move is from row i to $i + 1$, this constraint can be thought of as a HMM finite plateau transition prior centred around the previous MAP point. Importantly, this heuristic specifies not only a prior belief but also a *computational* simplification: it tells us to *consider* only those hypotheses in the plateau rather than all possible generating score states. HMMs allow us to generalise from this plateau prior to an arbitrary state transition matrix, with the 'distance' measures now interpreted as likelihoods. Such models are used in state-of-the-art academic (but closed-source) score followers. Rather than use score audio frames as states (as in DTW), score-following HMM researchers have tended to use a reduced model of the score, with one or several states per note [131], [123], and CHV or RGS statistics used as likelihood functions. Transitions are typically allowed between consecutive score states, self-transitions, and jumps to the end of the note, and their parameters fitted to previous performances. These models may be thought of as hidden semi Markov models (HSMMs). As with DTW, the next section tests a simple version of this architecture.

3.5.2.1 HMM experiments

We first implemented and tested a CHV model. Fig. 3.11 shows a scale played on the trombone; fig. 3.12(a) shows its spectra. Sampling was at 8kHz and large 0.5s non-overlapping windows were used). CHV values are shown in 3.12(b) and fig. 3.12(c) shows the maximum likelihood (ML) chroma. The ML solution is all correct except for the penultimate played note, which has been split into two parts (at around 25s on the horizontal time axis), the first part of which is incorrect. There is a stray ML note

Figure 3.12: (a) FFT spectra of trombone C major scale (clipped to useful frequencies). x=time, y=pitch, dark=high power. (b) Likelihood outputs from the harmonic filterbank. x=time, y=pitch, white=most likely (c) Maximum likelihood estimates of pitch state, from filterbank. x=time, y=pitch, white=most likely.

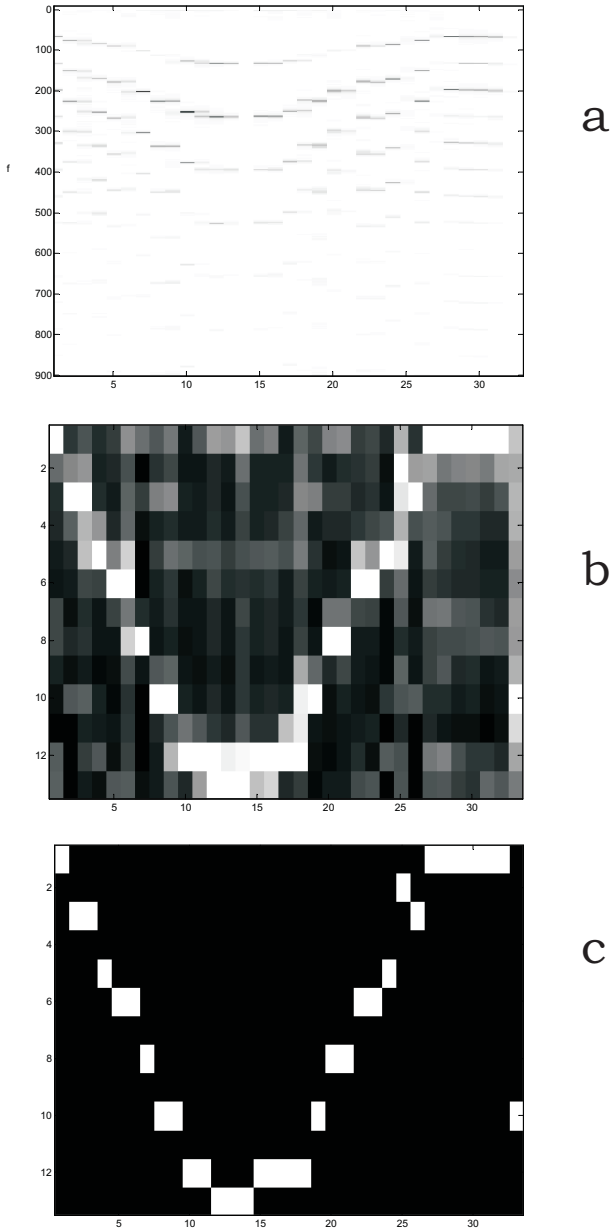

Figure 3.13: Left: Score position transition matrix. Note there are two types of row: for one-beat events and two-beat events. Right: PDF model for 'tied' pitch observations conditioned on score state.

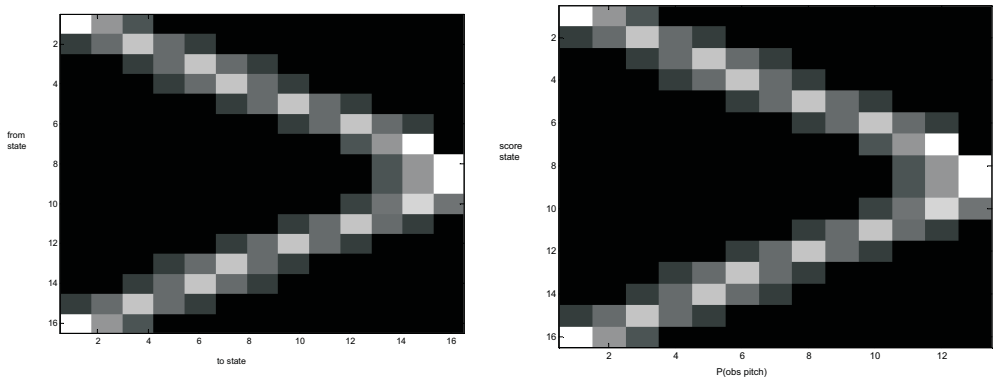

at the end of the performance, corresponding to silence in the audio. As likelihoods are normalised and there is no explicit 'silence' model, an essentially random note is produced in the ML interpretation. We noted the limitations of the FFT in the audio review section – specifically for bass instruments like the trombone we get poor resolution of low notes. Here a large window of 0.5s was used to compensate; though such a large time uncertainty would not not good enough for a real time system.

In a second experiment, an offline HMM score follower was constructed using the CHVs. The ascending and descending scale of fig. 3.11 was recorded, and a corresponding HMM constructed with one score state per note. Its transition matrix, shown in fig. 3.13(left) was tuned by hand to perform as well as possible. Following Raphael, 'tied' states were used, meaning that CHVs were conditioned only on the pitch of each score state rather than the score state itself. For example, the note D occurs twice in the score but these two states have identical CHV profiles. This was implemented by adding an extra layer of Bayesian network nodes between the hidden score states and the CHV observations (HMMs are a special case of BNs, and our HMM was implemented using a generic BN tool written for these experiments), as shown in fig. 3.14. These 'pitch' nodes have just 12 chroma states, rather than states for each score note, and have the transitions of fig. 3.13right. Using the large 0.5s frames as before, the HMM was able to infer correct score positions for the simple scale score as seen in fig. 3.14, using forward messages only.

A third experiment tested the CDV feature. A guitar was used to generate a performance of the chord sequence *ccggccffccgfccgfcc* for testing. To test robustness, the guitar was deliberately slightly out of tune and played quite badly, with around

Figure 3.14: Screenshot from the HMM software implementation, using similar graphical display to fig. 2.1 in the previous chapter. The Bayesian *nodes* have three sections, showing prior, likelihood and posterior distributions, from top to bottom. The two-sectioned *LINKS* show the prior (top) and likelihood (bottom) messages between nodes. For example, the top left node, *initScore* shows the prior score position at the start the performance: its prior and posterior are delta functions indicating certainty that the score state is the first note. (Its likelihood component however also suggests that the *last* note is also likely, being of the same pitch.) Moving to the right – through time – from the *initScore* node, we see the priors suggesting movement along the score, giving a high prior on the score position immediately after the highest posterior position of the previous node. The marginal maximum likelihood score positions for the seven time windows shown here are (1,2,2,3,3,3,4) corresponding to the first four notes of the score, (C,D,E,F).

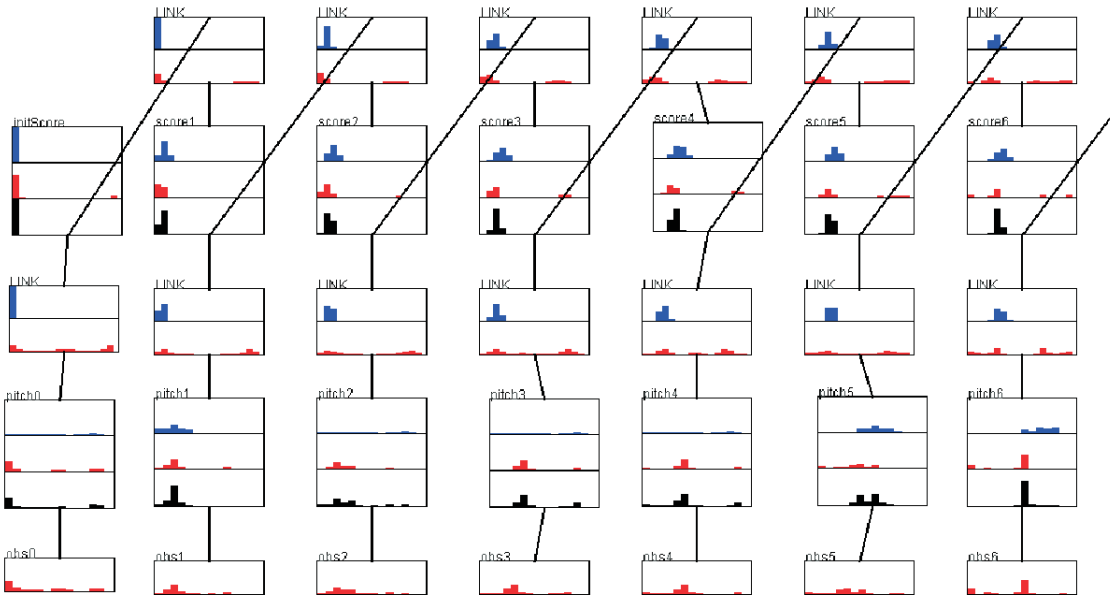

one in five chords played having one or more incorrect notes. There were also some brief open-string chords in the changeovers. The final c was held for about 2 seconds to fade out. Fig. 3.15(a) shows the 0.5s FFTs of the signal. The lowest string, E, on the guitar has fundamental 82Hz, and the low C of the first c chord has 128Hz. Corresponding CHV and CDV values are shown in figs. 3.15(c) and 3.15(d). The maximum likelihood CDVs are shown in fig. 3.15(e). The 'ground truth' chords actually played are shown in fig. 3.15(f) for comparison. CDVs ran in real-time with about 0.5s latency (the size of the FFT frames), allowing displays such as fig. 3.15(b) to show the currently-played CDV and ML chord estimate. The results show that the ML estimate is accurate about 85% of frames, and suggests that the errors could be corrected with temporal smoothing as in HMMs.

A fourth experiment, noting the reasonable accuracy of chordality recognition from a single guitar, tried applying it to a complete audio mix. This could allow transcription of chords symbols from MP3 recordings for example. A recording of The Beatles' three chord trick, *I Saw Her Standing There* was used as input to the previous ML-CDV system and its results are shown in fig 3.16. The detection is poor – many chords are completely incorrect and there is much random jumping around between likelihoods. In contrast, humans have no trouble perceiving the song as a simple series of three chords, showing that our perception of chords is not just based on instantaneous filterbanks and frequencies: we can still perceive a chord as e even if there are very few of e's notes in it, and the sound is cluttered with improvisations, non-chordal notes, and rhythm sounds. In particular, humans seem to perceive 'chordality' as a field covering whole bars, combining notes from all time-slices within them, rather than within single frames.

A fifth experiment tried to use the previous HMM implementation to follow the chord sequence in real time. In the previous scale-following test, the individual notes were used quite successfully as hidden states of the HMM. This worked for the simple test case because the audio frames were large (0.5s) and approximately the same duration as the notes themselves. The symbols from the chord sequence were similarly modelled by single hidden states. But in this case, the model failed due to an effect which we call *sandboxing*. This problem arises when performed symbol durations are much longer than frame lengths – in this case each chord symbol was played for a bar lasting about 2s. This means that each hidden score state must typically make four self-transitions before moving to the next score state. This is an inherently non-Markovian prior. It was possible to set the expected *mean* number of frames per hidden state by reducing its transition probability to the next state, p, but this does not capture the correct semantics. Instead, it gives a Poisson distribution over

Figure 3.15: (a) FFT spectrograms of chord signal. x=time, y=frequency. Dark=high power. (c) Octave-neutral pitches present. x=time, y=pitch, white=most likely. (d) Chord likelihoods. x=time, y=chord, white=most likely. (e) Maximum likelihood chord recovery. x=time, y=chord, white=most likely. (f) Ideal chord recovery. (b) (top right) Real-time chord detection: The caption reads 'I think you are playing D# major'. This is a screenshot from an animated Matlab screen, updated every 0.5s.

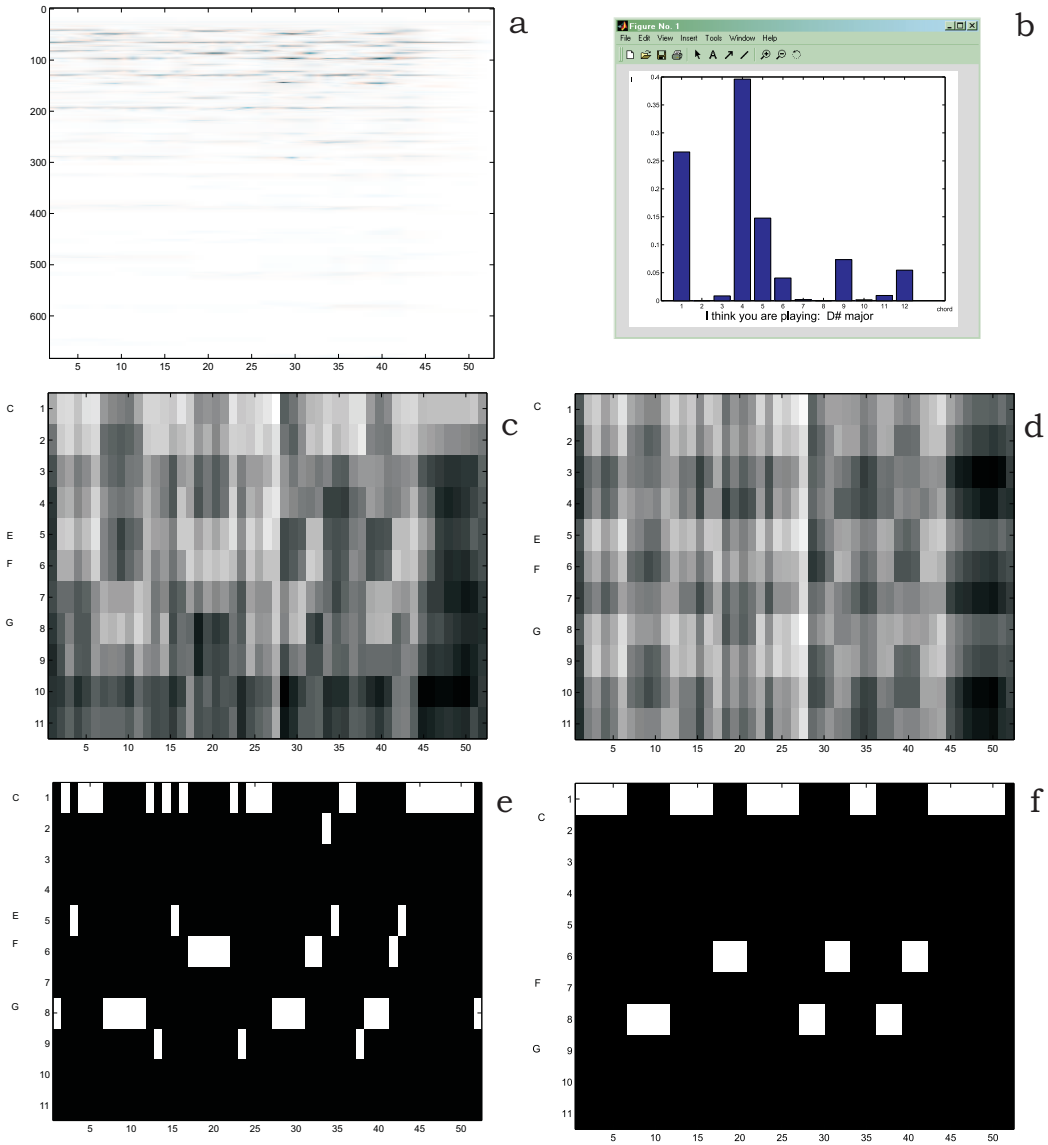

Figure 3.16: Left: Maximum likelihood chords for *I Saw Her Standing There*. Right: Corresponding notated ('ground truth') chords.

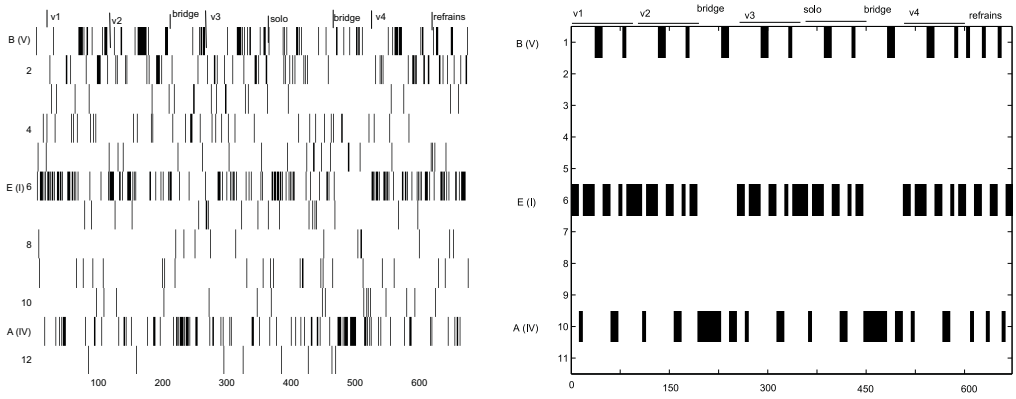

time spent in each state, which tends to make the score state priors dilute rapidly over time, as can be seen in fig. 3.17. (We named the effect 'sandboxing' because the priors resemble a stack of sand in the initial case, which is gradually tipped over time, spreading out into a wide pile.)

3.5.2.2 HMM limitations

The sandboxing problem can be fixed approximately by introducing multiple substates within each score symbol, as in Raphael's system, which uses about 10-20 substates per note[7] to obtain high accuracy with small frame lengths. Such an approach is similar to that used in DTW, where each note in the template has many audio frames. The only difference is that in DTW each template frame has its own statistic vector, but in note-based HMMs the statistics are generated from idealised note models rather than a prerecorded score. As with DTW, exact inference in such many-state HMMs then becomes impossible, so the set of hypotheses under consideration must be limited heuristically. Again, such limitations reduce the ability to recover from large jumps in the performance.

Accompaniment applications require very high accuracy predictions about near-future accompaniment time to allow advance scheduling and avoid latency. Unlike DTW, HMMs can be used to make such predictions ahead of time, by propagating forward messages *beyond* the current time to infer probable score states of near-future frames. However the accuracy is still limited to the resolution of individual frames, which may not provide the millisecond accuracy required by professional performers.

[7]Raphael, personal communication.

Figure 3.17: HMM for chord sequences, showing belief sandboxing on the score node priors. (These are the top distribution in the score nodes; observe that the priors spread out to the right, like a pile of sand being tipped over in a box)

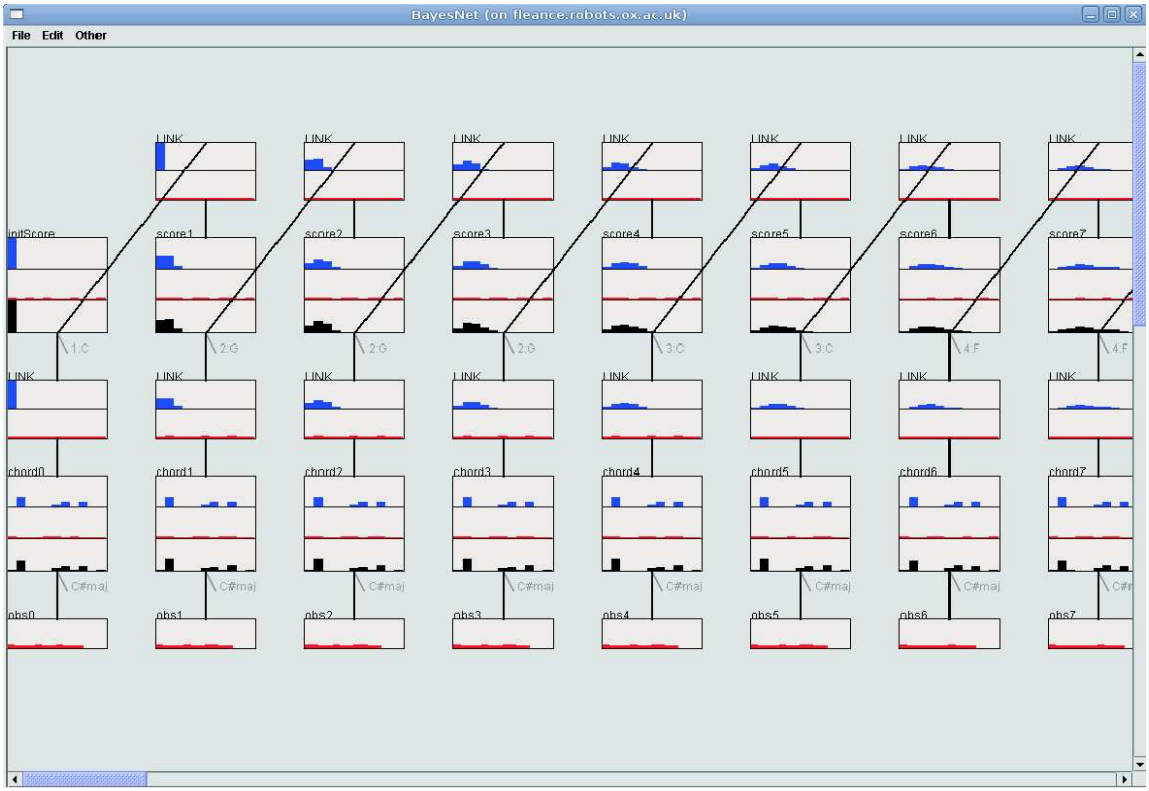

3.6 A novel priming particle filter score-follower

The software implementation and feature selection of this section were constructed in collaboration with John Quinn of Edinburgh University. The music application and priming ideas are the author's own. This text of this section is based on the peer-reviewed publication [60]:

- *C. Fox and J. Quinn.* How to be lost: principled priming and pruning with particles in score following. In *Proceedings of the International Computer Music Conference, 2007.*

While HMMs augment DTW with prior beliefs about transitions, they do not address the computational problem of which beliefs to *consider* in computations. As in DTW, practical HMMs generally apply some kind of cutoff threshold to limit the space of score states under consideration. For example, Raphael [131] used a heuristic which prunes all but a fixed number of most probable posterior hypotheses at each time step. These states tend to be closely clustered. This works well for Raphael's intended users: professional performers who are unlikely to make large errors, and whose small-scale tempo deviations from previous performances can be tracked with high accuracy. But for amateurs who may make very large leaps around the piece it runs the risk of becoming irrecoverably lost.

Particle filtering (section 2.2.2.4) is a general-purpose approximate inference method for probabilistic dynamic state space models. Rather than keeping the most probable hypotheses as in [131], it samples from an approximate posterior at each time step. This can allow for less probable paths to be explored in the hope that they may eventually provide a better global path than locally probable ones. Particle filtering has been applied to model-based score-following HMMs by [27]. This allows for larger leaps in the score than a 'take only the best' approach, but it is still possible for particle filters to become lost and they are then unlikely to recover.

Human musicians do not just rely on a prior information to select location hypotheses to consider: hypotheses can also be *primed* bottom-up from observed features. For example a song may have a distinctive chord change at the start of its chorus: when this change is heard, it primes us to consider that we might be at that location – even if our prior beliefs were focused elsewhere. The notion of priming will be key in much of this thesis, and we here introduce a simple computational model of its use.

Within the framework of particle filtering, we define priming as a heuristic injection of new samples into the system driven only by bottom-up features, regardless

of their priors.[8] We present a novel *priming particle filter* (PPF) which uses this technique to recover from being lost by recognising and allowing a probability for its own error, then creating new hypotheses based on bottom-up note changes. Unlike existing HMM score-followers, we have returned to the DTW-style audio-based score, and avoid the need for explicit note-based score models. To demonstrate the priming particle filter, we have used relatively simple features for likelihood computations, but we suggest that the PPF could be a useful addition to all state-of-the-art score followers with more advanced features.

3.6.1 Tempo model

At each time step of live performance time $t^{(l)}$, the hidden state is the position in score time, $t^{(s)}$ and the current tempo . We write the score time as a function of the live time, $t^{(s)}[t^{(l)}]$, and write the current tempo as $\dot{t}^{(s)}[t^{(l)}]$. The hidden state evolves as the damped switching stochastic process:

$$t^{(s)}[t^{(l)}] = t^{(s)}[t^{(l)} - 1] + \dot{t}^{(s)}[t^{(l)} - 1] + \epsilon_{t^{(l)}}$$
$$\dot{t}^{(s)}[t^{(l)}] = \rho(\dot{t}^{(s)}[t^{(l)} - 1] + \epsilon_{\dot{t}^{(l)}} - 1) + 1$$

where ρ is a damping coefficient and $\epsilon_{t^{(s)}}$ are from the Gaussian $N(0, \sigma_0^2)$ and $\epsilon_{\dot{t}^{(s)}}$ are from the switching mixture of Gaussians $\alpha_1 N(0, \sigma_1^2) + \alpha_2 N(0, \sigma_2^2)$ with $\alpha_1 + \alpha_2 = 1$ and $\forall i.\alpha_i \geq 0$. The two mixture components model a small tempo drift due to player or tracking errors and a separate large tempo change due to performer style changes. A mixture is used to encourage occasional large changes (e.g. at new phrases) whilst discouraging gradual large tempo changes (e.g. during notes). We do not perform any learning of parameters – they are simply set by hand ($\rho = 0.999, \alpha_1 = 0.99, \sigma_0 = 0.7, \sigma_1 = 0.1, \sigma_2 = 1.5$, with time measured in frames). Particles contain the 2-element state $(t^{(s)}[t^{(l)}], \dot{t}^{(s)}[t^{(l)}])$, i.e. a position and speed in the score.

3.6.2 Likelihoods

Offline score $x^{(s)}$ and online live $x^{(l)}$ audio is sampled at 2756.3Hz (=44.1kHz÷16) and cut into 512-point frames $y[t]$ with 448 point overlaps. We use the NDP feature on chroma vectors (CHV) as an approximate spectral likelihood $\lambda_s(X^{(s)}[t^{(s)}], X^{(l)}[t^{(l)}])$. E1 energy features $e[t]$ are computed and used to compute a further NOV feature v.

We use a Gaussian approximation of energy likelihoods:

$$\lambda_v(v^{(s)}, v^{(l)}) = \frac{1}{Z} \exp \frac{-(v^{(s)} - v^{(l)})^2}{2\sigma_v^2}$$

[8] This may destroy theoretical convergence properties in the infinite sample limit.

And assume that the total likelihood is the product of these spectral and energy likelihoods:

$$P(t^{(l)}|t^{(s)}) \approx \lambda_s(X^{(s)}[t^{(s)}], X^{(l)}[t^{(l)}])\lambda_v(v^{(s)}[t^{(s)}], v^{(l)}[t^{(l)}]).$$

3.6.3 Injecting primed particles

A fundamental assumption in Bayesian inference is that we possess the exhaustive set of hypotheses $\{H_i\}$ to explain some data D. It is this exhaustiveness that allows us to convert likelihoods into posterior probabilities. However in realtime score following we do not have computational resources to consider all possible score position hypotheses, we must consider only a subset of them. Previous models have used heuristics to choose this subset: we (with [27]) use sequential importance samples (particles) to make this choice in a principled way. The standard particle filter assumes that the particles form the exhaustive hypothesis set at each step. But this does not allow the model to represent the possibility of its own failure: in practice it is possible for a particle filter to get lost, and for the best hypothesis (and even the whole area around it) to be excluded from consideration. But the particle filter is blind to this – it assumes that the particles are an exhaustive set of explanations.

A precise definition of what it is to be lost is difficult when the state space is continuous. For discrete states, lostness at time t is easily defined: it occurs exactly when the ground truth state at t is s and there is no particle representing s at t. For a continuous space, no particle can ever represent the exact ground truth state, so some notion of an acceptable region must be used such that lostness can be defined as the condition of having no particle in the acceptable region around the ground truth state. For score following, one way to define this region is simply to ask users of the system what region would be acceptable to them, in the sense of having an accompaniment part played at the position and speed from that region. As we later approximate the probability of being lost heuristically, rather than compute it, there is no need to obtain the acceptability criterion explicitly. Instead, we may choose the heuristic approximation to maximise user utility directly. We assume that user's prefer a close match in positions between inferred states and ground truth throughout the whole score and choose a heuristic to approximately maximise this.

Ideally, we would like to compute the probability that all particles have irrecoverably failed (according to the acceptability criterion), $P(lost)$, and treat 'being lost' as an alternative explanation. When we know we are lost we will then consider a number of newly injected particles $\{H_j^*\}$ based on bottom-up priming, with

$$P(H_j^*|D, C) = P(lost|D, C)P(H_j^*|lost, D, C)$$

Figure 3.18: Chroma and change points of score performance

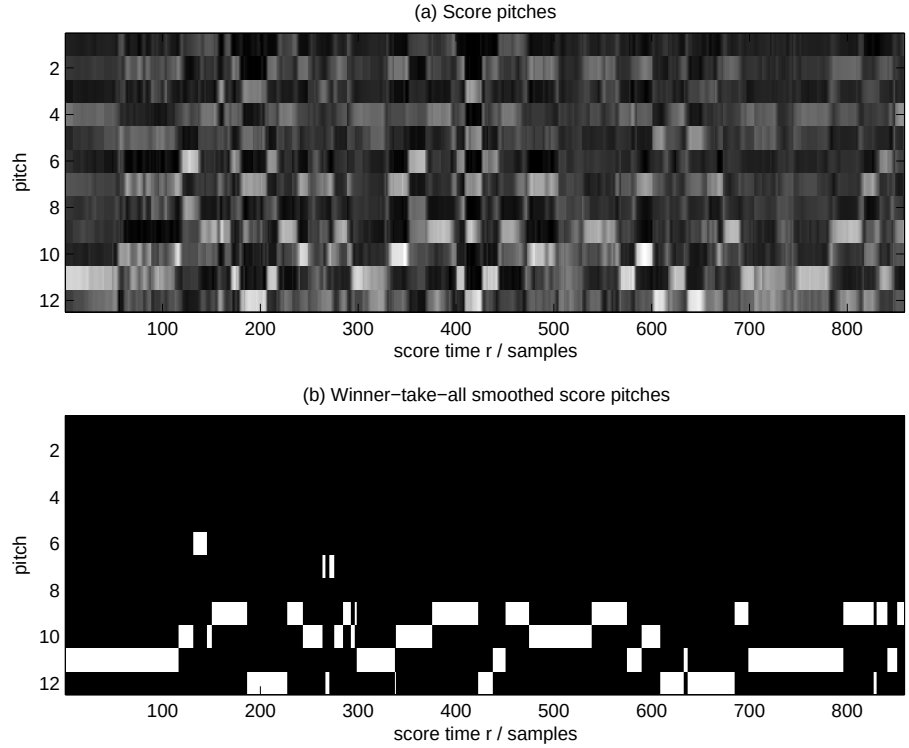

$$P(H_j^*|lost, D, C) \ = \frac{1}{Z} P'(H_j^*|feature(D)) P'(H^*|C)$$

where C is the context (i.e. the previous state for dynamic networks like HMMs), $feature(D)$ is some bottom-up priming feature computed from the data, and P' are probability *factors* (i.e. they are not necessarily normalised). In practice, all of the above terms are intractable (in the sense that computing them would require an exact solution of the very inference problem that the particle filter is approximating) but can be approximated from domain knowledge or historical statistics.

We approximate $P(lost|D, C)$ by looking at a windowed running average data likelihood. We use an exponentially weighted moving average of $P(D[t]|\hat{H}[t])$, the evidence of the MAP hypothesis at each step. When this average falls below a threshold we consider that we might be lost with a fixed probability. In practice we approximate this be removing the worst m particles from the set and replacing them with newly primed particles, where m is the number of these primes. (More detailed methods could model how probable being lost is given how far below threshold we are, and learn this model from historical data.)

$P'(H_j^*|feature[D])$ is approximated by a simple bottom-up priming scheme. We use sparse Boolean features and assume that all score states having the feature are equally likely given the presence of the feature when lost. For our score-following task,

Figure 3.19: Chroma and change points of live performance

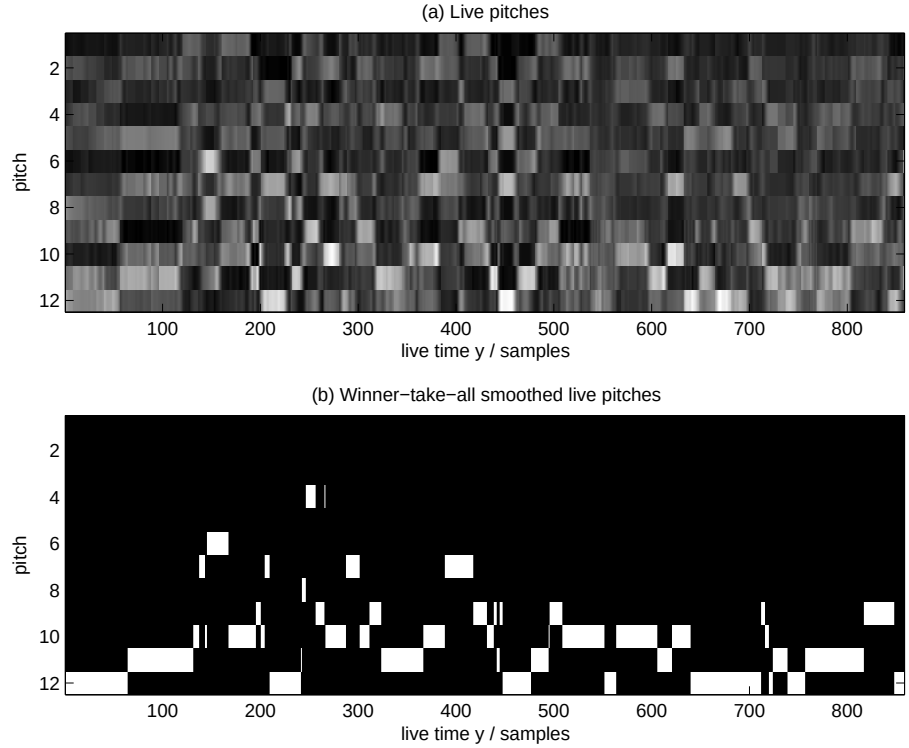

we use changes in the maximum windowed running average pitch as features. These *roughly* correspond to onsets of new notes. We maintain a cache of known positions of these features in the score, and consider these positions as hypotheses when the same features are found in a lost live performance. Speeds are created for these particles assuming that the tempo has been constant since the point of becoming lost.

$P'(H^*|C)$ can be approximated in score-following by considering how far removed the primed hypothesis H* is from where the particle filter's previous MAP estimate was, and penalising very large jumps. Our system uses a simple plateau function to allow only primes within a fixed distance of the previous MAP location. (In the results given below, the plateau allowed primes up to 200 frames either side of the MAP location).

3.6.4 Results

We demonstrate the priming particle filter on the first seven bars of the *Andante Cantable* from the Rimsky Korsakov *Trombone Concerto*. Recall that no symbolic score is required: an audio recording is used as the score. Fig. 3.18 shows the chroma vectors and priming features from the audio score; fig. 3.19 shows the same for the live recording.

Figure 3.20: Alignment without priming

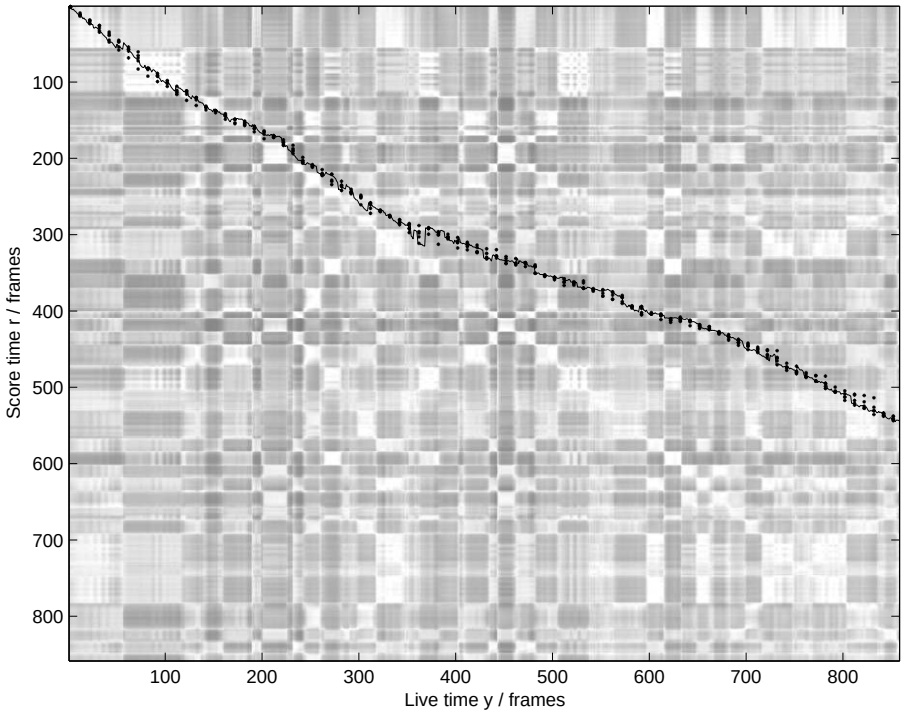

The live recording contains a short error around frame 200. Running the standard particle filter with 5 particles results in getting lost at this point as shown in fig. 3.20. The figure shows the complete spectral similarity matrix in the background, in which the central white diagonal stripe is the true path. The particles are plotted as dots and the MAP particle path is drawn as a line. Fig. 3.21 shows the same example running under the priming particle filter. The large jumps are where lostness recognition and priming has occurred. It can be seen that the filter gets lost several times but is able to recover every time.

3.6.5 Discussion

We have demonstrated the priming particle filter on a simple example for illustration purposes only, and running with more than 5 particles on this example generally avoids getting lost in the first place. Our demonstration PPF is a relatively simple score follower using very basic likelihood features and a Markov hidden state in contrast to state-of-the-art score followers such as [134], [28] which have more advanced features and higher-level state models. However we suggest that all state-of-the-art models could benefit from the simple addition of a PPF to allow them to recover from being lost when used by non-professional performers. Our HMM also illustrates how DTW-like audio templates can be used as HMM states, in contrast to existing

Figure 3.21: Alignment with priming

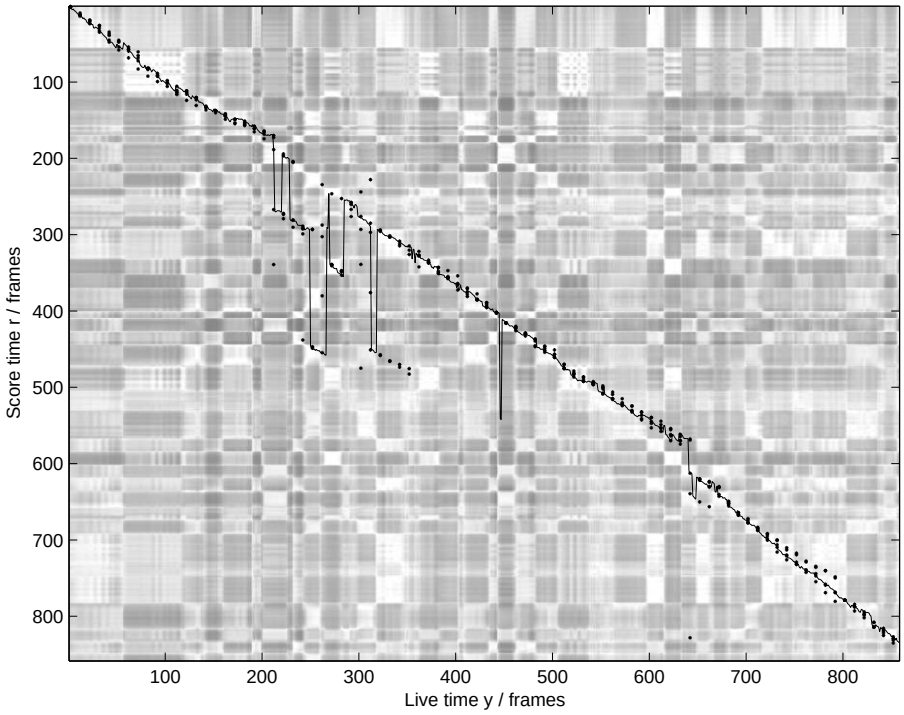

HMM systems which use symbolic scores with note templates. The notions of priming hypotheses and pruning improbable ones will recur throughout the rest of this thesis (though outside the context of particle filters).

3.7 Higher-level models in *Music++*

Having reviewed and evaluated simple DTW and HMM methods, it is useful to review a complete state-of-the-art score-following system in detail. It is useful to see what algorithms and heuristics are currently state-of-the-art, and in particular to see what kinds of special cases must be bolted on to standard algorithms to make them function in the real world. As the focus of this thesis is on hierarchical models of perception, it is also useful to see what higher-level models are deployed in a state-of-the-art system.

Raphael's *Music++* is perhaps the most prominent academic score-following system, taking the form of a closed-source, 65,000-line C program which performs monophonic deterministic following well enough to perform live accompaniment for Schumann's *1st Romance* at the NIPS 2001 conference [134]. The perception part of the program consists of an HMM and a higher-level Gaussian Bayesian network, driven by spectral and energy features from FFTs.

Music++ is aimed at professional and semi-professional classical musicians who make relatively few errors, and are musically competent to take control of a concerto's

tempo and expressivity, expecting the accompaniment to follow them. As input it takes a MIDI score and a prerecording of the accompaniment (for example, a full orchestral backing track). Its aim is to output the same sounds as a conducted orchestra would do when accompanying a professional concerto soloist, in real time.

Raphael has been developing the program since 1999 and whilst the source code was undocumented and not publicly available, parts of it are documented at the algorithmic level in a series of conference and journal articles [141, 138, 135, 140, 139, 136, 132, 137, 133]. I was able to obtain access to Raphael's source code and to interview Raphael[9] while employed by him at Indiana University to write the first source-level documentation of *Music++* [61]. Raphael's system has evolved over time so his papers may contain apparent contradictions – the following gives an original and coherent overview of the perceptual parts of the system as of late 2005.

A large part of the code base is a 'mini operating system' providing C functions for custom memory allocation and for scheduling the HMM and BN as well as controlling the audio accompaniment output. With our focus on scene perception we will not discuss these functions other than to take a warning that implementing real-time systems to industrial standards requires substantial time-consuming software engineering effort, and should be avoided in a thesis of the present scope to give preference to theory and concepts. Similarly we will not discuss training of model parameters or audio output generation here.

3.7.1 Architecture

Music++'s HMM takes the soloist's sound signal as input, and outputs a list of MAP estimated score note onset times, with variable latency. Latency varies because an onset is only reported once confidence in its position reaches some threshold. This generally requires waiting for some time after the onset has completed, and backwards messages are passed through the HMM to provide the extra information about recent onsets. Each onset is reported only once, when its threshold is reached.

The Bayesian network consists of Gaussian nodes which maintain marginal beliefs about the positions of performance and accompaniment notes. It takes the onset estimates from the HMM as observations and outputs an estimate of the predicted time of the next accompaniment note. Why is this network needed, when other systems (such as those used by IRCAM) claim to perform score-following using only an HMM? Raphael's experiments[10] suggest that whilst HMMs work well for localising

[9] under a non-disclosure agreement – the content of this section has been reviewed and approved for disclosure by Raphael.

[10] Raphael, personal communication.

the score state to the note or sub-note level, they do not give the millisecond precision demanded by professional classical musicians, typically because they must discretise the score states to a lesser accuracy. (Our priming particle filter has shown that continuous state space is possible in HMMs – however we certainly do not claim to have achieved professional quality accuracy with a real-time number of particles. We also note that IRCAM's score followers are generally used for contemporary electronic music which has less clearly defined beat and note positions than classical Western music.) By switching from a dynamic-state to a position-in-time model (section 1.3), the accuracy can be perfected, as the Bayesian network infers the expected times of each note rather than the expected (discretised) score state at each time.

The spilt between hard HMM onset reports and the Bayesian network is also useful with regard to action selection. Dynamic-state models – such as the HMM and the priming particle filter – can be used to report the most probable future states of the world, by making inferences over nodes representing the future. However these predictions may fluctuate rapidly. When action selection – rather than just prediction – is required, this becomes problematic because newly scheduled actions may be incompatible with previously scheduled actions, based on different fluctuating percepts. It is better to choose one interpretation and make a whole sequence of actions based on it. Ideally, such actions should be selected using the full posterior over future states, together with the set of already-scheduled actions and a utility function which penalises frequent switching between actions matching different percepts. The hard onset-reporting step may be viewed as a heuristic approximation to this scheme, reducing the amount of action switching because the data provided to the Bayesian network is updated only occasionally, when hard onsets are reported. (Section 6.3.1 will consider an explicit formulation of this type of task, modelling action coherence utilities as additional factors in a graphical model.)

3.7.2 Hidden Markov model

The sandboxing problem is reduced by modelling each score note as around 10-20 sequential substates. Most substates have a self transition probability p and a 'next substate' transition probability $(1-p)$, where p is a parameter shared by all substates of the note. Hence notes are parametrised by the tuple (n, p) where n is the number of substates used. Each substate thus has a discrete exponential distribution on its duration, and the distribution of the whole note length (i.e. the sum of substate lengths) is negative binomial,

$$P(T = t) = \left(\begin{array}{c} t-1 \\ n-1 \end{array} \right) p^{t-n}(1-p)^n.$$

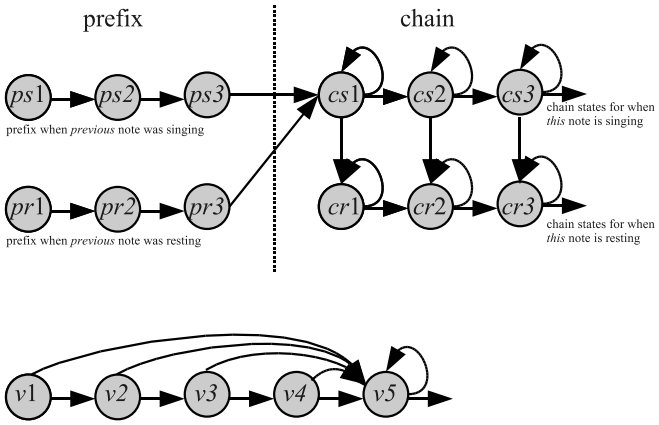

Figure 3.22: States for regular (top) and short (bottom) note models.

While it is unlikely that real performed musical notes happen to follow this conveniently parametrised distribution, its two parameters can be easily moment-matched to the mean and variance of empirical data to give a useful approximation.

The full note model, shown in fig. 3.22(top), is slightly more complex than a single chain of substates. It distinguishes between the attack and sustain parts of the note (left and right in the figure) which have different data-generating properties. It also distinguishes between notes whose attack follows immediately from a previous note (a rearticulation) and whose attack follows a rest – shown by the upper and lower left chains in the figure. Finally, the two right chains of the figure show two different paths for the sustained part of the note: the lower chain is of silent states, which occur if the player terminates the note early (e.g. to take a breath, or for a staccato effect.) The path may switch from the played sustain to the rests at any point during the sustain, but may not move back again. Very short notes (of around 15 frames long) are modelled differently as shown in fig. 3.22(bottom): these transitions allow performance to jump to the end of the note from any state, allowing for the whole note could be played as short as a single frame of audio. (The negative binomial model, even in the fastest case, is required to proceed through all states in sequence, giving an upper limit of n frames for its performance length.) These are examples of the fine details required by industrial-strength score-followers.

Input audio is sampled at 8kHz, and cut into 50% overlapping 512-point frames (32 frames/sec) and used to compute the three FFT-based features E1, RB and RGS.

E1 and RB are initially continuous valued, but are discretised. The combined vector of all the features is used as a single feature, and likelihoods $P(E1, RB, RGS|s)$ are used where s ranges over the quadrants of the note model in fig. 3.22 at possible pitch. Another real-life detail is optional additional conditioning on the most recent audio output of the accompaniment, a_i, which during non-headphone performance is likely to feed back into the input and must be accounted for.

Public descriptions of *Music++* do not explain how hidden state beliefs and the transition matrix are implemented in code. As discussed earlier, naïve implementation of the transitions as a matrix would become very slow due to the large number of states in the model. For example, a piece with 500 notes might have 20 nodes per note, giving a 10,000×10,000 transition matrix, and hidden 10,000 states per node, needing to be updated 32 times per second, which is infeasible on current computers. Detailed examination of the source code found a crucial heuristic contained in this small function (reprinted with permission):

```
static void graph_prune_list(list) {
  /*both dp cutoffs and low probability cutoffs */
  ACTLIST *list;
  int i,l;
  qsort(list->el,list->length,sizeof(NODEPTR),probcomp);
  for (i=list->length-1; i >= maxnodes; i--) del_list(list,i);
    if (list->length > 1)
      while(list->el[list->length-1]->prob<TEENY&&list->length>MIN_NODES)
        del_list(list,list->length-1); }
```

Here `list` is a list of 'active hypotheses' (i.e. those under computational consideration) having posterior probabilities `probcomp`; `qsort` is a quick-sort function; `del_list` removes elements from lists, and `maxnodes` is a threshold parameter. This function *prunes* all but some `maxnodes` most probable hypotheses, and shows that $P(s)$ is represented as a `list` of hypotheses rather than a naïve vector containing all possible states. We can view this is a crude form of particle filter, which always samples the `max_nodes` most probable hypotheses.

The most probable hypotheses tend to be closely clustered, and taking the most probable ones removes the ability to recover from large jumps in the score. For *Music++*'s target audience of professional performances of deterministic scores, this is rarely causes problems as professional players are unlikely to cause such errors in the first place. However for amateurs this is a problem and the system can become irrecoverably lost following some small errors. We suggest the use of the priming particle filter presented earlier as a possible cure for this problem with amateur musicians.

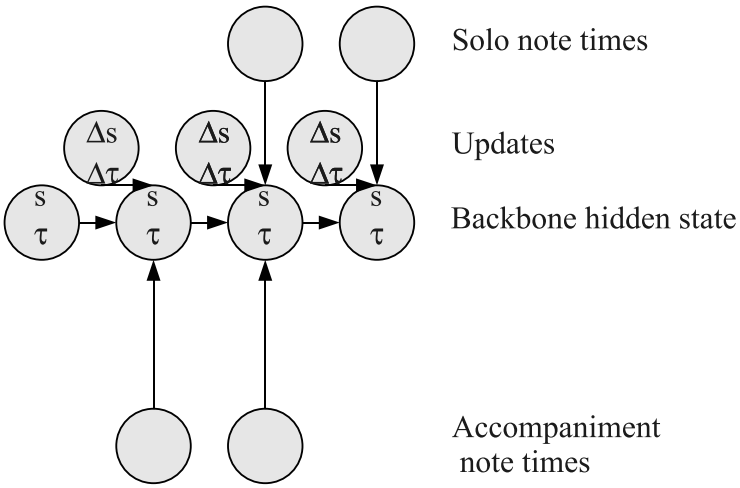

Figure 3.23: The Gaussian Bayesian network structure used in *Music++*.

Raphael's HMM shows up how low-level audio classification can be considered as a separate task from higher-level inference: there is no feedback information sent to the HMM from higher systems. The HMM functions in isolation as a smoothed onset detector, whose onset reports may be treated as symbols at the higher levels.

3.7.3 Gaussian Bayesian network

The Gaussian Bayesian network uses the stream of onset estimates from the HMM to predict and output the time and tempo of near-future accompaniment events. A typical fragment of the network is shown in fig. 3.23. Each *note* of the solo score is represented by a node, containing a PDF over its onset time and local tempo. Onset estimates are treated as noisy observations. The network also includes a node for each accompaniment event in the accompaniment score. This is because the system's own actions (playing accompaniment notes) will affect the performer's behaviour which in turn affects the predictions – the system's own behaviour thus becomes a feedback input for its later predictions. The solo and accompaniment onsets are treated as noisy observations of an underlying Markovian score process.

A real-time optimised version of the Pearl Gaussian message-passing algorithm (i.e. a Kalman filter) is employed to quickly obtain the marginal PDF for the onset time of the next unplayed accompaniment event in the score. This algorithm passes only the messages that are useful for updating the required note, and does not waste time updating other notes. The time of this next note, along with that of the latest observed note, is then used to estimate the current position and tempo.

Real music has several special cases where the regular GBN inference breaks down and custom behaviour is implemented. Once again we list such details an an illustration of the complexity of industrial score-followers. First, at a *cue point*, the temporal link along the backbone is completely severed and the new tempo prior is made uniform and thus independent of the previous backbone state. This is typically used at the first solo note after a cadenza. Second, an *exchange point* is similar to a cue, but is less severe: the tempo part of the state transition is severed in the backbone, but the time part is left connected. This is used for *a tempo*s and to reweight the solo/accompaniment control balance. Finally, *gated* accompaniment notes use the same transition structure and inference mechanism as regular accompaniment notes, but have a specified gating solo note preceding them, and are never played until the gating note has been explicitly reported by the HMM – even if the top-down inference in the GBN believes that its time has come.

Raphael's Gaussian Bayesian networks are deformable, position-in-time models of the performance. Similar deformable models have been used in vision [109], [155] [29], where they are visualised as wire-frames having elastic springs connecting their vertices. In the vision case, fitting the model is generally done by gradient descent on the 'energy' in the springs, corresponding to a prior probability over configurations. In the music case, the model is deformed over time rather than space. In contrast, Raphael's deformable model maintains marginal belief distributions over the 'vertex' positions (i.e. the notes of the model). It is possible to do this exactly using a Gaussian form of the Pearl equations because his models have no loops, existing only in one dimension rather than two-dimensions as in images.

For a deterministic score there is a single large accompaniment model. For our semi-improvised task, we are interested in recognising and accompanying collections of small fragments of music. This naturally suggests the idea of extending Raphael's models to a a collection of fragments, which could be dynamically assembled to construct a percept. We will see in chapter 4 that such score-free models need to make higher-level inferences than deterministic score models, as they must infer the positions of the underlying beats as well as the notes. Because of this they will be loopy, like visual deformable models. Unlike many visual tasks, their 'energy' surface will have many local minima so gradient descent is of little use. Maintaining beliefs over the parameters – like Raphael – will be useful but approximate inference methods must be used when large loops are present.

3.8 Onset detection and classification

Raphael's system provides the key concept of separating low and high-level inference mechanisms, using an HMM to report approximate onset times. We will use the success of his approach, and the success of experiments of this chapter, as justification for focusing in this thesis on higher-level mechanism, and assuming that similar low-level systems are available to report onsets and chroma. For semi-improvised music there is however an important difference: as no score is known in advance, we require methods which operate with no prior score information. This section gives a brief confirmation that this is possible. For segmentation into musical bars we would like to be given a list of estimated onsets and their types, similar to those produced by Raphael's HMM but with no prior score. We here provide a simple proof-of-concept method to obtain this type of information. Once again we do not aim to re-implement or extend the state-of-the-art, but merely confirm that it is possible.

As an illustration, we consider the task of constructing onset percepts from a rhythm guitar signal (though similar methods would be applicable to other instruments, especially drums). Rhythm guitars generally play bars containing chords, played with different rhythms which contain different types of *hits* of the strings. These hit types include: strumming all six strings together; strumming the bass strings only; strumming the top strings only; finger-picking single strings; *rasgueado* (flamenco strumming using finger nails); and 'ghost' hits where the strings are hit but muted with the left hand to make a percussive sound. These loosely correspond to various drum sounds found during similar rhythms.[11] There are two required tasks: first, to find the onset locations; second, to classify them by hit type.

88 bars of rhythm guitar audio were played, comprising a sequence of five 16-bar blues progressions playing using different rhythmic styles[12] and an eight-bar ending. It was sampled at 2756.3Hz (=44.1kHz÷16) and cut into 512-point frames with 448 point overlaps. NPDFT and NOV(E1) statistics were computed. Where NOV(E1) exceeded a threshold, an onset was declared. The NPDFT in a 16-frame region centred on the onset was re-quantised into four large frequency bins. These 4-dimensional vectors were input to a standard k-means unsupervised classifier ($k = 4$) [11].

A closeup of the results from the first eight bars is shown in fig. 3.24, and results for the whole audio file are shown in fig. 3.25. The closeup is shown with a subjective,

[11] An interesting piece of future work could be to automatically construct drum accompaniment to match such guitar hits.

[12] The blues is usually played using 12-bar progressions but programmers prefer 16 to simplify the arithmetic.

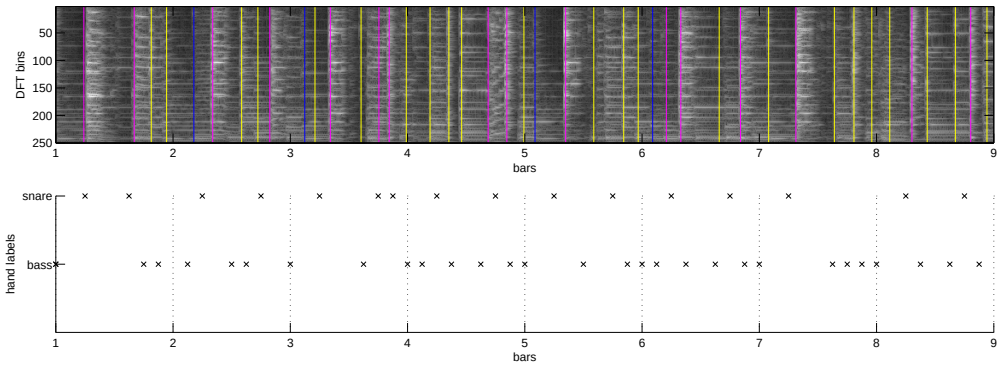

Figure 3.24: Onset detection and classification in first eight bars of guitar chord strumming. *Above*: detected onsets are shown as vertical lines, superimposed on the DFT spectrogram. Line colour indicates the class assigned by unsupervised k-means learning. Roughly, blue corresponds to bass strums and finger-picks; magenta to full (snare-like) strums and rasgueados; yellow to upper string and ghost notes (hihat-like); and red to muted finger-picked notes. For comparison, a subjective human bass and snare interpretation of the rhythm is shown *below*.

two-class human interpretation of the rhythms, in the sense of 'if you were to play the same rhythm with just a bass and snare drum, what would you play?'.

It can be seen from the close-up that constructed onsets correspond well to played onsets in the spectrogram. The classes corresponded roughly to full strums, bass sounds, high sounds, and muted picks. (Larger k values failed to yield satisfactory clustering into human-recognisable hit types using the relatively crude feature set – $k = 4$ yielded the most meaningful clusters.) The view of the whole file shows that the different style sections are distinguishable by the populations of hit types.

While this is a crude example of onset location and classification, it is sufficient for the purposes of this thesis as it shows that such perception is possible in principle. See [8] for current state-of-the art methods. In particular, improvements could be made using HMM smoothing as in *Music++* – the results presented here use only local frame information.

3.9 Beat Tracking Research

Beat tracking aims to segment non-deterministic performances into a unitary, coherent grid of bars and beats. Jukebox programs such as XMMS (`www.xmms.org`) have used simple bottom-up methods including peak-picking from audio signal energy autocorrelation. Generic generative models [22], [73] assume a hidden beat state similar to Raphael's Bayesian network, and assign generic probabilities for notes to be ob-

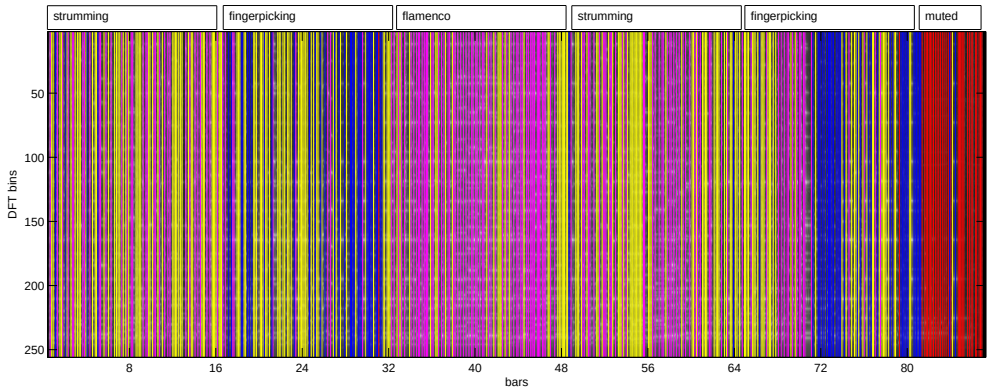

Figure 3.25: Onset detection and classification in the complete 88 bars of guitar chord strumming, finger-picking arpeggios and flamenco styles. The 16-bar sections are clearly visible from the distribution of onset types. Subjective human labels of the styles are shown above.

served on beats and at intervals between them. In contrast, Goto's non-probabilistic and highly heuristic BTS program [70] used a database of known rhythmic patterns to match against the input. Unlike generic models, BTS is able to deal with highly syncopated performances in which note locations rarely correspond to beat locations. It is able to perceive the notes *as* instances of models and infer the beats from those models.

3.10 Towards semi-improvised score following

Fig. 3.26 shows a sketch of an envisaged 'vertical iguana slice' architecture for semi-improvised, almost-known scene perception applied to the minidomain. Full generative inference is intractable as it requires exponential combinations of possible structures to explain the time series data. Several approximate speedups are used. DSP hash-classifiers reduce the data to useful features including onset positions and types. Rather than integrate over every possible bar-line segmentation, a unitary coherent rhythm grid is created from this bottom-up onset information only. 'Chordality' is approximated by a bottom-up feature within each bar. Larger-scale structures are constructed by agents on a blackboard (reviewed in detail in chapter 5) using priming hypothesis creation and testing. At this structural level this thesis is concerned only with chords, but similar methods could process melodic and other notes. Such a minidomain scene perception system could be used as a component in an automated accompaniment system if appropriate musical and synthesis modules were added. The architecture's three stages – features, segmentation and blackboard – are intended to be highly general to many forms of scene perception.

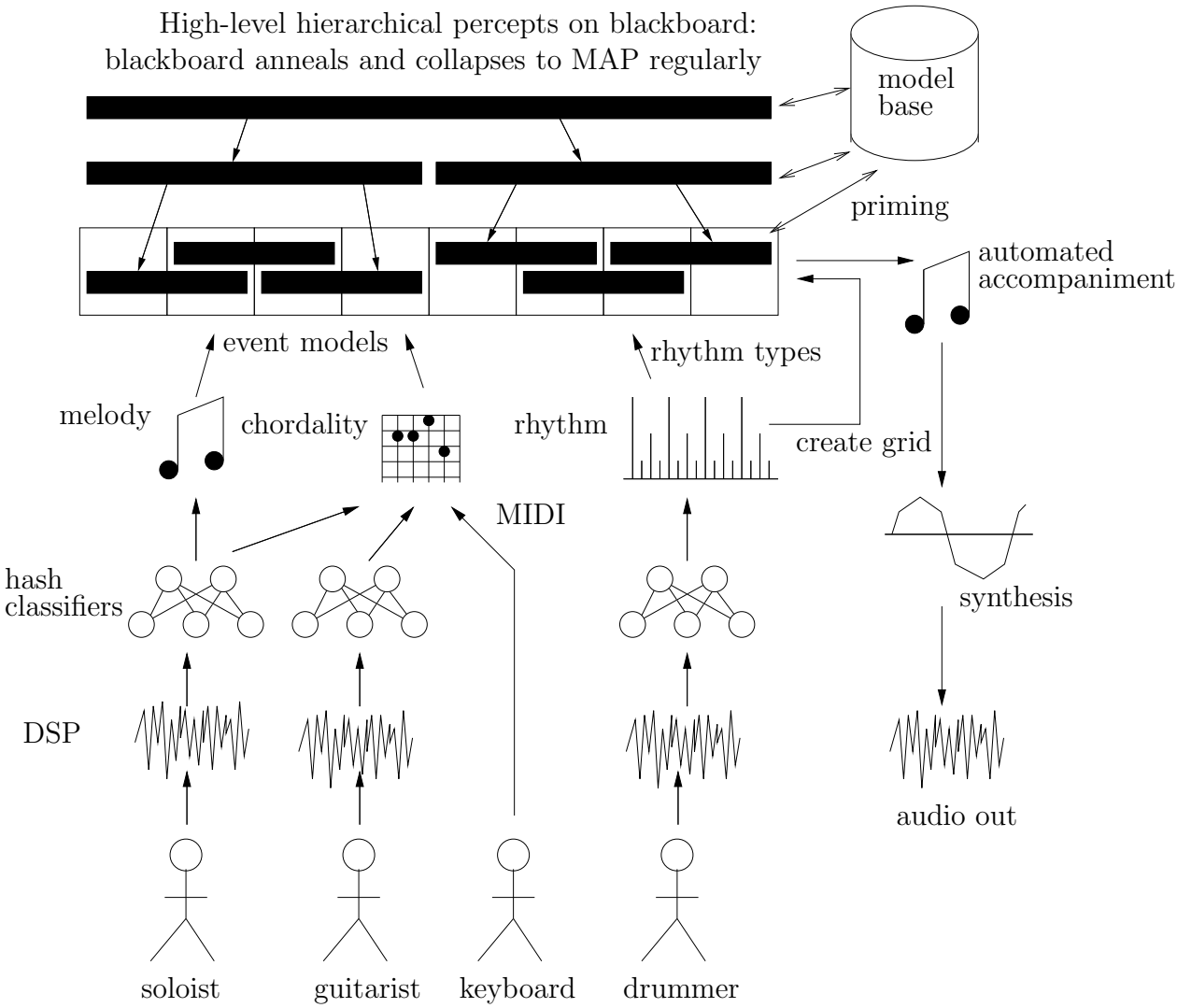

Figure 3.26: Architecture sketch.

This chapter has discussed the lowest of these levels. Chapter 4 gives a method for segmentation using Variational Bayes. Chapter 6 gives a framework for the blackboard and examples of inference using Gibbs and Variational methods. Chapter 7 shows how novel hardware could generalise both these methods to give increased inference speed in the blackboard component.

Chapter 4

Application of variational Bayes to segmentation of rhythmic scenes

The text of this chapter is based on the following peer-reviewed publication [62]. Rezek provided advice on standard theory only, Roberts provided advice on standard theory and on debugging techniques only:

- *C. Fox, I. Rezek, and S. Roberts.* Drum'n'bayes: Online variational inference for beat tracking and rhythm recognition. In *Proceedings of the International Computer Music Conference, 2007.*

It is useful for music perception and automated accompaniment systems to perceive a music stream as a series of bars containing beats. This is a form of segmentation which allows higher-level methods to construct hierarchical percepts on the temporal grid established by these bars and beats. This chapter presents a proof-of-concept implementation, *RhythmKitten*, of a system for simultaneous beat tracking and rhythm pattern recognition in the domain of semi-improvised rhythms. These are rhythms which consist mostly of known bar-long rhythm patterns in an improvised order, and with occasional unknown patterns. It applies Variational Bayes for perform inference. RhythmKitten uses position-in-time Bayesian network fragments representing individual bars and infers beat positions within them. Model posteriors provide principled model competition, and the system may be seen providing a Bayesian rationale for agent-based and blackboard systems – ideas which will be key in chapters 5 and 6. The psychological notion of priming is used to instantiate new candidate models.

As discussed in chapter 3, perception of beats and bars is difficult because there is scope for both within-bar and between-bar ambiguity. Both types of ambiguity are usually resolved by prior information. The genre of the performance favours certain patterns: a composition is unlikely to switch from military march to drum'n'bass

in consecutive bars. We expect – very strongly – that each new pattern will begin at exactly the time that the previous pattern ends, and – less strongly – that it will have a similar tempo. We formalise these ideas using Bayesian network models of single-bar rhythms to infer *within*-bar beat positions, together with a blackboard framework to select *between* these models. The required networks are highly loopy so exact inference is intractable. The variational Bayes inference approximation is applied because it seeks an estimate of the joint rather than the marginals, and in scene perception we are more interested in coherent explanations of whole bars than of individual notes. VB is fast enough to run in real-time, unlike sampling methods which may be very time consuming. VB runs iteratively, so may be terminated early ('anytime') to read off a 'best decision so far' which is useful in the real-time setting. Finally, in the semi-improvised setting we must compare rival explanations of bars and VB can provide a computationally cheap lower bound on the model likelihood using byproducts of its parameter computations. The real-time music perception systems reviewed in chapter 3 generally use one of two architectures. *Dynamic-state* models (e.g. [123] and the hidden Markov model component of [137]) update the state of the music at each point in time (typically each frame of audio). In contrast, *position-in-time* models (e.g. [22] and the Bayesian network component of [137]) maintain beliefs about the positions of a set of musical events – such as note onset or beat times. RhythmKitten is a position-in-time method, but unlike these previous systems it deals with *semi-improvised* music: rather than require the performance to be aligned with a fixed score, we consider sequences of known (and occasionally unknown) drum patterns played in an improvised sequence. Within each pattern, notes may also be omitted from or inserted into the standard pattern. In particular this means that unlike previous systems, we cannot assume a given mapping from input notes to model notes. We consider multiple rhythm models as hypotheses to explain the data: when the models are viewed as 'agents' this is a similar approach to non-probabilistic agent-based methods such as Goto [70] and Reis [142]. However our models have rigorous probabilistic semantics, for their internal parameters – in the manner of [137] and [22] – but also for their model posteriors. It is the latter that provides a rigorous probabilistic basis for agent competition.

We assume that some lower-level system is available (as shown in section 3.8) which reports incoming onsets with a belief over their time of occurrence and a discrete classification between bass, snare and hihat type hits. These could be extracted from drum audio or from other rhythmic instruments such as guitar chord strums.

4.1 Single models

We model the whole performance as a series of Bayesian networks, stitched together. Each network models a known four-beat, single-bar rhythmic pattern. At each bar, we compare several models to find the best fitting one, and the MAP values of its parameters. These parameters may then be used to extract the model's estimate of the past, present and future beat locations as required. (We leave aside the question of how and when to instantiate models, but will return to it in section 4.3.)

Fig. 4.1 shows a model for a very simple rhythm consisting of just two hihat (hh) notes. Fixed nodes are shown as squares and hidden nodes are circles. The diamond-shaped *multiplexer* nodes will be discussed later: for now, we may assume they simply forward incoming and outgoing messages unchanged.

The goal is to infer the beat positions $\{b_i\}_{i=1:5}$, along with the start time s and tempo τ. To utilise the efficiency of conjugate-exponential models, we work with the inverse tempo, τ^{-1} instead of τ. Both s and τ^{-1} are modelled as Gaussians, with fixed mean and precision priors.

The beat positions are modelled as linear combinations, $b_i = s + i\tau^{-1}$, and note positions are modelled as the weighted linear combination of their two nearest beats, $n_j = b_{i(j)} + w_j(b_{i(j)+1} - b_{i(j)})$ where $i(j)$ is now a function specifying the latest beat number i before the jth note, and w_j is a rational weight with $0 < w_j < 1$.

Incoming observations are shown in the lowest layer of fig. 4.1. We assume that an external system reports onset times x_k with associated detection precisions γ_k^D and discrete classes c_k (with values for bass, snare and hihat). The precisions represent possible errors in the detection process, not in any high-level sources of note deviations such as changes in tempo or performance timing errors. Once reported, x_k, γ_k^D and c_k are modelled as fixed. Note that a more fully Bayesian system would model them as random variables, allowing prior information from other parts of the music model to modify the onset detector's beliefs. In particular, priors from rival rhythm models could affect the observations, i.e. rival models' parameters would become dependent on each other. This would greatly increase the complexity of inference and it does not appear to give any practical advantages over independent models, as our task is ultimately to select one winning model. Forwarding messages to rival models without the usual co-parent dependency is performed by the special *multiplexer* nodes in the observation layer.

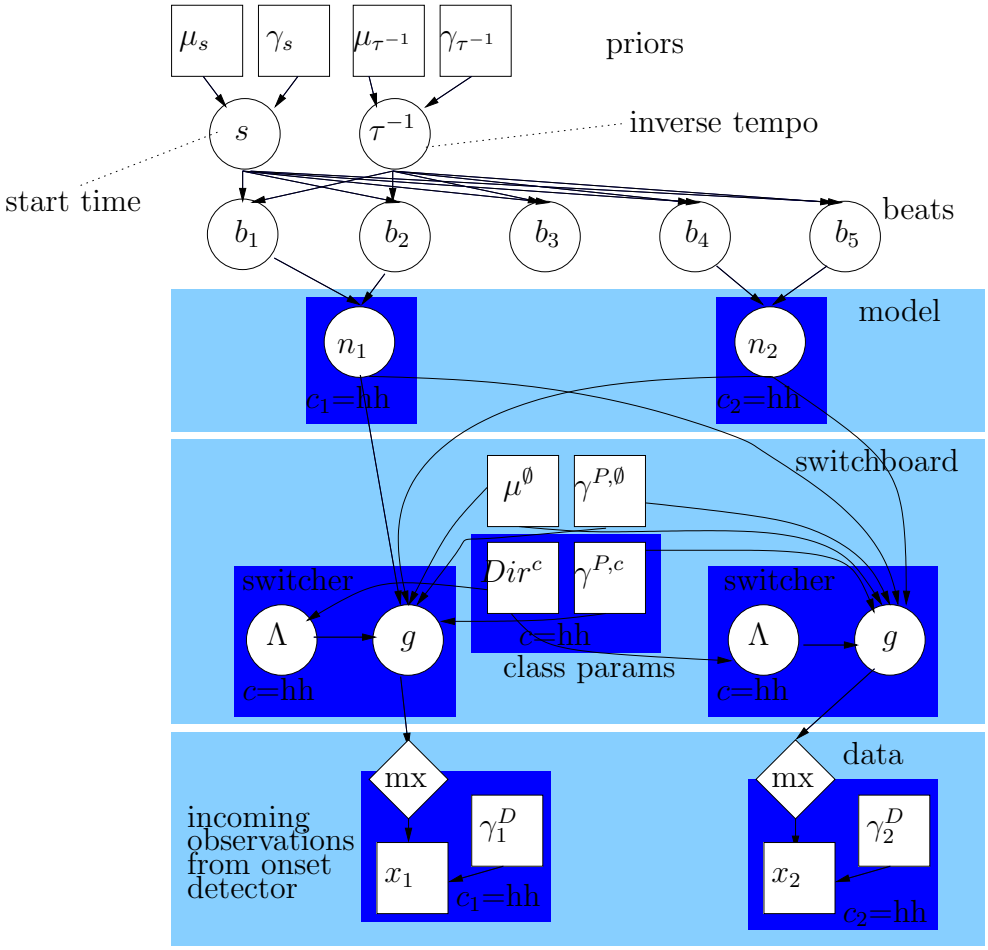

Figure 4.1: Schematic of a single-bar Bayesian network. The task is to infer the beat positions b_i. Both model and data in this simple example contain only two notes, both of class hihat ($c = hh$). The data region contains the reports from a lower-level onset detector and classifier. Classifications are hard (i.e. non-soft), as are the classes of model and switchboard nodes. The correspondence between observed and model notes is not initially known, so a switcher is constructed for each observed note. The switcher for an observed note of class c forms a (soft) Gaussian mixture g of the positions of all model notes of class c, to act as a prior on the observation position. The mixing coefficients Λ for each observation's switcher are to be inferred. For each note class c (hihat, bass, snare) the switchboard maintains a single pair of priors $Dir^c, \gamma^{P,C}$. Dir^c is a Dirichlet prior over mixing coefficients, whose dimension depends on the number of model notes of class c. $\gamma^{P,C}$ is the prior over performance precision for the class (caused by player deviation from the model rather than detection error). As some detections might not correspond to any model note, the switchboard maintains an additional pair of priors $\mu, \gamma^{P,}$ to describe the very wide Gaussian distribution of these 'sink' notes. Sink priors are included as components in all g mixtures.

4.1.1 Switchboard

We want to infer the positions of notes and beats from the set of observations. If each observed note x_k arrived with a label saying of which note n_j of the model it was an instantiation, this would be easy, as we could then connect the observed x_k to n_j and perform inference. Hence x_k would be treated as a noisy observation of n_j (as in the systems of Cemgil and Raphael). However we do not have such labels, we only have the class c_k of the observation. We are told that it is, say, a bass drum note, but not which of the (many) bass drum notes in the bar. Further, we want to allow the possibility that non-model notes may be played. This may occur for several reasons: (1) extra note played by accident, e.g. the performer's hand slipping; (2) performer is playing a variation of a known model, with deliberate extra notes; (3) performer is playing an unknown model. We must try to perceive the latter as a known model as best we can for now, then perhaps consider the known model's failings and update the model or learn a new model from them offline.

We solve the tagging problem by modelling the belief in the observation locations x_k as a Gaussian mixture models (GMMs), with one Gaussian source from each of the M model notes n_j that have the same class as that observation. The middle shaded layer of fig. 4.1 is called the switchboard, and consists mostly of clusters of nodes called switchers. (There are also some extra nodes which are shared across switchers.) One switcher is created per incoming observation k, and includes a GMM node, g, together with a discrete mixture weight node Λ, so that its prior is

$$P(g|\{\mu_m\},\{\gamma_m^P\},\{\Lambda_m\}) \propto \sum_{m=1}^{M} \Lambda_m \exp\left[-\frac{\gamma_m^P}{2}(g-\mu_m)^2\right]$$

where γ_m^P is a performance precision parameter for the mth parent (see section 4.1.2). This distribution is not in the conjugate-exponential family, but may be approximated:

$$P(g|\{\mu_m\},\{\gamma_m^P\},\{\Lambda_m\}) \propto \sum_{m=1}^{M} \exp\left[-\frac{\Lambda_m\gamma_m^P}{2}(g-\mu_m)^2\right]$$

This matches the mean and variance of the original GMM, and has the useful property that it tends towards it as $\Lambda_m \to \Delta_{mm'}$, that is, as the discrete mixing vector becomes a single peak at m'. This is useful for our task, as we wish to ultimately assign each observation to a single class.

All Λ nodes of each class c share a fixed Dirichlet prior, Dir^c, which have hand-set parameters favouring single-source explanations.

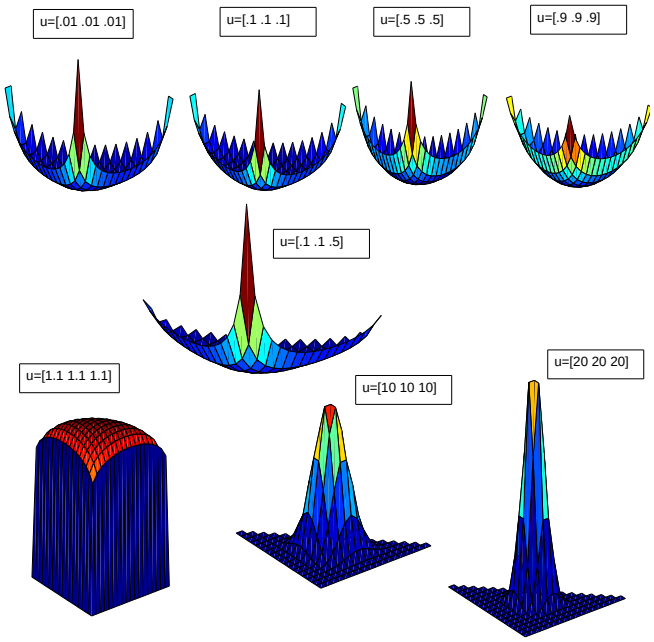

Figure 4.2: Examples of Dirichlet distributions on three variables.

$$P(p_{1:N}|u_{1:N}) = \frac{1}{Z}\prod_{i=1}^{N} p_i^{u_1-1}$$

Examples of three-variable Dirichlet distributions are shown in fig. 4.2. Note that when $u = [1, 1, 1]$ then distribution is flat. For u components above unity, it bulges in the centre (bottom row) encouraging mixtures of variables. For components less than unity (top row) it favours single-variable explanations. It is the latter kind of prior that we use here, as we want each switcher to be explained by a single component rather than a mixture. It is possible to favour particular components by changing relative values within the u vector, as shown in the centre row.

4.1.1.1 Sibling rivalry

In addition to this GMM formalism, we know something more about the relationship between the observed and model notes: each model note will be instantiated at most once in the data. Even if, say, two snare hits occur very close to each other and to an expected model note location, only one of them can be 'the' instantiation of

the note, and the other must be a spurious extra note. The standard GMM is not able to capture this 'sibling rivalry' between its children. GMMs are often used in data-intensive statistics where the task is to infer quantities from large numbers of noisy observations of them. In contrast, here we have at most one observation of each model note. The sibling rivalry problem is not unique to GMMs but is a general Bayes net problem: Bayes nets provide an automatic framework for competing *parents* to inhibit one another through the well-known 'explaining away' effect; but do not allow siblings to compete in any similar way.

To model our knowledge of sibling rivalry, we extend the Bayesian network into a graphical model containing both directed and undirected links. For each note class, we fully connect all the Λ nodes in the switchers of that class. We connect with inhibitory links, so that if one switcher lays claim to being an instance of a model note then it discourages other switchers from being instantiations of it. We extend the variational update for Λ nodes to include this undirected term (rightmost):

$$\log Q(\Lambda) \leftarrow \langle \log P(\Lambda | par(\Lambda)) \rangle_{Q(par(\Lambda))}$$

$$+ \sum_{ch(\Lambda)} \langle \log P(ch|\Lambda) \rangle_{Q(ch(\Lambda), cop(\Lambda))}$$

$$+ \sum_{riv(\Lambda)} \langle \log \Phi(riv, \Lambda) \rangle_{Q(riv(\Lambda))}$$

As riv and Λ are discrete distributions parametrised by $Q(\Lambda = \Lambda_m) = q_m^{(\Lambda)}$, $Q(riv = riv_m) = q_m^{(riv)}$ with $\sum_m q_m^{(\Lambda)} = 1$ and $\sum_m q_m^{(riv)} = 1$, we set the additional update terms to

$$\langle \log \Phi(riv, \Lambda) \rangle_{Q(riv)} = \begin{bmatrix} 1 - q_1^{(riv)} \\ \dots \\ 1 - q_M^{(riv)} \end{bmatrix}$$

where M is the number of components. This is a heuristic whose intent is to encourage pairs of discrete nodes to have large divergences between them (e.g. in the KL-divergence sense). Note that this does *not* assign zero probability to two discrete notes having the same component, because its effect is on the logarithm of the resulting joint, not the joint itself. Instead, it merely discourages such similarity, and we have found it useful enough for our purposes.

This scheme does not force any observations to match up with model notes: it merely discourages multiple observations from explaining the same model note.

4.1.1.2 Sinks

To allow for the performance of non-model notes, we construct an additional *sink* component for each note type. Sinks may be thought of as null hypothesis explanations for observations. They are modelled by Gaussians having their mean in the centre of the bar, and a very wide variance so that the distribution stretches all the way across the bar in one standard deviation. This wide spread has the classic dual effect of (a) catching observations from a wide range, enabling the sink to soak up all observations not well accounted for by other components; (b) assigning a low likelihood to each observation because it is so spread out; hence allowing non-null components to be favoured in their specialist locations.

This may be viewed as a crude approximation to a fuller sink model: there is information contained in non-model notes which we are currently throwing away. In particular, notes do not occur at completely random places in the bar: even if not part of an identifiable model, they still tend to occur on beats or rational subdivisions of beats. In fact many beat identification systems have been constructed in this way. For example Cemgil [22] constructed an intricate prior over subdivisions similar to:

$$P(x) = \frac{1}{Z} \sum_{D=1}^{K} \sum_{N=1}^{2^D} \delta(x; \frac{N}{2^D}) * \exp(-\frac{\gamma}{2} x^2)$$

(The left part of this forms peaks at major subdivisions, whose height increases with importance, as measured by number of factors. The right term convolves (*) with a Gaussian to blur the spikes.) Such priors could in principle be incorporated here as GMMs, with one GMM component per subdivision. The advantage of such a scheme is that tempo and phase may then be inferred in a 'model-less' manner simply from collections of notes and the prior. However this approach would be time-consuming in a real-time system due to the large number of additional components to consider. We also note that 'model-less' is something of a misnomer, as we would effectively be specifying a complete, general pattern based on subdivisions: in practice we can know most common models in advance and exploit this by using our set of particular models instead of this general one. We have found that there is usually enough information in the instances of model notes to infer the beats well, without having to rely on sink notes to improve the accuracy.

There is still one problem with our single wide Gaussian approximation to this intricate structure. As the Cemgil prior is made of peaks, this structure assigns slightly higher priors to sink notes around rational subdivisions than our Gaussian assigns, at the expense of having lower priors than our Gaussian at places away from

rational subdivisions. In practice, most (usually all) sink notes *do* occur at rational subdivisions. This means that our approximation will consistently assign lower priors to sink notes than the more accurate structure. To correct for this, we adjust the Dirichlet prior on the Λ nodes to give sinks a slightly higher prior than model notes. Empirically, $u = [0.10, ..., 0.10, 0.12]$ was found to work well, where the 0.12 is the sink component.

As discussed above, we constrain the GMMs with sibling rivalry links to prevent multiple observations mapping to a single model note. For sinks there is no such constraint: we allow multiple observations to be generated by the same sink. To accomplish this, the $\langle \log \Phi(riv, \Lambda) \rangle_{Q(riv)}$ term above is modified so as not to penalise sink-sharing.

4.1.2 Precisions

The switchboard contains two kinds of performance precision nodes. First, there is a single fixed precision $\gamma^{P,\emptyset}$ for sinks. This is used as an input to all GMMs, for the precision of their sink component, regardless of their class. It is set so that the standard deviation of the sink is one whole bar. Together with the Dirichlet prior amplification this produces a useful sink model. Second, for each note class c there is a fixed precision $\gamma^{P,c}$ which is shared between all switchers of that class. This performance precision models the player's accuracy in playing notes of class c. For example, the performer may be more accurate on the bass drum than on the hihat. Note that future versions of the system could extend this by allowing each model note to have its own performance precision, in the manner of *Music++*. This may be useful when the patterns become more complex, and the performer may try harder to play the on-beat notes very accurately at the expense of other more decorative notes. Alternatively, a simplified model might share just one performance precision across all note classes to allow faster inference.

Note that the performance precisions differ from the detection precisions γ^D – the latter being a measure of the detection error rather than the human player's deviation.

4.1.3 Visual display

The following demonstrations are illustrated using RhythmKitten's graphical displays. The format of these displays is similar to the schematic of fig. 4.1 but extended to show prior and posterior means and standard deviations for all positional nodes; to display nodes from multiple note classes (hihat,snare and bass) and to show mixture coefficients for the Gaussian mixture nodes in the switchers. A large quantity of

information is thus contained in these images, which may be difficult to read at first. To aid comprehension, fig. 4.3 gives a cartoon example of the display format.

4.2 Example of a single model inference

The RhythmKitten screen-shots in figs. 4.4-4.5 show four inference steps on a single model, as the message-passing progresses. Each step consists of a round of message passing, which includes a downward pass followed by an upward pass. The input observations consist of four hihat hits, one bass and one snare. The bass hit is slightly after the first hihat and the snare is slightly before the third hihat. The task is thus to find the best beat positions and assignments of noise to explain this data.

Fig. 4.6 shows the value of L, the lower bound on the log-likelihood during the above iterations. (As the observed nodes are delta spikes we are approximating the continuous probability *density* $p(d|M)$ which may have values above unity.) Note that – contrary to VB folklore – the lower bound does not improve monotonically, though it does converge. The reason for non-monotonicity appears to be the presence of the discrete switch nodes. While it is known that each individual update $Q_i(x_i)$ always improves the total $Q = \prod_i Q_i(x_i)$, this does not account for the fact that updating Q_i then has knock-on effects on other nodes, invalidating their Q_i's. This problem is especially apparent when discrete switches and rivalry are important.

4.2.1 Cyclic and divergent behaviour

As discussed above, variational Bayesian inference does not necessarily converge once discrete switch nodes are brought into play. The problem can become acute for highly ambiguous stimuli having multiple local minima, and having large loops in the graph. Such loops take time for information to propagate around, so for example it may take several steps before the effect of a switch node change is felt. In these cases it becomes possible for the network to oscillate between states, and even to diverge.

Fig. 4.7 shows an example of cyclic (and possibly divergent) behaviour: an ambiguous stimulus is presented to a standard *ROCK1* model (see fig. 4.10), and nine steps of inference are shown. The stimulus consists of just three hihat hits, with no immediately obvious underlying beat. Given priors on the start time and tempo as usual, the net oscillates between two configurations, labelled in the figure as L and R. In the R screen-shots, the notes are interpreted as occurring early, before the beats. In the L screen-shots, they are interpreted as occurring after the beats.

Fig. 4.8 shows the lower bound L during the oscillating run. Close inspection shows that the two apparently fixed points are actually slowly diverging.

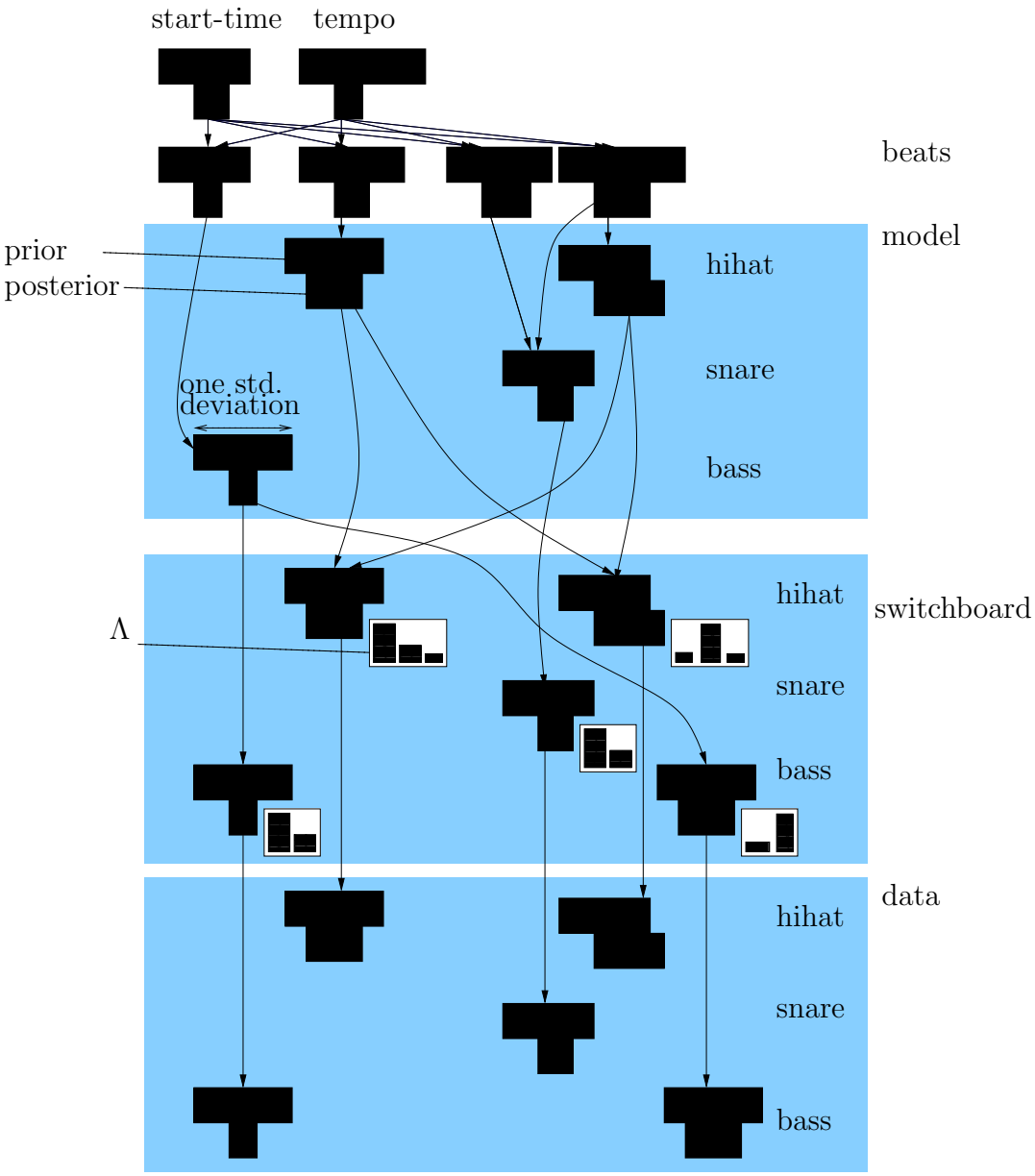

Figure 4.3: Cartoon of RhythmKitten's graphical display format. The horizontal axis represents time, and node priors and posteriors are shown as black bars extended over time. The position and width of these bars show the mean and standard deviation of the Gaussian prior (upper) and posterior (lower) node distributions. The model, switchboard and data regions are subdivided into layers for note classes: hihat, snare and bass. Each switchboard mixture node's associated mixture posterior is shown as a small bar chart. The rightmost bar in this chart is the sink component strength; the other bars are the strengths of the components from class-matching parent nodes in the model. (Hihat mixtures have three components as there are two hihat nodes in this model; bass and snare have two components as there is only one model note of each of these types.) In this example, the data contain an additional bass note which does not correspond well to the model: this note has been strongly assigned to the sink source. Nodes $\mu_s, \gamma_s, \mu_{\tau^{-1}}, \gamma_{\tau^{-1}-1,\mu,\gamma^{P,}}, \{Dir^c\}_c$ and $\{\gamma^{P,c}\}_c$ are not shown.

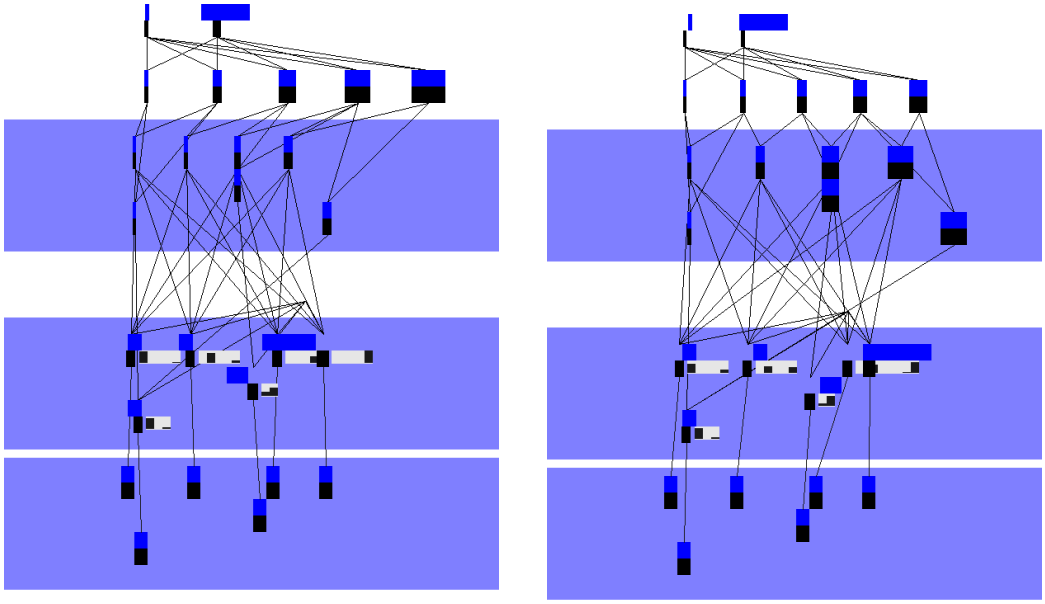

(a) In the first step, the *HIPHOP1* model (see fig. 4.10) has just been instantiated, with a tight prior on the start time and a loose prior on inverse tempo. *HIPHOP1* has hi-hats on all four beats, a snare on beat two, and bass on beat one and just before the end of the bar (the latter bass hit is the 'late' hit which provides the characteristic hiphop feel). The inverse tempo belief has already been greatly tightened by the messages from the beats. The beat position beliefs still obey the start-time and tempo priors more than the observations. This is because messages from the observations have not yet propagated to the beat layer. They have however propagated to the model layer, as its nodes show substantial deviation from where the beats would predict them. The switcher nodes assign the final hihat to the sink, misassign the penultimate hihat to the third beat instead of the forth; and are uncertain whether the snare was generated by the (only) model snare on beat 2 or by the sink. Overall the model is far from the solution and out of balance as its tempo is still too slow and the beats last much longer than the observed notes; meanwhile the model notes are too fast and do not last as long as the observations.

(b) The same musical bar after a second step of inference. In the second step, the beat positions have been corrected and now span a similar range of time to the set of observations. (Note there are five beats rather than four as the model represents the *end* of the bar as well as its internal beat positions.) However the model notes have sprung out beyond the observation range – affected by the *previous* version of the beat beliefs. The snare switcher is assigning a strong sink belief due to the *previous* location of the model snare note, as can be seen by the bar chart next to the snare node in the switchboard. At this still-early stage of inference, there is still much uncertainty in the switchboard's beliefs about the third and fourth hihat notes – even though the corresponding model beliefs are comparatively tight (but wrong). This is because information has yet to propagate from the model to the switchboard.

Figure 4.4: The first two of four steps of inference in a single-bar rhythm network.

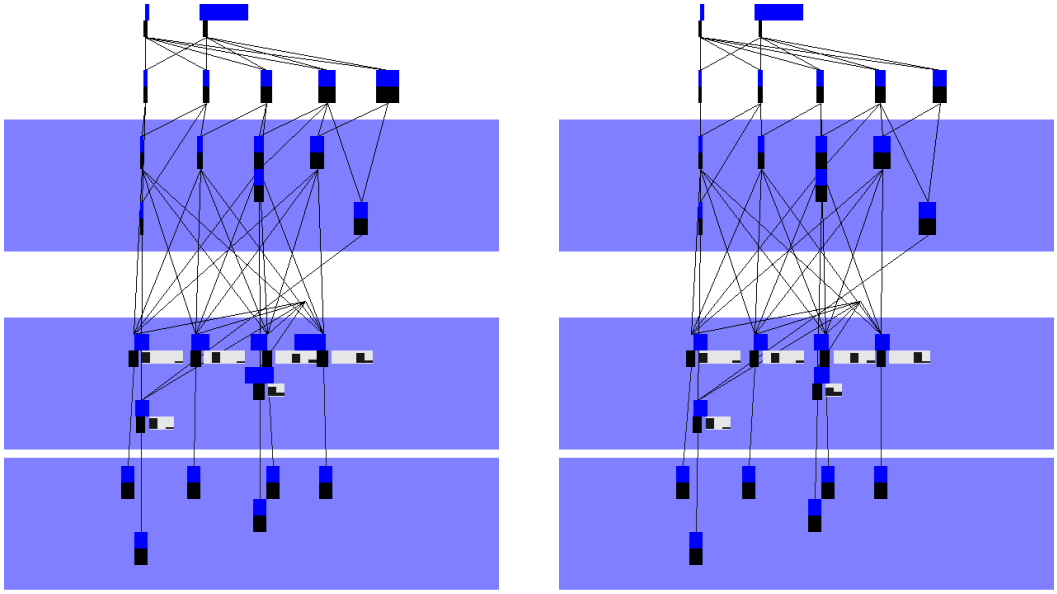

(a) By the third step, the oscillations have largely calmed down, and the beat and model note positions now agree with each other and with the switchboard. The snare hit is correctly assigned and so are are the other switchboard notes, which all show fairly decisive switch assignments.

(b) By the fourth step there is very little change in each step. All notes are correctly assigned, though each note – especially the snare – maintains a small probability of being sink-generated. This is because the played bass and snare do not coincide exactly with the hi-hats beats so it is possible they were played intentionally as extra non-beat notes rather than played incorrectly as on-beat notes. Even at convergence, the positions of the beats grows increasingly uncertain towards the end of the bar. This is because the tight start-time prior becomes diluted by the relatively loose tempo prior, and also as there are few observations towards the end of the bar. Little visual change occurs if additional steps are run beyond this point (though numerically the network continues to converge to a limit point).

Figure 4.5: The final two of four steps of inference in a single-bar rhythm network.

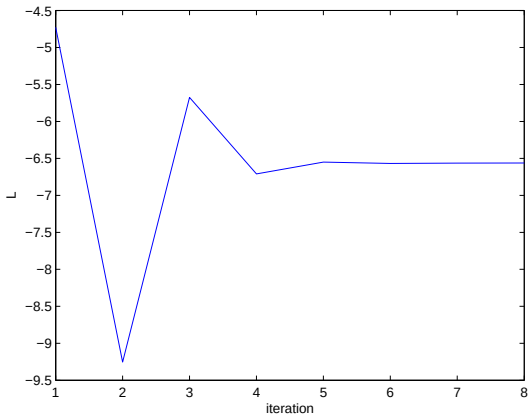

Figure 4.6: Log-likelihood during variational inference in the single-bar rhythm network.

Convergence is affected by the model priors: a main reason for the oscillation above is that the model assigns similar priors to the L and R configurations. If the model was instantiated with less ambiguous priors then a single optimal state would have been found. Convergence can also be affected by node firing order. In the run of fig. 4.7, we used the best firing order that we have found: one iteration consists of a complete down-pass followed by a complete up-pass. Earlier versions of the system used iterations consisting of a down-pass only, or up-pass followed by down-pass but we found this tends to lead to oscillation more often. Indeed, under the latter scheme, highly ambiguous tasks such that of as fig. 4.7 can sometimes produce unstable oscillations in which the difference between the bistable percepts grows rapidly at each step, the beat and model note positions moving towards $\pm\infty$ until the program crashes due to numerical underflow errors.

4.2.2 Annealed variational message passing

To reduce the possibility of belief oscillations during message passing, we use variational annealing. In this scheme we do not seek $Q \approx P$ directly, rather we infer a sequence of *heated* distributions $Q^{1/T_i} \approx P^{1/T_i}$. The temperature T begins at a number greater than unity, and is gradually reduced to unity. Further, if an MAP solution is sought rather than a joint approximation, T may be reduced below unity and toward 0, in which case $Q^{1/T}(x) \to \delta(x; \hat{x})$, giving an estimate of the MAP. In practice, this MAP estimate is a near-delta spike at a local maximum of the posterior. As the cooling schedule slows and the initial temperature is raised, the probability of arriving at the global maximum increases. We extend the variational message passing

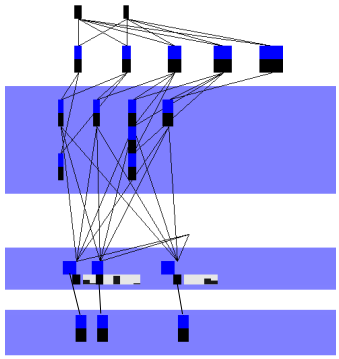

(a) Step 1. (R config.)

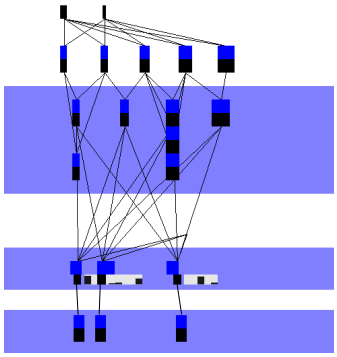

(b) Step 2. (L config.)

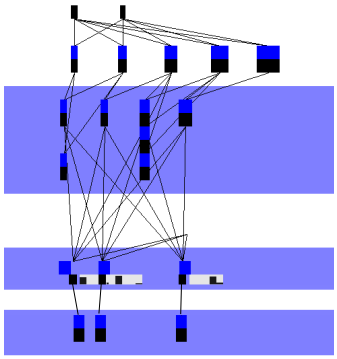

(c) Step 3. (R config.)

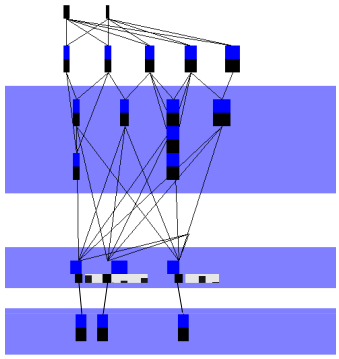

(d) Step 4. (L config.)

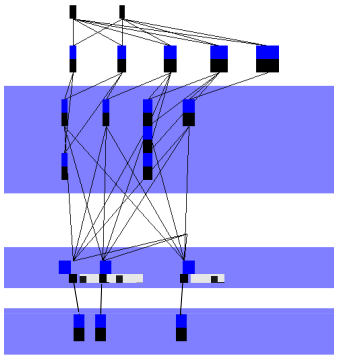

(e) Step 5. (R config.)

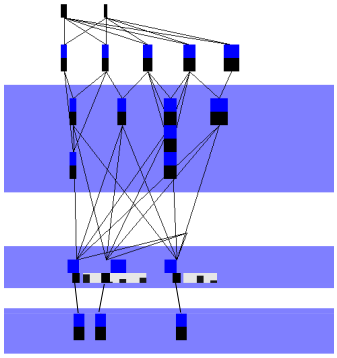

(f) Step 6. (L config.)

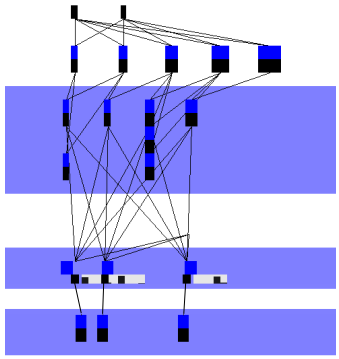

(g) Step 7. (R config.)

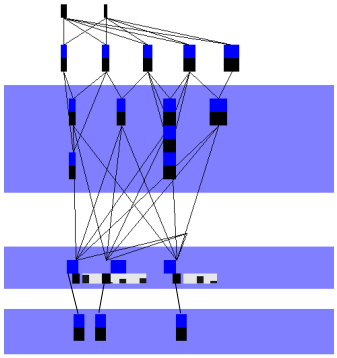

(h) Step 8. (L config.)

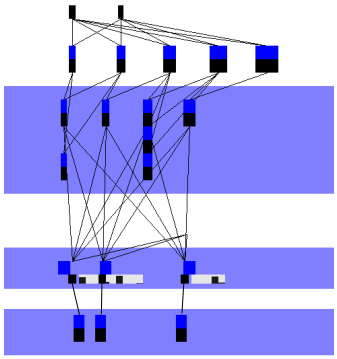

(i) Step 9. (R config.)

Figure 4.7: Cyclic behaviour for an ambiguous percept and weak prior. The beat positions oscillate between two approximately stable configurations, L and R.

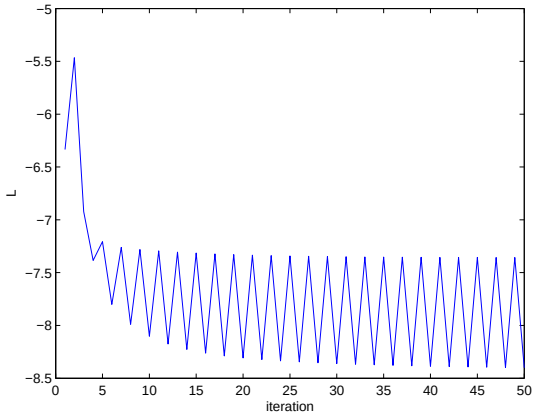

Figure 4.8: Log-likelihoods for the cyclic example. Oscillations are clearly seen: local variational Bayes updates do *not* always lead to global improvements in log-likelihood.

framework to include annealing by giving each node a temperature parameter (for our conjugate exponential models this simply multiplies the parameter vector.)

Fig. 4.9 shows a difficult three-onset inference problem: the notes fall in such places as to be highly ambiguous under the position and tempo priors. Without annealing this causes the network to oscillate and diverge during inference; annealing cures this problem. The distributions on the nodes begin by becoming very wide as messages are received; then gradually reduce as cooling takes place. (See section 4.4 for a description of the display.)

4.3 Hypothesis management

So far we have considered rhythm models of individual bars: test data was created representing a single bar's content of music, and the postulated model had to explain all the data. However in the wild, the situation is more complex: we receive a stream of events over a period of several minutes (the song) and we do not know initially which events belong to which bar and hence to which model.

The ideal Bayesian approach would be to consider all possible models instantiated at all possible points in time-tempo space, together with a prior on which combinations of them are allowable and mixture switches to allow data points to be explained as mixtures of models. The prior would act to allow only sets of rhythm models which are contiguous throughout the whole song, and could further specify Markovian or grammatical priors on the probabilities of particular sequences of models.

This approach is impractical because it requires an infinite number of models, and even quantising the possible model instances would require a very large number

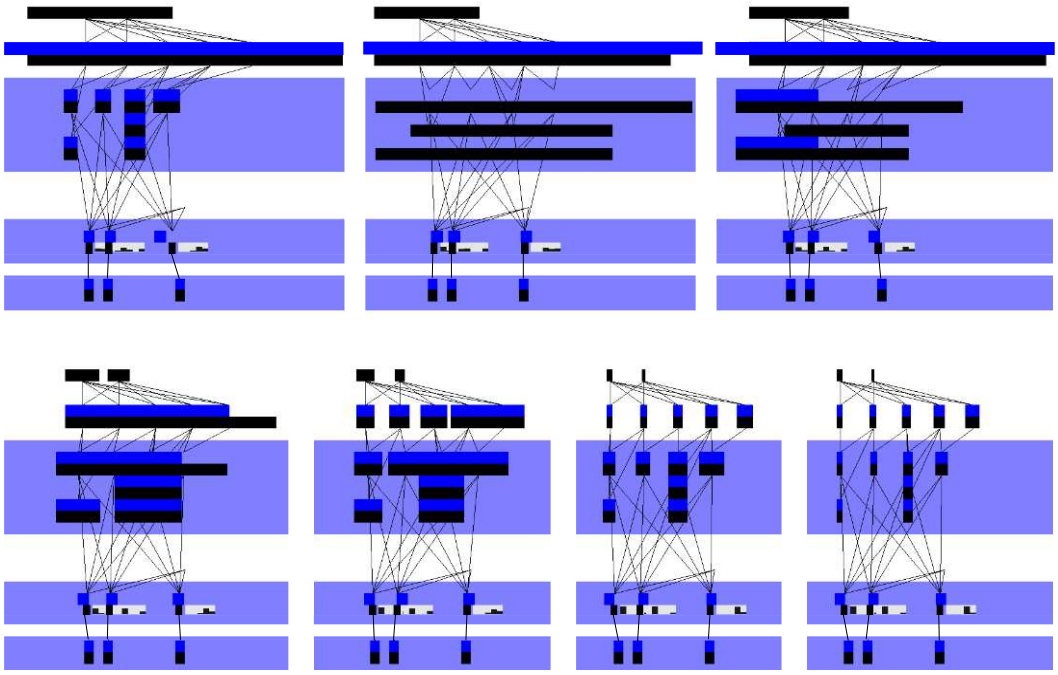

Figure 4.9: Seven steps of annealed variational inference on an ambiguous three-onset problem. As inference progresses, the heated initial beliefs converge to the correct VB posterior. Without annealing, the network can oscillate and diverge during inference.

of models. In particular the prior would have to operate on the power set of these models which is intractable. So we must use heuristics to approximate the Bayesian ideal.

The heuristics we use are based on the ideas of priming and pruning presented by [142]. Reis modelled symbolic sequences using a set of *agents,* each agent being a detector for a particular pattern. When an agent A successfully completes its pattern (by observing the exact required sequence – Reis' work was non-probabilistic) it competes with completed *rival* agents, and the winner W primes all other agents to start looking for their patterns beginning at the point that W completed. Rival agents are those which share one or more symbols of the data stream. Losing agents are deleted (*pruned*).

We extend this method to the case of continuous time events (opposed to sequences of symbols). We replace discrete symbol sequence detecting agents with our variational models. Reis handled competition between models with a heuristic, but in contrast, we are able to use the variational lower bound on model likelihood to provide a more rigorous foundation for competition. The principal difficulty is the lack of sharp boundaries between models together with the uncertainty in note arrival times: in the symbolic domain is simply to say 'if the new note time is after the end of agent A then add it to the next agent instead of to A' but the meaning of this

is less clear in our probabilistic domain: there will instead be some probability that the new note lies inside or outside the model. Pragmatically, we simply set a probability threshold and declare the new note to be outside the model if it is exceeded. Pseudo-code is shown in algorithm 1.

Algorithm 1 Reis-like algorithm for hypothesis management with priming and pruning. $d_M$is the set of data points attached to model M and $|d_M|$ is the size of this set.

```
prime initial model set
set initial models to incomplete state
for each incoming note n do
  for each incomplete model M do
    if P(n after M < threshold) then
      link n to M
      update temperature T
    else
      set M to completed state
      winner W ← M
      for each rival model R (overlapping M) do
        if R completed then
          if log Q(R|d_R)/|d_R| > log Q(W|d_W)/|d_W| then
            W ← R
            prune R and descendants of R
          end if
        end if
      end for
      prime from W
    end if
  end for
end for
```

There is an issue regarding model comparison when two rivals R and W have different numbers of data points. Instead of raw model posteriors, we compare the log posteriors *per data point*, dividing the lower bounds by the number of data. This statistic may be thought of as an approximate log probability *density* per unit time, with data points as a proxy for time. (Log posterior densities are typically negative, so dividing them *increases* their value.) The reason for comparing *log* probability per data point is as follows. Suppose we have N models in a sequence, $M_1, M_2, ..., M_N$ which together cover a complete song. The issue is that data points near model boundaries may fall under the model at either side of the boundary. We do not wish to penalise either case in the ideal *global* distribution of models. So we note that our statistic has this property: the score for the whole song is

$$\frac{\sum_{i=1}^{N} \log P(d_{M_i}|M_i)}{\sum_{i=1}^{N} |d_{M_i}|}$$

From the point of view of the global distribution, the denominator is constant so does not penalise any particular assignments of data to models. However recall that we are using a heuristic to approximate the global distribution, namely that we make a hard decision about which models to keep and reject at the end of each bar. And from the viewpoint of these individual bars, the statistic *does* make a difference, namely that of transforming our measure of log likelihood into log likelihood per data point explained, which aids our greedy search through the space of sequences of models as required.

Note that we have included the annealing schedule as part of the node linking cycle. We want the model to start as 'hot' when first created, then to cool as *real* time progresses, so that it reaches the true probability scale as it completes. We use the time of the latest received note as a proxy for elapsed time, and have found that a useful schedule is to cool linearly from $T = 8$ to $T = 1$ during the course of the bar.

4.3.1 Priming

In the present work we have used a simple Markov transition matrix to specify priors on sequences of models. (e.g. the low probability of a drum'n'bass pattern following a military march pattern.) There is an important practical difference between transitions of zero probability and those of small but non-zero probability. Conceptually these are similar, but the former will *not be primed* whereas the latter are primed but are unlikely to be chosen as the final winner. This makes a huge difference to the amount of computation that takes place, but there is the classic tradeoff that in setting unlikely transitions to a hard zero, we rule out the ability to use them to explain uncommon situations, so in the unlikely event that those situations occur, the model will fail. (Primed models are 'known unknowns', as they still contain much uncertainty but are under active consideration'; unprimed models are 'unknown unknowns'.)

Newly primed models are instantiated having a start time with mean equal to the MAP end time of the previous (completed) model – shown by the dotted line in fig. 4.1 – and inverse tempo mean equal to the MAP of the previous inverse tempo. Parameters specify precisions of these beliefs, which at present are global and hand-set. However it would be conceptually simple to use an EM method as in [137] to learn precisions for each bar and also to learn priors on tempo transitions.

4.4 Evaluation

It is more instructive to present a walkthough of a real RhythmKitten test run than to give only statistics of its results. A data set was recorded by a human drummer using a MIDI kit, and standard deviations of 100ms attached to notes of all types to simulate a level of uncertainty that would be typically be attached to onset-detected notes (as in the experiments of section 3.8). The data consists of 48 bars of rhythms lasting about 2 minutes and including over 250 hits, which is a typical amount of data for beat tracking evaluations in the literature, (e.g. [26]). The rhythms begin as simple known patterns and get progressively more complex, and more errors are introduced. A knowledge base of six models was used, shown in fig. 4.10, which includes three regular rhythms and three fills.

RhythmKitten is written in interpreted Lisp research code, and no effort has yet been made to optimise its execution for real-time online inference. However the test run was performed on a 1.6GHz Pentium in quasi-realtime of half the original performance speed, suggesting that real-time optimisation would be possible with further development work.

To aid understanding, figs. 4.11-4.13 give close-up pictures and discussion of the results from the first 12 bars. Bar numbers are displayed above each model, and only the winning models are shown, in their final collapsed form. The reader may examine the remainder of the run in fig. 4.14, noting the near-losses of tracking around bars 26-28 and 36 and subsequent recovery; and the eventual failure due to complex unknown rhythms at the end.

4.4.1 Comparison with naive tracking

Fig. 4.15 shows the deviation of the played onsets from 'ground truth' beats (as labelled by hand, offline), and can be seen as a measure of the accuracy of the playing. The x axis measures fractions of a beat deviation from the nearest labelled beat. Note the clusters around ± 0.5 beats which are notes played half way between beats. Excluding these notes, the standard deviation (player error) from the beat is 0.07 beats, corresponding to 35ms at 120bpm.

Fig. 4.16 shows a histogram of errors of the system's MAP beat positions from the ground truth. Only the correctly-tracked bars 1-38 are included. The standard deviation of the errors is 0.12 beats, which corresponds to a musical semi-quaver, or 60ms for a track played at 120bpm. However this large deviation includes the outliers shown in the graph which arise during the near-loss of tracking around bar 27. Excluding these incorrect models gives a deviation of 0.056 beats over 129 data

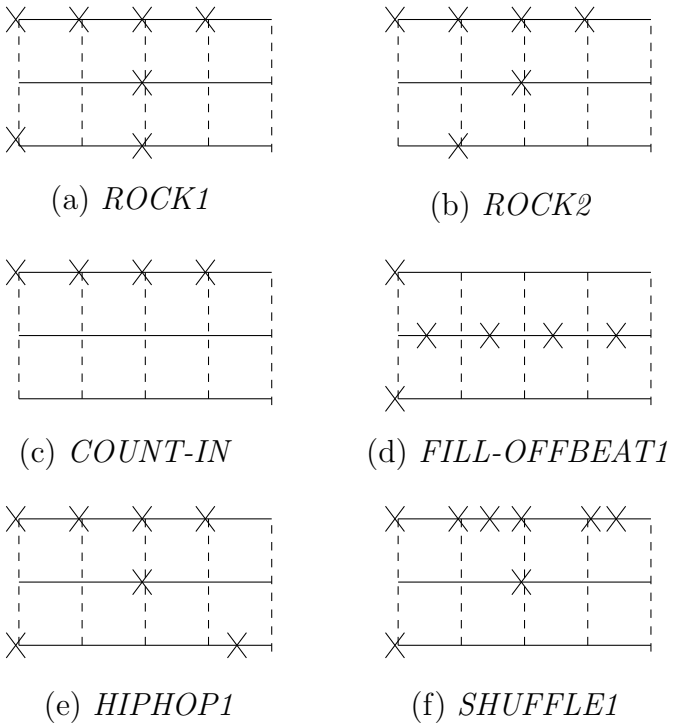

(a) *ROCK1* (b) *ROCK2*

(c) *COUNT-IN* (d) *FILL-OFFBEAT1*

(e) *HIPHOP1* (f) *SHUFFLE1*

Figure 4.10: Model-base used in the evaluation. Each model is a four-beat pattern containing hihat (top), snare (centre) and bass drum (bottom) hits. Beat positions are shown as dotted lines.

points, equivalent to 28ms at 120bpm. This is a significant (a χ^2 test gives $P(s^2 \leq 0.056^2 | \sigma^2 = 0.07^2, N = 129) = 0.0004$) improvement from the 35ms player latency above (for example if the raw onsets had been used as beat locations.) Typical home music software has a latency of around 10ms in comparison. Inspection of the worst errors shows them to occur in bars where the tempo changes within the bar rather than at the bar-line, this is of course expected as our current model assumes a single tempo within each bar.

4.4.2 Issues and extensions arising from the evaluation

4.4.2.1 Need for missing children penalties

In several cases we saw over-complex models being used to interpret simpler data. For example there is no implicit penalty for using a *HIPHOP1* model to explain a *ROCK1* pattern above. This can give unintended results, for example we saw this occur in bar 3, because there is some small chance that the extra bass note was a very early hiphop note. The problem becomes acute in cases like bar 43 where a completely wrong rhythm has been selected because just one or two notes match; and its remaining notes then deform the perception. In bar 43 it would have been better

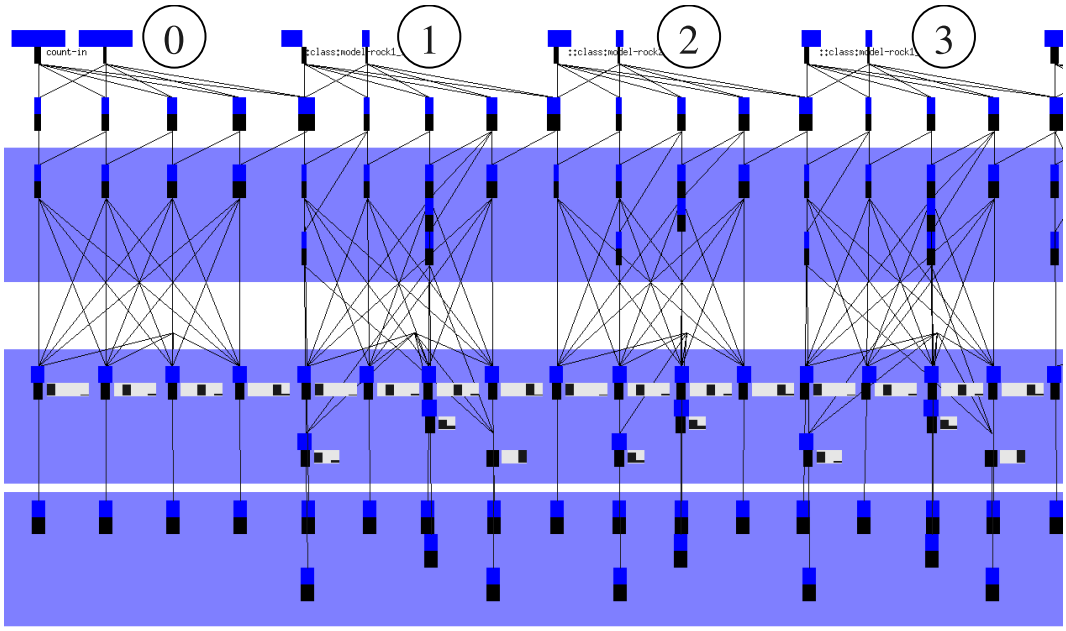

Figure 4.11: Bars 0-3 of the evaluation run. Bar zero is a simple four hihat count-in: the program is initialised with a single *COUNT-IN* model at the correct time and roughly correct tempo, much as a human musician would require. Bars 1 and 2 form a pair of *ROCK1* and *ROCK2* patterns. There is a high prior on such a transition. In bar 1, an additional bass drum hit is played on beat 4. This is is not part of the pattern so is assigned to the sink. The second bass hit of bar 3 is treated similarly.

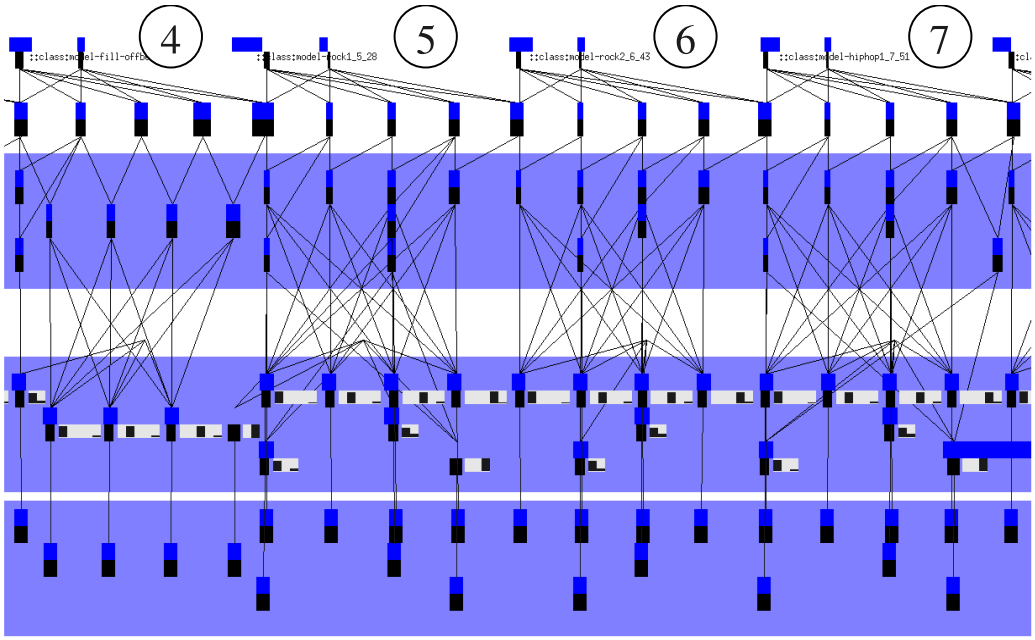

Figure 4.12: Bars 4-7 of the evaluation run. Bar 4 contains a performance of the highly syncopated *FILL-OFFBEAT1* pattern: four snare hits played between the beats instead of on them. This kind of pattern is likely to confuse conventional beat trackers that operate by looking for correlations and phase of onsets and assuming beats match strong onsets. But RhythmKitten knows this pattern is a fill, albeit with a low occurrence prior, and is able to infer the beat positions correctly. Bars 5 and 6 see another standard *ROCK1-ROCK2* pair. Note the change in s belief in bar 5: the posterior (lower half) s is later than one standard deviation away from the prior (upper half), due to the player losing time when recovering from the offbeat fill pattern.

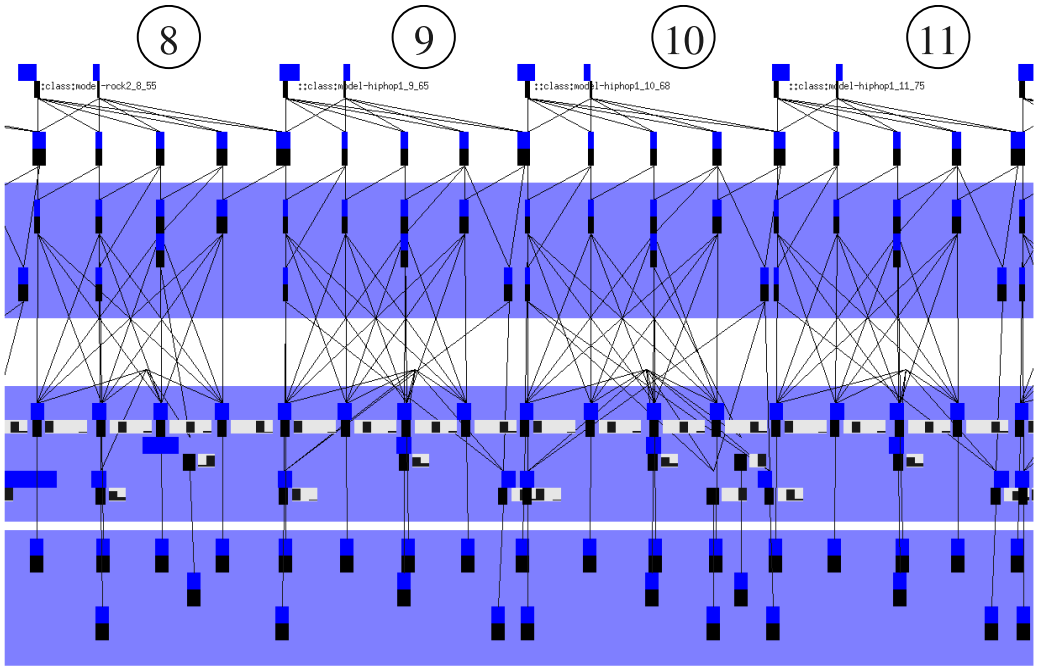

Figure 4.13: Bars 8-11 of the evaluation run. Bar 8 is a $ROCK2$ pattern, but the snare hit has been intentionally played half a beat late: it is assigned to the sink (the rightmost bar in its bar-chart). (Future work – instead of modelling such notes from the sink – might explicitly model them as played intentionally late; a human listener primed to expect *ROCK2* is likely to hear the note in this way and in fact it is this feeling of lateness that creates the laid-back mood of this pattern, sometimes called a 'lounge' beat.) Bars 9-11 switch to a $HIPHOP1$ pattern, due to extra hits at beat 4.5.

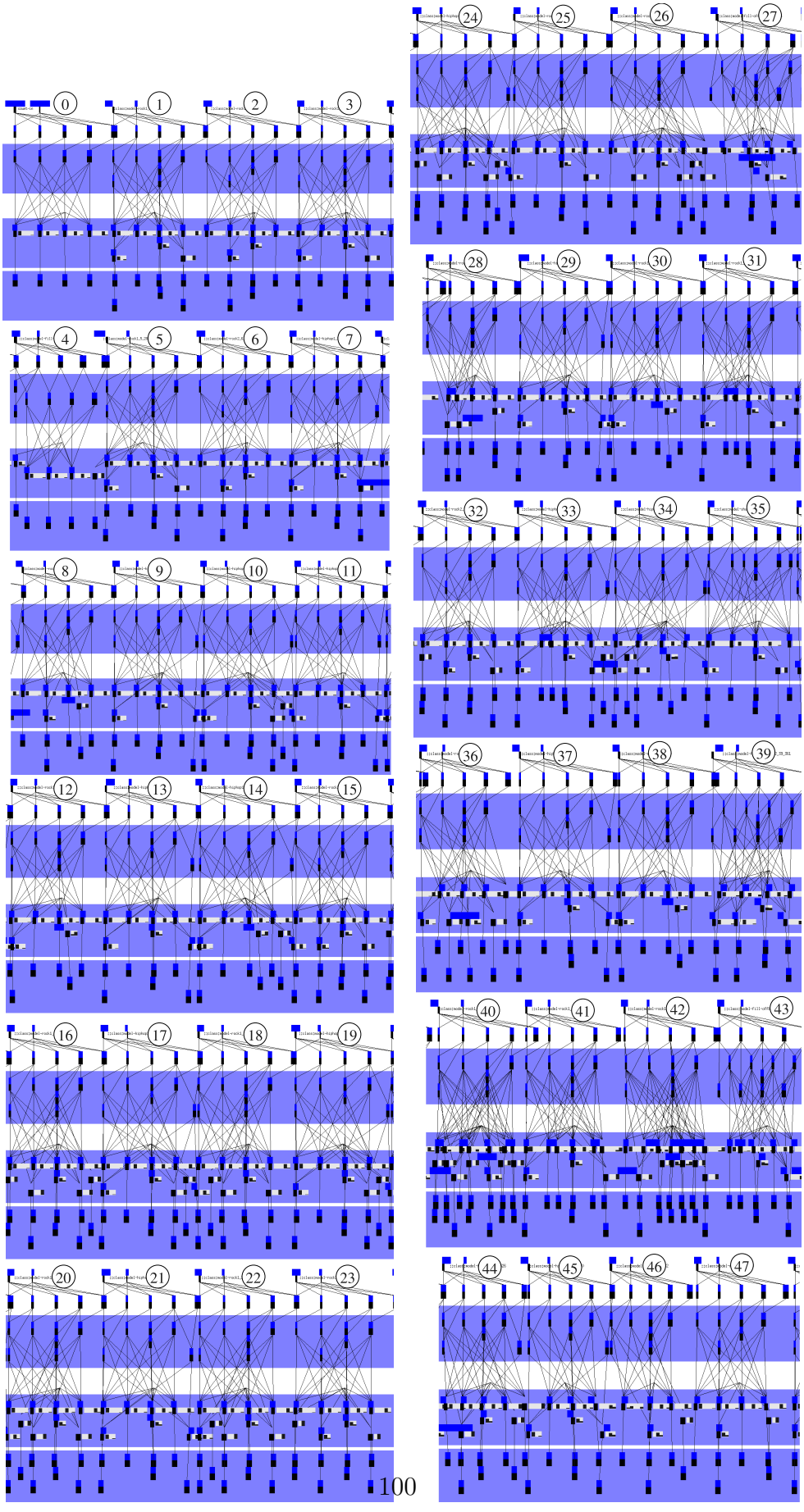

Figure 4.14: Complete 48-bar test run results.

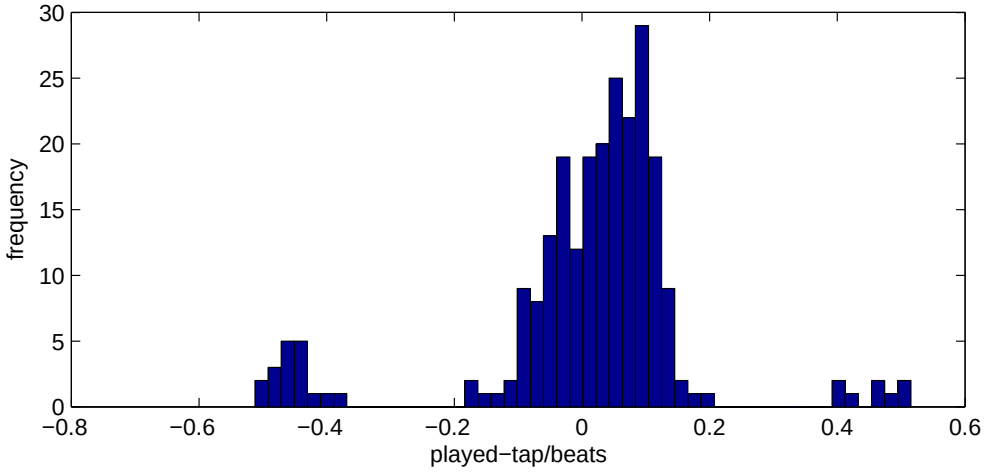

Figure 4.15: Error of played onsets from hand-tagged beats.

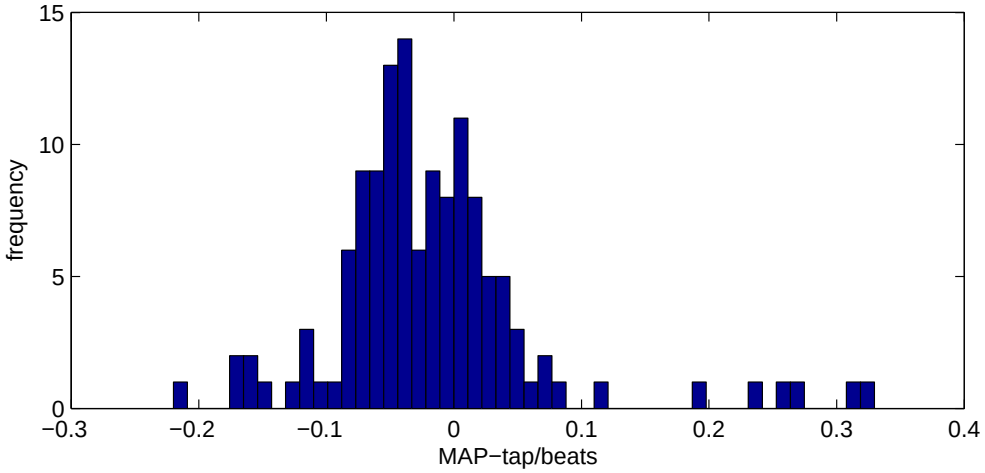

Figure 4.16: Error of played onsets from auto-tagged beats.

to select a simple standard model (like *ROCK1*) to fit the few notes. RhythmKitten could be extended to penalise models with many missing children. However the penalty should not be too strong as humans do often 'fill in' their perceptions of missing beats. For example, if listening to a *HIPHOP* beat for several minutes and a *ROCK1* bar is played, the 'missing' hiphop note will still be heard (and danced to.) So clearly missing child penalties must balance the ability to occasionally fill in against the problem of perceiving hugely over-complex patterns in very simple data.

4.4.2.2 Tempo changes in bars, and tempo priors

Music++ models tempo as changing at each event, and learns priors on these tempos using an EM algorithm run after each new performance. In contrast, RhythmKitten currently assumes that tempo is constant within each bar, and is thus unable to track gradual tempo changes. To extend RhythmKitten towards industrial performance, a more detailed tempo model should be constructed. This is conceptually simple – essentially a re-implementation of Raphael's structures – but requires additional software engineering effort.

4.4.2.3 Learning new models

This thesis is concerned primarily with Bayesian models of perception and computation on those models – but learning is always complimentary to perception and makes an obvious research extension. Learning new models is time-consuming from a software engineering point of view – so we merely discuss it rather than implement it. Future work could provide software implementations of these methods.

New concepts are usually learned as variations on existing concepts. A simple algorithm to learn new models here would be as follows. Recall the generic Cemgil prior discussed in section 4.1.1.2. A generic model based on this generative distribution should be implemented and always primed but with a low model prior. It would then be able to catch all bars that fall below some threshold of explanation by the other competing models. The particular set of note types found at subdivisions would then define a temporary new model class. As in Reis' scheme, temporary models could be given a fixed lifespan: if the model is useful and is found to re-occur then it is kept and its prior grows stronger. If it was a one-off then its prior decays and the model removed once the prior falls below a threshold.

When dealing with learned models there is always a problem that several variations of an ideal single model may be learned separately. However it would be reasonable simple to create a heuristic: a sub-task that periodically (like a garbage collector)

checks the model database for sets near-duplicates and tries to compute a generalised replacement for them. Research from classification theory and unsupervised learning could perhaps be applied here to make good heuristics.

A more advanced alternative to learning new models as specialisations of the Cemgil prior would be to learn them as specialisations of other existing models. For example, in the walkthrough we touched on the idea that patterns like the 'lounge' beat in bar 8 could be perceived as regular patterns with particular transformations applied to certain notes. Swing beats, the hiphop note (when considered as a preemption of the start of the next bar), and salsa rhythms (which play notes slightly early to drive the music forward) are further examples. Similarly, several of the bars in the walkthrough contain a standard pattern but with notes played on different drums than usual. For example the final snare hit in bar 15 could be seen as the hiphop note but 'transposed' from the bass to the snare. Future work could consider how to model these transforms and learn new models based on them. (The transposition case could perhaps be handled more easily by allowing the low-level hit classifier to report uncertainty over hit type likelihood; RhythmKitten could then change its type assignment under prior information from the rhythm model. But a more general transformational approach could capture both this and the positional movements of the lounge and swings beats described above.)

4.4.2.4 Data-model mis-assignments

Mis-assignment of data to models is not a cause of failure but is a major cause of the inability to recover from it. It prevents models from correcting themselves because they do not have access to the data points that would help the corrections.

Within models we created a system based on GMM nodes to handle uncertainty of mapping from data to notes *within* the model. A similar scheme could be used to handle uncertainty of mappings between models, though heuristics may need to be invented to prevent computational explosions. In this case, the multiplexer nodes would be replaced by GMMs with switches between models, and models of previous bars may have to be kept alive for longer to explain data pushed out of following bars.

Once multiplexers are replaced by GMMs it would also be natural to treat *rival* models in this way as well. Then information could flow between rival models. This is a more fully Bayesian approach to rivalry, however the question of whether it is useful for this application remains to be answered. (An even more Bayesian approach could be to have all rivals sharing the same set of beat nodes – this way, predictions of future beats would be formed by automatically averaging over all models. However the view of this thesis is that it is useful for perception to periodically stop and collapse its

inference to a single unambiguous explanation of the world rather than computing averaged Bayesian predictions.)

4.4.2.5 Non-Markovian priming

The Markov assumption is somewhat limiting, for example most songs contain sections of four bars which use an alternate rhythm (or 'fill') to mark the final bar. Similarly real songs contain larger-level structure such as verses and choruses that are likely to have more unusual fills to mark their endings, as these endings are important musical events. The Markov assumption is unable to capture these ideas, so if we are ever to recognise a fill, we must prime it after every bar, which can be computationally wasteful. It is envisaged that RhythmKitten could later be used as a mid-level, grid-establishing component in a larger music perception system, which could include higher-level grammatical models (such as those of ThomCat in chapter 6) that send prior messages back to RhythmKitten to prime models and specify their priors. Again such connectivity is conceptually simple but is a large software engineering task beyond the scope of the present work.

An alternate way to reduce the number of models is to prime upwards from features in the lower level data. For example, the presence of a 'late' hiphop-like beat may alert us to the possibility of a *HIPHOP* model, which may be primed and tested. Bottom-up priming is explored in chapter 6.

Like most beat trackers, RhythmKitten is currently very brittle with respect to errors of start-time phase and tempo multiples. These errors do not arise often but once they have occurred they are usually the cause of irrecoverable error, as we saw around bar 42. The standard solution (e.g. [70]) to make trackers more robust is to prime additional models with different phases and multiples. For example, at each model completion, we could prime four extra models of each type, having: phase -1 beat; phase +1 beat; double tempo; and half tempo. The obvious problem is that this would need to be done for *each* primed model type, so would increase the amount of computation by a factor of four. This may not be a problem in a code-optimised RhythmKitten but would have slowed down our experiments in the research prototype. A useful technique would be to determine when the perception is in a state of 'crisis', i.e. when the models posteriors are consistently falling below some threshold, and only then switch to this more desperate form of inference. It would also be useful to alter the annealing schedule at these time to allow a wider range of possibilities to be considered *within* the models. Both the introduction of extra primes and the higher-temperature annealing within them are examples of 'tempering' or 'high-temperature thinking': when one's perception of the world is in

crisis, one must be willing to step back and consider possibilities that are a priori more far out, in an attempt to find some new theory to make sense of the data.

For some applications it may be useful to reinterpret historical data once a crisis is resolved. For example, if grammatical priming was active, a reinterpretation of the genre of the last 8 bars could affect what types of models are considered in the future.

4.5 Discussion

We emphasise the general architecture of RhythmKitten: while an industrial system for drum tracking could be built by extending it with the ideas above and more software engineering, this is not our goal in this thesis. Rather, the aim to begin thinking about how perception in general can construct interpretations of low-level data. We take a Bayesian constructionist view: since Kant [87], we have been accustomed to the idea that the world in itself (noumena) is not available to us; rather we construct a best (phenomenal) interpretation of what reaches our senses. Kant held that the basic framework of perceptual space and time must be hard-wired in order for the process to begin: here we are presented with measurements of events in time. We then construct higher-level interpretations of those events in terms of known models. Which models are used will depend on RhythmKitten's subjective priors: if set up to expect drum'n'bass patterns then it will perceive them rather than military march patterns, in the same data. This is a useful illustration of how (phenomenal) models exist only in the head, not in the external (noumenal) world.

In making the mapping from data to model, we found it useful to employ a three-layered system, shown by the shaded bands in the figures. The lower and upper bands are the data and the model respectively, but intermediate between them is a *switchboard* layer, which deals with selecting which data to map to which model components, and with rivalry between explanations. This is unconventional in Bayesian networks, and is present because we are working with a scene perception problem in which the data-model mapping is not given a priori. We will extend the idea of the intermediate switchboard layer into the *thalamus* component of ThomCat in chapter 6.

Our modified Reis scheme regularly makes 'collapses' of the PDF to unitary interpretations. As data arrive, several competing models are active in explaining them; as time progresses the temperature is lowered; then at the end of the period the single best model is chosen as the winner and the others are pruned. Effectively, the parameters θ *within* the winning model are also collapsed to their MAP at this point as we read off the mean belief in the beat positions and export them as RhythmKitten's

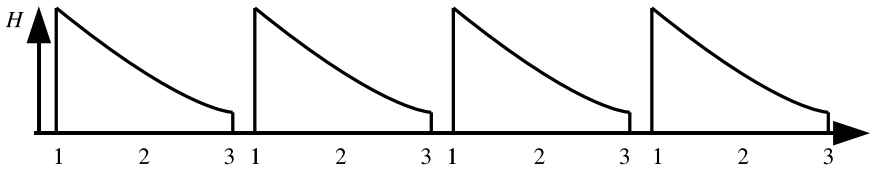

Figure 4.17: Phases of annealing cycles for perception. (1) Start of cycle, high uncertainty; (2) temperature reduction; (3) collapse to unitary coherent percept.

output (along with the name of the model type). At this point the new batch of models is primed from the winner and the cycle begins again.

Fig. 4.17 shows conceptually the three stages present in our approach, where the axes show the amount of uncertainty (H) over time. At the start of the cycle (1) several models are primed, and we are very uncertain about both the models existence and their parameters. Over time (2) inference takes place and temperature is lowered, creating a reduction in uncertainty. At some stage, (3) we make a hard decision based on our best (and hopefully quite certain) belief, and collapse the percept to a single best explanation. Immediately after this collapse, the process begins again with new primes (the diagram shows a small gap to separate the phases, but this gap is an infinitely small 'moment' in practice.) We will see these three phases reappear again in the following chapters' Gibbs and quantum Gibbs perception algorithms of this thesis.

While our proof-of-concept implementation of the variational and blackboard ideas described here is not yet of industrial quality, we have explained how and why the approach is useful for solving higher-level rhythm and beat perception tasks than those tackled by current beat-trackers. By incorporating psychological ideas of model-based perception, priming and a global workspace, the approach may also lead to clarifications of perceptual music psychology concepts and could even serve as a framework for empirically modelling human rhythm perception, especially for interesting ambiguous percepts. This thesis is about scene perception, and RhythmKitten has extended the notions of priming and pruning – that we first saw in the priming particle filter – to position-in-time models. It has also introduced the highly general concept of the annealing cycle for perception. However RhythmKitten is Markovian in its one-dimensional sequence of models and has no conception of perceptual hierarchies. It is these concepts that we next explore in a study of blackboard systems.

Chapter 5

Blackboard systems review

5.1 From sets to sequences to hierarchies

RhythmKitten used simple Markovian transitions between hand-set pairs (2-grams) of models. In the general scene perception task, non-local dependencies such as n-grams and hierarchies come into play, along with completely global factors such as the key of a musical performance or the location of a visual scene. General scenes do not necessarily consist of *sequences* of models: there may be areas of the scene which are unexplained, and models which are 'free-floating' – i.e. not part of any larger structure such as a sequence or hierarchy. Auditory scenes may allow *some* types of model to exist simultaneously at the same location, for example a chord and a rhythm played simultaneously; or two notes played simultaneously. Alternatively it is useful to think of the scene as existing in more than one dimension with non-overlapping explanations: for example, we might think of the musical score as a 2D piano-roll type grid, where previously overlapping notes now exist at separate vertical coordinates on the pitch axis. Similarly we can allow separate scene areas for rhythms and chords. This approach brings the auditory scene perception task closer to the visual scene perception task, which also has high dimensions, free-floaters, and global factors. We stress that this is part of our intention: to model the general scene perception process, not just the example minidomain of semi-improvised musical scene perception.

This chapter discusses the concepts involved in moving to general, hierarchical scene perception, and reviews existing relevant work. We will see that classic AI work from the 1970s and 1980s laid the groundwork before lying dormant during most of the Bayesian revolution – but can be usefully fused with the latter into the domain of 'Bayesian blackboards'.

5.1.1 Music-related issues

Most work on scene perception has focused on the special case of visual scene perception, neglecting other domains such as auditory and tactile scene perception, and more abstract domains such as the perception of analogies, mathematical proofs and scientific theories. While most of the visual concepts carry across to other domains, including our music minidomain, much vision work has focused on static image perception, neglecting the temporal aspect of perception which is of crucial importance in the general case. For example, in tactile scene perception, a rat finding its way around in the dark using its whiskers receives only a small about of information at each point in time, but still constructs (and presumably perceives) a complete map of its environment. For tactile scenes, active perception is important – choosing where to focus attention in order to construct the scene. Recent visual systems [13] have begun to model the movement of attention over time, in both static images (like a human moving the fovea around a photograph) and more challengingly, in video clips. However these scenes are still usually static at each moment of time: the percept is of the state of the world *at* the moment that perception is taking place. The auditory case (and video scenes, if done properly) is different: the percept is of an *interval* of time, which may or may not contain the moment that the perception is happening at. For example, in music, we are usually aware of the last four bars or so of music, and also of a prediction of what will happen next. Our percept is of an interval of time stretching four bars into the past and maybe on bar into the future. Less typically, we might 'cast our minds back' to what happened in the previous verse, in which case our percept consists of the four bars that happened some time ago, and we are mostly ignorant of what is happening around us at the time of this percept (like the absent-minded History professor oblivious to the traffic around him as he perceives some medieval battle in the past). Importantly, we may recall the past in two ways: first, by recalling the same actual interpretation of a historical event as we did at the time of the event itself; or second – and more usually – by *reconstructing* an interpretation of recalled models in terms of our *currently available* model set. For example, humans who have changed their politics towards libertarianism over the last ten years are likely to recall their teenage activism as part of their current framework than their actual teenage socialist framework: 'Yes I've always marched for freedom, it wasn't the *corporations* we were protesting against but the *government's* involvement with them', (c.f. [54]). We may also focus our perception onto the future, or onto a different place than our actual location, for example when we are making distant plans

or guessing what our friend is doing in the states right now. Most visual scene perception programmes have completely ignored this aspect of scene analysis, and the music minidomain provides a way of bringing it to the fore, as it as of unavoidable importance in our task.

Questions about creativity and 'where models come from' have an interesting perspective brought upon them from the music perception task. Previous work [56] constructed a genetic algorithm for musical composition, in which random changes were proposed to an L-system representation of a musical scene, and human listeners provided an acceptance function. The system evolved new compositions from initial, existing compositions. However a notable omission from the work was that the existing compositions had to be hand-parsed by human music experts into the L-system form. So the work of perception was pushed out of the system onto human pre-processing, along with the work of artistic judgement. The supposedly 'creative' composing stage of making random changes was much easier to automate than the two listening (parsing and acceptance) stages. There is a great similarity between the two human stages: they both involve perceiving the music as a hierarchy, that is, they are musical scene perception tasks. They both require creativity in the sense of choosing what models to use in the percept – whereas the automated composing stage only shuffles around these models. So there is a sense in which good listening is harder than composing – and good perception in general may form the hardest part of creativity.

5.2 Blackboard systems

Many constructionist ideas were realised in the classic Hearsay-II speech recognition system [51] during the 1970s. Hearsay-II was designed to recognise sentences from a known simple grammar and a 1000 word vocabulary. It operated by first performing a heuristic hard segmentation of the audio signal into syllables (analogous to our hard segmentation of music into bars) then assigned a likelihood vector $P(segment|syllable)$ to each segment (analogous to assigning chord likelihoods to bars of music, for example). A probabilistic grammar was used to define probabilities of the segment sequence under all possible sentences. Rather than instantiate all possible words and sentences in all possible positions, hypotheses are primed in various ways when they may be useful. Priming schemes include bottom-up (for example, a syllable with likelihood above a threshold primes all possible words that contain it); top-down (a sentence primes word hypotheses); and sideways (a word primes neighbouring words from 2-gram probabilities). Likelihoods are propagated

upwards through the hypotheses, in a similar style to the Inside-Outside algorithm. When no more hypotheses can be created, or the program runs out of resources, there may be one or more complete sentence hypotheses on the blackboard that explain the complete data set (all others are ignored), and the one with the highest probability is chosen as the winner. (The authors mention other prior probability sources such as priors on what sentences are common in the domain, which can convert the propagated likelihoods into posterior beliefs.)

The likelihood propagation used is both a strength and a limitation. Its strength is that it is a tractable exact probabilistic algorithm (given the model that is constructed heuristically). Its weaknesses are critical in the general scene perception problem (including our music task), outside the limited domain of speech recognition. First, there is no allowance for global factors, such as the global musical key or the location of a visual scene. Second – crucially – the use of a limited grammar prevents the perception of free-floating objects. In speech (at least where the generating grammar is known exactly) this is not a problem, as sentences are single entities which fill the scene exactly from the start of the data to the end of the data. But other scenes do not have such a global grammar – at least not of tractable size. For example, a grammar which specified all the possible positions of houses in a photograph would need a huge number of rule applications to do this. (It could be done with few rules, using recursive rules, but the likelihood propagation would no longer work in that case.) In music, we must allow the possibility for non-grammatical events to occur free-floating, for example it is possible for a player to insert an extra bar on the fly. Initially we must perceive this as exactly that – as an extra bar free-floating between a *VERSE* and *CHORUS*. Once we have done this we may proceed to consider learning a new rule *SONG→VERSE,EXTRA-BAR,CHORUS* to better explain the floater. Music is less grammatically rigid than speech, so we must emphasise such possibilities. (Though they do also occur in speech, for example when we are first exposed to new regional dialects and grammars that need to be learned.)

Hearsay-II thus appears to have the same grammatical power as the inside-outside (IO) algorithm, i.e. it makes inferences about SCFGs. It is a heuristic approximation to IO as it uses thresholds to prime only locally probable hypotheses, whereas IO considers all possible hypotheses at each start and end location. As such, it may be seen as essentially the same algorithm as the Early parser [50], which likewise uses priming heuristics (taken from standard symbolic chart parsers) to restrict the inside-outside hypotheses to be tested.

Two further criticisms of the SCFG approach in general – including Hearsay and Earley-like methods – are as follows. First – like our rhythm segmentation and

Raphael's onset detector – they rely on initial hard segmentations of near-continuous input data to convert it into a sequence of symbols. This appears to be wasting information, as no top-down information can be used to guide the segmentation. Ideally, segmentation and parsing should occur simultaneously, and inform one another. However this is an open and probably intractable problem, as the space of possible segmentations is $O(t^N)$ where t is the number of discretised time steps and N is the maximum number of allowed segment boundaries. t is generally very large, for example speech may be sampled at 8000 steps per second. (Though it may perhaps be possible to use some form of coarse-to-fine search to approximate the segmentations in the future?) In vision too, the idea of hard initial segmentation is popular, for example [99] where good results have been achieved without the need for top-down segmentation priors.

The second, more serious problem is that the SCFG approach to inference does not generalise to multiple dimensions. IO and its relatives all exploit the fact that each hypothesis has only two parameters: its start and end times; hence there are $O(Ns^2)$ hypotheses to consider, where N is the number of models and s is the number of segments. However objects in spaces of two or more dimensions do not collapse into such a simple parametrisation. A shape in a 2D image or spectrogram can have many corners whose positions would all be parameters. Even highly symbolic representations of music tend to have at least two dimensions, to allow for multiple notes to be active at the same time. The centre-surround algorithm [149] used IO extended with an EM algorithm to perform 2D parsing, where each area is subdivided by a line at an EM-optimised angle. Position-encoded dynamic trees [151] similarly provide 2D parsing, assuming each node is modelled as the centre of a Gaussian which generates a cluster of children, and a fixed number of nodes with probabilistic connections between them – this approach does not use SCFG semantics but models images in a similar spirit (variational Bayes was used to approximate the NP-hard inference problem).

Hearsay-like blackboard systems have been applied heavily from the 1980s to the mid 1990s by a group of researchers now associated with the IET Corporation, in scene analysis domains including production line object recognition, medical imaging and military battlefield analysis. [10] summarises the general principles used by these systems, which include: hard segmentation; interest-point detection; use of the segments and interest points as leaf nodes on the blackboard; and highly loopy graph structures dynamically constructed to explain the scene. Much of this work was done before the 'inference revolution' so heuristic approximations to the Pearl equations were used in the loopy graphs, rather than principled modern approximations such

as mean-field and Monte Carlo methods. The work is also notable for introducing the concept of utility of *perceptual* actions into scene perception: many of their systems are real-time so computation is a limited resource. Priming heuristics were augmented with discounted expected utilities [100] which compute the approximate expected utility of the prime, by considering what top-level objects (e.g. tanks) the prime could lead to, and how useful it would be to recognise those objects at the expense of computation time.

5.2.1 The Copycat approach to scene perception

Inspired by Hearsay-II and methods from Statistical Mechanics, Hofstadter and colleagues constructed a series of models [81] during the 1980s and early 1990s leading up to the Copycat model. Though descended from the same influential Hearsay project, the Copycat models have developed largely independently and in parallel to most mainstream AI research, which has led to a confusion of terminology between the two communities and under-appreciation and misunderstanding of each others' work. One of the aims of this thesis is to correct this misunderstanding: the ThomCat model developed in chapter 6 will draw heavily from Copycat but will be derived entirely from modern Bayesian AI ideas: by doing this we will demonstrate the similarity of the two approaches and show how concepts may be translated between them. It will emerge that many supposedly 'modern' ideas in the AI community are pre-dated by Copycat and the other blackboard systems reviewed here.

Hofstadter's training was in Statistical Physics, so he was familiar with Ising models, Gibbs samplers and simulated annealing at a time when most of the AI community was still working with symbolic methods such as theorem provers and Prolog. For example, [80] refers to all of the above concepts by name (and also makes the connection to the 'Boltzmann Machine', an early name for Ising Models/MRFs used by the neural modelling community). Following the general Physics approach, Hofstadter tried to construct an artificial ('laboratory') setting for the scene analysis task, which simplified it to its bare, more easily observable essentials. This is the microdomain approach.

In Copycat, the chosen microdomain is the perception of short sequences of letters, for the task of making analogies between them. i.e. the task is essentially to try to perceive pairs of strings in the 'same' way. Copycat has been of interest to dedicated analogy researchers, but this thesis views the analogy-perception as a microdomain of general scene perception. Copycat's scenes consist of sets of letter strings, and the task is to perceive them so as to have similar parses, and 'fill in' the missing percepts.

However, the specifics of the analogy task may distract more general scene perception researchers, so we will examine one of Copycat's simpler predecessors, Numbo, in its place.

5.2.2 Numbo: an example of the Copycat family

Numbo solves the mathematical game of *Le compte est bon*, also known as 'the numbers game' on British television's *Countdown* game-show. The player is given six integers between 1 and 10, and a larger target integer between 1 and 500. The goal is to combine the given integers using the operators $\{+, -, \times, \div\}$ into an expression which evaluates to an integer as close to the target as possible. Each number can only be used once in the expression, and there is a time limit of a few minutes.

While it is probably possible to solve the problem with a brute force tree-search method on a fast processor, this approach would not scale to larger problems, and does not appear to be how humans solve it. Rather, we use our powers of 'perception as' to guide our search though the space. We maintain a 'knowledge-base' of rote facts about small numbers (such as '6=2×3', a fact about the number 6) and about certain classes of large numbers (e.g. 'numbers ending in 5 are divisible by 5'). These allow us to perceive number *as* playing roles within these facts. For example, perceiving the number 2 *as* 'the number which, when multiplied by 3, gives 6'. We use certain well-known numbers as 'landmarks' or intermediate solutions. For example, if the target is 128, it is useful to try and make 100 first to get into the right 'ball park', because we know many facts about 100. The facts are heuristics used to guide the search. If we have the number 6 available this may prime 2 and 3 because they occur in a fact with 6; if we seek 128 and we know the fact '128 is a power of 2', then 2 will be primed again – so we make a connection, and will now become very interested in thinking about how to make a 3. We have started to perceive 6 and 128 *as* powers of 2. We are constructing a 'mathematical scene' containing objects (instantiated numbers and operators) that eventually make up the required expression. Unlike visual and auditory scenes, this scene exists in an abstract space rather than Euclidean space or time. However this space still has many general properties such as: rivalry – a number cannot be used twice in the derivation, so different percepts of it must compete to 'explain' it; and the unitary coherent requirements of the solution.

The Numbo architecture seeks to simulate this mathematical scene perception process. It consists of three main components, which are general across the whole Copycat family of models. First, a *slipnet* stores permanent known (non-parametric) models. These include numbers and models representing rote facts about them. Weighted

association links are maintained between concepts. (The Copycat models do not address the issue of how to learn such models, instead they are hand-coded.) Second, the *workspace* is an area of memory where object instances of models can be placed. Objects may be 'explained' by instantiated mathematical relations connecting them. Construction, connection and removal of model instances is performed by the third structure, the set of *codelets*. The workspace always represents the current best solution, in terms of parts of the final expression tree that are under consideration.

When models are instantiated on the workspace, their activation in the slipnet increases and spreads to neighbouring models via association links. Construction agents select random highly-active models and try to instantiate them on the workspace – a form of priming. For example, if 128 and 6 are instantiated and active, the number 2 and the relations '$\times$' and 'power of' will become active and may become instantiated as 'explanations' of the previous objects. If explanations are already present, these new instantiations are rivals. Heuristic 'energies' are defined to measure the quality of explanation, and rivalry is resolved by taking the lowest energy option (though with an annealing-like acceptance system to allow escape from local minima).

The percept is thus constructed by small codelet changes, changing a lot at first, and stabilising into a solution. Temperature is controlled by simulated tempering: unlike simulated annealing, it forms a feedback loop with the system; if the system becomes stuck in a local minimum and shows so signs of changing, the temperature is increased until it can escape.

Substituting 'blackboard' for 'workspace', and 'knowledge base' for 'slipnet' and 'priming and pruning heuristics' for 'codelets', the Copycat/Numbo architecture can be seen as a blackboard system running something very similar to Gibbs sampling with simulated tempering.

5.3 Blackboards in musical scene perception

5.3.1 Pre-Bayesian blackboard music models

The blackboard architecture has been applied to low-level music perception in attempts to build automated polyphonic transcription systems. This task is to recover the notes from a recording, offline, as accurately as possible. It is complicated by the fact that notes are made of harmonics, some of which may be missing, and it must be decided which harmonic belongs to which note.

Early work was done in Japan by Katayose and Inokuchi [90] but is not available in English. The Machine Listening group at MIT continued Katayose and Inokuchi's

approach [106] [107]. Their model base consists of track, partial, note, interval and chord models. 'Track' here refers to the raw DFT or AR-like spectra, hard-segmented by bottom-up methods as in chapter 3. Like Numbo's codelets, they employ around 20 'agents' which bring models on and off the blackboard, depending on its current content. (However there is no concept of spreading activation – rather the experts preconditions are tested in a simple cycle until one of them is triggered to act. This simple scheduling does not scale. Probabilities are not used, instead there are various ad-hoc 'ratings' and thresholds. The closest concept to activation is heuristic 'sources of uncertainty', which tag blackboard elements, and instructs other experts to ignore them if they are very uncertain.) The system can transcribe simple polyphonic tonal music which has been synthesised by a known piano synthesiser (so the exact generative model of the note harmonics is available). Like humans, it has difficultly distinguishing between octaves, so is limited to a two octave range. The system is intended as an extensible proof of concept, not a full solution.

The OMRAS project [46], [6], [7], [128] takes up such an extension of the MIT transcription work. As in the MIT systems, segmentation is hard, onset-based, and bottom-up only; and ad-hoc non-probabilistic 'ratings' are used to score hypotheses. For priming, they add an MLP neural network which hash-classifies 256-point DFT frames *directly* to a bank of top-level chord hypotheses – bypassing the causal chain (DFT←track←partial←note←interval←chord). The intermediate structures are then constructed top-down from the chord hypotheses. The MLP acts as a cheap priming device; more rigorous (though non-Bayesian) work is then done by the 'experts' to fit these models in more detail. It appears to be a small step to make a Bayesian system from this architecture, though this has not yet been done. The interesting innovation here is the demonstration that priming does not always need to be local. This quick-recognition-plus-top-down-fitting scheme seems to fit well with human experiments (e.g. [73]) which show human transcribers tend to recognise chordality first, before fitting (or simply making up) individual notes.

Reis [142] worked in the domain of higher-level music blackboard perception, assuming a series of symbolic notes was available, and grouping them into hierarchical structures. Frequentist probabilities were used to score competing hypotheses, based on actual counts of previous occurrences. 'Agents' competed for positions on a unitary blackboard; as in RhythmKitten, rival agents were allowed to remain active until they completed, then competition and pruning of losers was performed. As in RhythmKitten, this is a heuristic that gains speed at the expense of long-range correlation modelling. Reis' priming was from all possible explanations and children of active agents using an inverse dictionary. Reis' agents have no domain knowledge: all

symbols appear the same to them, and they simply respond to repeated sequences of symbols (and recursively, to sequences of lower-level agents). The same domain of symbolic pitch sequences is used in the recent Copycat descendant, *Seek-Well* [94], [122]. Unlike Reis agents, Seek-Well agents have some musical domain knowledge, such as preferring notes from the tonic chord of a key, and preferring to perceive pre-defined structures such perceptual musical 'forces' of 'gravity, inertia and magnetism' that have been identified by Music Psychology [94]. At the time of writing, the detailed design and implementation of Seek-Well is in progress.

5.3.2 Dynamic Bayesian network music models

Recent music models have used explicitly Bayesian models to perform blackboard-like tasks, but using dynamic-state Bayesian networks rather than position-in-time blackboards.

Kashino and colleagues [88] used a two-level HMM structure to perform recognition of notes and chords from audio. Audio was bottom-up hard segmented as usual, and each segment treated as an observation. A particle-filter-like scheme was used to prime and prune hypotheses at the note and chord levels (top-down, bottom-up and sideways), which is reminiscent of blackboard knowledge sources. The Pearl equations are used for inference on the active hypotheses. This system is of interest because it illustrates a mixture of Blackboard position-in-time and DBN dynamic-state architectures. In later work [89], lateral connections were made at the note level as well as the previous chord level, leading to a loopy DBN: in this case standard Gibbs sampling was used for inference after the hypothesis priming step.

Cemgil [21] used a similar approach to perform more detailed polyphonic transcription up to the note level, and cast the problem explicitly as a 'switching' Kalman filter with pruning heuristics. Researchers at Cambridge [68] dropped the temporal dependence between arbitrary short audio frames and used reversible-jump MCMC (RJMCMC) to explore the space of note sets in each independent frame, using a finely detailed note model including variable partial harmonic frequencies and amplitudes. The RJMCMC kernel is tailored to the particular problem, and includes musically-meaningful proposals such as adding and removing whole notes, partials, changing overall note pitches and detuning partials. It forms another example of bringing blackboard-like priming knowledge into the DBN framework. (This approach could be easily extended by restoring the temporal links and Rao-Blackwellising the time-steps using the RJMCMC within each step and standard particle filtering between steps.)

A Hearsay-like blackboard approach has been used recently in the linguistics community, together with MCMC sampling, under the guise of data-oriented parsing (DOP) [14]. We have not discussed most work in linguistics because of the special cases it presents: in particular, the absence of the ungrammatical free-floaters which are common in more general scene perception. However DOP can easily be extended to allow this. DOP postulates that language is parsed as collections of known grammatical *chunks* rather than single rules. These chunks form a hierarchy, and must be fitted together like a jigsaw puzzle to make a parse. Like most jigsaw puzzles, this is an NP-hard problem, and loses the classic SCFG exact polynomial algorithms – though gains the ability to represent a stronger class of language. Inference in DOP has been run with various algorithms, including approximations to Viterbi and various MCMC algorithms. These sampling algorithms are of interest because they again begin to look very much like Copycat-style blackboard systems. DOP has been applied to parsing similar symbolic melodies as input to Seek-Well and Reis' agents [15]. We note that, coming from linguistics, it aims to parse scenes into complete 'sentences', made up of known fragments. In contrast, general scenes must allow free-floating objects. However this approach could lend itself to free-floating extensions if we allow a non-zero probability of non-sentence level hypotheses to exist without parents.

5.4 Inference algorithms on Bayesian logics

While not specifically aimed at scene perception, interest in Bayesian logics and inference algorithms on them using dynamically constructed networks has recently appeared in the Machine Learning community. Classical symbolic AI represented hard, true facts by symbols, with no scope for uncertainty. Theorem-proving methods were used to make hard inferences in response to queries, using heuristics to guide the search through the space of possible proofs. Bayesian logics conserve the use of symbolic logics (for example, first-order schemes representing objects and relations between them) but then use them as domains over which to define PDFs.

In inference algorithms on Bayesian logics, the old search heuristics may become priming schemes; statements about symbols and relations may become network nodes; and proof methods such as unification may become the basis for linking the nodes together. Posterior beliefs over query formulae may then be computed from the constructed network.

Early work with standard diagnostic Bayesian networks soon found that it was tiresome to manually specify networks by hand for tasks which shared similar enti-

ties. [69] presented a human-writable language for specifying network fragments corresponding to entities, from which situation-specific networks could be constructed.

Object-oriented Bayesian networks (OOBNs) [93] formalised the entities described by these fragments into classes, including 'is-a' and 'part-of' relations. This representation ensured that each class had a well-defined encapsulating interface, allowing inference algorithms to automatically construct BNs for queries regarding properties of objects.

Multi-entity Bayesian networks (MEBNs) [95] describe network fragments which do not necessarily correspond to classes. Conditions for joining fragments together are given by logical terms: two or more fragments can be joined if these terms are unifiable. As there is no longer any clean-cut notion of encapsulation (because fragments, like DOP's linguistic fragments – can be any shape and size, and overlap heavily), noisy-OR and similar rules are needed to specify how priors from multiple fragments should combine onto a common child.

As with OOBN inference algorithms, MEBN inference algorithms can construct a standard BN in response to a query. For ideal inference on MEBNs, fragments are retrieved and unified until observed nodes make the query nodes independent from the rest of the network. In practice, domain-knowledge-based priming heuristics may be used to limit the construction. The standard junction-tree algorithm may be used to perform inference on the BNs constructed from OOBNs and MEBNs.

Similar recent Bayesian logic systems include probabilistic relational models [66], the relational OOBN extensions implemented by SPOOK [127], and BLOG [110].

5.5 Summary

Excluding special cases such as certain linguistic 'scenes' which have single roots, scene perception is generally an intractable task, so some kind of heuristics must be used. In Blackboard systems the percept is *constructed* dynamically, using the partial results of inference to guide the construction, to explore interesting areas in more detail, once they are believed to be interesting.

Most of the models discussed feature the now-classic tripartite blackboard architecture. First, a symbolic knowledge base such as a grammar, logic or semantic association network, is used to look up primes – i.e. related hypotheses to those currently under consideration – in the manner of a hash-table. Second, a blackboard is used as a central place in which to construct the percept. At the end of inference, the blackboard should contain a unitary coherent percept; during inference it may contain rival alternative hypotheses, as in populations of particle filters and genetic

algorithms, Gibbs samplers at high-temperatures, and Pearl-like spreads of belief until the MAP result is selected. Third, a set of priming and pruning heuristics (sometimes called 'agents') are used to control the application of the knowledge base to constructing the network. In very small tasks it may be possible to construct the exhaustive set of all possible scenes, though in general, thresholds are used to limit where to make constructions. Goal-based systems may use heuristics which approximate the value of information from the construction. Priming is usually performed in a local sense, with nodes priming parents, children or rivals – though some systems such as OMRAS allow hash-table priming direct from very low to very high levels. Any hash-classifier can be used for priming if it proves empirically useful. Pruning generally consists of removing nodes which have low beliefs, sometimes only if sustained over time.

All the systems run using symbolic information, typically extracted from near-continuous input (e.g. an audio or radar stream) using bottom-up hard segmentation in the manner of RhythmKitten's bar-line output and Raphael's hard HMM onset output. An open question is whether top-down information can be fused into the segmentation, performed simultaneously with the scene analysis – though this appears to be intractable due to the huge space of possible segmentations. Further heuristics may however be possible to obtain useful improvements.

In early work, inference was performed approximately, using heuristic 'rankings' or 'ratings' of hypotheses, which can be thought of as approximations to posterior beliefs. Hearsay-II used real probabilities wherever possible; Copycat's system is essentially Gibbs sampling so does not experience problems with loopy propagation like Hearsay. These models were built before the invention of the junction-tree algorithm, which is now often used as the standard inference engine. In real-time inference, the notions of attention and temperature become important in many domains. Attention trades off the size of active inference in an area of the scene for accuracy in computation there. Temperature arises in relaxation methods such as annealing and tempering; again, a slow schedule will give more accurate results at the expense of computing time and hence size of attention.

Human perception varies according to goals. Some models – such as Bayesian logics – construct entire networks on the fly, from scratch, in response each new query. This means that only inference relevant to the query is performed. However in the real world, we can usually expect a series of related 'queries' about what actions to take to occur over time, and rather that construct a whole network from scratch each time, it appears to be useful to construct and maintain an ongoing, unitary coherent percept of the scene which may be used to answer a range of likely queries. Such

a scene percept is still goal-directed, but in the more general sense that is directed towards a set of possible future goals rather than a single logical query.

This chapter has provided a unifying review of a wide range of fields, developed by different communities using very different languages, but using similar architectures. Where domain-unspecific changes have occurred, they have mostly been in the inference methods used within the networks: the early IET work introduced the Pearl equations; Copycat introduced Gibbs inference; more recent models have used junction trees. The DBN community has reconstructed many blackboard ideas by designing custom Metropolis-Hastings kernels that are equivalent to priming and pruning heuristics, and drawing the states of system in HMM-like diagrams rather than position-in-time blackboard diagrams. Although the basic blackboard concept has changed little over the years, it has been re-invented and extended under new names many times. There is much to be gained by providing a unified view of blackboard systems using contemporary Bayesian language: this will allow the different communities to see their ideas in a common framework; and will allow the power and wide selection of modern inference algorithms to be fused with classic architectural ideas. This chapter has contributed a unifying qualitative review to this end. The next chapter will make this view more concrete by deriving a new Bayesian blackboard system, ThomCat, from Bayesian network principals to show quantitatively how the blackboard ideas emerge from well-defined Bayesian heuristics. It will show how a Copycat-like system emerges naturally from these heuristics and Gibbs inference. Bringing Copycat-like systems into the Bayesian framework then allows alternative inference algorithms to be used, and as examples we will demonstrate variational Bayes and cluster sampling in addition to standard Gibbs sampling.

Chapter 6

Perceptual construction and inference in Bayesian blackboards

The text of this chapter is based on the peer-reviewed publication [58]:

- *C. Fox.* ThomCat: A Bayesian blackboard model of hierarchical temporal perception. In *Proceedings of the 21st AAAI International Florida Artificial Intelligence Research Society Conference, 2008.*

Two musical perception systems have so far been constructed in this thesis. The first was non-hierarchical, a priming particle filter for following deterministic musical performances. This is a highly limited domain as it assumes that the structure of the scene is known entirely in advance, up to tempo changes. However it allowed us to construct a first Bayesian network and to illustrate the use of sampling inference. It also demonstrated the concepts of priming and pruning to control the search space and allow recovery from mistakes by allowing for a heuristic probability of its own error. Becoming less deterministic, RhythmKitten then considered the use of limited-depth hierarchical models in semi-improvised rhythmic scene perception. RhythmKitten introduced simple structural generative models (i.e. tempos and beat positions generating played and heard notes), and extended the previous priming and pruning ideas into a simple blackboard system based on Reis' [142] symbolic agents algorithm.

This chapter will generalise further to fully hierarchical semi-improvised musical scene analysis. It considers the minidomain task of online perception of semi-improvised chord sequences. These are sequences generated from an almost-known probabilistic context *sensitive* grammar. In contrast to RhythmKitten, which used discrete models chained together in a sequence by a Markov process, we now allow for models of structure at arbitrary levels such as bars, riffs, verses and songs, and fuse the models into a single dynamically-constructed Bayesian network. Scene perception

here means explaining the data in terms of the presence of these hierarchical structures. 'Almost-known' means that we allow for the possibility of new rules being used in the performance that are not previously known to be in the grammar. This setting is typical when listening to a new composition in a known genre. For example, in popular music we may maintain probabilistic rules such as *SONG→VERSE,CHORUS, VERSE,CHORUS;p=0.6* and *SONG→VERSE,CHORUS,VERSE,MIDDLE8,CHORUS; p=0.4*, showing that we expect most songs to follow one of these standard patterns with prior probabilities p. Similarly we may have *VERSE→A,B,A,B;p=0.4* and *VERSE→A,A,A,B;p=0.6* indicating two well-known verse forms (where A and B are arbitrary substructures). The grammars bottom out with terminal chord symbols, of which we have uncertain observations.

Context sensitivity arises where there is a global (but not directly observable) musical key which makes all chords mutually dependent. Due to this sensitivity and the requirement to allow for new rules, standard natural language processing techniques such as the inside-outside algorithm lack the power to model this domain. Our concept of 'semi-improvised' is thus extended beyond the Markovian bars of RhythmKitten, to allow the performer to generate chords from an almost-known probabilistic grammar with global context. The concept of accounting for one's own fallibility from the priming particle filter is carried over to the 'almost-known' nature of the grammar: again we must allow for things happening that we are unable to model with our current knowledge – and perhaps try to learn new knowledge from these occasions. Again, standard parsing methods are unable to do this.

We describe a proof-of-concept system, ThomCat, which implements these ideas. It will emerge that the behaviour of ThomCat is very similar to that of Hofstadter's Copycat family of models, however we will derive it from more rigorous Bayesian principles in contrast to the many ad-hoc heuristics used in Copycat. We view Copycat as a pioneering exploratory model – ThomCat (named after Thomas Bayes) is intended to build a more solid, rigorous structure on this ground. It also shows the way for fusing other recently developed inference algorithms (such as Bethe propagation and variational Bayes) with Copycat-like scene construction architectures.

Like RhythmKitten, ThomCat is a position-in-time model, in contrast to hierarchical dynamic-state models such as HSMMs. As discussed in chapter 5, the two types of structure can be made equivalent but we hold that position-in-time models are more intuitive to work with, and could provide useful insights about real cognition.

ThomCat assumes that a sequence of bars containing chord likelihoods is known. For example, this could be obtained by segmenting the bars with RhythmKitten, then computing chord likelihoods as in the priming particle filter's likelihood model.

It appears that this kind of pre-segmentation, while not Bayes optimal, is extremely useful in reducing the complexity of inference.

The priming particle filter and RhythmKitten included increasingly complex notions of *attention* and ThomCat continues to extend them further. The priming particle filter was a dynamic-state model, running forward inference only. As such, its only question is "what is the state of the scene *right now*?". Dynamic-state models such as Raphael's HMM [131] extend this slightly by including a short backward pass, asking "what is the state of the scene right now and in the 100ms window before now?". Position-in-time models, in principle, can answer queries about events occurring at *any* time in the scene, though in practice inference should be limited to a *window of attention* if the system is to run in real-time. We restrict on-line inference to a window around the current time, 'freezing' the results of inference outside it. This is a simple version of a 'window of attention', and gives insight into how attention and reconstruction of the past could operate in other domains.

ThomCat currently uses Gibbs sampling similar to Copycat, but improved to exploit independence of causal influences (ICI) using cluster sampling. As the architecture is brought into the graphical models framework, this opens the way for other inference algorithms to run on the same structures, which we demonstrate. The 'almost-known' allowance for unseen rules to be perceived in terms of their known parts gives a framework for online learning of new rules as well as Hebbian-like learning of rule probabilities, discussed in section 6.3.2. Section 6.3.1 will further discuss how the architecture could be extended to bias perception according to action selection and rewards. Again, learning and action can be discussed in the Bayesian framework that ThomCat provides for Copycat-like models.

The goal of this thesis is not to perform efficient inference on a serial desktop PC, but to give a detailed, quantitative and plausible account of the general scene perception process. The implementations used here are proofs of concept, illustrations, and are used as tools for the encouraging of clear thinking during the development of the algorithms, but are not strictly part of the thesis itself. That said, we hope that future implementation of many parts of the algorithms will be useful for practical musical tasks. This thesis uses the computer to illustrate a distributed model of the perceptual process. All of the inference architectures simulated in this thesis are inherently distributed and would perform best on parallel architectures – we could imagine fast FPGA or biological neuron implementations.

In common with many scene perception domains, the music minidomain contains some representational complications concerning hypotheses of variables sizes, so before introducing the full musical task we will consider an even simpler microdomain

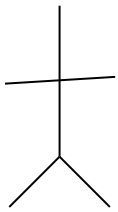

Figure 6.1: A single complete matchstickman.

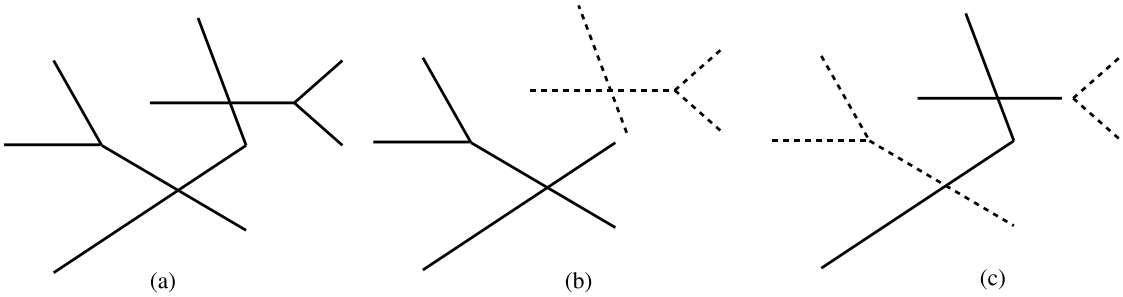

Figure 6.2: (a) An ambiguous scene. The task is to interpret it in terms of non-overlapping matchstickmen. (b) A good interpretation: two complete matchstickmen and no clutter. (c) A poorer interpretation: two incomplete matchstickmen and two clutter lines (dotted).

to help fix ideas about network construction and inference. We have construed an extremely simple visual perception task, the Matchstickman problem, to illustrate the basic architectural ideas that will be used in ThomCat. Such a domain also serves to reinforce the point that the general architecture proposed here is transferable to many forms of scene analysis such as vision, not just the musical minidomain.

6.1 The matchstickmen microdomain

The matchstickman microdomain is a simple 2D scene analysis task, similar to the famous Necker cube rivalry. The scene is comprised of a number of matchstickmen, each made of four lines, as shown in fig. 6.1.

Some of the lines may be missing, and extra *clutter* lines may be present. Lines may not be shared by multiple matchstickmen. The task is to find the most probable interpretation of the scene, assigning lines to hypothesised matchstickmen or to clutter sources. Fig. 6.2(a) shows a scene. Fig 6.2(b) shows its best interpretation; fig. 6.2(c) shows a sub-optimal interpretation in which there are two men each with some missing parts and two clutter lines.

Figure 6.3: Matchstickman template showing cues. Cues are located in the scene and used to instantiate instances of the template as hypotheses for testing.

The matchstickman domain is simpler than ThomCat's music domain because there are only two levels of hierarchy: lines and matchstickmen. In the music domain there are many levels of hierarchical hypotheses, and dealing with rivalry between them is more complicated. Music examples grow large very quickly and are harder to understand and debug. The scene perception networks introduced here will carry over to the music domain, with observed musical bars analogous to visual lines; and musical structures analogous to visual matchstick men.

6.1.1 Hypothesis generation by priming

Unlike standard inference problems, we are not initially given a graphical model – we are only given the low level data. This is a set of lines $\{l_i\}$. The first task is thus to construct a graphical model, using cues in the data to prime hypotheses (i.e. candidate matchstickmen). The psychological literature suggests that low-level surface features are used to create hypotheses, so we follow this approach. As in the priming particle filter, we use informative low-level features (cues) to heuristically hash to (prime) sets of candidate explanations. In this case we examine the data for two features that are characteristic of matchstickmen: (a) pairs of crossed lines (which may form the torso and arms) and (b) pairs of lines joined at acute angles (which may form the legs). A hypothesis is defined by a candidate torso line and its head-waist direction. Fig. 6.3 shows examples of the two cues.

Each line l_i also primes a *free-floater* hypothesis, $\pi^{\emptyset}_{l_i}$, modelling the prior belief that it is clutter rather than generated by an underlying matchstickman m_j. (The empty-set symbol is used as the set of higher-level generating parents is empty.) Each line must be explained by exactly one hypothesis, so we add undirected inhibitory (*rivalry*) links between all parents of each line. The matchstickmen themselves are freefloating with priors $\pi^{\emptyset}_{m_j}$. The priming process gives rise to highly-loopy graphical models such as fig. 6.4.

This is a heuristic approach. Ideally we would instead model the entire scene S by a generative process, beginning with a top-level choice from all possible matchstickmen *combinations*, then adding clutter. However this would require us to model all possible combinations of hypotheses, which is intractable. This intractability does not require any context sensitivity, rather it arises from the intractable set of possible scenes given by combinations of matchstickmen. For example, dynamic programming algorithms such as inside-outside would require an exponential number of rules to describe these scenes, of the form

$$S \rightarrow m_1(s_{m_1}) \cap m_2(s_{m_2}) \cap ... \cap m_M(s_{m_M}) \cap l_1(s_{l_1}) \cap l_2(s_{l_2}) \cap ... \cap l_L(s_{l_L})$$

where $m_i(s_{m_i})$ means there is a matchstickman m_i having position s_{m_i} and where $l_i(s_{l_i})$ means there is a clutter line l_i having position s_{l_i}, assuming there are at most M matchstickmen and L clutter lines in the scene. For a finite number of position states $|s|$ there must be $O(|s|^{LM})$ rewrite rules for the high-level scene S, which is exponential in the number of scene objects. This is sufficient for intractability. In more general scenes the situation is even worse as the number of possible position states may be very large or continuous, for example in vision tasks. Although inside-outside and related dynamic programming algorithms are polynomial time in the number of rules, this is of no use in scene perception tasks as the number of rules is itself intractable. In contrast, we are constructing only the primed hypotheses from the bottom-up cues, and inserting inhibitory rivalry links to compensate for the lack of a top-level scene model.

6.1.2 Parameters

The matchstickmen and clutter hypotheses are assigned priors $\pi^{\emptyset}_{m_j} \propto 0.8$ and $\pi^{\emptyset}_{l_i} \propto 0.1$ respectively, set by hand in this case to approximate the frequencies of the objects occurring in the scene. These should technically be improper as there is a flat continuous space of possible matchstickmen and clutter positions. However we only care about the *ratio* $\pi^{\emptyset}_{m_j} : \pi^{\emptyset}_{l_i}$ and wish to find the MAP solution, so we may scale them by an arbitrary factor and set $\pi^{\emptyset}_{m_j} = 0.8$ and $\pi^{\emptyset}_{l_i} = 0.1$.

The observed lines are modelled as noisy-OR nodes, as they are caused independently by their parent hypotheses:

$$P(l_i = 1|m_1, ...m_k) = 1 - (1 - \pi^{\emptyset}_{l_i}) \prod_{j=1}^{k} (1 - m_j P(l_i = 1|m_j = 1))$$

where k is the number of matchstickman parents m_j of line l_i. All nodes are Boolean valued and treated as 0 and 1 arithmetically.

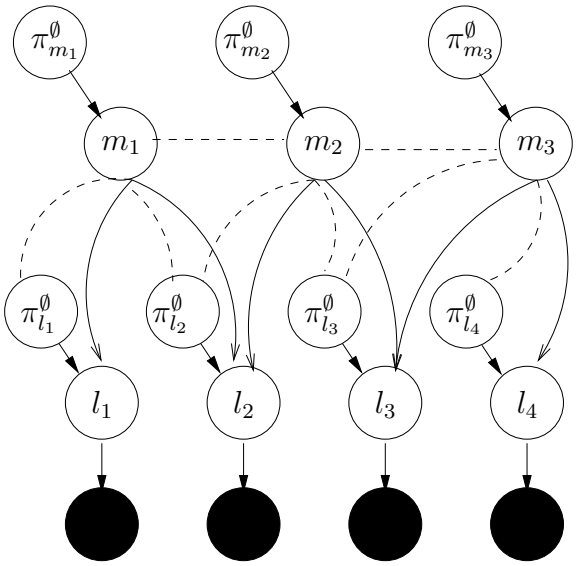

Figure 6.4: Graphical model for a simple scene. We have noisy observations (shaded nodes) of the four lines l_i. These may be explained by freefloat priors $\pi^{\emptyset}_{l_i}$ or by primed matchstick hypotheses m_j, which themselves have freefloat priors $\pi^{\emptyset}_{m_j}$. Hypothesis pairs competing to explain the same datum are connected by a (dashed) inhibitory undirected link.

For convergence of annealed inference methods, we must ensure that all probabilities are soft, so we set $P(l_i|m_j) = 1 - \epsilon, \forall ij$ and give each datum a small probability of being true even when no parents are true, $P(l|\bar{m}_1...\bar{m}_k) = \epsilon$. Similarly, we set the undirected rivalry link potentials to

$$\begin{pmatrix} 1 & 1 \\ 1 & \epsilon \end{pmatrix}$$

meaning that no penalty (a factor of 1) is applied when zero or one rivals are on, and a factor of ϵ is applied for each pair of concurrent rivals. Empirically, for our annealing schedules, we found $\epsilon = 0.01$ to be a useful value.

6.1.3 Noisy-OR vs. feedforward neural networks

It is interesting to compare our generative network with classical feed-forward sigmoidal neural networks, as it gives useful intuition about how the sigmoids emerge in the latter.

Feed-forward networks only propagate messages upwards, from data to hypotheses. In contrast, our more general noisy-OR networks also send top-down messages. If we assume that no pairs of rival hypotheses are ever on together (as in the derivation of inside-outside messages in section 2.4.1), the bottom-up messages are then given by inverting the generative probabilities using Bayes theorem:

$$P(h_j|x_i) = \frac{P(x_i|h_j)P(h_j)}{P(x_i|h_j)P(h_j) + \sum_{k\neq j} P(x_i|h_k)P(h_k)} = \frac{1}{1 + \sum_{k\neq j} \frac{P(x_i|h_k)P(h_k)}{P(x_i|h_j)P(h_j)}}$$

$$= \frac{1}{1 + \frac{1}{P(x_i|h_j)}[\frac{1}{P(h_j)} \sum_{k\neq j} P(x_i|h_k)P(h_k)]}$$

For a feedforward neural net with fully certain observed data layer and unobserved hidden layers, the bracketed term is a constant, $\ln c$, and we can write this in sigmoidal form, retrieving the standard feedforward messages:

$$P(h_j|x_i) = \frac{1}{1 + \exp\{-\ln P(x_i|h_j) + c\}}$$

However that the bracketed term is *not* constant in the more general Bayesian case, where observations may be uncertain and modelled by other hypotheses; or even missing; and hypotheses have top-down priors and interactions. Hence the feedforward network emerges as a special case of the more general Bayesian noisy-OR network.

6.1.4 Inference with Gibbs sampling, or 'spiking nodes'

Scene perception graphs are highly loopy once hierarchies are present, so exact inference is generally #P-hard. Two suitable approximation methods are Gibbs sampling and variational methods, both of which use only local message-passing operations. The important difference between them is that Gibbs sampling can model correlations between nodes whereas variational methods cannot. Variational methods are usually faster at reaching their best approximation, because this approximation is simpler (having no correlations) than the best approximation available to Gibbs sampling. Chapter 2 reviewed two types of variational method: the variational Bayes approximation, as used in RhythmKitten, which locally minimises $KL[Q||P]$ by node updates of the form

$$Q(x_i) \leftarrow \exp\langle \log P(x_i|mb(x_i))\rangle_{Q(mb(x_i))}$$

and the Bethe variational method, which approximates the node marginals using Pearl node updates of the form

$$Q(x_i) \leftarrow \langle P(x_i|mb(x_i))\rangle_{Q(mb(x_i))}.$$

As with Gibbs sampling, both of these methods are easily converted to MAP searchers by annealing. In the infinite annealing schedule limit, they should both converge to

a Delta spike at the MAP. Delta spikes contain no correlations so VB's mean-field assumption becomes irrelevant; similarly the marginals of a Delta distribution are equal to its mean-field factors so Bethe is still appropriate. However it is questionable – and perhaps impossible to analyse – when variational methods will behave well and converge to the correct basin of attraction in finite-time scene perception problems. This is because of the strong influence of rivalry connections, which inherently describe strong correlations between nodes. Such links are not well captured by non-Delta variational models, and pilot software experiments suggested that very long annealing schedules are needed to obtain sensible MAP solutions to matchstickman scene perception tasks.

A further complication with variational methods on noisy-OR nets is that the transfer function is non-linear and lacks an analytic variational expectation integral, so the upwards messages

$$msg_{x_i \to h_j} = \langle \ln P(x_i, h_k, h_j \rangle_{Q(x_i, h_k \in cop(x_i))}$$

would have to be computed by brute-force summation,

$$\sum_{x_i, h_k \in cop(x_i)} \left(\prod_k Q(h_k) \right) Q(x_i) \ln P(x_i, h_k, h_j)$$

where the sum is over the exponentially-sized configuration space of the hypotheses. Further approximations [83] to this integral are possible using methods from convex analysis, but this adds to the code complexity of the implementation, reduces the quality of the approximation, and is applicable to particular cases only.

Due to these drawbacks with variational scene perception, annealed Gibbs sampling was chosen as the primary inference algorithm for our task, examples of variational inference attempts will be given in section 6.2.8.3. It was found empirically that a useful Gibbs annealing schedule for the matchstickman task was $\beta = 0.0005$ to $\beta = 3.0000$ with steps of $\Delta\beta = 0.0005$, where β is the inverse temperature, modifying acceptance probabilities by $P \to \frac{1}{Z} P^{\beta}$.

6.1.5 Matchstickmen results

Fig. 6.5 shows the four most probable results from many runs of the matchstickman scene with Gibbs sampling. Following Mitchell [111] we show a simple bar chart of their probabilities. We could easily increase the probabilities of the best solutions arbitrarily – at the expense of computation time – by using longer annealing schedules.

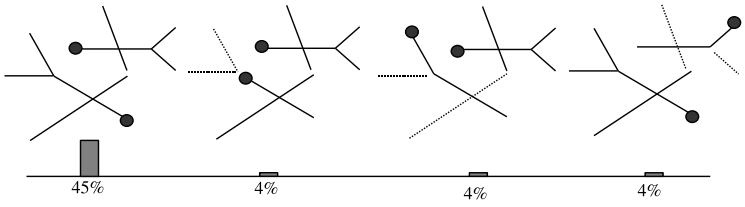

Figure 6.5: The four most probable results of the matchstickman scene, from about 100 trials. Winning hypotheses are shown by circles at their head positions. Dashed lines are explained as noise.

Such an increase occurs for two reasons. First, assuming the Markov chain converges at each temperature, the final distribution of scenes states S is

$$P(S) = \frac{1}{Z} P(S)^{\beta}$$

so the increased inverse temperature β can be see to produce an arbitrary sharpening of the observed annealed scene probabilities. Second, fixing the maximum value of β but decreasing the step size (or similarly, performing multiple sampling rounds at each temperature) gives improved observation probabilities up to a point. This is because the first explanation assumed perfect Markov chain convergence at each step, which only occurs in the infinite limit. Faster annealing deviates further from this ideal and is noted empirically to produce poorer solutions.

6.2 The music minidomain

The Matchstickman microdomain shows the basic idea of how hierarchical scene perception networks may be constructed and inference performed on them with annealed Gibbs sampling. We now consider scaling up to the larger-scale musical understanding minidomain. The task is to listen to a sequence of incoming chords from a 'semi-improvised' performance of an 'almost-known' probabilistic grammar with context-sensitive factors, and make sense of the performance. *Semi-improvised* here means that the performer is using known fragments of a composition (such as verses and choruses, or sub-verse fragments, or chord substitutions) and improvising the order they are played in according to conventions for that performance. This could occur in simple jazz performances, or to a lesser extent in pop/rock bands who may decide to insert or omit extra sections and play variations on them. *Almost-known* means that we must be able to account for the performance of occasional unknown rules, and preferably be able to learn these new rules. This is analogous to the allowance for clutter in the matchstickman domain, and as with that domain, would require an

exponential number of scene description rules if written as a fully-known grammar with explicit rules for scenes containing freefloaters. Context-sensitive factors are important in music as in most kinds of scenes (with the notable exception of artificially simplified context-free sentences in linguistics). In music, such factors include the global musical key, and the use of repeated musical motifs throughout the piece (in Copycat, non-local factors were referred to as the 'national mood').

In particular, the requirements for almost-known-ness and context-sensitive factors exclude the possibility of using polynomial-time dynamic programming algorithms such as inside-outside variants for general scene perception.

We assume we are given the positions of incoming bars of music, and a set of chord likelihoods for each bar. We do not attempt to track melody or anything else other than chordality here. We also assume we have prior knowledge of a context-sensitive probabilistic grammar describing the song being played. This is specified by a basic context-free grammar together with a set of global modulatory potentials. The task is to construct the MAP interpretation of the scene. Note that the hierarchical grammar plays the analogous role to Marr's visual hierarchies [105] – but by choosing the music microdomain we avoid large amounts of low-level processing – we are concerned with high-level perception here.

6.2.1 Formal task specification

The task is to perceive a sequence of incoming chord observations as the maximum a posteriori (MAP) unitary coherent structure which generated them, or as close an approximation to it as possible. We assume that a musical bar segmentation (such as provided by RhythmKitten) and chord likelihoods within those bars (such as the hash-classifier likelihoods used by the priming particle filter) are available as input. At each bar t, we receive a set of chord likelihoods $\{(c_i, \lambda_i)\}_{i=1}^{N_t}$, where c_i are chord symbols (such as *em, g, a♭*) and λ_i are likelihoods $\lambda_i = P(D|c_i)$ with D being the raw data received by the chord detector, such as a sound wave or MIDI stream. We allow for major and minor chords from each of the 12 possible root notes. (There are no more complex chords such as dominant sevenths – such chords if encountered will be reported as the best-fitting chords from the allowed set by the external chord detector module.)

We are given a prior SCFG generation model, modified to become context sensitive with a set of key coherence factors and to allow for 'almost-known' structures. We also known that the data may occasionally be generated by rules which are missing from the grammar. The SCFG is a set of rewrite rules of the form $(X_i \rightarrow \{Y_k\}_k, p_i, \pi_i^{\emptyset})$

where X and Y are symbols. If a symbol ever appears as the left hand side (LHS) X_i of some rule i then it is called a non-terminal. If it does not appear in this way it is called a terminal, and is assumed to be a lowest-level chord symbol. Terminals are written in lower-case type to distinguish them from non-terminals. p_i is the transition probability $P(\{Y_k\}_k|X_i,)$, that is, the probability that the LHS term is rewritten as the RHS sequence rather than as some other RHS sequence, given that the LHS already exists.

The $\pi_i^\emptyset$ values in the rewrite rules are *free-floating probabilities*, used in understanding 'almost-known' structures which allow the possibility of occasional new rules being used in the performance which are not known to be part of the grammar. We consider the case of new rules whose RHS are comprised of known symbols. To allow the possibility of learning such rules, we must first be able to perceive the sequence of RHS structures as existing in perceptual space, but with no parent structure (e.g the K in fig. 6.11). Such percepts are called *free-floating*, and we allow each known symbol X_i to free-float with probability $\pi_i^\emptyset$. This is an important feature in general scene perception tasks. For example, in visual scenes there is usually no explicit top-level grammatical structure, rather the scene is made of objects at arbitrary positions in space, which in turn are comprised of hierarchies of sub-objects. This is a key difference between scene perception and language processing, the latter almost always assuming the existence of some top level 'sentence' structure which ultimately generates everything in the linguistic 'scene'.

We assume that the whole performance is in a single musical key κ, which affects the chord percepts c_i via compatibility factors, $\prod_i \phi(\kappa, c_i)$ so the total probability of a scene interpretation is given by the probability product of all the rewrite and floating rules used in the derivation, multiplied by this factor and normalised. We assume a flat prior over 12 keys, assuming relative major and minor keys to be identical[1]. This gives rise to dependencies between all chord percepts and hence to context sensitivity.

We require *quasi*-realtime inference, meaning that complexity should not increase as the performance progresses. (However ThomCat is presented as a perceptual model rather than a practical application, so is not currently required to run in real-time on a desktop PC). Scene perception is generally used to make predictions of the near-future, so to illustrate this we will require a near-optimal prediction of the musical structure of the next bar, and preferably a rough prediction of the structure of the entire future performance.

[1]In reality they would generate slightly different PDFs over the same set of scale notes due to the change of emphasised home note.

6.2.1.1 Example song

In this text we will refer to the following simple complete song grammar, where lower case symbols are terminal major and minor single-bar chords, and S, V, C represent a simple song, verse and chorus:

$$\begin{aligned} p(S \to V, C, V) &= 1 \\ p(V \to A, A, B) &= \frac{3}{4} \\ p(V \to B, B, A, A) &= \frac{1}{4} \\ p(C \to K, L, K, L) &= 1 \\ p(A \to c) &= 1 \\ p(B \to c, g) &= 1 \\ p(K \to f, am) &= 1 \\ p(L \to f, g) &= 1 \end{aligned}$$

The song is simple because it has only a four possible forms:

$$\begin{aligned} S \to V, C, V \to A, A, B, K, L, K, L, A, A, B \\ S \to V, C, V \to B, B, A, A, K, L, K, L, A, A, B \\ S \to V, C, V \to A, A, B, K, L, K, L, B, B, A, A \\ S \to V, C, V \to B, B, A, A, K, L, K, L, B, B, A, A \end{aligned}$$

6.2.1.2 Freefloat priors

For all songs we assume that the free-floating probabilities are a function of the *level* of each rule, defined as the minimum (over all possible rewrite sequences) of the maximum number of rewrite applications needed to reach a nonterminal (over all nonterminals given by the rewrite sequence). In the example song, the levels of A, B, K and L are 1, the levels of V and C are 2, and the level of S is 3. We assume that larger structures are a priori more probable to exist as free-floaters than smaller structures. For example, performers will more frequently insert an extra verse or chorus into a song than insert an extra riff into a verse or an extra bar into a riff. The prior of a freefloating song should be especially high as we expect there to be a song in the scene with no further explanation. Hence we set the freefloat prior for rule r to

$$\pi_r^{\emptyset} = \frac{1}{20} level(r)$$

which is a heuristic that has been found to give useful results.

6.2.1.3 Key factors

We assume there are 12 possible major keys and that the 24 major and minor chords are the only chord symbols. The table below shows the assumed chord factors $\phi(\kappa, c)$ which are unnormalised factors, set by hand based on the statistics of typical popular music.

$\phi(\kappa, c)$	I	II♭	II	III♭	III	IV	V♭	V	VI♭	VI	VII♭	VII
major	8	1	1	1	1	5	1	6	1	1	2	1
minor	2	1	4	1	4	1	1	1	1	5	1	1

6.2.1.4 Simplifications

The example song and factors described above is a highly simplified domain based on real music, but chosen to illustrate the important properties of the music perception and general scene perception tasks. Real music may have many more context-sensitive factors, which would operate with similar machinery to the key factors. For example, real music tends to repeatedly apply the same forms of transform from the probabilistic rewrite rules (e.g. preferring to always use the same verse rewrite rule from the two available in the example song). Real music may change key during the piece but our model assumes a single global key. Real music may have more complex chords than just major and minor, and more possible keys than just major ones. The example song is a grammar with only one nondeterministic rewrite rule; real semi-improvised songs may have many more. In particular the architecture is intended to be applicable to grammar representing whole *genres* of songs which are highly nondeterministic but still characterisable by loose grammars with many freefloaters. We work with single sequences of chord symbols, arranged in the time dimension. Again the architecture could easily be extended to allow for simultaneous objects such as melodies, chords and rhythms.

6.2.2 ThomCat architecture: static structures

We view the scene generation process as (causal) Bayesian networks as shown in the example of fig. 6.6. The existence of each musical structure (called a *hypothesis*), such as a *SONG* causes its components to exist, with a probability given by the grammatical rewrite rule. Each possible hypothesis can also exist as a free-floater, with a

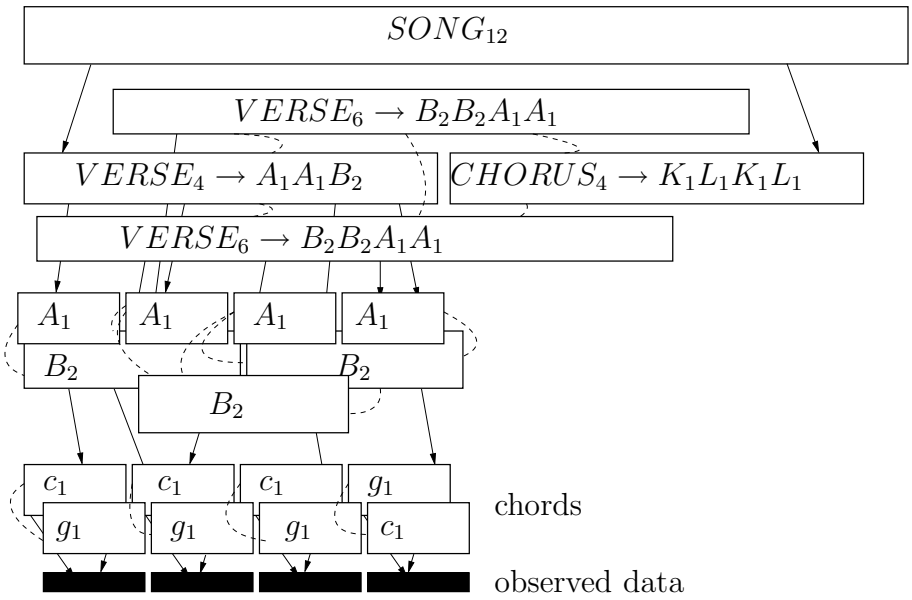

Figure 6.6: A network instantiated from the test grammar

probability[2] $\pi^{\emptyset}$. The probability of a hypothesis is given by the noisy-OR function of its parents and its free-floating probability as in the matchstickman domain.

The lowest level hypotheses are the chords reported by the external bar and chord classifier. To handle these in the same framework as the rest of the grammar, we construct a lowest-level set of nodes called 'observed bars' or *ObsBars* which represent the raw data observed by the external classifier. ObsBars then have transition probabilities conditioned on the reported possible chords c_i, $P(obsBar|c_i)$ which are set to the reported likelihoods from the classifier.

As in the matchstick example, the dashed links in the figure connect pairs of rival hypotheses. As a unitary coherent explanation of the scene is required, we cannot allow the existence of pairs of hypotheses which overlap in time and level of explanation. Formally, these links represent pairwise probability factors, $\phi(h_1, h_2) = \epsilon h_1 h_2 + (1 - h_1 h_2)$, as in section 6.1.2, which when multiplied into the scene joint distribution, set scenes with overlapping rivals to have probability zero, and have no effect otherwise.

6.2.2.1 Internal and external hypothesis parameters

In the matchstickman (MM) domain, a hypothesis described a matchstickman occupying a particular position, scale and orientation in 2D space. These parameters can

[2]In our microdomain these are probabilities as the possible structure locations and sizes are discretised by the bars. In more general scene analysis this is not the case, and probability *densities* would be used over continuous space and size.

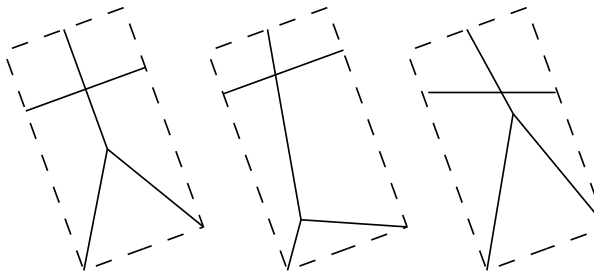

Figure 6.7: MM hypotheses with identical external parameters and variable internal parameters.

be thought of as 'externally' visible, meaning that they would be of interest to higher-level entities (discussed below). In contrast, 'internally', its sub-components could be thought of as having various parameterisations controlling how the matchstickman's total space is shared out by the sub-components. For example, three matchstickmen with identical external parameters but differing internal parameters are shown in fig 6.7. The external parameters in this case are location, orientation and scale. These parameters define a bounding box around the matchstickman. Inside (internally) the coordinate frames of the boxes, the matchstickmen are different. In the coordinate frame of the whole, (externally) they are identical. Fig. 6.8 shows the converse: the external parameters (the bounding box) vary, while the internal parameters (the positions of the sub-components) are identical.

The concept of external and internal parameters was unimportant in the matchstickman domain because inference stopped at the level of matchstickmen: there were no higher level explanations of why those matchstickmen were there. For example, there could instead have been a discrete 'karma sutra position number' variable which selected a global configuration of positions of multiple persons. When such higher-level hypotheses come into play, the distinction becomes important: only the external parameters of the n^{th} layer affect the likelihoods of the $(n+1)^{th}$ layer, whilst the internal parameters are irrelevant. This is a case of shared optimal substructure: we may aggregate the effects of multiple level n instances to pass to level $(n+1)$. The distinction becomes important in general scene perception, including the music minidomain.

In the music domain, a hypotheses is an instantiation of a rule, whose external features are its starting position in time and its total length. It also has internal parameters which describe what subcomponents it has. Importantly, the notion of 'which subcomponents' is specified using the *external* parameters of the subcomponents: two subcomponents with identical external parameters are treated as identical

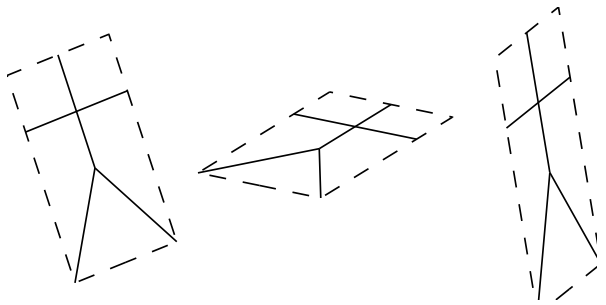

Figure 6.8: MM hypotheses with different external parameters and identical internal parameters.

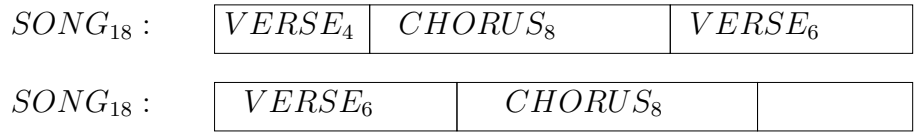

Figure 6.9: Two *SONG* hypotheses with identical external parameters and variable internal parameters.

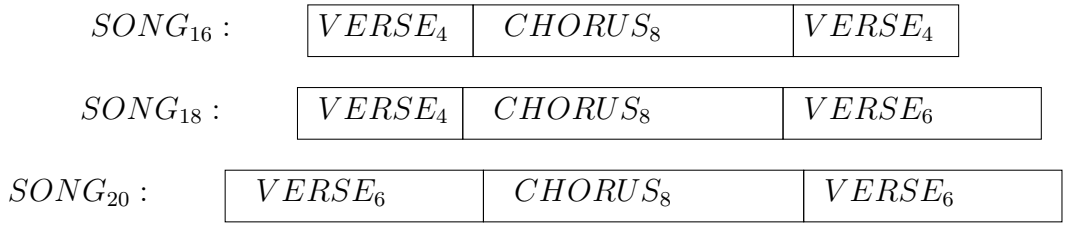

Figure 6.10: Three *SONG* hypotheses with differing external parameters.

for this purpose. For example, fig.6.9 shows two *SONG* hypotheses with differing internal parameters but identical external parameters. It is possible to generate both from the example grammar. Fig. 6.10 shows three *SONG* hypotheses with different external parameters which can be generated from the grammar. Hypothesis lengths in bars are shown as subscripts in the figure.

6.2.2.2 Lengthened grammars

ThomCat's scene hypotheses are of the form 'there is a structure of type X which exists in temporal space starting at time t and having length L'. In general, grammars allow the same type X to exist having different lengths, depending on how it becomes expanded later. In our framework this is important because such alternative expansions give rise to rival hypotheses such as the two $VERSE$ structures at the start of fig. 6.6, of lengths four and six bars. So hypotheses do not use the raw grammars as seen so far, but instead make use of compiled *lengthened* grammars (*l-grammars*), constructed from SCFGs. l-grammars split up SCFG rules which can exist in different lengths – into sets of individual rules which make the lengths explicit – and convert the transition and free-float probabilities appropriately.

This section shows how to construct an l-grammar from an SCFG, by running a novel message passing scheme on an intermediate structure called a *lengthened p-stripped grammar*. This structure contains all possible lengthened rules but lacks any probability information. It is constructed from the original SCFG. First the probability information is removed from the SCFG. Then recursively, the set of all possible lengths for each rule in the grammar is constructed, beginning with the lowest level rules and working upwards. We then run algorithm 2 for each rule in the lengthened p-stripped grammar, which constructs a *derivation tree* where each node contains a partially re-written version of the rule.

Algorithm 2 Construction of lengthened grammars

```
create top level hypotheses node from the rule
while any leave nodes contain nonterminals do
  for each leaf node l do
    x ← the leftmost nonterminal in l
    look up all rules which rewrite x
    for each of these rules r do
      create child of l, in which the RHS of r replaces x
    end for
  end for
end while
```

On this derivation tree, we then perform a top-down, dissipative (α) round of message passing followed by an upwards agglomerative (β) round with

$$\alpha_n = \alpha_{par(n)} T_{G(par(n)\to G(n))}$$

and

$$\beta_n = \begin{cases} \sum_{m \in ch(n)} \beta_m : \text{for non-leaves} \\ \alpha_n : \text{for leaves} \end{cases}$$

where n ranges over nodes and we introduce the notation $G(par(n)) \to G(n))$ to indicate the rule R in the unlengthened grammar G whose LHS is the symbol in $par(n)$ which was substituted in the transition to the RHS of R. At the end of this process we obtain β values in the first layer of children which summarise the the probabilities of those parameterisations of the top-level rule, and sum to 1 (so β at the root node is 1). The child β values are the required transition probabilities to insert into the lengthened grammar. Having formed the tree above and passed messages, it is simple to obtain the lengthened $\pi^{\emptyset}$ by $\pi_{\emptyset}(S_{9.5}) = \pi_{\emptyset}(S).\beta(S_{9.5})$. This works because the top-level $\beta(LR)$ for lengthened rules LR compute the prior $P(LR|R)$ where R is the corresponding unlengthened rules.

The following shows the l-grammar constructed by this scheme from the example grammar used throughout this chapter:

$$\begin{aligned} S_{16} \to V_4 C_8 V_4 : p = 1.0, \pi^{\emptyset} = 0.253 \\ S_{18} \to V_4 C_8 V_6 : p = 0.5, \pi^{\emptyset} = 0.084 \\ S_{18} \to V_6 C_8 V_4 : p = 0.5 \pi^{\emptyset} = 0.084 \\ S_{20} \to V_6 C_8 V_6 : p = 1, \pi^{\emptyset} = 0.028 \\ V_4 \to A_1 A_1 B_2 : p = 1, \pi^{\emptyset} = 0.15 \\ V_6 \to B_2 B_2 A_1 A_1 : p = 1, \pi^{\emptyset} = 0.05 \\ C_8 \to K_2 L_2 K_2 L_2 : p = 1, \pi^{\emptyset} = 0.2 \\ A_1 \to c_1 : p = 1, \pi^{\emptyset} = 0.05; B_2 \to c_1 g_1 : p = 1, \pi^{\emptyset} = 0.05 \\ K_2 \to f_1 a m_1 : p = 1, \pi^{\emptyset} = 0.05; L_2 \to f_1 g_1 : p = 1, \pi^{\emptyset} = 0.05 \end{aligned}$$

In addition to musical structure hypotheses, we also model beliefs about the global key. There are 12 possible keys, each is either true or false, and all are mutual rivals so that only one key is allowed in a single coherent scene. Undirected links are added to the chord-level hypotheses, connecting them to the 12 key nodes and applying the pairwise compatibility potentials from section 6.2.1. A flat prior is placed over the keys by giving each key an equal $\pi^{\emptyset}$ probability factor.

6.2.2.3 Discussion of the static structure

The scene network is a causal Bayesian network in the sense that it respects Pearl's *do* semantics [125]. It is a position-in-time model rather than a dynamic-state model as it conceives of the nodes as existing in a temporal space, and makes inferences about what exists in each part of space. There is much independence of causal influence [166] in the network which might be exploitable by the various inference algorithms we may choose to run on it[3].

The multiple hypotheses that may be instantiated from these lengthened rules are similar to those which appear in the context-free inside-outside algorithm, which instantiates *every* possible rule at *every* possible start time and *every* possible length. The l-grammar method is generally more efficient as it only ever instantiates hypotheses which can actually ever exist. In the example grammar, there is no way that a $SONG$ of length less than 12 can ever exist, so it is wasteful to consider such hypotheses. This speedup is especially important when we move away from polynomial solvable context free structures to NP-hard context sensitive ones. Ideally, we would instantiate all possible hypotheses allowable by the l-grammar, giving rise to a single, large Bayesian network (not as large as that used by inside-outside – but lacking polynomial-time dynamic programming algorithms) and run inference on it. However such a network would still grow as $O(RT^2)$ like inside-outside, with R the number of lengthened rules and T the total number of bars, both of which are likely to be large in music and other domains of scenes, rendering even approximate inference impractical [32]. Worse still, to generalise away from the music microdomain to continuous scene analysis domains such as vision, an infinite continuum of hypotheses would be needed which is clearly uncomputable.

6.2.3 ThomCat architecture: structural dynamics

Rather than instantiate all possible hypotheses from the outset, we turn to the blackboard architecture for heuristics. Blackboard systems such as Copycat aimed to *construct* a single unitary percept by allowing multiple agents to add, change and remove parts of the percept. Each agent, when called upon, searches the blackboard for any changes it could contribute. If the changes improve the percept, they are made; if they make it worse, they may be made anyway, according to some heuristic, to help escape from local minima. Randomising the orderings of agents to call upon also adds stochasticity which helps to break symmetries and escape such minima. In Copycat, changes proposed by agents are accepted with approximate Gibbs

[3]ICI is also known as 'causal independence' in older literature.

probability $P = \frac{1}{Z}\exp(-E/T)$ where T is a variable temperature parameter and E is a heuristic 'energy' function. (Copycat's exact tempering equations are found in the functions `get-temperature-adjusted-probability` and `update-temperature` in source file `formulae.l` in [112]). Extending the simulated annealing algorithm to simulated tempering, Copycat defined temperature as a function of the current 'stuck-ness' of the inference: if there is little change, suggesting a local minimum, then temperature is increased to escape from it.

Classical blackboard systems always maintained a unitary coherent state, even if that state is unlikely and is part of a path between local minima. Each proposal in sequence was either accepted and updated on the blackboard, or rejected and forgotten. In Copycat, proposals occur rapidly and repeatedly, resulting in a 'flickering halo' [81] of accepted proposals flashing briefly into existence around the local minimum. This set of nearby potential but usually-unrealised percepts is analogous to James' [85] notion of the *fringe* of awareness: the set of percepts which *could* be easily perceived if required – and which may now be quantified using psycho-physical priming experiments, which show faster responses to fringe members than to non-members [159]. In Copycat and other classical blackboards, this fringe is an implicit notion, defined by an observer of the program to be the set of hypotheses which tend to flicker around the current solution.

ThomCat provides a new formulation of the fringe, derived from a heuristic that makes its network structures tractable. We discussed above how instantiating all possible hypotheses is intractable. But luckily there is some domain knowledge in scene analysis tasks that may inform a heuristic to limit the size of this search space *at each step* of inference. The implicit search space will remain the same, but at any point during inference, only a small subset of it will be instantiated and used to run inference. Recall that the task is to seek MAP solutions, not full joints. Consider a candidate solution set X of hypotheses that together explain the data (i.e. a set of nodes all having value 'true'). Now consider solution set $X' = X \cap x_d$ where x_d is a 'dead' hypothesis. A *dead* hypothesis is one with no 'true' parents or children. Recall that all hypotheses in our models have *small* free-float priors, in this case $\pi_\emptyset(x_d)$. Because the hypothesis is floating, setting its value to 'true' will always decrease the total network configuration probability. So as we only seek the MAP solution we know that we can exclude configurations with floating nodes from consideration and computation.

This fact gives a rigorous foundation for a *Bayesian blackboard* approach. The hypothesis nodes may be treated as objects on a blackboard, which may be inserted and removed *during* inference. *Cues* in 'true' low-level hypotheses *prime* (i.e. instantiate)

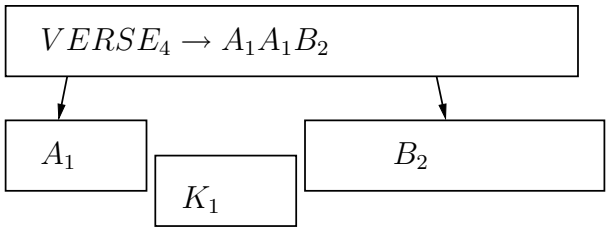

Figure 6.11: A missing child, and a floating replacement.

higher-level hypotheses and vice-versa, known as bottom-up and top-down priming respectively.[4] This gives rise to a 'spreading activation' of hypotheses, starting at the lowest level of received observations, and spreading up the levels of abstraction, and down again to their top-down predictions. Some of these top-down predictions will eventually reach the lowest level of perception and provide us with the 'what chords come next' prediction that is our ultimate goal. Hypotheses from the exhaustive set now fall into *three* classes: instantiated-and-'true' (the current percepts, as in classical blackboards), instantiated-but-'false' (the fringe, now explicitly instantiated), and uninstantiated.

Priming may be done by any hash-classifier that rapidly and approximately maps from a central object to the set of its fringe members. In classic blackboard systems, Hopfield-like association networks and semantic networks were popular; classical neural networks are also useful hash-classifiers for priming. The grammatical nature of the music minidomain allows an especially simple form of priming: when a (lengthened) term is asked to prime, we simply search the grammar for all rules containing it in their LHS or RHS, and instantiate them at the appropriate locations. Pruning is performed in two ways. First, *Conway* pruning (after Conway's *Life* [67]) removes hypotheses which are 'false' and have no 'true' neighbours. Second, a garbage-collection sweep removes any resulting islands of nodes having no chain of connectivity to observed data.

In music as with most scene domains, it is unlikely that an object (hypothesis) would exist without one of its constituent parts. Initially it may appear that the model lacks a mechanism for penalising such omissions. In a visual example, a $TABLE$ with a missing LEG is improbable: but if there was data and *instantiated* hypotheses only about three legs, and the scene probability was

$$\pi^{\emptyset}(TABLE) \prod_{i=1}^{3} P(LEG_i|TABLE)$$

[4]Sideways temporal priming – as used in RhythmKitten – is also a possibility but is not used in the current ThomCat architecture.

then this scene would be assigned a *higher* probability than a similar scene with data about four legs, because the latter scene would include an extra term in the product from the fourth leg. To handle such cases, we may wish to include extra probability factors into the joint (as with keys) which specifically penalise the absence of components. The former visual scene would then be assigned probability

$$\frac{1}{Z}\pi^{\emptyset}(TABLE)\phi_{mc}\prod_{i=1}^{3}P(LEG_i|TABLE)$$

where ϕ_{mc} is an explicit 'missing component' penalty. Early implementations of our system included such penalties, but they are in fact superfluous in the music minidomain because we are guaranteed that every bar will contain some chord, and require some explanation. Fig. 6.11 shows an example: the hypothesis corresponding to rule $VERSE_4 \rightarrow A_1, A_1, B_2$ is instantiated, but one of the A structures is missing, and a free-floating K takes its place in explaining that bar. However for the K to be 'true' it must have been generated by the free-float prior, which is small compared to the top-down prior on its rival A, so the scene as a whole does receive a penalty. In practice, the missing A will generally be instantiated anyway if the parent $VERSE$ is 'true' due to the fringe priming method, in which case a penalty will be received because $P(A|VERSE)$ is high so $1 - P(A|VERSE)$ is low.

6.2.4 Inference

So far, descriptions of hypothesis states as being 'true' and 'false' (for example,, during decisions about what to prime) have been used informally, as the discussion has been on the network structure and construction rather than inference. We now consider inference over the structures, which gives meaning to these node states. In the present implementation, hypotheses contain an abstract *inferlet* object, which provides a standard event-based API which may be implemented by various inference algorithms. Events include 'hypothesis just created', 'request made to run a local inference step (fire)', and 'tell me if you are 'true' or 'false".

The nearest inference method to classical blackboard systems is annealed Gibbs sampling, in which each instantiated node has a single Boolean state, updated according to the Gibbs probabilities given its Markov blanket. In this particular case, 'true' and 'false' are simply these Boolean Gibbs states at the moment the node is queried. We extend standard Gibbs to sample from *clusters* of co-parents rather than single nodes. The rivalry links impose a strong form of independence of causal influences on the network: we know a priori that pairs of rivals will never be on together, so we need not consider these scenarios – they are not part of the 'feasible set'.

Unlike Copycat, ThomCat runs online, updating its percept on the arrival of each new bar (about 2s of music). Inference runs under an annealing cycle: at the initial arrival of the chord likelihood data, the temperature is raised to its maximum. Sampling and cooling run during the bar, and a schedule is chosen so that it reaches near-freezing just before the arrival of the next bar. At this point the Gibbs distribution is almost a Delta function, at a local (and hopefully global) maximum scene probability. An additional 'collapse' step is performed which sets this to an exact delta function, yielding the MAP estimate.

Two other inference algorithms have been implemented in ThomCat, annealed Bethe and annealed variational Bayes [11], using different inferlet classes. The notion of hypotheses being 'true' or 'false' as used in the priming mechanism now become vaguer, and we use the heuristic that hypotheses with $Q_i(h_i) > 0.5$ are classed as 'true' for this purpose only. Many typical grammars have troublesome symmetries in their generating probabilities, which can cause variational methods to get stuck at an average between two solutions, or diverge, or converge very slowly. Empirically it was found that adding a small stochastic component to each node's $P(h_i|pa(h_i))$ at each step is a useful way to break these symmetries and allow convergence to a single solution.

6.2.5 Attention

Real-time domains require that complexity of inference does not increase over time as the scene grows, so we cannot keep growing the network and running inference on all of it as more and more data is received. Rather, it is better to focus *attention* on a fixed-size region of interest. Attention in this case means computing power used to run inference on nodes. It is not usually useful to focus on distant past events, rather we should focus on the region around the current events.

ThomCat assumes that the region of interest consists of a few bars either side of the most recently received bar: this is where it is worth applying most effort to get good MAP approximations. We typically take six bars of the recent past, and two bars of the immediate future as the 'window' of attention. Hypotheses having any part inside the window are treated as active, and their inferlets participate in inference. Interactions between attention and priming and pruning need to be handled carefully. Fig. 6.12 shows an example of the window around the current time. It is important that the high level nodes such as $VERSE$ still receive likelihoods from out-of-attention past events that are 'true', such as the leftmost A structure. Such information acts as part of the prior when interpreting the current window. However,

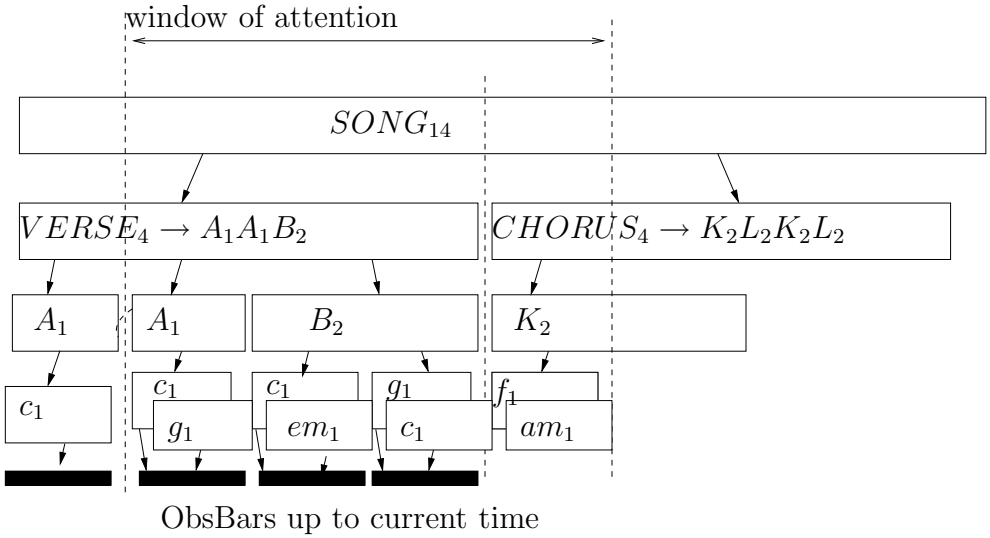

Figure 6.12: Attention includes the recent past and near future.

'false' past hypotheses can be pruned once they fall outside the window, as they contribute no such prior and can never become 'true' again (unless a movable, 'mind-wandering' window was implemented – but in that case they would become re-primed when their region is attended to.) Similarly, new hypotheses are not primed outside the window, including in the future. We do however prime hypotheses in the *near* future inside the window, such as the K, f and am of fig. 6.12. Inference runs as usual on these hypotheses (though there are no *ObsBars* yet to provide bottom-level likelihoods) and the inferred state gives a prediction of the future, which could be used for example to schedule automated accompaniment actions to play along with the performer. The window moves along by one bar each time an *ObsBar* is received – at the same time as the annealing schedule is reset to its starting maximum temperature.

6.2.6 'Thalamus' and 'hippocampus' as structural speedups

After naive implementation of the system with simple data structures, profiling, and optimising language-dependent constructions, it became apparent that structural algorithms were consuming vastly more processor time than inference proper, particularly during the single task of searching for pairs of rivals in a global hypothesis list. A large speed gain was made by constructing a central topographical map of the temporal space, and using it to hash (i.e. map directly from a location to a list of objects at that location) the locations of all hypotheses to allow rapid look-up of rivals. We call this structure 'thalamus' as it has a similar structural connectivity to the hypothesis space as the biological thalamus has to cortex.

A similar performance gain was made by pre-caching hash maps of all possible primes from each l-grammar rule in a 'hippocampus' structure to avoid online look-up. Again this name come from the biological analogy: the biological hippocampus is believed to provide fast associative look-ups amongst other functions.

Once these speedups were implemented, the number of inference rounds per structural update was balanced so as to make the structural updates insignificant with respect to inference proper.

6.2.7 Software architecture

The large-scale architecture of ThomCat is shown in fig. 6.13. The architecture has been designed to be extensible to other domains, priming schemes and inference algorithms. The major structure is the `blackboard`, instantiated as a singleton. The `blackboard` maintains a collection of instantiated `percept`s, which have a Boolean `gibbsState` indicating whether they are 'on' or 'off', where 'off' percepts correspond to the fringe. (We will see later how different inference algorithms will make use of this state variable in different ways.) The public interface of the `blackboard` allows it to receive new `ObsBar`s and to run inference, priming and pruning. Keeping the parent-child links between `percept`s up to date is one of the major structural tasks, and may be combined with priming for speed since both tasks involve searching for possible or actual candidate neighbours. The `thalamus` and `hippocampus` singletons maintain fast look-up tables for active percepts and potential primes respectively. `Percept` is an abstract class providing a standard interface which is specialised by the various particular types of `Percept`. The methods `getPGivenPars` and `getTotalPContribution` get part of all the `percept`'s contributions to the total network or cluster probability, using the `percept`'s own `gibbsState` and the `gibbsStates` of its Markov blanket. Care is taken to avoid double counting of pairwise factors. The `Hyp` class represents unobserved temporal structure hypotheses; `ChordHyp` is a special subclass for chord-level hypotheses, which receive extra factors due to the global key. `Key`s are also a type of `Percept`, but are not `Hyp`s as they do not exist in temporal 'space'.

`Percept`s do not perform any inference themselves – instead they contain an `Inferlet` which handles inference. `Inferlet` is an abstract class, providing an interface which is implemented (in the object-oriented programming sense) by subclasses containing different inference algorithms. `InferletGibbs` implements `fire()` as the clustered Gibbs sampling described earlier. It uses the Boolean `gibbsState` variable of its owner's Markov blanket along with the `Percept` functions `getPGivenPars` and `getTotalPContribution` to compute and draw from the cluster posterior.

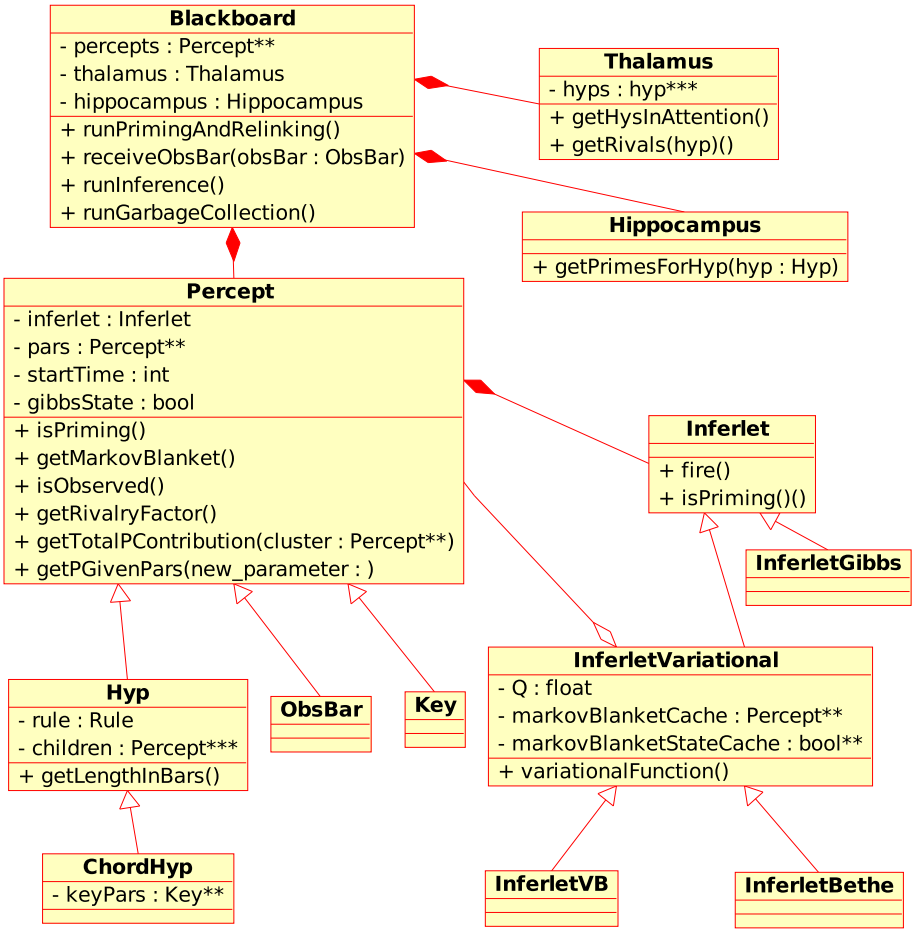

Figure 6.13: Simplified UML diagram showing large-scale ThomCat implementation architecture

The two types of variational inferlet – VB and Bethe – differ only in their implementations of their `variationalFunction(Ps,Qs)` and share the rest of their code. Variational inferlets must consider all possible Boolean configurations of their Markov blankets rather than just its current `gibbsState`s. The `gibbsState` variables are used as temporary states, and the inferlet iteratively set these states to each possible configuration during their computations of the variational expectations. The result of these computations is stored in their `Q` variables, representing $Q(on)$.

6.2.8 Results

This section presents detailed walkthroughs of the Gibbs and VB run modes, along with statistics for the Gibbs version and a demonstration of recognising freefloaters. (Statistics from large numbers of complete runs are provided later in section 6.2.8.6.) The walkthroughs are illustrated using 3D visualisations of the blackboard. True and false hypotheses are shown as red and blue respectively when in attention, and grey

when outside attention (all past out-of-attention hypotheses are true as false ones are removed.) In the VB case, there is a continuum of Q values between true and false, shown by shades of red, magenta and blue. The current time is always that of the latest observed bar, and the latest set of chord hypotheses. A window of attention of 6 bars of past and 2 bars of future is used in these trials, as it was found to be a useful size. The current temperature, β^{-1}, is shown graphically by the level of a graphical thermometer. β always runs from 0 to 1.5, though various step sizes are tested. Early test ran to 1.0 but were found to give occasional non-optimal samples, so the extra cooling to 1.5 is used to approximate the 'collapse' of the Gibbs distribution to the required Delta spike at the MAP probability. The figures also show the musical key hypotheses – limited to just C and G in these examples – below the thermometer. Note that unlike the structural hypotheses, the key hypotheses are non-'spatial' as they refer to global properties of the scene rather than existing 'in' it. (Philosophers who insist that all percepts must be spatio-temporal may be interested by this.) The walkthroughs were generated by a single random trial and commented upon during the runs. The first such trial was reported to avoid reporting selection bias. Our presentation of walkthroughs followed by success statistics is based on the Copycat evaluation chapters of [111].

6.2.8.1 Gibbs walkthrough

This walkthough, shown in figs. 6.14 - 6.21, shows snapshots of the blackboard running in Gibbs mode, with a step size of $\Delta\beta = 0.05$. A new bar of evidence arrives at the end of each annealing cycle, then a new cycle begins. Each cycle consists of several *rounds* in which all nodes are fired (in a random order) at one temperature in the annealing schedule. At most medium to low temperature steps there is little change in the blackboard state, so after the initial high-temperature fluctuations, snapshots are generally taken only when something changes.

6.2.8.2 Gibbs bar-end collapsed percepts

The walkthough gave snapshots during the inference process, occurring mostly within bars. Complementing it, fig. 6.22 shows the state of the blackboard at the end of each bar's annealing cycles (i.e. when 'collapse' to a single interpretation has approximately occurred – as can be seen by the zero readings on the thermometer graphics). These states are important as they are the ones on which actions would be based, for example if this perception scheme was used to drive an automated accompaniment system. The end-of-bar percepts are all correct except for bar 5 (fig.

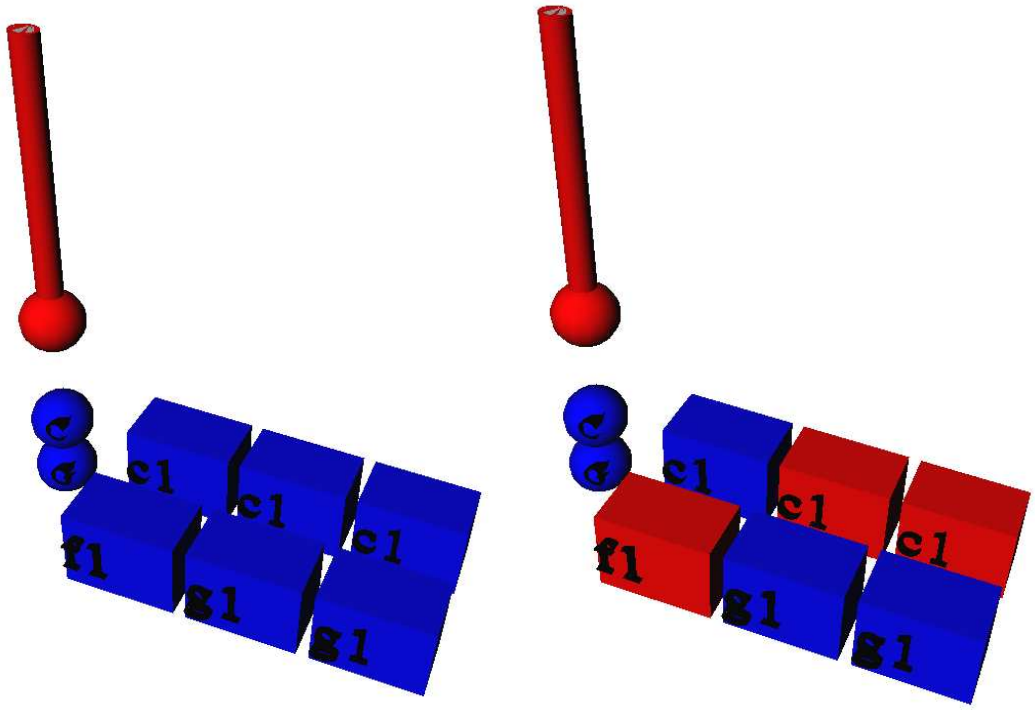

(a) The start of the simulation. Perceptual time is shown left to right. Three bars have been heard before inference is started. The ground truth chords (as generated from the grammar) are *c,c,c*. They are corrupted by the hypothetical chord detector, which reports the normalised likelihoods of the correct chords as about 0.8, with the remainder of unity in each bar given to random confuser chords, in this case *f,g* and *g*. Chord hypotheses are created for the reported likelihoods, and initialised to the off state (blue). The two spheres marked *C* and *G* on the left are key hypotheses, also initialised to off. The temperature is at is maximum as an annealing cycle is about to start – this is shown by the fully-red thermometer on the left.

(b) Six hypotheses have fired so far, still within the first round of inference in the annealing cycle. Three of them have switched to the on states. The two *c*s are correct, the *f* is incorrect, but is accepted as the temperature is very high.

Figure 6.14: Gibbs walkthrough.

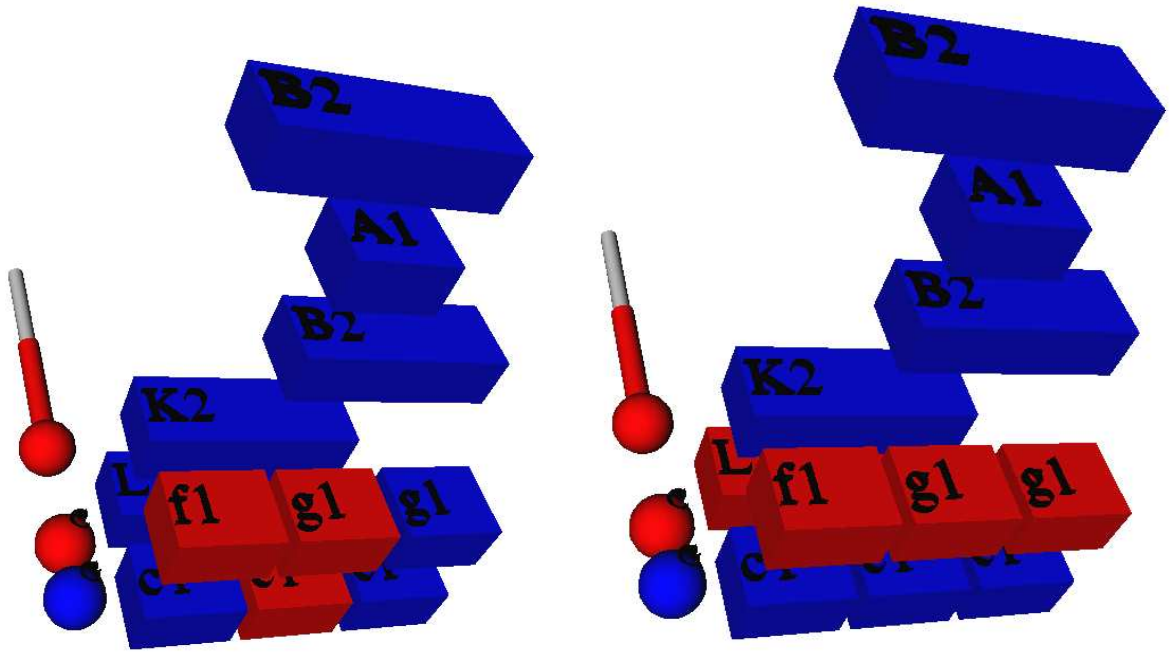

(a) After another 12 firings, the first inference round is over. Temperature is reduced to the next member of the schedule, shown by the thermometer dropping (temperature is reduced exponentially over time so the first drop appears very large). At the start of the new round, priming and pruning is performed. There is no pruning yet, but each of the on hypotheses primes its possible parents. These are initialised in the off state, and form a 'fringe' or 'conceptual halo' around the current on percepts. The key percepts have also had chance to fire by now, and the C key is currently on.

(b) A further 12 firings have passed within this round. Temperature is still high so an unusual interpretation is currently instantiated, with all the chords perceived wrongly, and an L_2 structure activated to explain the first two incorrect percepts. This incorrect structure could become a self-reinforcing local minimum as it grows larger – luckily the temperature is still high so there is time for it to be eroded.

Figure 6.15: Gibbs walkthrough.

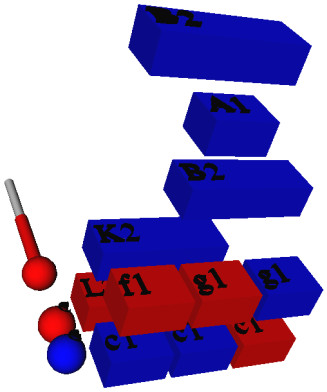

(a) Another 12 firings have passed, at the same temperature; the latest c has jumped back to the ground truth interpretation, the others are unchanged.

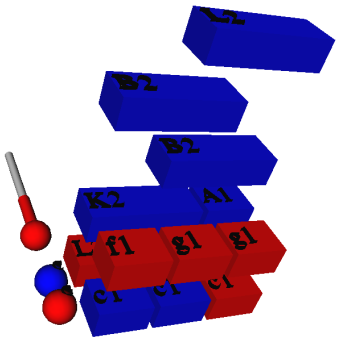

(b) Another 4 firings have passed. As the temperature is high, two rival hypotheses are allowed to be on together on the right. The key has also jumped to G, due to the predominance of 'true' g chords.

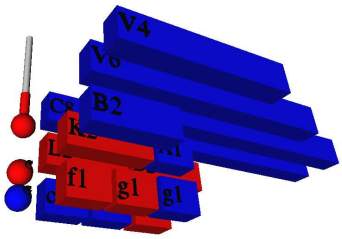

(c) Another 45 firings have passed, the inference round has completed, temperature is reduced and priming and pruning occurs.

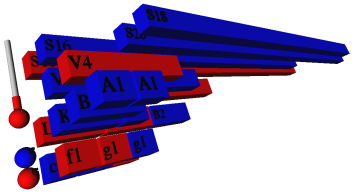

(d) Another 70 firings have passed, and a new round has begun. The ground truth V_4 hypothesis has been primed and is currently on. However the first two bars are still incorrect and are mutually reinforcing with the L_2 explanation and the G key.

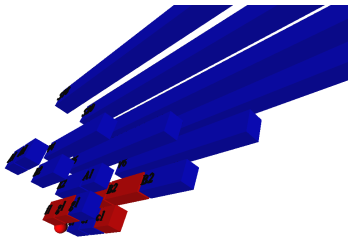

(e) 40 more firings. The third bar now has a correct B_2 explanation, though the first two bars and key are still stuck in the wrong explanation.

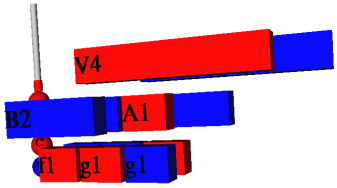

(f) 50 more firings. An alternative explanation, A_1, of the third bar's c is being explored.

Figure 6.16: Gibbs walkthrough.

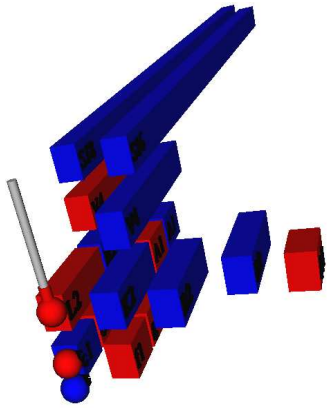

(a) 80 more firings. Priming has just occurred.

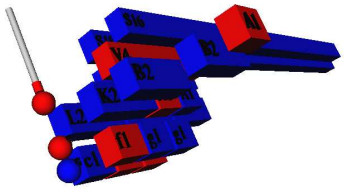

(b) 20 more firings. The incorrect mutually-reinforcing block in the first two bars is breaking down.

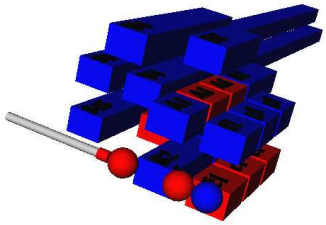

(c) 30 more firings. All chord hypotheses now happen to be matching the ground truth, however there is not much explanation above them.

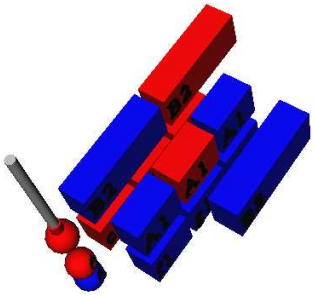

(d) 50 more firings. Priming and pruning have just occurred, this time there is a large amount of pruning. The A_1 and B_2 hypotheses are both correct.

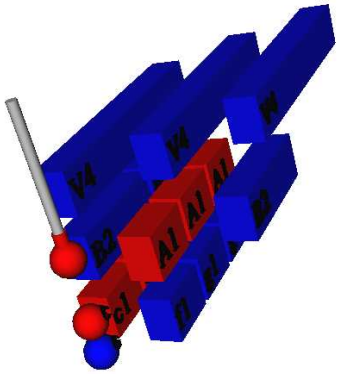

(e) 50 more firings. Priming has just occurred.

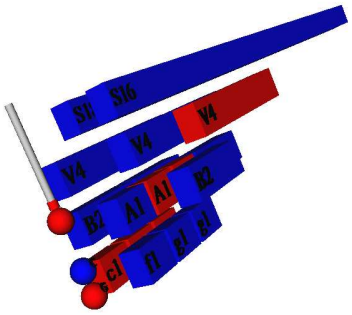

(f) 50 more firings. Note that between most of these illustrated steps there is little change in the state – images are taken when something interesting happens.

Figure 6.17: Gibbs walkthrough.

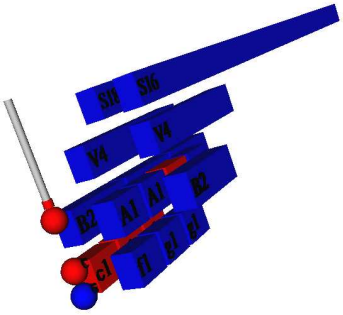

(a) 50 more firings. Priming just occurred.

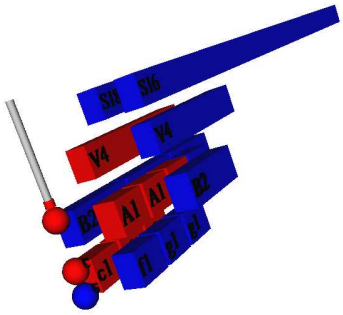

(b) 20 more firings. The first two bars are now being correctly explained by the high-level V_4 hypothesis. Bar three is still wrongly explained by another A_1 – it should be B_2.

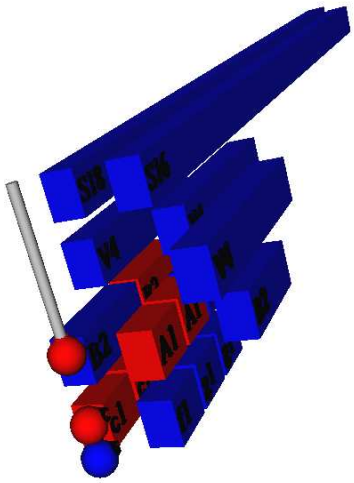

(c) 20 more firings, including a new round. Temperature is now getting low, but the correct A_1, A_1, B_2 explanations are in place (though we have lost their higher-level V_4 hypothesis).

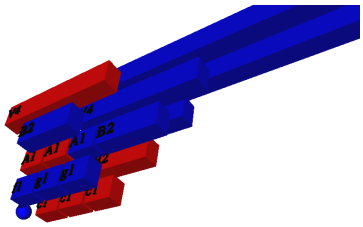

(d) 10 more firings. The correct V_4 is now on – the whole explanation is currently correct (but could be improved by postulating a *SONG* to generate the *V4* instead of it freefloating)

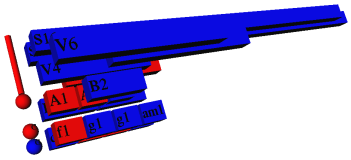

(e) 30 firings. In this period the annealing cycle completed and a new bar has been delivered. Its ground truth chord is *g* and its confuser is *am*. The annealing cycle begins again, so the temperature is maximum.

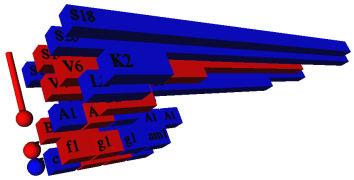

(f) 40 firings. As temperature is high many hypotheses are being considered and concurrent rivals are allowed.

Figure 6.18: Gibbs walkthrough.

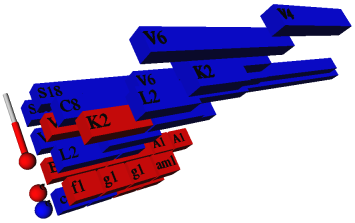

(a) 70 firings. The first round at maximum temperature has just completed; the temperature has just decreased but is still very high.

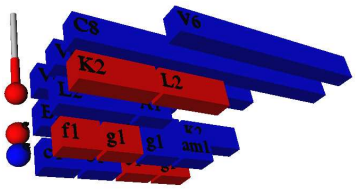

(b) 70 firings. Temperature is still very high.

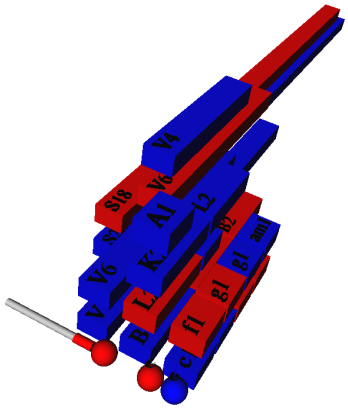

(c) 100 firings.

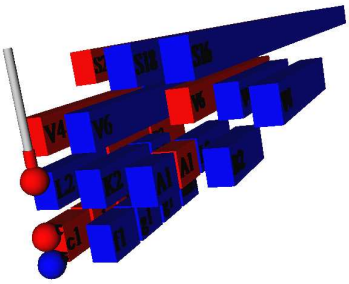

(d) 100 firings. Temperature still high; correct V_4 has reappeared at the start.

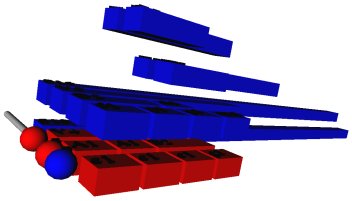

(e) 100 firings. The complete correct V_4 explanation is showing.

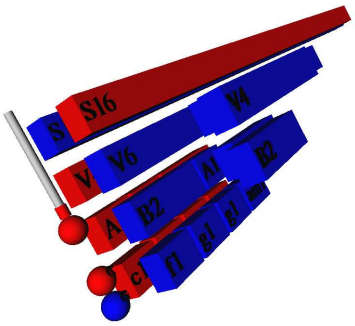

(f) 30 firings. The V_4 has primed a $SONG_{18}$ hypothesis – we now have a complete explanation of the scene, which can be used to make predictions about events right up to the end of the song if required.

Figure 6.19: Gibbs walkthrough.

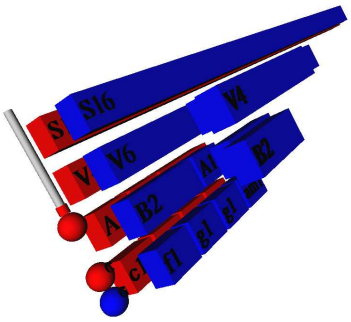

(a) 150 firings. There is now very little change in state, except for occasional flickerings between the two rival *SONG* hypotheses (of different lengths; both equally well supported by the evidence, though having different priors) and sometimes both *SONG*s are 'false' allowing the verse to freefloat.

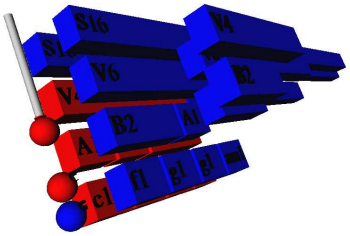

(b) 150 firings. Temperature now very low, occasional flickerings of the songs as above. The V_4 freefloat hypothesis is good at this stage as there is not yet a chorus or second verse to support a *SONG* hypothesis.

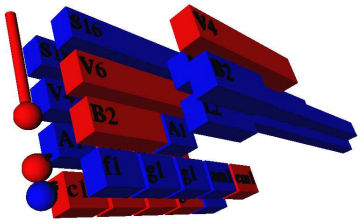

(c) 120 firings. The end of the annealing cycle – a new bar has arrived, having correct chord *f* and confuser chord *em*. A new annealing cycle has started; temperature is at maximum so much change and exploration is occurring.

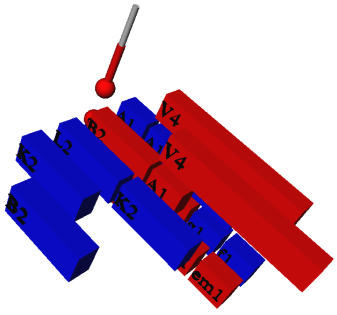

(d) 80 firings. Temperature still high, priming and pruning recently taken place.

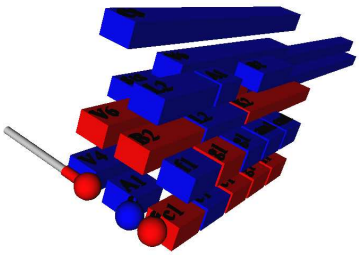

(e) 150 firings. The latest chord (*f*) is the start of a chorus, which has the L_2 structure to start it.

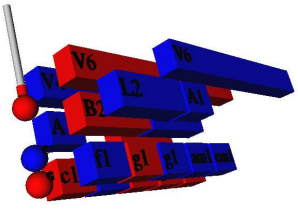

(f) 250 firings. Apparently stuck in a local minimum, having B_2 as the first two bars. Temperature still medium so there may be time to escape.

Figure 6.20: Gibbs walkthrough.

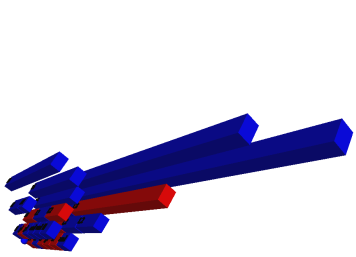

(a) 60 firings. End of annealing cycle; first two bars still wrongly perceived as B_2 at collapse. However the newly arrived bar is reinforcing the K_2 structure and its parent chorus, which may prime a song again, which in turn will provide strong top-down priors to correct the interpretation of the first two bars.

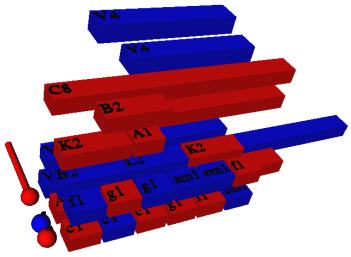

(b) 60 firings. Temperature at max, many hypotheses being explored. Note that the attention window (6 bars of past) now encompasses all the received bars – when the next bar arrives, the window will leave the earlier part of the song.

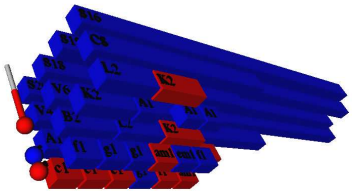

(c) 120 firings. Temperature still high, much exploration taking place.

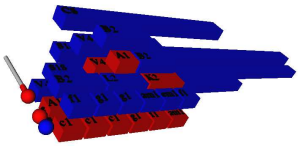

(d) A further 120 firings. Temperature is medium, some exploration taking place.

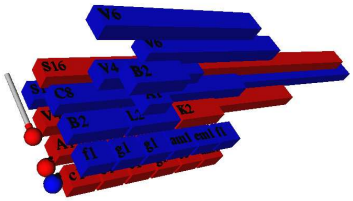

(e) 350 firings. Temperature is quite low, and the state is now fairly stable at the correct explanation. Stability is stronger and occurs earlier in the annealing cycle now that more bars of evidence are available.

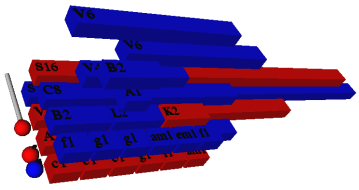

(f) 200 firings. End of annealing cycle, the interpretation is unchanged since the previous image.

Figure 6.21: Gibbs walkthrough.

6.22(05)) in which the first few bars are being interpreted as $V_6 \rightarrow B_2 B_2 A_1 A_1$ rather than the ground truth $V_4 \rightarrow A_1 A_1 B_2$ – probably as a consequence of high noise in the evidence making the former temporarily more probable. This percepts is rapidly overruled by later data which alters the noisy chord data by top-down priors. The correct key of C is perceived by the end of all the bars.

6.2.8.3 VB walkthrough

As predicted by our preliminary experiments, the variational methods – VB and Bethe – did not perform well in the ThomCat minidomain. Inference steps were extremely slow, often taking 30 minutes of computation time per step. This is because of the brute-force summations required in the update equations, which are computationally exponential in the size of the Markov Blanket. It is not uncommon for hypotheses to have 10 to 18 neighbours (in the Markov Blanket sense) once all rivals and possible children are taken into account. This can give $2^{18} = 262144$ elements in the sum, required to update a single node! Another problem is that even on very simple scenes with small-step annealing schedules, convergence can still be much slower than the analogous Gibbs inference if there are multiple solutions having similar posteriors. In this case, the network state oscillates slightly between them, converging *in the infinite limit* to the single best one, but spending most of its finite runtime in a mean-field average of the two. These intermediate averages are not very useful if computation is halted early, as they ignore rivalry correlations between hypotheses. A particular problem in our minidomain was that being a small domain, many pairs of hypotheses have *exactly* equal probabilities, causing variational methods to get completely stuck 'on the fence' at the average of the two solutions – opposed to Gibbs, which randomly falls into one or the other. This problem was solved by adding a small random perturbation to every computed Q, which breaks the symmetry and allows convergence to begin. (Interestingly, this can be seen as a simple kind of variational-Gibbs hybrid method – if the perturbation was made larger and dependent on the Markov Blanket, inference would behave more and more like a Gibbs sampler and less like a variational method.)

The inference speed could be improved in future versions by using Jordan's QMR approximation, and possibly by designing a cluster-variational algorithm (as discussed, though not implemented by [161], and roughly analogous to the cluster Gibbs speedup used earlier in ThomCat). Such a speedup would allow more gradual annealing schedules and so possibly improve the mean-field problem by allowing closer convergence to individual minima that is currently possible. However the purpose of the variational implementations here is not to beat the Gibbs algorithm, but merely to

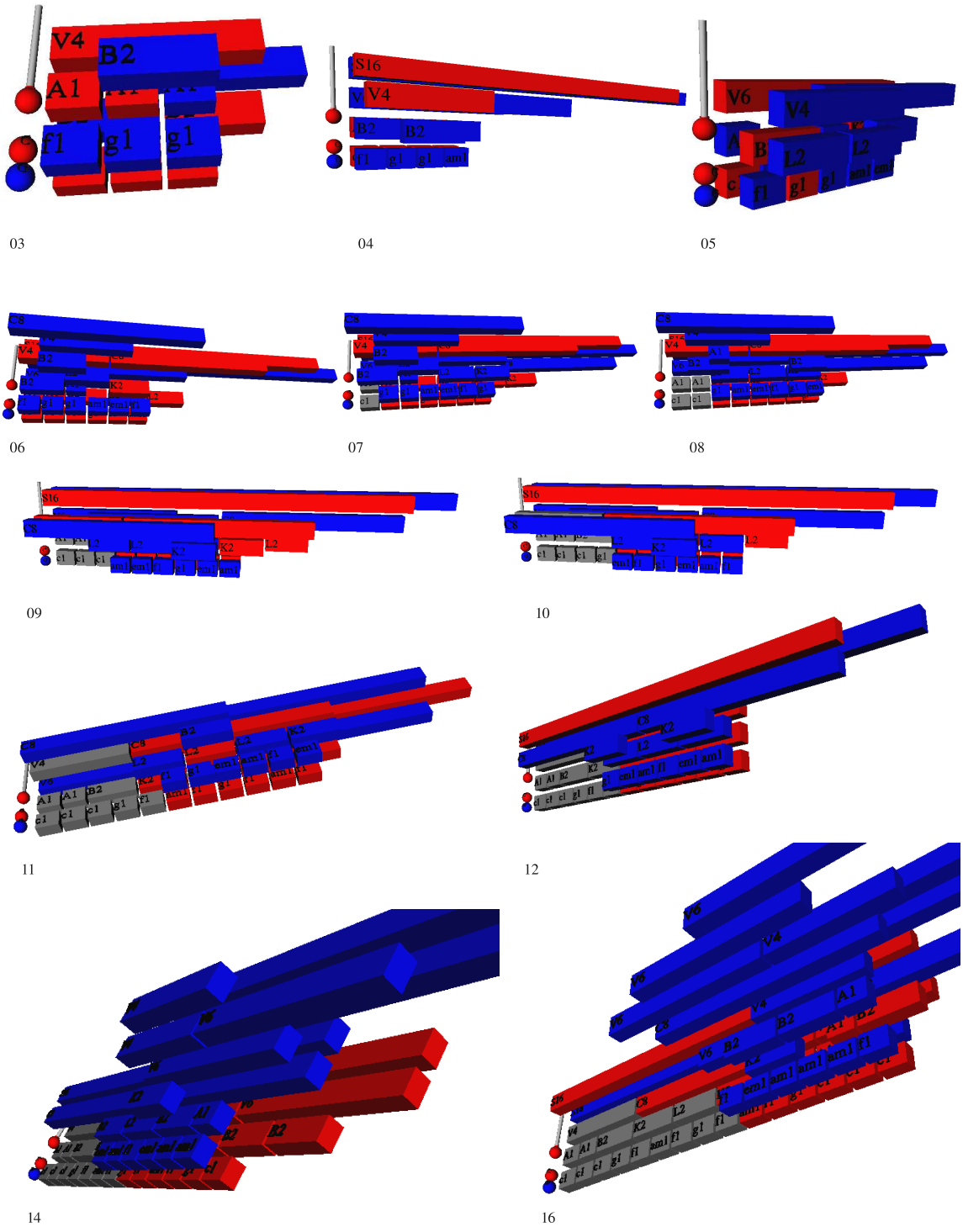

Figure 6.22: Gibbs end-of-bar collapsed percepts

illustrate how Copycat-like blackboard systems may benefit from a rigorous Bayesian formulation by allowing other standard algorithms to be run on them. The variational implementations are simple proofs-of-concept that this can be done, which we hope will encourage other authors to consider importing more detailed and appropriate fast algorithms into Copycat-like domains.

We have been unable to distinguish any difference in performance between VB and Bethe implementations, as both run extremely slowly and only a few bars of single runs can be computed. Hence we present only a short walkthrough and end-of-bar states for the VB implementation on a few bars. The walkthrough is shown in figs. 6.23 and 6.26 and commentated on below.

6.2.8.4 VB bar-end collapsed percepts

The end-of-bars states of the VB run are shown in fig. 6.27. The majority have converged to single Delta-like near-collapsed states (seen from the binary red and blue decisions); of note is bar 3 (03) in which the V_6 hypothesis is still around 0.5 belief, due to the slow convergence properties discussed above. In this case, its rivals are the overlapping V_6 as well as all the freefloat priors of its children (not shown in the figures).

6.2.8.5 Effects of annealing schedule on Gibbs performance

As noted earlier, the speed of Gibbs annealing is a tradeoff between accuracy and running time. For real-time applications such as musical scene analysis the latter is especially important. To test the effects of different annealing schedules, we ran repeated trials of various schedules with various noise levels on samples drawn from the example song grammar (with no freefloaters). We wish to infer the probability of successful perceptions occurring for each (schedule, noise level) scenario. A successful percept is defined as on which matches *exactly* the generative sampling ground truth at the *end* of the song. (There are many other ways to define success which could equally well have been chosen. For example considering the state of the percept at the end of each bar rather than at the end of the song.) For each scenario we assume a flat Beta prior on $\pi = P(success)$, run n trials and observe x successful trials, having a Binomial distribution given the Beta prior. We may then plot our beliefs in the mean and standard deviation of the success probability for each scenario in fig. 6.2.8.5 using the standard equations for this Beta statistics as shown below. For each schedule, we also note the average running time and express as beats per minute, a standard measure of musical tempo. Most popular music has tempo between 100 and

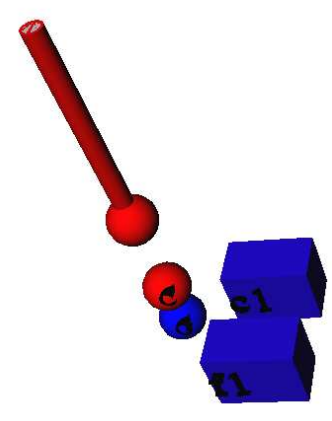

(a) Initial state, no inference has started yet, just one bar is presented (to reduce the computational complexity of this demonstration). Nodes are instantiated with $Q = 0$.

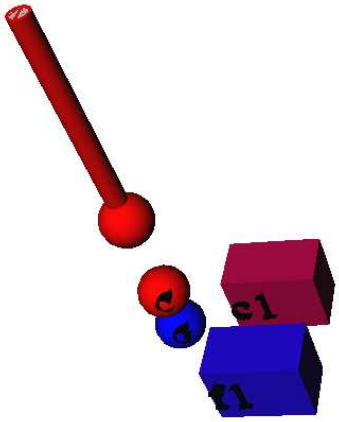

(b) c has fired and increased its Q, since its rival f is still completely off.

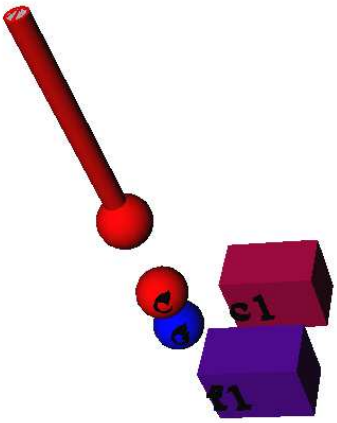

(c) f fires and increases its Q slightly, though not as much as c

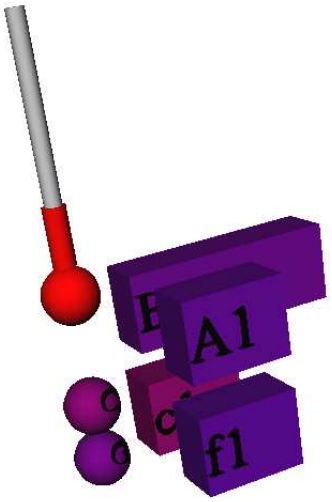

(d) 20 firings later.

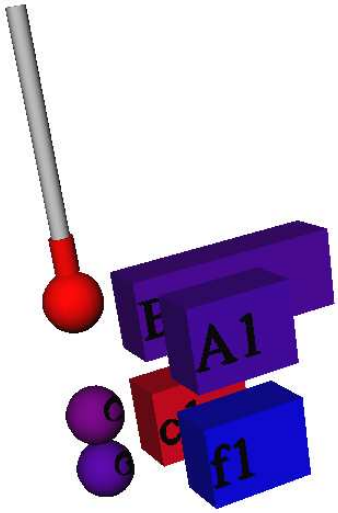

(e) Another 10 firings later. c is winning the contest with f: as c strengthens, f weakens.

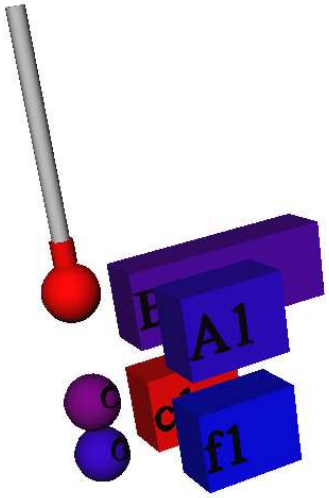

(f) 10 firings. The above trend continues, and c's explanation, B_2, grows stringer with c. Unlike Gibbs sampling this all takes place very smoothly.

Figure 6.23: VB walkthrough.

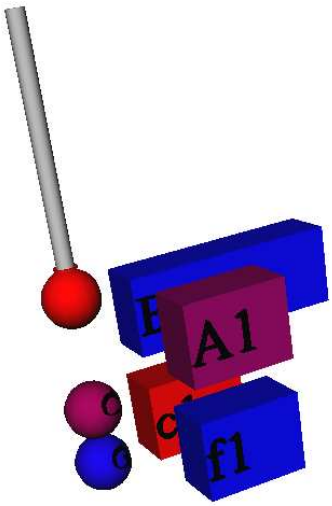

(a) 5 firings. A_1 has gradually taken belief away from B_2.

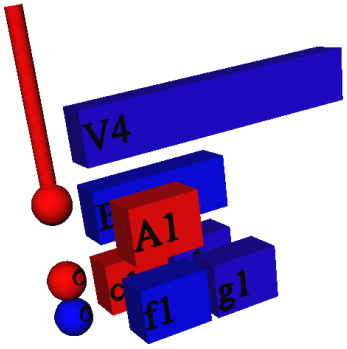

(b) 5 firings. Annealing cycle has completed, a new bar is received and temperature is set back to maximum. A_1 has primed a verse to explain it.

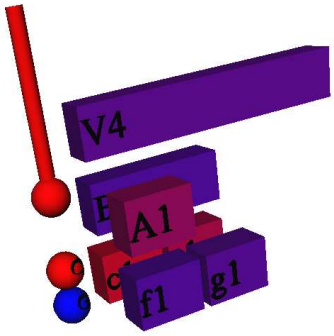

(c) 10 firings.

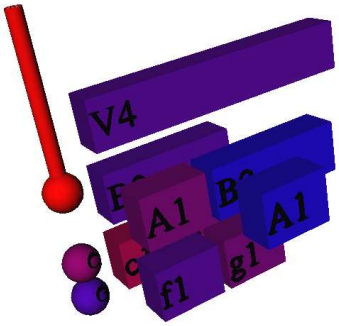

(d) 10 firings. The second c bar has grown strong and primed an A_1 explanation, which fits with the high-level V_4.

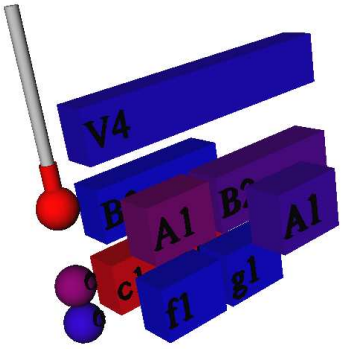

(e) 30 firings. An alternative explanation of the second c is under consideration using a B_2 structure. This is able to take belief away from its rival A_1 if it has a stronger freefloat prior, or through the random variational perturbations implemented to escape local minima.

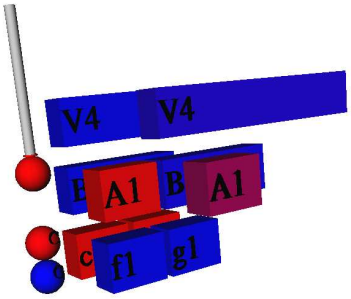

(f) 50 firings. The B_2 has faded again, being beaten by the A_1. Temperature is getting low – it is nearly time to receive the next bar.

Figure 6.24: VB walkthrough.

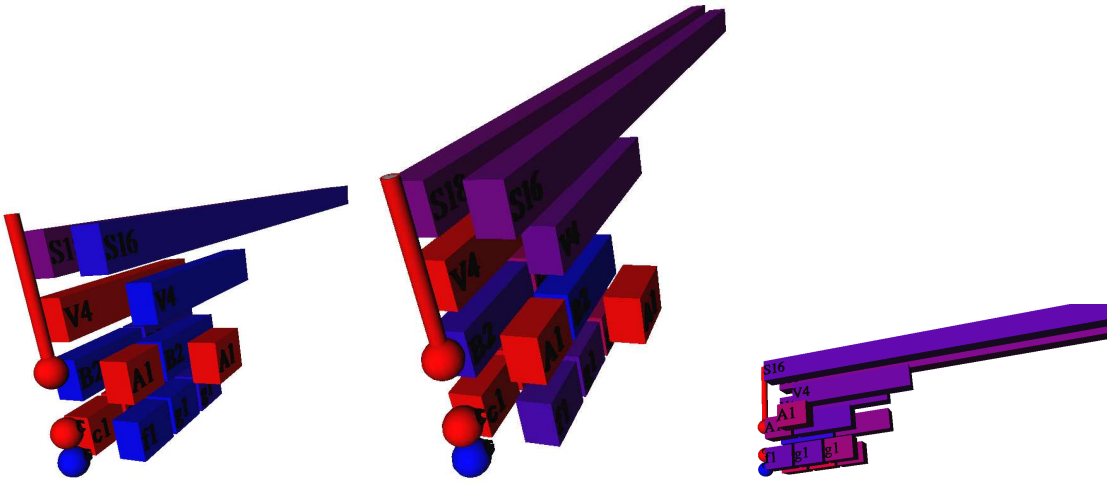

(a) 20 firings. The next bar has just been received; V_4 has become strong and primed a *SONG* explanation. The temperature is reset to maximum.

(b) 20 firings. Two rival songs both exist in approximately $Q = 0.5$. There is no evidence to discriminate between them yet.

(c) 20 firings. Temperature is still at maximum, and all nodes become closer to $Q = 0.5$.

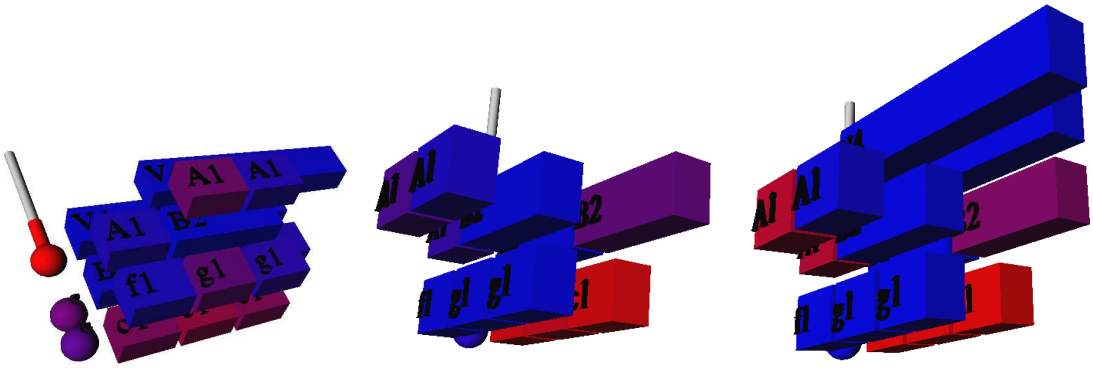

(d) 50 firings. Temperature is still high, but some clusters of nodes are now being pruned as they fall below $Q = 0.5$.

(e) 40 firings. Medium temperature; the correct A_1, B_2 interpretation is growing in strength.

(f) 40 firings. A_1, B_2 still growing.

Figure 6.25: VB walkthrough.

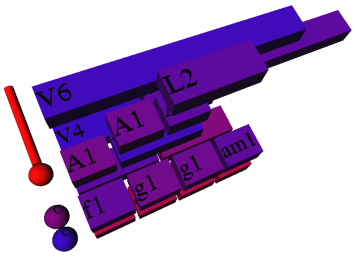

(a) 110 firings. The next bar has arrived and the network is heated up again.

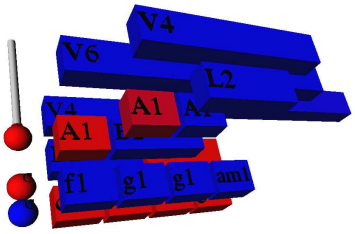

(b) 150 firings. Temperature is getting low. Correct A_1, A_1, B_2 in place; V_4 not fired recently enough to pick it up.

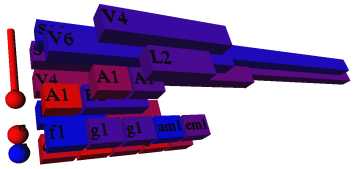

(c) 150 firings. V_4 became active, and primed song parents. A new bar recently arrived and the network is heated up again.

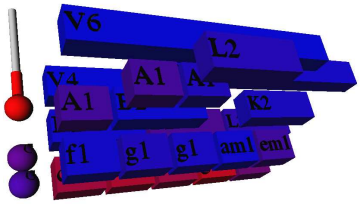

(d) 150 firings. Temperature is still high. Inference is starting to become sluggish.

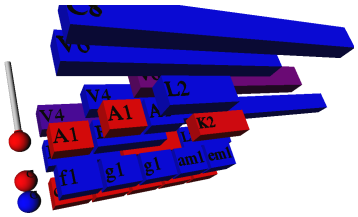

(e) 150 firings. The correct solution's strength is growing, including V_4 at start and K_2 at bar 5. Temperature is very low, an the annealing cycle is almost complete. (V_4 is still weak at it has multiple good rivals which affect it.)

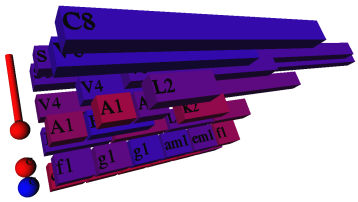

(f) 100 firings. The next bar has arrived, and the network is heated up again. Inference is now very slow (taking more than 10 minutes for 100 firings). The trial was aborted here.

Figure 6.26: VB walkthrough.

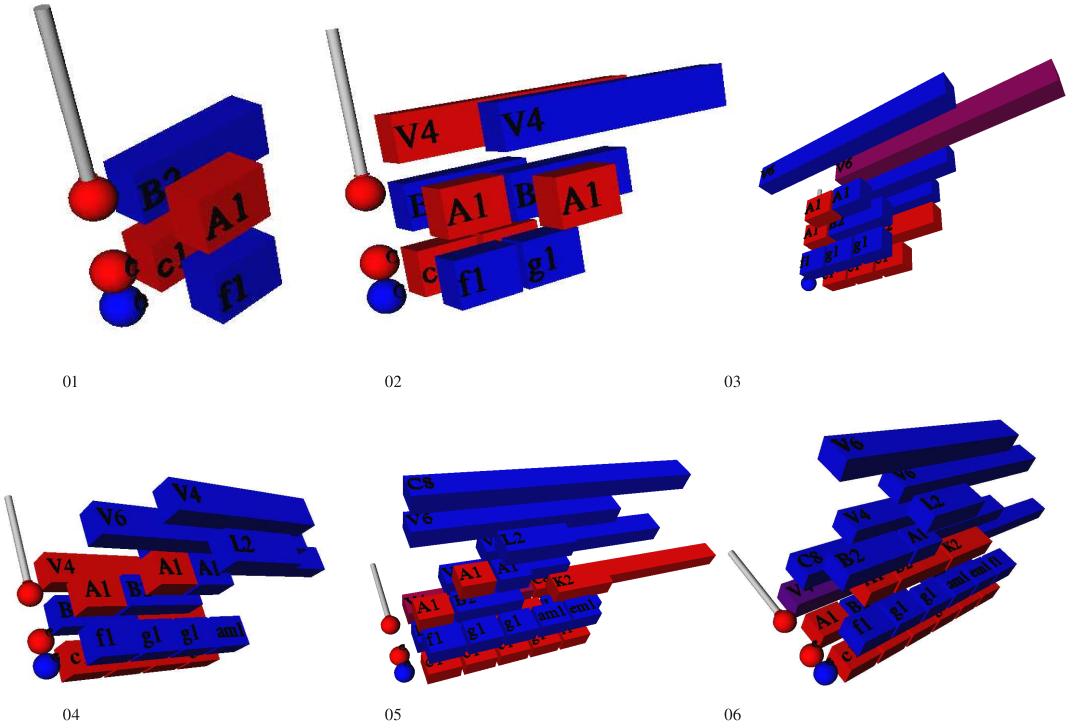

Figure 6.27: VB end-of-bar collapsed percepts

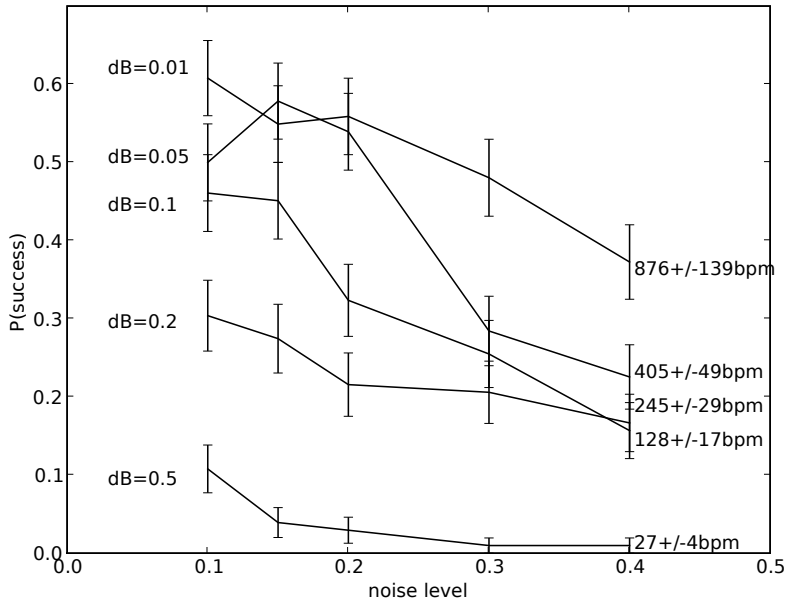

Figure 6.28: Effects of annealing schedule on Gibbs performance

180 bpm so running speeds around this range are roughly suitable for real-time on the Intel P4 1.6GHz machine used in the tests and using the simple example song grammar.

$$P(x|n,\pi) \sim Bin(x;n,\pi) = \binom{n}{x}\pi^x(1-\pi)^{n-x}$$

$$P(\pi) \sim Be(\alpha=1,\beta=1) \propto \pi^{\alpha-1}(1-\pi)^{\beta-1} = 1$$

$$P(\pi|x,n) \propto \pi^{\alpha+x-1}(1-\pi)^{\beta+n-x-1} \Rightarrow \alpha' = \alpha + x, \beta' = \beta + n - x$$

$$\langle \pi|x,n \rangle = \frac{\alpha'}{\alpha'+\beta'} = \frac{1+x}{2+n}$$

$$std(\pi|x,n) = \sqrt{\frac{\alpha'\beta'}{(\alpha'+\beta')^2(\alpha'+\beta'+1)}} = \frac{1}{2+n}\sqrt{\frac{(1+x)(1+n+x)}{3+n}}$$

6.2.8.6 Performance with freefloaters

In the above trials, sample performances were generated from the SCFG to be interpreted by ThomCat. Although noise was added to the individual chord bar likelihoods, there were no freefloaters in play. We give results which do include freefloaters. First we must define a generator of samples which include freefloaters. Recall that the purpose of allowing freefloaters is to provide the ability to understand almost-known scenes which include known structures but in unknown combinations. For example, the grammar used in this chapter does not include the rule $S \rightarrow C, C, V$ but a performer may decide to play such a structure, comprised of known verse and chorus structures. In this case, the C,C and V should be perceived as freefloaters (and future systems may perhaps hypothesise a new song form from this percept). To draw samples including freefloaters we must specify sample probabilities. Domain knowledge tells us that changes tend to be more *a priori* probable at higher structural levels than lower levels. Performers more frequently insert and remove extra verses and choruses than insert extra riff repetitions within those structures; and more frequently change the arrangement of the riffs than the individual bars comprising them. This knowledge was encoded in the perception system by assigning higher freefloat priors to larger structures. We use a similar scheme to draw samples with freefloaters. Beginning with a sample from the SCFG as before, we proceed to make alterations to each of the rule applications used in that sample. Each application of a rule of level l has probability

$$p(mutate|l) = p(mutate|L) * \frac{1}{2^{L-l}}$$

where L is the level of the top-level song. Essentially this means that the top-level song mutates with some constant $p(mutate|l)$ (set to 0.2 in our trials), then the probability of mutations at successively lower layers is divided by 2. This typically produces one or two mutations in samples from the example grammar of this chapter, mostly occurring at high levels. One a mutation is determined to occur, it type is drawn (uniformly) from three options: (1) deletion of a random RHS term; (2) insertion at random location of a new random RHS term (having the same level as a neighbouring term); (3) substitution of a random RHS term for another RHS term of the same level. (These mutations are similar to, and influenced by, the genetic algorithm proposal distributions used in previous work [56].)

A trial is defined to be a success if the following two conditions are met. (1) All subcomponents of mutated and non-mutated rules are perceived as in the sample; (2) All hypotheses that have no mutated descendants are perceived as in the sample.

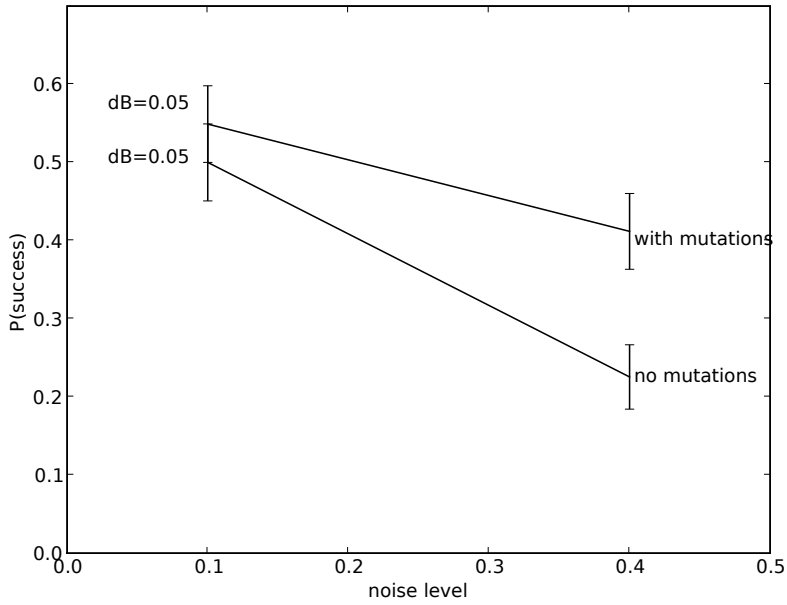

Figure 6.29: Effects of annealing schedule on Gibbs performance with random mutations, including insertions, deletions and changes of substructures.

Intuitively, this means the scene is perceived as best possible: as known structures where possible, and as freefloaters where mutations have occurred.

Fig. 6.29 shows the results of 100 trials with such freefloaters for the single annealing schedule with $\Delta\beta = 0.05$, compared to the previous Gibbs results having the same schedule. (Only two noise points are used as the results are analysed by hand which is time-consuming.) The performance is comparable with the previous results, showing that ThomCat is able to handle almost-known scenes using freefloaters just as well as fully grammatical scenes. This is something that dynamic-programming approaches such as inside-outside are completely unable to do. (In fact, the performance on freefloaters is actually slightly *better* than on fully grammatical scenes. This is probably because scenes with freefloaters typically contain fewer hypotheses in total than fully grammatical scenes, as there are less parents. For example, the fully grammatical scene $S \rightarrow V, C, V$ requires the song S to be perceived correctly in addition to the verses and choruses. In contrast, the freefloating scene $S \rightarrow C, C, V$ only requires the three substructures, all free-floating, so there is less scope for error as there is no S hypothesis which could go wrong.) Fig. 6.30 shows an example of a successful free-floating percept.

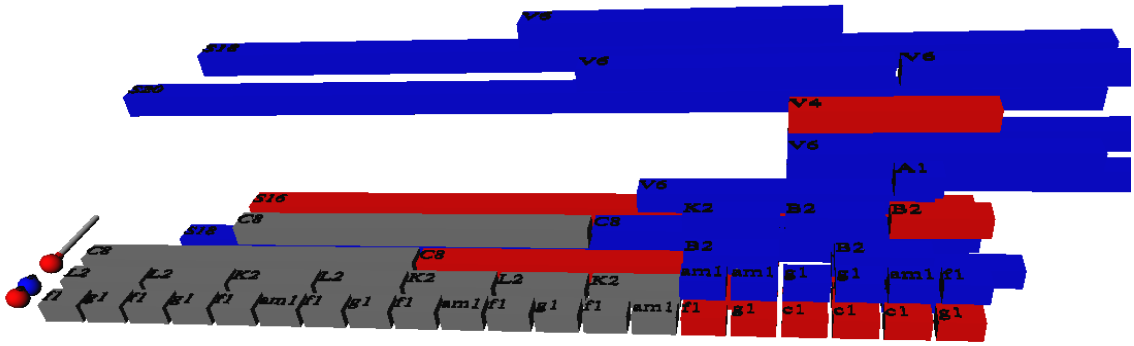

Figure 6.30: A successful freefloating percept. The mutation is high-level, $S \rightarrow C, C, V$. The substructures C, C, V have been perceived correctly as freefloaters. (The perceived S is ignored in classifying success as it has mutated descendants.)

6.3 Future extensions

This chapter concludes by discussing some possible future extensions to ThomCat, for which outlines of concepts and algorithms are provided, but no software implementation. It discusses the extension of the architecture from a passive scene perception system into an active decision maker based on the scenes; how to perform various types of learning; the movement of attention; and larger musical domains. These extensions could be implemented in ThomCat to make further progress towards an integrated musical listening and accompaniment system, for more varied styles of music, and perhaps – eventually – fully improvised music. Discussion and refinement of the concepts may contribute to clarifying the corresponding human psychological ideas; and the following also serves as an example of how formalisms such as ThomCat can contribute to such discussions.

6.3.1 Action and utility

> "There are five fingers there. Do you see five fingers?"
> "Yes"
> And [Smith] did see them ... a moment of luminous certainty, when each new suggestion of O'Brien's had filled up a patch of emptiness and become absolute truth, and when two and two could have been three as easily as five, if that were what was needed.
> – George Orwell, *1984*

Standard graphical models represent the joint PDFs $Q(x_{1:N})$ over variables. Normally this is used to model $Q(x) = P(x)$, a true distribution; we have seen how it can

be cooled to $Q(x) = \delta(\hat{x})$ as a means of finding the MAP solution, i.e. the most probable percept of the scene. However in real-world scene analysis we are less interested in the most *probable* interpretation of the data than in the most *useful* one. For example, a hungry agent has a vested interest in perceiving an uncertain object an *food* rather than a ball, because this can initiate an action to try eating it, which prevents the animal from dying of starvation. Similarly, a trombonist who has got slightly lost in the sheet music has an interest in perceiving his place as being at the quiet flute section rather than the loud brass fanfare entry, because it is more damaging to the performance (and the trombonist's pay cheque) to play a loud part over a quiet one than vice versa. Even when the data strongly favour a perception, utility can overrule it. Like Orwell's Smith, we really can and should perceive improbable things if it it is strongly in our interests to do so. In this section we discuss how ThomCat's $Q(x)$ could be altered to model these ideas and to produce high utility actions if, for example, used in an automated musical accompaniment system. We will see that unitary coherent percepts are of no use in finding the ideal but typically intractable maximum expected utility plans, but may be useful for *quickly* finding maximum utility percept-plan pairs, which often give useful though suboptimal plans.

6.3.1.1 Tree searching and hashing in AI

The text of this section is based on the peer-reviewed publication [59]:

- *C. Fox, N. Girdhar, and K. Gurney.* A causal Bayesian network view of reinforcement learning.. In *Proceedings of the 21st AAAI International Florida Artificial Intelligence Research Society Conference, 2008.*

Action selection is a classic problem in AI, Economics and Operations Research. It can be shown [9] that the only coherent, optimal way for an agent to act is to maximise an expected utility function, when suitably defined. When sequences of actions (plans) are considered, this is generally an intractable problem. Classical AI [147] made heavy use of *tree-searching* methods to search over all possible combinations of actions, and showed that some combinations could be omitted (for example in 'alpha-beta' pruning). In the probabilistic domain, this requires that each plan be evaluated against all possible worlds, and the expected utility computed for each plan. This is doubly intractable because both the set of plans and the set of possible scenes (in scene analysis) is exponential in size. We can view classical tree search as a dynamic Bayesian network (DBN) with decision nodes as in fig. 6.31(a). (In some tasks, actions such as asking questions may affect the amount of *information* available about the state of the world. If this is the case, then the state must be expanded

to model future states of *knowledge* about the world, and the model is known as a partially observable Markov decision process [153].) An external global controller fixes plans $\{a_t\}_{1:T}$ into the action nodes, then infers the current expected utility, or 'value', v_1:

$$v_1(\{a_\tau\}_{1:T}) = \langle \sum_{\tau=1:T} \rho^t r_\tau \rangle_{\{s_\tau, a_\tau\}_{1:T}}$$

where ρ is an temporal discounting factor. The global controller then resets the action nodes to the next possible plan and runs inference again, and repeats until all plans (perhaps with some pruning or sharing of partial computations between plans) have been simulated. The plan with the highest v_1 is then selected, and the first action of that plan is performed. If new information arrives about the state, then the whole decision process is rerun. We may compute v_1 by assigning similar value nodes to each future point in time:

$$v_t(\{a_\tau\}_{t:T}) = \langle r_t + \rho^{t+1} v_{t+1} \rangle_{\{s_\tau, a_t a u\}_{t:T}}.$$

This way of computing the value is shown in the figure. (Curiously, the links between values are causal, respecting Pearl's *do* semantics, even through they flow backwards though time. This is because the current discounted value is a construct which deliberately measures future expectations, and is therefore dependent on future events, and caused by our pre-perception of those events. This is a strange form of causality but is not paradoxical because nothing in the 'real world' is causing previous events: the events and causations are all within the phenomenal world of perception.)

An alternative, heuristic, method of action selection in AI is to assume there is some hash-classifier $v_t \approx v(s_t, a_t, \theta)$ where s is the current state of the world and θ is a learnable parameter, and try to optimise this with respect to θ to give the best actions, by trial and error. *Reinforcement learning* (RL) [152] is one way to do this. These methods have the advantage that once learned, they are very fast, as they simply call the hash function to obtain actions direct from states. A novel view of RL is show in fig. 6.31(b)-(c) (which encompasses both 'classical RL' [152] and the 'Bayesian RL' of [39]). It consists of two phases, which change the structure of the previous tree-searching net in different ways to approximate the full solution. In the *acting* phase (a), all links are removed, and replaced by the hashing function. This is an acausal directed link (it does not respect the Pearl semantics) but allows a rapid search for a the next single action a_t to maximise the approximated value. Then in

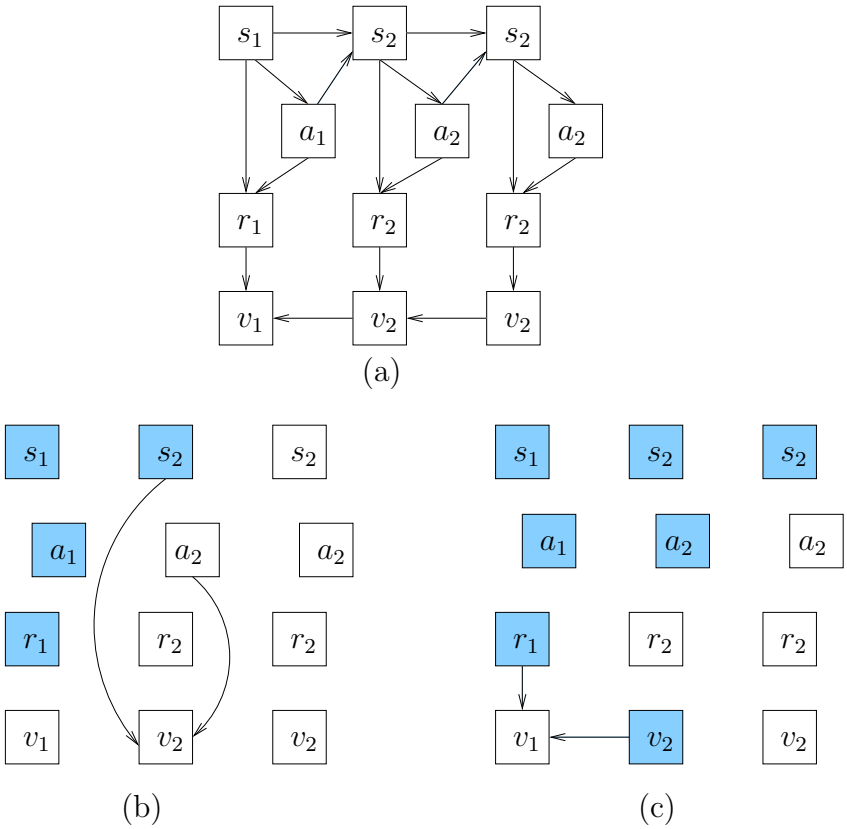

Figure 6.31: (a) Classical tree-searching may be viewed as instantiating a sequences of plans $\{a_i\}$ and computing their present value v_1. (b) The action step of reinforcement learning may be viewed as cutting links and replacing them with acausal hash links. (c) The learning step of reinforcement learning reinstantiates the relevant causal links.

the *learning* phase, the obtained value v_t is then used along with the previous step's reward r_{t-1} to update the hashing function for the previous value (with $0 < \alpha < 1$):

$$v_{t-1}(s_{t-1}, a_{t-1}) \leftarrow \alpha v_{t-1}(s_{t-1}, a_{t-1}) + (1 - \alpha)(r_{t-1} + \rho \max_{a_t} v_t(s_t, a_t))$$

It is generally accepted (e.g. [37]) that real humans and animals use both tree-searching and hashing methods for action selection, with tree-searching for novel, high-level tasks, and hashing for low-level routine tasks. Tree-searching itself in classical AI generally 'bottoms-out' as a heuristic, hash-classifier evaluation function, essentially combining some tree-searching with some hashing. (For example in chess programs, the hash-classifier is some learned mapping from board state to valuation.)

6.3.1.2 Unitary coherent scenes vs. optimal actions

An interesting recent extension of the junction-tree algorithm [97] extends it with action and reward nodes, and passes pairs of messages which result in a 'locally optimal' plan being computed (in the sense that changing any single action would reduce

the expected utility). This algorithm operates on a similar graph to fig. 6.31(a) but without the value nodes. The first element of the message is identical to the standard junction-tree algorithm, and passes marginal probabilities. The second element passes corresponding expected utilities. From the perspective of this thesis, there are several problems with this approach. First, the solution is only locally optimal. Second, it requires junction-trees to be computed, which is NP-hard and seemingly not biologically plausible. Third, it requires two independent sets of messages to be sent between nodes, which again seems biologically difficult. Most importantly, it does not compute an MAP scene description, as all the nodes represent marginal probabilities. This raises an interesting question: if we can compute good approximate plans without computing a unitary coherent (MAP) scene, then why does real perception bother to do so? Why not just compute marginals and expected utility maximising plans? But yet we know from our own perception of the world that we *do* perceive a unitary coherent percept rather than a 'Bayesian blur' of possibilities. So what could this unitary coherent percept be for?

This is a deep question at the heart of cognition, and we do not expect to give a solution here, though we tentatively suggest that a coherent unitary scene interpretation lends itself to fast, simple priming of actions, and also ensures that actions in a plan are compatible with *each other*. For example, Raphael's music accompaniment system [132] includes additional heuristic code to prevent the played accompaniment from jumping around in the score, even if the marginal beliefs about the position jump around. Even if the individual notes are played according to their MAP locations, there is an additional penalty for non-smooth playing that must be accounted for.

There appear to be at least three forms of action selection and perception used by humans. First: very low-level actions in response to low-level stimuli, for example at the level of psychophysics experiments. Humans are known to perform almost optimally in many such experiments [48] but are unable to report justifications for these actions. Such low-level perception may involve hashing functions and does not appear to use scene perception. Second: immediate, reportable scene perception-driven action selection. For example, seeing a unitary coherent scene containing *food* and therefore reaching out to grab it. Actions based on single percept cannot be optimal as they do not depend on the distribution of scenes. However they may be useful for the reasons given above, and will will show how ThomCat could be extended to model them. Third: very high-level, reportable action selection based on conscious consideration of the distribution of scenes. For example, although perception of the face/vase stimulus is never instantaneously ambiguous or incoherent, we may use

our memory and high-level cognition to notice that over time we are considering different interpretations, and may use reportable mathematics and probability theory to work out a maximum utility action over them. Such actions are very difficult to compute, for making complex actuarial tasks only skilled mathematicians armed with large computers are able to make good decisions. (These three forms bear a passing similarity to the Freudian id's unconscious decisions; the ego's conscious decision making; and the super-ego's meta-level monitoring of ego activity.)

Unitary coherent scene-driven actions may thus be viewed as a useful heuristic for quickly finding good but suboptimal sets of coherent actions. The following gives a brief sketch of a theory of unitary scene-driven actions in the ThomCat framework, which could be extended and implemented in future work. The sketched system computes annealed approximations to

$$\arg\max_{s,a} P(s)R(s,a)$$

which is the maximum utility percept and plan (where both scene and plan are made of multiple components), as opposed to the optimal but intractable and non-unitary MEU solution,

$$\arg\max_{a} \sum_{s} P(s)R(s,a).$$

6.3.1.3 Network extension

Fig. 6.32 shows how action and reward nodes could be used to extend the ThomCat network. Note that both actions and rewards can depend on scene structures at many levels, not just low-level chords. For example, it may be important to play a *VERSE* accompaniment pattern as well as playing that pattern in the chord of *em*.

The figure shows actions and rewards as single nodes for each bar, assuming that the bar is the smallest unit of alternative actions. In this type of network, all possible actions for the i^{th} bar are grouped into a single multistate node a_i, and the reward node r_i is a function of these multistates and all possible relevant scene configurations. (Relevance is shown by links from scene to reward nodes, and means the scene nodes whose states alter the reward under any action.) An equivalent architecture – more in keeping with ThomCat but requiring a more complicated figure to explain – would be to convert these action and reward nodes into collections of Boolean nodes corresponding to each state of the multistate nodes; and add rivalry links between them. The latter are suggested for parsimonious implementation with ThomCat.

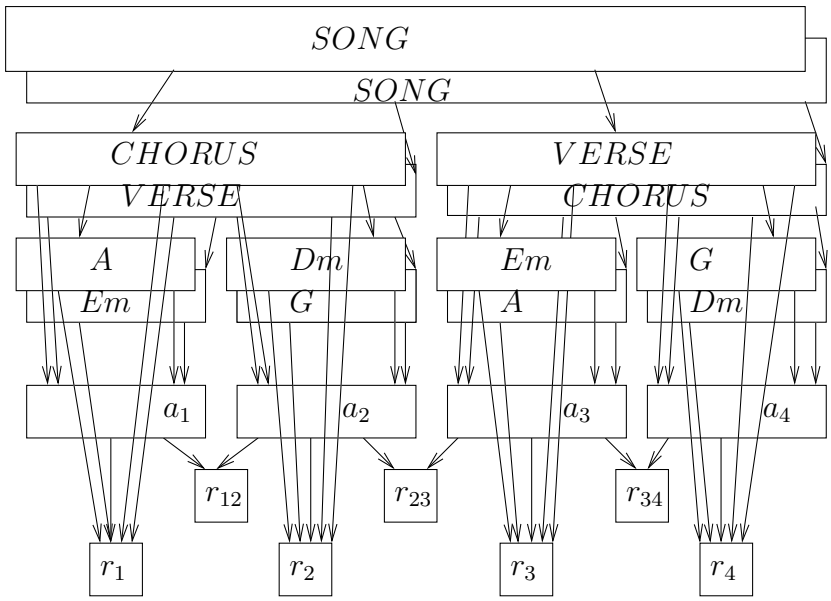

Figure 6.32: A simple ThomCat scene extended with action and reward nodes.

We wish to find the configuration of the whole network – both scene and action nodes – with the maximum utility,

$$\arg\max_{s,a} P(s)R(s,a)$$

As usual, the scene probability is

$$P(s) = \prod_i P(s_i|pa(s_i))$$

where $s = \{s_i\}$ are all the hypothesis and observed data nodes. Assume that the total reward R for a plan $a = \{a_j\}$ under a scene percept s is written as a product of local r_i factors as in the figure, $R(s,a) = \prod_k r_k$. Then we have

$$P(s)R(s,a) = \prod_i P(s_i|pa(s_i)) \prod_k r_k(s,a)$$

which is of the same form as a Bayesian network with joint

$$P(s,a) = \prod_i P(s_i|pa(s_i)) \prod_k P_k(s,a)$$

when $P_k(s,a) = r_k(s,a)$. That is, we may treat the local reward components exactly as if they were probabilities. The reward nodes can thus be modelled as regular Bayesian network nodes with CPTs containing their local rewards, and regular annealing will converge to give the maximum utility scene and plan combination.

The conversion of reward into probability may be of interest to pragmatist philosophers (c.f [84]) who have argued qualitatively that truth and utility are the same thing. This Bayesian network formalism shows quantitatively how this idea could be useful for action selection. Pragmatism is often summarised by the maxim 'truth is measured in dollars', meaning that we should take a model as being 'true' if and only if it does some good – which ultimately translates into monetary value. Our reward factors are multiplicative but if we consider

$$r_k = \exp m_k$$

where m_k are monetary rewards such as dollars, then we can make these monetary rewards additive as would be expected of a currency. Under this interpretation, each $\ln 2$ currency units corresponds to a doubling of the probability, so we are saying that we prefer an outcome having $\ln 2$ units two times as much as we prefer an outcome having zero units (and four times as much as an outcome having $-\ln 2$ units etc.) This suggests that within the maximum utility approximation scheme, and assuming such a mapping from currency to preferences, James' notion can be written more accurately as '*log* truth is measured in dollars'!

Future work could perhaps extend the ideas above to produce different, related types of approximation, and perhaps look for signs of their existence in human behaviours. In particular, could we quantify the mapping from actual dollars to probability – what is the empirical 'exchange rate'?

As discussed, the reason for the existence of unitary coherent percepts – useless for MEU action selection – is one of the biggest questions in Cognitive Science and the detailed study of such approximations could perhaps shed some light upon it.

6.3.2 Learning

ThomCat as currently presented requires a user-specified SCFG prior. In deterministic music, this will be a deterministic grammar, having only one parse which specifies the whole composition. In general semi-improvised music there will be some non-unitary probabilities allowing for a specified distribution of possible performances. There is a continuum from 'semi-improvised' to 'improvised' music as the distribution increases in entropy: even the most apparently 'free' jazz solo is usually made up of at least some recognisable motifs and transforms of those motifs. For practical musical applications it is inconvenient and probably inaccurate to rely on human specification of these SCFGs. Instead, it would be useful to automate at least some of the specification by learning from previous performances, and fine-tuning the learning during later additional performances (even during a live accompaniment concert).

From a cognitive viewpoint, it is again useful to consider such extensions as a way to model and test human learning behavioural concepts and performance.

This section considers several types of learning, from tuning of parameters to creation of new models. These discussions are relevant not only to ThomCat, but to the other music perception models constructed in this thesis: the priming particle filter score-follower and RhythmKitten, and are intended to be relevant to general hierarchical perception systems. Perceptual model creation has been debated by philosophers for centuries so we do not expect to give a definitive account, but we will at least suggest some potentially useful heuristic methods, applicable to both the engineering application and as candidate cognitive theories.

6.3.2.1 Tuning parameters

The simplest and best-understood form of learning in the Bayesian framework is parameter updating. If we have a top-level node X with prior $\pi(X)$, the standard way to learn is to parametrise the prior, for example adding new Dirac Delta nodes $\{\theta_i\}$ as parents of X so that $\pi(X) = f(\{\theta_i\})$. This structure was used (though not yet for learning) in RhythmKitten's rhythm networks (fig. 4.1) to specify the start time and tempo priors, and Dirichlet mixture priors. A method to (locally) optimise the priors for a single model in a single performance is to use the EM algorithm. Usually though we wish to learn parameters which are useful in a variety of performances (including unobserved future performances). A naive way to approximate this is to compute the optimal $\hat{\theta}_i(D_i)$ for each available performance i, and update $\theta \leftarrow (1-\alpha)\theta + \alpha\hat{\theta}_i$ where α is a heuristic 'learning rate'. A more rigorous method is to maintain a count of the number of training examples seen for each parameter, and update in accordance with this (e.g. see [98]).

This method was used by Raphael [131] to train his low-level HMM segmenter and to update his high-level Bayesian network score model. Identical methods could be added to the priming particle-filter score follower and to RhythmKitten as well as ThomCat. A similar method is used by the inside-outside algorithm [4] to train its grammar, and we could carry it over to ThomCat to update its grammatical – and other – probabilities. Essentially parametric learning simply updates the priors to make them more compatible with the current data, hence making them suggest similar data in the future. (This is similar to biological and simulated Hebbian learning [38], in which neural weights are modified to make the current configuration more probable in future.)

Of particular interest in ThomCat are the free-float priors, $\pi^{\emptyset}$, which allow for free-floating structures that do not appear in linguistic models such as inside-outside.

Strengthening these priors for structures which appear to free-float regularly could play a useful role in higher-level model learning, discussed next.

6.3.2.2 Learning new models

Much less well understood than tuning – and probably intractable – is the problem of learning new models. In the data mining literature (e.g. [75]) heuristic methods such as genetic algorithms are often used to search some large candidate space of network *structures* to explain data, with some approximate prior assigned to each structure (for example, as a function of the number and types of operations used to construct it). These methods typically require operations that make small and hopefully useful changes to existing candidate models, or combine existing models. This issue was introduced in section 4.4.2.3; here we make further suggestions about possibly useful operations for altering music models and for constructing new models from scratch.

First though, is the question of *when* to bother creating a new model, rather than using an existing one and accepting that it may be a poor fit. In science this is the question of when to perform a 'paradigm shift'. For example we may have a *ROCK1* rhythm in RhythmKitten that is repeatedly failing to explain a re-occurring extra snare drum note at beat 3.5; or in which one of the bass drum hits is regularly missing; despite being the best available explanation. One option is to continue to use the model, updating its parameters to allow for this wider set of data to be generated from it. The alternative is to consider the probability that our own model base is incomplete, and try adding a new model. Computing such a probability is intractable, and the issue is similar to that faced in the priming particle filter, that we must consider an approximate probability of our own failure. As in the PPF, we suggest simply using some hash-classifier $P(failure|circumstances, \theta)$, where θ and the function form are set by trial-and-error to be empirically useful.

One way to create new models is as variations on the previous best fitting model. In RhythmKitten, the models make inferences about which data points are unexplained (i.e. assigned to sink priors) and which model notes are missing from the data, so an obvious way to create candidate changes is to produce models that include extra notes at the positions of unexplained data, and which omit missing data. The analogous situation in ThomCat arises when a rule repeatedly has a missing child in the same place, and a the same free-floater in that location. For example, the rule $VERSE \rightarrow A,A,B$ may repeatedly be perceived as $VERSE \rightarrow A,\emptyset,B$ (where $\emptyset$ denotes a missing child) but with a free-floating K structure at that location as in fig. 6.11. This suggests creating a new rule $VERSE \rightarrow A,K,B$ as an alternative, with a probability influenced (somehow) by the free-floater's learned $\pi^{\emptyset}$ prior. If the new

rule is successful in later performances, the free-floater's $\pi^{\emptyset}$ prior should also then be reduced by the parametric learning described earlier.

Another way to create new models is based on bottom-up regularities. For example, if we notice that the freefloaters *A,B,A,B* often occur in that sequence with no rule to explain them, then we could postulate the rule $NEWRULE \rightarrow A,B,A,B$ to explain them. Once postulated, *NEWRULE* will then appear as a free-floater itself (having an appropriately heuristic, tunable $\pi^{\emptyset}$ prior, based on its frequency of occurrence) and may later become part of larger structures using the variations and bottom-up rules described here.

To avoid an explosion in the number of models, we need methods to remove as well as create models. Pruning of models could occur if they have not been used for some heuristic period of time. More interestingly, pairs of models could be merged if they grow to resemble each other via parameter learning. Again, the question of when two models are alike enough to be seen as "the same thing" is a deep cognitive and philosophical one [64]. In robotics, the problem of 'loop closure' [120] is similar to this: deciding when two known locations are the same; in science, realising that concepts such as temperature and molecular motion refer to the same thing is a key type of innovation. Again we suggest the use of some empirically useful hash-classifier to take the place of this philosophising.

6.3.3 Extended musical structures

ThomCat currently operates in the highly constrained minidomain of semi-improvised musical scene perception from chord-bar sequences. But as a general scene perception architecture it could be applied to other, more difficult musical scene perception tasks, of which we give some examples.

Parallel input percepts have already been mentioned: for example considering both rhythmic types (from RhythmKitten) and the chords played within them, possibly by multiple instruments.

Rather than following large-grained bars of chords, another musical task is to perceive scenes of melodies of smaller-grained notes and their relationships. A new Copycat descendant, Seek-Well, is currently under development [121] which groups melodic notes into percepts such as rising and falling streams, 'leaps' and 'steps', and possibly higher-level relations between these structures. These ideas could be brought into ThomCat's Bayesian blackboard framework, along with the melodic agent ideas of Reis [142].

Melodies – and to a lesser extent, chord sequences – may exist in transformed instantiations in many musical styles. Transforms include shifting pitch and time-stretching existing structures. (In Baroque music especially, more advanced transforms include reversing and harmonically inverting melodies.) Such transforms have been modelled in automated composition systems as extensions to grammars similar to those used by ThomCat [56]. Perception systems could try to perceive such structures by considering the space of transformed hypotheses in addition to their standard forms. New priming hash-classifiers would be needed to navigate through the enlarged search space.

Moving from notes to even lower-level structures, blackboard systems have previously been used for musical transcription directly from sound waves, for example by constructing hypotheses about individual harmonics, notes and chords, without the use of pre-processing or segmentation. The ThomCat architecture could be used to provide principled handling of rivalry, which has often been handled heuristically in other systems. For example, the matchstickman network of fig. 6.4 could equally well refer to individual harmonics l_i being explained by the presence of notes m_j. This task is a little harder than the matchstickmen because the latter assumed each Boolean l_i was generated by at most one m_j. In the harmonics case the l_i may have continuous energy, generated by the sum of several sources, so ThomCat would need to be extended to account for this.

Modelling global correlations is an important aspect of scene perception. ThomCat included just one – key – as a proof-of-concept. Real musical scenes have many other global factors including identity of the players (what are their favourite chords and riffs?), venue of performance (rock riffs are unlikely in a concert hall) and perhaps most importantly, consistency of rewrite rule selection (if rule $V \rightarrow A,A,B$ was used to form the first verse, the changes of it being used in the second increase.) All can be modelled similarly to global key in ThomCat.

A highly challenging task would be to extend ThomCat to perceive unknown musical compositions in real time, based only on a general stylistic grammar. For example, such an extended ThomCat could perceive an unknown pop song on the radio using only knowledge of the pop genre in general. Such music – whilst deterministic from the performers viewpoint – is effectively semi-improvised from the listener's view. Indeed while the 'semi-improvised' concept used throughout this thesis has appeared somewhat artificial, it is this 'semi-improvised' perception of deterministic music through uncertain priors that forms the bulk of everyday human musical perception.

6.3.4 (Re)constructing the past and future

The current implementation of ThomCat assumes that the region of interest is always around the current position in real time: its 'window of attention' is always centred on the latest bar of observed data. Although this is usually the case in human music perception – we attend to the current state of the world – there are occasions when we 'cast our mind' back to what happened in the past ("I just noticed this movement is in a different key... so did I play all those notes wrong at the beginning?"), or 'think ahead' to predict what will happen in the distant future ("I have 50 bars rest but then there's a difficult brass fanfare, how does that go...?" or "what should I do in my next jazz solo if the guitarist keeps making that chord substitution?"). For such cases, ThomCat could be extended to move the window of attention around to focus inference where it is needed. The need for controlled movement of attention is of course more evident in domains such as (foveal) visual scene perception, but a ThomCat-like system would capable of capturing the idea in simpler musical minidomains. Choice of where to place the focus of attention should be based on the expected utility of the decision, such as the (hash-classified) value of information to be found there, and the value of the actions made there.

ThomCat does not currently remove winning structures from the past when the window of attention moves on from them: they are left in the computer's memory (and appear in the graphical parse as 'frozen'). This works well for our chosen minidomain but there may be cases when memory is limited and non-attended objects should be pruned. If this occurs, then attention is moved back to the past, the historic scene must be reconstructed. Reconstruction could be based on the current high-level percept acting as a top down prior on what happened (for example, if I know I am three minutes into a *SONG*, then I can reconstruct the *VERSE* at its start based on the grammar and the position of the whole *SONG*). A limited form of memory may also be of use, remembering particularly unusual deviations of the data from the most probable top-down construction. In general the reconstructed past will not form the same percept as was originally perceived, because new top-down information is available and the set of models used to perceive it may have changed through learning.

6.3.5 Modelling human cognition

A recent movement in Psychology is *Bayesian Cognitive Science* [24], [57] which assumes that humans behave in a Bayesian (near-)optimal way, then seeks to extract details of what models, parameters and heuristics are being used under this assumption. As ThomCat has been designed based on ideas about human cognition, it could

perhaps form the basis of a Bayesian Cognitive Science study, and could be extended to try to model human percepts and actions as accurately as possible.

More speculatively, architectural concepts from ThomCat might be used as broad-brush predictions about what biological neurons might be doing. In particular, it has been speculated that cortical columns might perform Pearl message passing [77]. ThomCat's considerations of loopiness, rivalry and correlations suggest that a Gibbs inference engine on these Bayesian columns may be more appropriate for scene perception.

6.4 Discussion

The ThomCat architecture continues the MAP-seeking annealing-cycle approach to scene perception used by RhythmKitten (and to a lesser extent, the priming particle filter). The approach is extended to hierarchical scenes featuring global correlations. The generative Bayesian networks for such scenes are highly loopy, and intractably large if all possible hypotheses are instantiated. They feature strong correlations due to rivalry, but contain much independence of causal influences which may be exploited by inference algorithms. This set of properties leads to annealed Gibbs sampling being a useful inference method. We extended standard Gibbs sampling to sample from clusters of co-parents (to exploit ICI) and fused dynamic structure-building ideas from blackboard systems into the Gibbs sampler itself, choosing active Gibbs nodes to prime from.

Questions about the use of MAP percepts in action selection were discussed. An important open question in Cognitive Science is why humans bother to perceive a unitary coherent scene at all, when Bayesian theory shows that optimal actions are only achieved by considering the 'Bayesian blur' of all possible worlds. However such computations are highly intractable. Extending ThomCat with action and reward nodes tentatively suggests that unitary coherent percepts may produce fast ways of selecting good but suboptimal actions.

Even with these priming, pruning and cluster-sampling speedups, inference in ThomCat is still very slow, requiring longer than real-time to run on the relatively simple musical minidomain problems discussed here. At least on classical computers, slowness seems to be unavoidable due to the NP-hardness of the underlying loopy networks. This presents an apparent dead-end for more realistic scene perception models. However, the next chapter will investigate another, even more impressive speedup for Gibbs sampling, making use of quantum computational hardware, which

we will see achieves a quadratic speedup over the classical case, so could make larger scene problems amenable to real-time perception.

Chapter 7

A quantum generalisation speeds up scene perception

The text of this chapter is based on the following peer-reviewed publication [63]. Rezek and Roberts provided advice on standard Bayesian theory and on presentation only.

- *C. Fox, I. Rezek, and S. Roberts.* Local quantum computing for fast probably map inference in graphical models. In *Proceedings of the Second AAAI Symposium on Quantum Interaction, 2008.*

We have examined the general problem of hierarchical perception in a Bayesian framework, using the minidomain of semi-improvised musical scenes as a recurring example. The view developed here of how scene perception could work has comprised three levels of computation: First, low-level approaches to raw data hash-classification as in chapter 3. These are useful because low-level data is usually large and full Bayesian inference (for example, considering all possible instruments, physical locations, environments and playing styles that could generate a raw sound wave) is intractable at this level in real time. Heuristic hash-classifiers can rapidly (though approximately) map the raw data to a higher level of abstraction. In the music minidomain, these are chords and drum onsets; in vision, the analogous classes would be low-level edge and corner detectors, and perhaps features such as SIFT features [101]. Second, chapter 4 discussed segmentation at the mid-level. This makes a *hard* decision about region boundaries. In the music minidomain, RhythmKitten segmented the input into bars. In vision [99] segmentation can be done using colour boundaries for example. The segmentation step is useful to reduce the complexity of the third stage, hierarchical scene construction. Given the mid-level set of segmented objects (chords in bars in the music minidomain; visual regions with their properties in vision), hierarchical perception dynamically constructs a Bayesian network of candidate phenomenal objects using priming and pruning.

The key problem with this view is what happens next. Chapter 6 showed how to construct the network and move a window of attention around it, and the next task as that of finding a maximum utility percept of the contents of this window, which can be formulated as an MAP problem given suitable utility and action percepts. The key problem is that this MAP task is unavoidably #P-hard. Chapter 2 reviewed the inside-outside and CYK algorithms, which solves the hierarchical perception task in polynomial time but only for a very limited class of percepts, i.e. those which are context-free. General hierarchical scene perception does not have this property. For example in the music case there are global properties such as musical key and style; in vision research there is the analogous ideas of global 'gist' [114].

We have seen several methods for approximate MAP inference in Bayesian networks, as required in hierarchical scene perception: deterministic annealing in Bethe message passing; annealed variational Bayes, and annealed Gibbs sampling. When running in real time, all of these methods take the form of a rapid series of annealing cycles: the network is 'heated' then cooled during inference towards a Dirac delta distribution. The near-delta distribution is then 'collapsed' to the MAP by reading off the node modes. The collapsed state is then used as the starting point for the next cycle (as all these algorithms have multiple local minima and are sensitive to starting point) and to schedule actions in response to the percept. However it is known [32] that even such *approximate* inference in Bayesian networks is still #P-hard, in the sense of number of computations required to reach an arbitrary error rate. This is a very serious problem for a theory of perception: after all our work in low-level heuristics, segmentation, network construction and attention restriction, we are still stuck with an #P-hard problem to complete the inference. The experiments with ThomCat in particular showed that even simple minidomain tasks such as chord sequence perception can become slower than real-time on a modern PC once more than about seven objects with their fringes are inside the attention window.

One commonly discussed possibility for speeding up such inference in Bayesian networks (and hence hierarchical scene perception) is the use of massively parallel computer hardware. All of the above algorithms are effectively parallel algorithms anyway – when implemented on a serial computer they run by choosing some random update ordering or clocking scheme to simulate the parallelism – so implementation on a parallel machine is simple. While this has achieved useful speedups (for example, Google's large Bayesian networks[1]) it still only provides a linear speedup: with N machines we can do N times as much computation, where N is the number of nodes.

[1]Details not publicly available.

A radically new idea to speed up hierarchical scene perception is to make use of another new kind of hardware: quantum computing. We consider this due to desperation and beauty: desperation as we are stuck with an #P-hard problem at the highest level of perception, and approximations and parallel hardware do not seem good enough to solve it efficiently; beauty because we will see that the fundamental structure of quantum computing theory is intriguingly close to that of Bayesian theory. Quantum computing theory was developed in the 1980s and in recent years has become a working, implemented commercial technology [31] – though the size, expense and speed of current devices still resemble the room-sized paper-tape and mercury-line machines that first implemented Turing machines. However there is every reason to believe that like those machines, quantum hardware will in time reduce in scale and cost. We should not be put off discussing useful algorithms for our theoretical problem of hierarchical scene perception just because the commercial hardware market cannot yet sell us equipment on which to run them at an affordable price. (We can of course simulate them, albeit slowly, on a current PC to provide proofs of concept.)

After reviewing the relevant yet simple concepts of quantum computing theory and previous work, this chapter will present a novel algorithm for speeding up the MAP inference task required in hierarchical perception by a quadratic factor: in the sense that only $\sqrt{N}$ cycles are needed to obtain the same trajectory probabilities as the classical Gibbs sampler used in ThomCat. Unlike standard quantum algorithms for search [71] that achieve similar speedups but requiring complex global operations, our algorithm uses only small, local messages as in regular Bayesian networks. The algorithm combines aspects of the other approximation methods discussed so far. Recall that the fundamental problem of Bayesian computation is that joint distributions have a size exponential in the number of nodes, so representing and computing with them is unavoidably exponentially hard. We have discussed how the approximations try to work around this. The Pearl/Bethe approach does not attempt to represent the joint, but approximates its marginals. The mean-field approach represents an approximate joint as the cross product of its marginals, but at the expense of losing all representation of correlation between nodes. The MCMC approach represents the joint by a sequence of samples – a *path* – drawn from it over exponential time. Like Bethe, the quantum algorithm will represent node marginals at each node. Like mean-field, the marginals will also represent part of the joint. But unlike mean-field, the quantum algorithm is able to represent the *correlations* between nodes. Like all the algorithms, the quantum algorithm will use rapid annealing cycles, beginning

with the previous MAP solution and ending with a collapse step to reduce a near-delta distribution to a pure delta spike. Like the Gibbs sampler, each node's state will make transitions according to the Gibbs probability given its neighbours, and this proposal is always accepted. However it extends the Gibbs sampler by exploring all possible sample paths *simultaneously* using quantum parallelism. The quantum algorithm solves the same hierarchical perception problem as the other approximation methods: MAP inference in an attentional window –and has been developed as a generalisation of all of them. As such it forms the culmination of this thesis.

Strictly in passing, we note that a form of quantum perception has been proposed in a highly speculative, vague, qualitative sense by several authors [126, 74] as a candidate mechanism for *biological* perception, though largely for prior philosophical reasons rather than computational gains. The constructive engineering approach of this thesis cannot say anything about the biological plausibility of these ideas – that is clearly an empirical question for empirical scientists. However if we can show that a quantum version of our existing perceptual approximation schemes can give a significant improvement in speed, then this would make these speculative claims more *likely* because there would then have been a higher chance of them being selected by evolution. While the claims are extremely speculative, they have a potentially large impact on major problems in philosophy if they do turn out to be correct; however that is not the focus of this thesis: we are instead merely concerned with making our existing hierarchical scene perception algorithms run as fast as possible in spite of their #P-hardness.

7.1 Quantum computing theory

We begin with a brief overview of quantum computing theory. Despite the huge amount of intellectual effort that was required to develop quantum mechanics and quantum computing, the theory delivered to us by its inventors is in fact very simple, being couched only in 'high-school' finite-dimension linear algebra. Because of this form it is highly amenable to representation in the Matlab programming language, which is strongly based around vectors and matrix structures. To aid the development of the quantum perception algorithm, a Matlab library, QCF [55], was developed to simulate quantum computer operations. We give QCF examples of the basic concepts, to show how simple quantum computing is from the Machine Learning programmer's point of view. QCF programs could in theory be run on real quantum computers; here we use the QCF simulator on a classical machine to give the same results but

```
>> phi_1=bin2vec('011')
0
0
0
1
0
0
0
0
>> phi_2 = dec2vec(5, 3) %second argument is how many bits in the register
0
0
0
0
0
1
0
0
```

Figure 7.1: QCF representation conversion functions, called from a Matlab session.

requiring much longer to run. For a more detailed review of quantum computing theory, see [119].

A classical (non-quantum) computational register of bits exists in a single state, for example, a three-bit register could store a configuration of three Boolean MRF nodes such as 101 (also notated as the decimal 5). Such classical states may also be thought of as basis vectors in an 2^3-dimensional space. To emphasise this view we use 'ket' notation[2]:

$$|101\rangle \equiv |5\rangle \equiv [00000100]^T$$

where ^{T} denotes a transposition from row to column vector. Here, the three bits of the classical register provide $2^3 = 8$ basis vectors, representing numbers from 0 to 7. The number 5 is the sixth such number (as the first is zero) so the vector representation contains a '1' in the sixth element and zeros in the others.

In QCF, the functions *bin2vec* and *dec2vec* convert binary and decimal numbers into ket (i.e. vector) representation as shown in fig. 7.1.

Classical operations that map register states to register states may then be represented by a 2^3 permutation matrix. For example, the operation 'subtract 1 (mod 8)' is represented by:

[2]Ket notation is a hangover from Quantum Mechanics, in which it generalises to infinite-dimension Hilbert space. Quantum Computing works only with finite-dimension vectors, so for our purposes the ket is synonymous with a column vector.

$$U = \begin{bmatrix} 0 & 1 & 0 & 0 & 0 & 0 & 0 & 0 \\ 0 & 0 & 1 & 0 & 0 & 0 & 0 & 0 \\ 0 & 0 & 0 & 1 & 0 & 0 & 0 & 0 \\ 0 & 0 & 0 & 0 & 1 & 0 & 0 & 0 \\ 0 & 0 & 0 & 0 & 0 & 1 & 0 & 0 \\ 0 & 0 & 0 & 0 & 0 & 0 & 1 & 0 \\ 0 & 0 & 0 & 0 & 0 & 0 & 0 & 1 \\ 1 & 0 & 0 & 0 & 0 & 0 & 0 & 0 \end{bmatrix}$$

and when applied to the previous 5 state we compute 5-1=4:

$$U\,|5\rangle = |4\rangle$$

$$\begin{bmatrix} 0 & 1 & 0 & 0 & 0 & 0 & 0 & 0 \\ 0 & 0 & 1 & 0 & 0 & 0 & 0 & 0 \\ 0 & 0 & 0 & 1 & 0 & 0 & 0 & 0 \\ 0 & 0 & 0 & 0 & 1 & 0 & 0 & 0 \\ 0 & 0 & 0 & 0 & 0 & 1 & 0 & 0 \\ 0 & 0 & 0 & 0 & 0 & 0 & 1 & 0 \\ 0 & 0 & 0 & 0 & 0 & 0 & 0 & 1 \\ 1 & 0 & 0 & 0 & 0 & 0 & 0 & 0 \end{bmatrix} \begin{bmatrix} 0 \\ 0 \\ 0 \\ 0 \\ 0 \\ 1 \\ 0 \\ 0 \end{bmatrix} = \begin{bmatrix} 0 \\ 0 \\ 0 \\ 0 \\ 1 \\ 0 \\ 0 \\ 0 \end{bmatrix}$$

Note that U is unitary (i.e. $U^\dagger U = I$) – only unitary operations are allowed in quantum computing. Note that the ket and unitary operation representations are similar to those used in hidden Markov models, having state vectors and transition matrices.

When two registers are brought together and considered as a single system, the Kronecker (or 'tensor') product – notated $\otimes$, or `kron` in Matlab – of their state vectors gives the state vector for the combined system. This is the same operation used in Bayesian networks when we consider and iterate over the combined state space of a set of parent nodes. The $\otimes$ symbol can be omitted, and the 'bringing together' property means that the product can be written as a single ket containing a concatenation of the bits:

$$|10\rangle \otimes |01\rangle \equiv |10\rangle\,|01\rangle \equiv |1001\rangle$$

$$[0010]^T \otimes [0100]^T = [0000000001000000]^T = |1001\rangle$$

It follows that the operation U comprised of two independent operations U_1 and U_2 acting on separate subspaces is given by $U = U_1 \otimes U_2$, so that

$$U_1 |a\rangle \otimes U_2 |b\rangle = U |ab\rangle$$

So far the discussion has been equally applicable to classical and quantum computers: we have simply notated classical registers and operations as vectors and unitary matrices. Classical computing is a special case of quantum computing in which states are limited to the basis vectors of the register (i.e. the vectors always contain exactly one '1''and the other elements are '0'; and the unitary matrices are permutation matrices). Unlike classical computing, quantum computing allows systems to exist at any point on the complex unit radius hypersphere in the state space, rather than just the classical basis vectors. For example a register can be in a *superposition* of basis states $|000\rangle$ and $|110\rangle$:

$$|\Psi\rangle = \alpha_{000} |000\rangle + \alpha_{110} |110\rangle$$

where the α are complex numbers chosen to describe a hypersphere location, $\sum_i |\alpha_i|^2 = 1$. General unitary matrices may operate on the state vectors rather than just the special permutation cases. Unitary matrices may be thought of as rotations on the hypersphere. For example, the *Hadamard matrices* H_n map n-bit classical states to superpositions:

$$H_1 |0\rangle = \frac{1}{\sqrt{2}} |0\rangle + \frac{1}{\sqrt{2}} |1\rangle$$

Hadamard operators are defined recursively by

$$H_1 = \frac{1}{\sqrt{2}} \begin{bmatrix} 1 & 1 \\ 1 & -1 \end{bmatrix}, H_{n+1} = H_n \otimes H_1$$

and QCF provides a function `hadamard(n)` to generate them, e.g.:

```
>> hadamard(2)
ans =
    0.5000    0.5000    0.5000    0.5000
    0.5000   -0.5000    0.5000   -0.5000
    0.5000    0.5000   -0.5000   -0.5000
    0.5000   -0.5000   -0.5000    0.5000
```

Each $|\alpha_i|^2$ describes the probability of an *observation* collapsing the register into state $|i\rangle$. An observation is a random non-linear operator, which when applied, draws a probability from this distribution, and *changes* the state to the classical basis vector

$|i\rangle$.[3] This is the only non-linear operator allowed in this form of quantum computing theory[4]. Its physical meaning is still debated by philosophers [3] but empirically it appears to correlate with the act of a subject looking at, or otherwise obtaining information from the system. Note that the observed vector is drawn from the set of basis vectors for the system *as a whole*, rather than drawing bits independently. For example, making an observation on the state $\frac{\sqrt{3}}{2}|00\rangle + \frac{1}{2}|11\rangle$ gives the following *joint* observation distribution on the two bits:

$$P(00) = \frac{3}{4}, P(01) = 0, P(10) = 0, P(11) = \frac{1}{4}$$

In this case the values of the two observed bits are perfectly correlated. After observing one bit's value, we know for certain that the other bit has the same value. This is a form of *entanglement*: we say that the two qubits are entangled because observation of one affects the observation distribution of the other.

The QCF `measure` function simulates the nonlinear observation operation by computing these probabilities then randomly drawing from them, for example:

```
phi = sqrt(3)/2 * bin2vec('00') + 1/2*bin2vec('11')
phi =
    0.8660
         0
         0
    0.5000
>> pretty(phi)
ans =
 0.86603|00> + 0.5|11>
>> phi=measure(phi)
phi =
     1
     0
     0
     0
>> pretty(phi)
ans =
 1|00>
```

[3] In general, observations in arbitrary bases and subspaces are possible, however we do not need these in our algorithm.

[4] See [119] for a discussion of general 'POVM' measurements. We assume that all observations are made in the standard basis here.

This will give the above result, $|00\rangle$, three quarters of the time, and the other possible result, $|11\rangle$ one quarter of the time. (The QCF `pretty` printing function converts the vector representation back to binary ket notation for display.)

7.1.1 Summary of quantum computing theory

The above discussed all the postulates of quantum computing theory, which can be seen to be merely simple applications of linear algebra and probability theory. The theory can be written concisely as four postulates (based on [119]) in addition to standard linear algebra:

1. Associated with any finite physical system – such as a collection of discrete Bayesian network nodes – is a complex vector state space. The system is completely described by its state vector, which is a unit vector in this space.

2. Except for observations, all operations on the system are described by unitary operators.

3. The state of a composite system having substates $|a\rangle$ and $|b\rangle$ is the Kronecker product $|a\rangle \otimes |b\rangle$.

4. An observation of state $\sum_i \alpha_i |i\rangle$ changes the state to $|i\rangle$ with probability $|\alpha_i|^2$ and the resulting state is knowable by the observer.

Note that in general, states are unknowable, because observing them generally changes them. We have seen that using entanglement, states are able to represent and compute with the set of all possible classical states each with an amplitude, but we cannot generally read all of this information. We can compute with it, but making an observation reduces it to a single basis state that we can know. This is extremely interesting from the view of our task of hierarchical perception, because we wish to make computations on the joint distribution of many nodes, but we do not need to report the joint. We only want to report a particular function of it, namely the location of the MAP state. This is the beautiful structural similarity between Bayesian theory and quantum computing theory: they both compute with exponentially large joints, but only report the result of a function of those joints. It is therefore worth considering how this structural similarity can be exploited in our hierarchical perception task.

7.1.2 Comparison to existing work

Quantum optimisation methods have been featured in the physics literature in recent years (e.g. [82], [49], [20]). However this work has not generally been framed in the context of discrete local quantum computation, the MAP Bayesian network task, or

the language of the Machine Learning community. The novel contribution of this chapter is to give a purely quantum-computational algorithm for graphical model MAP optimisation as required in the general hierarchical perception task, which generalises the previous approximate algorithms and which we show achieves a quadratic speedup over the classical Gibbs sampler. The algorithm uses only local operators, in contrast to various extensions of the standard Grover algorithm to parameter search. Grover's algorithm was one of the first quantum algorithms, used as the basis for many others, so we review it below; this review also provides a first example of a quantum algorithm in action, implemented and simulated in QCF.

7.1.2.1 Grover's algorithm

Grover demonstrated that quantum computers can perform unstructured database search faster than their classical counterparts, which must consider each element in turn taking $O(n)$ computation. In this simple example of Grover's algorithm, we use a function, *haystack*, to represent the database. We are searching for a needle in the haystack, i.e. there is one element of the database that we require. The *haystack* function returns 1 if queried with the correct needle element, and 0 for all the other elements. In this example, *haystack* is defined for a 5-qubit input, and returns 1 for element 8 ('00100' in binary):

$$haystack(i) = \begin{cases} 1 : i = 8 \\ 0 : i \neq 8 \end{cases}$$

Grover makes use of the fact that for any function f with a binary string input and a Boolean output, we can define a corresponding unitary matrix V_f, whose action on input strings $|i\rangle$ is to invert their amplitudes if and only if $f(i) = 1$; otherwise, it does nothing:

$$V_f(|i\rangle) = \begin{cases} |i\rangle : f(i) = 1 \\ -|i\rangle : f(i) = 0 \end{cases}$$

The QCF library provides a function `vf` to create such matrices. First the Boolean function is defined, continuing our example:

```
function b = haystack(i)
if i==8
    b=1;
else
    b=0;
end
```

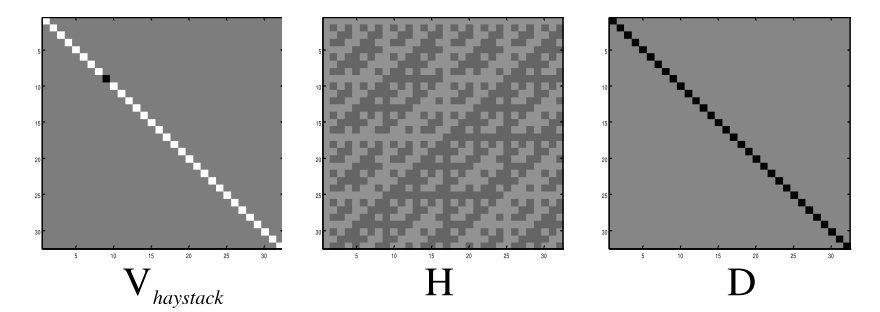

Figure 7.2: Graphical display of matrices used in Grover's algorithm for 5-bit search space. White=+1, black=-1.

Then `vf` converts it into unitary matrix form (where n specifies the number of bits to act on):

```
n=5;
V_haystack  = vf('haystack', n);
```

The output in this case is a 32×32 matrix (too large to write out here, but shown graphically in fig. 7.2 as $V_{haystack}$) which can be seen as an identity matrix but having $V_{haystack}(8,8) = -1$ instead of the usual 1.

The other operation used by Grover is an 'inversion about the average' matrix, D_N, defined by

$$D_N \begin{bmatrix} a_0 \\ a_1 \\ \dots \\ a_{2^N-1} \end{bmatrix} = \frac{1}{N} \begin{bmatrix} \sum_{i=0}^{2^N-1} a_i - a_0 \\ \sum_{i=0}^{2^N-1} a_i - a_1 \\ \dots \\ \sum_{i=0}^{2^N-1} a_i - a_{2^N-1} \end{bmatrix}$$

where N is the number of bits to be operated on. Continuing our example, we construct an inversion about the average operator for three bits, D_3 using the QCF command

```
D = ia(5)
```

Again this produces a large 32×32 matrix, shown graphically in fig. 7.2. We will also make use of a 5-bit Hadamard operator H_5 as shown in the same figure:

```
H = hadamard(5)
```

Grover's algorithms works by iteratively applying $V_{haystack}$ and D to the current state. Each iteration amplifies the probability of a measurement collapsing the state to the correct 'needle' value. Grover showed that performing a measurement after $\sqrt{(}2^N)\pi/4$ iterations is highly likely to give the correct result. Here is the algorithm in QCF:

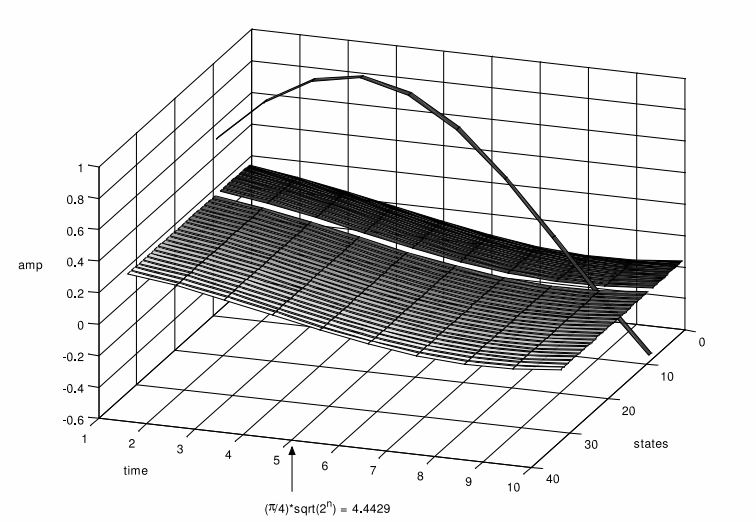

Figure 7.3: Results of Grover's algorithm simulated in QCF. At each time step, the graph shows the probabilities of an observation giving each of the 32 states. The amplitude of the sought state, $|8\rangle$, increases over time relative to the others, reaching a maximum at $\sqrt{(}2^N)\pi/4 \approx 4$ iterations.

```
phi = bin2vec('00000');
phi = H*phi;
for i=t:10
    phi=V_haystack*phi;
    phi=D*phi;
end
phi=measure(phi);
```

Fig. 7.3 shows the amplitudes of the different 'needle' candidates over time (i.e. number of iterations). We chose to keep the algorithm running for 10 iterations, but note that the amplitude for 8 (the correct needle value) reaches its peak at about $\sqrt{(}2^N)\pi/4 \approx 4$ iterations, as predicted by Grover. The N bits can represent $n = 2^N$ numbers (from 0 to 31 in our case), so rather than the classical $O(n)$ search speed we have reached $O(\sqrt{n})$.

Grover's algorithm is general in that it can be used to search any discrete finite space for any property representable by a V_f function. It was generalised by [82] to optimisation search problems (which are #P-hard rather than NP-hard so do not have an available f function). This work reported heuristic results that were, unimpressivly, 'at least comparable to classical heuristics'. A similar generalisation [49] reported a quadratic speedup. [145] noted that it could be used to search for weights in a neural network. However these Grover-like algorithms are still problematic in

practice because they require large global unitary operators to be constructed. Much of quantum computing research is devoted to finding collections of smaller, local operators which are easier to implement. But it is not known what the smallest local operators are to achieve Grover-like speedups. We note that classical message passing in Bayesian networks has already been formulated as a set of operators [143], so a good question to ask is if this approach can be extended to the quantum domain.

7.1.2.2 Adiabatic optimisation

A recent development in quantum optimisation is the *adiabatic* method [52], which uses a different global operator to match Grover's $\sqrt{N}$ unstructured search speedup [146]. This speedup is dependent on prior information on the difference in probability between the first and second most likely states, and would not be achieved for general optimisation such as MAP inference. It is an open question how it could be exploited in those particular inference tasks where we do have some such information. (The private Canadian company D-Wave claims to have demonstrated a working 16-bit adiabatic machine [31].)

7.1.2.3 Physical annealing

Physical *quantum annealing* (e.g.[20]) uses continuous quantum mechanics (rather than discrete quantum computing theory) and physical temperatures (rather than temperature as an abstract numerical parameter) to physically cool systems towards their ground states. This work is fascinating but has been couched in the language of continuous physics and is generally inaccessible to AI researchers. Our algorithm achieves a similar goal to this work but using pure quantum computing operators. Furthermore, it is presented to be accessible to AI researchers and as a ThomCat speedup, and as a generalisation of the variational and Gibbs approximate inference methods seen so far.

7.1.2.4 Bayesian models of quantum systems

In contrast to our algorithm and the above work, another strand of research [154], [96] has generalised Bayesian networks to make inferences *about* quantum systems.

7.2 Quantum hierarchical scene perception

The hierarchical scene perception task requires us to find the MAP state of a graphical model. We will present a quantum computational algorithm capable of performing

MAP inference in graphical models. The algorithm quickly finds a probably MAP or near-MAP configuration with a quadratic speedup over classical Gibbs sampling, in the sense that after the same number of sampling steps it yields observation probabilities $\frac{1}{Z}Pr_{obs}(\tau)^2$ of trajectories τ where $Pr_{obs}(\tau)$ are the classical Gibbs observation probabilities and Z is a normalising coefficient. A trajectory specifies the *history* of the sample as well as its final state, as quantum computing is reversible. The algorithm uses only small local operators and makes essential use of decoherence – which is usually thought of as a hindrance rather than a feature in quantum computation. Unlike Grover and other algorithms, all state amplitudes remain real and positive throughout.

Simulating quantum computing on a classical machine is an extremely intensive task – this is of course to be expected as the whole point of quantum computing is to be faster than classical machines. Simulation is intensive of both memory and time, as all possible register states must be modelled. This means that even a 16-bit register requires 2^{16} complex-values amplitudes to represent it: and a single operation on it requires a $2^{32} \approx 4.3 \times 10^9$ element complex-valued matrix. Because of these huge computational requirements, we must at this point abandon the music minidomain, as running simulations on typical ThomCat windows of attention would require unavailable computational resources. Instead we will simulate very small toy problems which will serve as a proof of concept for a future quantum ThomCat (which must surely be named 'ErwinCat'). To simplify the size of the simulations further, we will switch from working with Bayesian networks to Markov random fields. Any graphical model can be written in MRF form (e.g. [117]), by introducing more nodes and simplifying the links potentials. MRFs have only one link type, specifying undirected pairwise potentials: this is simpler to work with that the full Pearl equations which require priors and likelihoods to be distinguished. However throughout the discussion it should be borne in mind that a real quantum computer would be capable of working directly with ThomCat's analogous directed Bayesian networks, without the need for conversion.

We work with an undirected, loopy, pairwise Markov random field with N Boolean-valued nodes X_i. Let nodes have potentials ϕ_{ii} and links have potentials ϕ_{ij} so that the joint is

$$P(x_{1:N}) = \frac{1}{Z}\prod_i \phi_{ii} \prod_{ij} \phi_{ij}$$

where Z is a normalisation coefficient. We restrict our discussion to potentials which may be defined by integer-valued *energies* E_{ii} and E_{ij} such that

$$\phi_{ii} = \exp(-E_{ii}), \phi_{ij} = \exp(-E_{ij})$$

We wish to find the MAP configuration $\hat{x}_{1:N}$ to maximise $P(x_{1:N})$. This is generally NP-hard [148].

Our quantum notation uses upper and lower case letters as follows: A refers to a state space; $|A\rangle$ is a general vector in that space; a is an integer (in decimal or binary notation) denoting a basis state; $|a\rangle$ is the basis vector in A with coding a. (Such binary codings will be used to represent Boolean MRF configurations.) We write true and cooled *model* probabilities as $P(a)$ and $Q(a)$ respectively, in contrast to quantum *observation* probabilities $Pr_{obs}(a) = |\alpha_a|^2$.

7.3 Representing joints by superpositions

A quantum register of N qubits ('quantum bits') is able to store and represent amplitudes of all its 2^N possible classical configurations simultaneously. A fundamental problem in machine learning is that the joint distribution of N variables has exponential size. The structure of quantum amplitudes is very similar to that of joints so we can use the α_i to store our probabilities (up to normalisation; recall that our probabilities normalise to 1 but amplitudes normalise so that $\sum_i |\alpha_i|^2 = 1$), requiring only N qubits instead of exponential resources. We will try to set the α_i so that $\alpha_i = \frac{1}{\sqrt{Z}} Q(i)$ where Q is some probability distribution of interest over the space of binary registers I, and Z is chosen for correct normalisation of the amplitudes. Distributions Q of interest include the true joint $Q(i) = P(i)$ and the MAP-Dirac delta joint, $Q(i) = \delta(i; \hat{i})$. The latter is of interest because it guarantees that an observation on the system will yield the MAP state, $|\hat{i}\rangle$. We may move gradually from a flat $Q(i)$ to $Q(i) = P(i)$ then to $Q(i) = \delta(i; \hat{i})$ via a series of *cooled* distributions, $Q(i) = P(i)^{1/T}$.

We have seen that it is possible to represent joints in linear resources on a quantum register. The problem is how to bring the register into such a representational state.

Grover's method [71] performs quantum unstructured search over N items in $O(\sqrt{N})$. However this algorithm requires the use of large operations over the whole space, applied in series. It also only finds target values whose target-ness is a function of their value only, rather than of their relationship to other values as in optimisation problems. In contrast, we present an algorithm using small local operators which may be applied in parallel during each overall sequential step, as in the local node updates of an annealed Gibbs sampler or Boltzmann machine [78]; and which seeks targets that are global and near-global MAP states.

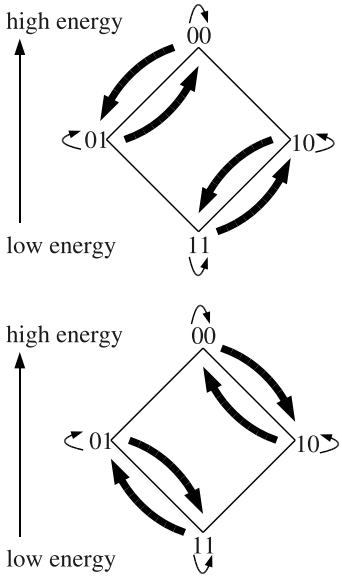

Figure 7.4: Top: A unitary operator that maps states to a superposition of themselves and the state reached by flipping their rightmost bit. Bottom: A similar operator for the leftmost bit.

7.4 Side-stepping the unitary requirement by extending the state space

The key idea is to construct and apply operators which transfer low-probability (high-energy) states to high-probability (low-energy) states. A difficulty with this is that quantum operators must be unitary. This means that as much amplitude must flow out of each state as flows in, in a similar sense to 'global balance' in Markov chain theory. Initially this may seem to prevent our approach being possible, as the high-energy states must ultimately flow back to low-energy states. This is indeed the case when a fixed-size system is considered. Consider fig. 7.4(top) and fig. 7.4(bottom), which respectively illustrate unitary operations acting on single qubits to flip the left and right qubits of a two-qubit register. In general, single-qubit operators may have some portion of self-transition as well, shown by the thin loops. The widths of the arrows illustrate the transition probabilities. (Note that this state transition diagram is not an MRF, but could represent moves between *configurations* of a Boolean MRF with two nodes.) Suppose the two variables are elements from an MRF whose configuration energies satisfy

$$E(|00\rangle) > E(|01\rangle) = E(|10\rangle) > E(|11\rangle)$$

where $E(|\psi\rangle) = \sum_i E_{ii}(|\psi\rangle) + \sum_{i,j} E_{ij}(|\psi\rangle)$ with the second sum over linked pairs of nodes.

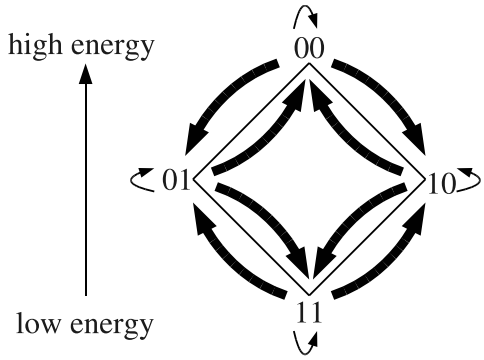

Figure 7.5: The same operators as fig. 7.4, plotted together as a single figure. Note that unitarity is equivalent to the requirement that there is an equal amount of total flow into and out of each node.

In this case we would like to design operators that tend to make the probability amplitudes flow away from the high-energy state $|00\rangle$ and down towards the low-energy state $|11\rangle$. This is not possible with ordinary unitary operators on the 2-qubit space because unitary operators must have as much flow out of states as into them.

However by adding *new* bits to the system at *every* operation we will be able to make the state space grow and keep on providing new places for the accumulating high-probability states to flow to. The algorithm is reminiscent of – and inspired by – the idea of blowing a constant stream of *coolant* particles over a machine to cool it. The particles then flow away as *garbage* (or 'exhaust'), carrying away information (cf. Feynman's heat computers, [53]). They can then be ignored for the final measurement, but their existence is the key part of the algorithm. This process of spreading the superposition across a large garbage space is a form of *decoherence* (e.g. see [119]).

As we are considering only operators which – like the Gibbs sampler – flip only single qubits (and/or don't flip them) we may depict whole collections of such operators by a single diagram, as in fig. 7.5. Depending which of the bits is chosen to be considered next, one may read off the appropriate flow arrows without ambiguity.

Fig. 7.6 shows how the 2-variable system from fig. 7.5 may be extended with a garbage qubit to achieve the desired flows. This qubit is notated by the rightmost bit in the state labels, and is initialised to $|0\rangle$. Our node operators now act on the combined space of the node together with the garbage bit – i.e. the garbage bit's value may change as well as the node of interest. The figure shows how the low-energy state $|11\rangle$ may now act an attractor: the flow out of $|11\rangle|0\rangle$ does equal its flow in, but most of this flow is into $|11\rangle|1\rangle$, which maintains the $|11\rangle$ state of the nodes. We don't care about the resulting value of the garbage bit. For each operation a new, fresh garbage qubit, initialised to $|0\rangle$, is introduced to the system.

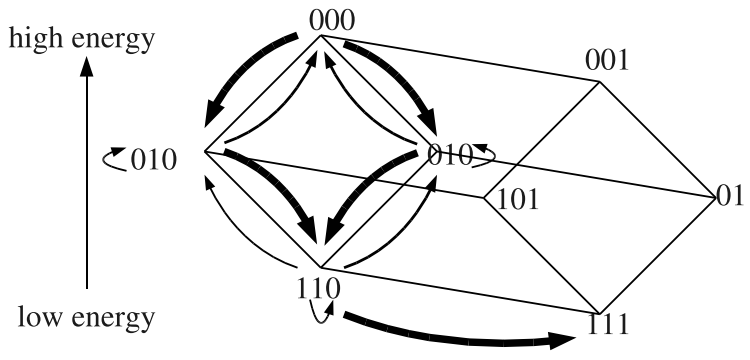

Figure 7.6: The rightmost qubit is new, introduced to extend the state space.

Because we are introducing *new* qubits at each step, we are able to control all of their initial states – setting them to $|0\rangle$. So we know that the initial complete state will have all its amplitude in the left half of the diagram. We can set up our unitary operator to have large flows from the left half to the right half, and vice versa. But we know that the flows from right to left (called 'shadow flows' and not shown on the diagram) will never actually be used. The states in the right half are called 'shadow states' and are never realised as initial states, only as resulting states.

7.5 Intuitive explanation

The algorithm is based on a simplified analogy to physical atoms being bombarded by photons. Each new coolant is like a photon; each node is like an atom. At each step, one coolant and one node (and its neighbours) interact, and like Gibbs sampling, the node may or may not flip as a result.

If the energy of the coolant/photon is exactly zero and an energy emission is possible from the atom/node, then the node flips and energy {emission} occurs. If the coolant has zero energy but the node is unable to emit energy then {no emission} occurs.

If the energy of the coolant is exactly the right amount to raise the atom/node to a *higher* energy state, then the node flips and {absorption} occurs. If coolant has energy but not the exact amount then {no absorption} occurs.[5]

[5]There is one special subcase where flipping the node would 'emit' zero energy, i.e. flipping makes no energy difference. In this case we make a superposed transition, {both flip and not flip} simultaneously. Amplitude thus disperses over equiprobable states, and this is required to escape from plateaux in the PDF. An alternative would be to always flip in such cases, but this would lead to undesirable random-walk MCMC behaviour as discussed in [118].

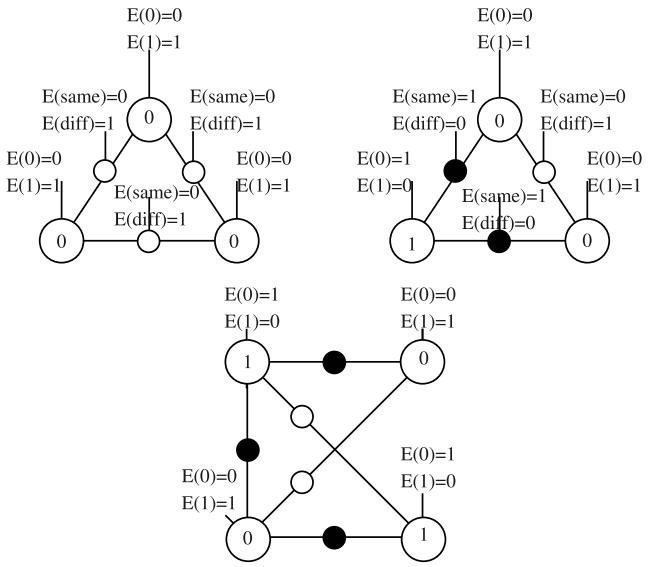

Figure 7.7: Top left: the $\hat{x} = 000$ test MRF. Top right: $\hat{x} = 010$ test. Bottom: $\hat{x} = 1010$ test. White and black links prefer same and differing nodes respectively. Nodes are labelled with optimal values.

The terms in braces above refer to cases in the algorithm pseudo-code in section 7.6.2. Note that they refer to transitions between basis configurations of nodes and coolants: in the general quantum setting, nodes and coolants will be in a superposition of states, so all of these cases can occur simultaneously. As in classical Gibbs sampling, we would like to encourage the emissions to occur more often, and absorptions to occur less often, whilst still allowing energy increases to escape from local minima. We can control the rates of emissions and absorptions by manipulating the composition of the coolant superpositions. Initially we create 'hot' coolants with relatively high amplitudes of high energy states. Then we reduce the temperature to make the low-energy states more likely. Use of the term 'temperature' is analogical: the algorithm itself may run on a standard quantum computer.

As discussed above, all operators are required to be unitary. As well as 'energy bits', our coolants contain 'change bits' which act as in fig. 7.5 to construct shadow states and transitions. As before these states are never realised as inputs, but exist as outputs; they are a book-keeping device to allow unitarity to be maintained. The algorithm in section 7.6.2 is a constructive proof that this is possible.

7.6 Formal algorithm description

We consider Boolean MRFs so each node may exist in state $|0\rangle$ (false) or $|1\rangle$ (true). Initially, the system state space Ψ_0 is just the state space of the nodes:

$$\Psi_0 = X_1 \otimes X_2 \otimes ... \otimes X_N$$

This system state is initialised by an N-bit Hadamard transform H_N to a superposition of all possible configurations (this may be though of as the limit of high temperature, the flat distribution):

$$|\Psi_0\rangle := H_N |00...0\rangle = \frac{1}{\sqrt{Z}} \sum_{\psi=0}^{2^N-1} |\psi\rangle$$

At each step s of the algorithm we extend the state space with a new *coolant* state space $(\Gamma_s \otimes C_s)$, so as the algorithm progresses, the space grows very large:

$$\Psi_s = \Psi_0 \otimes (\Gamma_1 \otimes C_1) \otimes (\Gamma_2 \otimes C_2)... \otimes (\Gamma_s \otimes C_s)$$

Each coolant has two parts: $|\Gamma\rangle$ is generally made of several qubits, and is called the *energy register*. It is analogous to a fresh particle being blown over the system to heat or cool it; or to a photon striking an atom to transfer energy in or out of it. $|C\rangle$ is a single qubit and is called the *change bit* because we will use it as a book-keeping device to record whether the node changed state (allowing us to create 'shadow states' and to make our operators unitary). Initially each of the coolants are created in the state:

$$|\Gamma C\rangle = \frac{1}{\sqrt{Z}} \sum_{\gamma=0}^{\Delta_{max}E-1} \exp(-\gamma/T) |\gamma\rangle |0\rangle$$

(where as usual Z is chosen so that the sum of squared amplitude moduli is unity). The amplitudes follow a Boltzmann distribution. T is a temperature parameter, and is chosen so that $\sum_{\gamma=1}^{\Delta_{max}E-1} \exp(-\gamma/T) > 1$.[6] As in classical Gibbs annealing, T will be gradually reduced. It should be follow a similar schedule as used in classical Gibbs; these schedules are generally heuristic. We will show that the quantum algorithm produces a speedup for the same schedule as its classical counterpart. $\Delta_{max}E$ is chosen to be the first power of two above the highest possible change in network energy that would occur from flipping one Boolean node, $\log_2 \Delta_{max}E = \max_{i,x_i,m_i} \lceil \log_2 \Delta E \rceil$, with $\Delta E = |E_i(x_i, m_i) - E_i(\bar{x}_i, m_i)|$, described in section 7.6.2.

[6] This is to encourage more energy emission than absorption.

7.6.1 Algorithm

First construct an operator U_i for each node X_i as detailed in section 7.6.2. At each iteration k, choose a random node ordering (as in classical Gibbs sampling). For each node X_i in the ordering, create a new coolant and add it to the system. The size of the state space thus keeps growing. Apply the node's associated operator U_i to the subspace consisting of X_i and its neighbours M_i. Ignore old coolants – they are garbage. When all nodes in the ordering have been operated on, lower the temperature according to the cooling schedule and progress to the next iteration. With appropriate hardware, each iteration's operations could be applied in parallel instead of random series.

The system converges to a superposition of local minima, and usually to a global minimum with high amplitude. Unlike the classical Gibbs sampler, all possible histories of proposal acceptances and rejections are explored in parallel by the superposition.[7]

7.6.2 Constructing the local operators

Before running the quantum iterations we first define one operator U_i corresponding to each node X_i. These operators are local in the sense that they act only on the reduced state space Ψ_i comprising the node X_i, its neighbours $M_i = \bigotimes_{X_j \in neigh(X_i)} X_j$, and a coolant system $(\Gamma \otimes C)$:

$$\Psi_i = X_i \otimes M_i \otimes \Gamma \otimes C$$

Define $E_i(x_i, m_i)$ to be the energy contribution due to the prior on X_i and the links to its neighbours:

$$E_i(x_i, m_i) = E_{ii}(x_i) + \sum_{X_j \in neigh(X_i)} E_{ij}(x_i, x_j)$$

Each U_i is constructed by algorithm 3 (refer to section 7.5 for descriptions of the cases):

As part of the purpose of this chapter is to present the QCF library, and show how simple quantum computer *programming* can be, we give the Matlab/QCF code for the algorithm in Appendix A.

[7] This is reminiscent of an 'exact particle filter', which adds new particles at each step to ensure all possible histories are explored. Information carried away by coolants could be used to recover the trajectory histories.

Algorithm 3 Pseudo-code for the construction of the U_i operator matrices. This is a classical algorithm which simply inserts numbers into matrices. A quantum algorithm will later apply these operators to the nodes and coolants. Refer to the text for descriptions of the various cases.

for each x_i configuration; each m_i configuration; each $\gamma = 0 : \Delta_{max}E$ **do**
  $\Delta E := E_i(\bar{x}_i, m_i) - E(x_i, m_i)$
  {network's energy gain by flipping}
  if $\Delta E \neq 0$ **then**
    if $\gamma = 0$ **then**
      {coolant carries no energy – possible cooling}
      if $\Delta E < 0$ **then**
        $U\,|x_i, m_i, 0, 0\rangle := |\bar{x}_i, m_i, -\Delta E, 1\rangle$
        {emission}
        $U\,|\bar{x}_i, m_i, -\Delta E, 1\rangle := |x_i, m_i, 0, 0\rangle$
        {shadow transition}
      end if
      if $\Delta E > 0$ **then**
        $U\,|x_i, m_i, 0, 0\rangle := |x_i, m_i, 0, 0\rangle$
        {no emission}
        $U\,|x_i, m_i, 0, 1\rangle := |x_i, m_i, 0, 1\rangle$
        {shadow transition}
      end if
    else
      {coolant carries energy – possible absorb}
      if $\Delta E = \gamma$ **then**
        $U\,|x_i, m_i, \gamma, 0\rangle := |\bar{x}_i, m_i, 0, 1\rangle$
        {absorption}
        $U\,|\bar{x}_i, m_i, 0, 1\rangle := |x_i, m_i, \gamma, 0\rangle$
        {shadow transition}
      else
        $U\,|x_i, m_i, \gamma, 0\rangle := |x_i, m_i, \gamma, 0\rangle$
        {no absorption}
        $U\,|x_i, m_i, \gamma, 1\rangle := |x_i, m_i, \gamma, 1\rangle$
        {shadow transition}
      end if
    else
      {equi-energy special case – flipping node has no energy effect}
      $U\,|x_i, m_i, \gamma, 0\rangle := \frac{1}{\sqrt{2}}\,|x_i, m_i, \gamma, 0\rangle + \frac{1}{\sqrt{2}}\,|\bar{x}_i, m_i, \gamma, 0\rangle$
      {flip and not flip}
      $U\,|x_i, m_i, \gamma, 1\rangle := \frac{1}{\sqrt{2}}\,|x_i, m_i, \gamma, 1\rangle - \frac{1}{\sqrt{2}}\,|\bar{x}_i, m_i, \gamma, 1\rangle$
      {shadow transitions}
    end if
  end if
end for

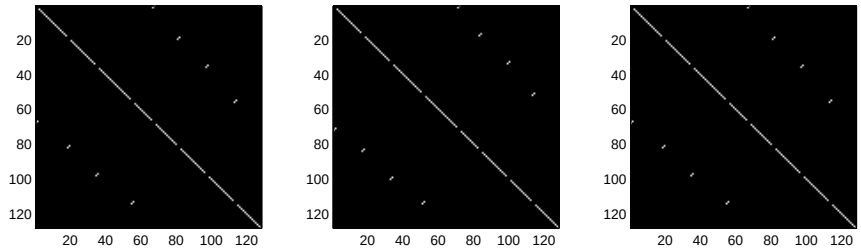

Figure 7.8: Operators U_0, U_1 and U_2 constructed for the $\hat{x} = 010$ task by the algorithm in section 7.6.2. There is one operator for each node. In this simple case the matrix representations of the operators are all of size 120×120. Matrix elements are always 0 or 1 (except in special equi-energy cases). After the operators are constructed, the quantum computing itself may run. Applying U_i to node i and its neighbours is analogous to a classical Gibbs step of updating one node.

7.7 Results

Simulations were performed using the above QCF/Matlab code. Due to the exponential resources required to simulate quantum devices, the present work is restricted to giving only proof of concept demonstrations. We consider the 3-node and 4-node Boolean MRFs in fig. 7.7. The first net has unit energy penalties for nodes with value 1 and for links whose neighbours are different, i.e. $E_i = x_i$, $E_{ij} = \Delta(x_i, x_j)$, so its MAP state is 000. The second net has asymmetric penalties and MAP state 010. The third is a more complex net with MAP state 1010. Fig. 7.8 shows the three operators constructed for the $\hat{x} = 010$ task.

A naive state-vector-based computer simulation would require resources exponential in the number of iterations, due to the expanding state space from the new coolants (e.g. of size about 2^{50} after 4 iterations of the 4-node net). However as we don't care about the resulting states of the coolant – they are garbage – we may make use of the density matrix formulation of quantum computing (e.g. see [119]), which allows us to 'trace out' over these coolant states. This essentially provides us with the analogous operator to the 'sum' in the 'sum-product' algorithm (the 'products' corresponding to the unitary operators). It is the lack of ability to sum out states – which reduces information – that prevents us from using quantum algorithms without garbage bits to do inference. Summing these traces uses the bulk of computing time on a classical computer simulation.

The performance of the quantum algorithm was compared to the analogous classical Gibbs sampler, as currently used in ThomCat, whose acceptance probabilities are $\frac{1}{Z}\exp(-E/T)$. The same arbitrary cooling schedule was used in both algorithms, and was chosen prior to the experiments: at the k^{th} iteration we set $T = \frac{1}{k+1}$. Each

classical sampler was run for 100,000 trials, each trial initialised with a random configuration. The table below shows the empirical probability of the classical sampler (C) reaching the MAP solution after the final iteration, compared with the (deterministic) quantum observation probabilities (Q), for the three tasks with MAP targets 000, 010 and 1010. The quantum algorithm appears to lag the classical sampler for the first two iterations before overtaking.

	000		010		1010	
step	C	Q	C	Q	C	Q
1	.68	.51	.68	.43	.63	.35
2	.80	.76	.81	.70	.84	.72
3	.84	.84	.82	.86	.89	.92
4	.84	.87	.84	.92	.92	.98
5	.84	.89	.84	.94	.94	.99
6	.85	.89	.84	.96	.95	.999

7.8 Discussion

7.8.1 Comparison to classical Gibbs sampling

A fundamental problem in Machine Learning is that the joint over N nodes generally requires exponential resources to represent it – whether as a brute-force table or the classical Gibbs sampler's use of ensembles of N-node configurations over exponential time. We have shown how by using quantum amplitudes to represent joint probabilities, it is possible to represent the exponential-sized joint of N nodes instantaneously using only N physical nodes. However, moving the state vector into this representation is non-trivial and we showed how to use a unitary quantum analog of Gibbs sampling to get there. Further, we showed how it can be cooled towards the MAP solution, $Q(x) \to \delta(x; \hat{x})$.[8]

The algorithm does not make use of phase cancellations (all amplitudes are positive real), so trajectories in the state space starting from each of the superposed initial states evolve almost completely independently of each other.[9] When we make a measurement after the cooling, we are therefore selecting just a single trajectory history to have occurred, and discarding the others.[10] It may be asked what advantage this has over the classical Gibbs method of simply sampling a single s-step trajectory

[8] $Q(x) \approx P(x)^{1/T}$ is represented implicitly as the marginal of the explicit $Q(\tau) = Q(x, \gamma_{1:s}, c_{1:s})$. The coolant space was introduced as it was not possible to carry out marginalisation explicitly by unitary operators.

[9] The unimportant exception being the special plateaux case.

[10] The computation is reversible, so reachable basis states including coolants specify historical trajectories.

$\tau = \{x_{1:N}\}_{1:s}$ without the need for quantum hardware – what is the use of the unobserved trajectories? The answer is that as we are representing cooled *model* probabilities $Q(\tau)$ by *amplitudes*, α_τ, our probability of *observing* a particular τ is given by the (renormalised) *squared* probability of its occurrence in the corresponding classical sampler, $Pr_{obs}(\tau) = \alpha_\tau^2 = Q(\tau)^2$. This gives a quadratic amplification of the probabilities $Q(\tau)$ from the classical sampler. This quadratic speed-up appears to fit in spirit with the result [165] that the optimal quantum search speedup is $O(\sqrt{N})$, however full mathematical analysis of the algorithm's nature could form the basis of future work. Such analysis could also try to explain why the first two iterations give poorer results than the classical sampler: we believe this is due to the sub-optimal nature of our sampling, as for simplicity we excluded the possibility of low but non-zero energy states absorbing energy.

7.8.2 Comparison to variational inference

Although we have presented the algorithm largely as a quantum extension of the classical Gibbs sampler, an alternative and interesting view is as a quantum extension of classical variational methods [11] such as variational Bayes and loopy (Bethe) message passing. Such methods approximate the true joint $P(x_{1:N})$ by a product $Q(x_{1:N}) = \prod_{i=1}^{N} Q_i(x_i)$ which ignores correlation structure but is typically more tractable to compute. In the Gibbs analogy, we view our algorithm as a multitude of Gibbs samplers, running in 'parallel worlds'. An alternative view is to consider the amplitudes over individual node subspaces as being like variational Q_i factors. However they are extended from classical variational methods because they are entangled with the other nodes, so representing the correlation structure. A re-derivation of the algorithm from this perspective could be interesting future work.

Chapter 8

Conclusion

We presented an architecture for unitary coherent scene perception, in the context of a minidomain. The architecture comprises three stages: features, segmentation and blackboard, and is intended to generalise to other domains. Bayesian theory was used within all stages and to join them together. The stages would be unnecessary in ideal inference, which would consider the exhaustive set of explanations. But we have viewed features, segmentation and blackboards as heuristics to approximate inference in practical computation time.

The blackboard heuristics in particular shed light on two philosophical issues. The attention heuristic shows how reports about the past are subject to change, providing an alternate view to those of Dennett [40]. Treating rewards as likelihoods to infer the unitary coherent percept with maximum utility gives a quantitative version of James's pragmatism [84]. ThomCat as a whole provides a constructive demonstration of rigorous Bayesian foundations for Hofstadter's Copycat research programme.

The quantum algorithm gives a quadratic speedup in the blackboard stage, using the quantum ability to represent complete N node joints instantaneously with only N physical nodes. While other quantum annealing methods exist, ours is a pure quantum computing method, presented in the language of Machine Learning, and we hope that it will contribute to mutual understanding between the two fields. It generalises the variational and Gibbs methods. Although non-toy simulations are not currently possible, we gave proof of concept examples to illustrate the speedup that a future 'ErwinCat' blackboard would have over its classical ThomCat counterpart. Such an annealed quantum, Bayesian message passing, hierarchical priming and pruning system would fuse the fields of quantum computing, Machine Learning and blackboard systems and would truly be *an Entangled Bayesian Gestalt*.

Appendix A: Matlab/QCF code

Listing 8.1: MATLAB/QCF code implementing the quantum algorithm.

```
function rho_phi=run_net(node, link, E_max, E_bits)


%compile a list of neighbors of each node from the links
for i=1:length(node)
    node(i).neigh=i;
end
for i=1:length(link)
    node1 = link(i).node1;
    node2 = link(i).node2;
    node(node1).neigh = [node(node1).neigh node2];
    node(node2).neigh = [node(node2).neigh node1];
end
for i=1:length(node)
    node(i).E_phi=zeros(2^(length(node(i).neigh)), 1);
end

%make links bidirectional (speed up searching)
L=length(link);
for i=1:L
    link(L+i).node1 = link(i).node2;
    link(L+i).node2 = link(i).node1;
    link(L+i).E     = link(i).E';
end

%phi format is:  |i,1,n2,...,nm> for node i with neighbours n

for i=1:length(node)

    %make a table of energies for each state
    n_neigh = length(node(i).neigh);
    for phi_dec=0:2^(n_neigh)-1
        phi_bin = dec2bin(phi_dec, n_neigh);
        E_phi = compute_energy(i, node, phi_bin, link);
        node(i).E_phi(phi_dec+1) = E_phi ;  %NB offset
    end

    %init U_i.  The last bit is change bit
    U_i = zeros( 2^length(phi_bin) * 2^E_bits * 2^1 );

    %make U_i
```

```
%for each input  |in>  = |phi>*|E>*|0>      (final bit is change bit)
%make      output |out>
for phi_dec=0:2^(n_neigh)-1
    phi_bin = dec2bin(phi_dec, n_neigh);

    %consider the possible output |psi> got by flipping node i
    psi_bin    = phi_bin;
    psi_bin(1) = num2str(not(str2num(psi_bin(1))));
    psi_dec    = bin2dec(psi_bin);
    %lookup energy of |phi> and |psi>
    E_phi = node(i).E_phi(phi_dec+1);
    E_psi = node(i).E_phi(psi_dec+1);
    dE    = E_psi - E_phi;   %energy gain BY the system

    %E=0 is the possible emmission case -- different from the rest
    for E=0:E_max

        %complete |in> state
        in_bin    = [phi_bin  dec2bin(E,E_bits)  '0'];

        b_split=false; %flag for sepc case of equienergy

        if (dE~=0)
            if (E==0) %possible emission, or equienergy flip
                if (dE<0) %energy lost by system -- transition
                    out_bin    = [psi_bin    dec2bin(-dE,E_bits)  '1'];

                    sh_in_bin  = out_bin; %shadow transition
                    sh_out_bin = in_bin;
                else   %no change, E>0
                    out_bin    = in_bin;   %self transition

                    sh_in_bin  = [phi_bin    dec2bin(E,  E_bits)  '1'];
                    sh_out_bin = sh_in_bin;   %shadow self transition
                end
            else      %E>0 are possible absorbtion cases
                if (dE==E) %energy absorbed by system -- transition
                    out_bin    = [psi_bin    dec2bin(0,  E_bits)  '1'];

                    sh_in_bin  = out_bin;
                    sh_out_bin = in_bin;
                else   %no change
                    out_bin    = in_bin;   %self transition

                    sh_in_bin  = [phi_bin    dec2bin(E,  E_bits)  '1'];
                    sh_out_bin = sh_in_bin;   %shadow transition
                end
            end
        else   %dE==0, any E
            b_split=true;

            out_bin    = [psi_bin    dec2bin(E,E_bits)  '1'];
            sh_in_bin  = out_bin; %shadow state, opposite transition
            sh_out_bin = in_bin;
```

```
            end

            %complete |out> and |shadow out> states
            in_dec       = bin2dec(in_bin);
            sh_in_dec    = bin2dec(sh_in_bin);
            out_dec      = bin2dec(out_bin);
            sh_out_dec   = bin2dec(sh_out_bin);

            %insert transition into U   (+1 adjust matlab idx)
            if (~b_split)
                U_i(in_dec+1,    out_dec+1)    = 1;
                U_i(sh_in_dec+1, sh_out_dec+1) = 1;
            else %special case of equienergy
                U_i(in_dec+1,    out_dec+1)    = 1/sqrt(2); %flip
                U_i(in_dec+1,    in_dec+1)     = 1/sqrt(2); %dont flip
                U_i(sh_in_dec+1, sh_out_dec+1) = 1/sqrt(2); %flip shadow
                U_i(sh_in_dec+1, sh_in_dec+1)  = -1/sqrt(2); %flip shadow
            end

            node(i).U = U_i;

        end
    end
end

%now we need to scale up U to the whole net; and add new garbage...

%  |i1 i2 i3 > |E> |g1> |g2> ... |gn>

%init phi
phi = zeros(2^length(node),1);  %bin2vec('0000');
phi(1,1)=1;
H = hadamard(length(node));
phi=H*phi;              %create superposition of node states

%this is always constant now we've moved to density version:
idx_E_bit_start = log2(length(phi))+1;  %index of 1st new E bit in |in>

rho_phi = phi*phi'; %density representation

temperature = 1/2;     %at 1/2 no change will occur?

for iter=1:160  % *** THE MAIN QUANTUM COMPUTATION LOOP ***

    temperature = 1/(1+iter);

    %update each node, by firing a NEW energy chunk and NEW change bit at it
    for i=1:length(node)


        E = temperature.^(0:2^(E_bits)-1)'; %exp superposition of energy
        E = renormalise(E);
        ch = bin2vec('0');        %change bit

        rho_E = E*E';      %density versions
```

```
        rho_ch = ch*ch';

        rho_in = kron(rho_phi,rho_E);
        rho_in = kron(rho_in, rho_ch);  %create whole system density

        nbits_in = log2(length(rho_in));
        idx_new_garbage = idx_E_bit_start:nbits_in;

        %now expand U to all the qubits
        %and permute it so it applies to the right bits
        %dont change the rest of the qubits - ie the rest of the net and
        %old garbage
        I_rest = identity(nbits_in- (length(node(i).neigh)+E_bits+1)  );
        U_raw = kron(node(i).U,  I_rest);
        perm  = [node(i).neigh      idx_new_garbage];
        perm  = [perm               setdiff(1:nbits_in, perm)];
        U     = permute_matrix_bits(U_raw, perm);
        % U is now in same basis as |in>

        %apply coolant operator to density matrix
        rho_out = U*rho_in*U';

        %trace out energy and ch bits
        rho_phi = trace_out(rho_out, E_bits+1);

        disp(iter);
        disp(temperature);
        disp(diag(rho_phi));

    end
end
```

Bibliography

[1] Emile Aarts and Jan Korst. *Simulated Annealing and Boltzmann Machines*. Wiley, 1988.

[2] Hagai Attias. A variational Bayesian framework for graphical models. In *Advances in Neural Information Processing Systems*. MIT Press, 2000.

[3] Jim Baggott. *The meaning of quantum theory*. Oxford University Press, 1992.

[4] J. Baker. Trainable grammars for speech recognition. In J. J. Wolf and D. H. Klatt, editors, *Speech communication papers presented at the 97th meeting of the Acoustical Society of America*, pages 547–550. MIT Press, 1979.

[5] Adrian Barbu and Song-Chun Zhu. Cluster sampling and its applications in image analysis. Technical Report 409, Dept. of Statistics, UCLA, 2004.

[6] J. B. Bello and M. Sandler. Blackboard system and top-down processing for the transcription of simple polyphonic music. *Proc. COST G-6. Conf. on Digital Audio Effects*, 2000.

[7] J. B. Bello and M. Sandler. Techniques for automated music transcription. *International Symposium on Music Information Retrieval*, 2000.

[8] J.P. Bello, L. Daudet, S. Abdallah, C. Duxbury, M. Davies, and M.B. Sandler. A tutorial on onset detection in music signals. *IEEE Transactions on Speech and Audio Processing*, 13(5):1035–1047, 2005.

[9] J.M. Bernardo and A.F.M. Smith. *Bayesian Theory*. Wiley, 2000.

[10] Thomas Binford and Tod Levitt. Evidential reasoning for object recognition. *IEEE Tranactions on Pattern Analysis and Machine Intelligence*, 2003.

[11] Chris Bishop. *Pattern Recognition and Machine Learning*. Springer, 2006.

[12] C.M Bishop, J.M.Winn, and D. Spiegelhalter. VIBES: A variational inference engine for Bayesian networks. In *Advances in Neural Information Processing Systems*, 2002.

[13] Andrew Blake and Alan L. Yuille, editors. *Active Vision*. MIT Press, 1993.

[14] Rens Bod. *Beyond Grammar: An Experience-Based Theory of Language*. Center for the Study of Language and Information Publications, Stanford CA, 1998.

[15] Rens Bod. A unified model of structural organization in language and music. *Journal of Artificial Intelligence Research*, 17:289–308, 2002.

[16] A.S. Bregman. *Auditory Scene Analysis*. MIT Press, 1990.

[17] G. L. Bretthorst. *Bayesian Spectral Analysis*. Springer-Verlag, 1985.

[18] Rodney Brookes. The whole iguana. In Michael Brady, editor, *Robotics Science*. MIT Press, 1989.

[19] Stephen G. Brush. History of the Lenz-Ising model. *Reviews of Modern Physics (American Physical Society)*, 39:883–893, 1967.

[20] Giuseppe Castagnoli and David Ritz Finkelstein. Quantum-statistical computation. *Proceedings of the Royal Society A*, 459(2040):3099–3108, 2003.

[21] Ali Taylan Cemgil, H. Kappen, and D. Barber. A generative model for music transcription. *IEEE Transactions on Speech and Audio Processing*, 2004.

[22] A.T. Cemgil. *Bayesian Music Transcription*. PhD thesis, Radboud University of Nijmegen, 2004.

[23] D. Chalmers, R. French, and D. Hofstadter. High level perception, representation and analogy. In *Fluid Concepts and Creative Analogies* [81].

[24] Nick Chater, Joshua B. Tenenbaum, and Alan Yuille. Probabilistic models of cognition: where next? *Trends in Cognitive Sciences*, 10(7):292–293, 2006.

[25] R. Chatterjee. *Statistical Thought*. Oxford University Press, 2003.

[26] Nick Collins. Drumtrack: Beat induction from an acoustic drum kit with synchronised scheduling. In *Proceedings of the International Computer Music Conference*, 2005.

[27] A. Cont. Realtime audio to score alignment for polyphonic music instruments using sparse non-negative constraints and hierarchical HMMs. In *IEEE Int. Conf. Acoustics and Speech Sig. Proc.*, 2006.

[28] A. Cont and D. Schwarz. Score following at IRCAM. In *International Symposium on Music Information Retreival*, 2006.

[29] T. F. Cootes, G. J. Edwards, and C. J. Taylor. Active appearance models. *Lecture Notes in Computer Science*, 1407, 1998.

[30] R. Cowell. Advanced inference in Bayesian networks. *Learning in Graphical Models, ed. Jordan*, 2001.

[31] D-Wave. World's first commercial quantum computer demonstrated. http://www.dwavesys.com/, 2007.

[32] Paul Dagum and Michael Luby. Approximating probabilistic inference in Bayesian belief networks is NP-hard. *Artificial Intelligence*, 60(1):141–153, 1993.

[33] R. Dannenberg. An on-line algorithm for real-time accompaniment. *Proceedings of the International Computer Music Conference*, 1984.

[34] R. Dannenberg. Real-time computer accompaniment of keyboard performances. *Proceedings of the International Computer Music Conference*, 1985.

[35] R. Dannenberg. A stochastic method of tracking a vocal performer. *Proceedings of the International Computer Music Conference*, 1997.

[36] R. Dannenberg and N. Hu. Polyphonic audio matching for score following and intelligient audio editors. *Proceedings of the International Computer Music Conference*, 2003.

[37] N.D. Daw, Y. Niv, and P. Dayan. Uncertainty-based competition between prefrontal and dorsolateral striatal systems for behavioral control. *Nature Neuroscience*, 8:1704–1711, 2005.

[38] P. Dayan and L.F. Abbott. *Theoretical Neuroscience*. MIT Press, 2005.

[39] Richard Dearden, Nir Friedman, and Stuart J. Russell. Bayesian Q-learning. In *AAAI/IAAI*, pages 761–768, 1998.

[40] Daniel C. Dennett. *Consciousness Explained*. Penguin, 1998.

[41] Department of Chemistry, University of Oxford. *Quantum Pharmacology - 30 years on. (A Special Conference in Honour of Prof. W. Graham Richards)*, 2006.

[42] David Deutsch. *The Fabric of Reality*. Penguin, 1997.

[43] Diane Deutsch. *Muscial Illusions and Paradoxes*. Philomel Records, 1995.

[44] D.J.MacKay. *Learning in Bayesian Networks, Ed. M.I. Jordan*, chapter Introduction to Monte Carlo Methods. MIT Press, 1999.

[45] A. Doucet, J.F.G. de Freitas, and N.J. Gordon, editors. *Sequential Monte Carlo Methods in Practice*. Springer-Verlag, 2001.

[46] M. Dovey, T. Crawford, D. Byrd, J. Montal, J. Pickens, J. Bello, G. Monti, and M. Sandler. Overview of the OMRAS project. *Journal of the American Society for Information Science and Technology*, 2004.

[47] J. Stephen Downie, Kris West, Andreas Ehmann, and Emmanuel Vincent. The 2005 music information retrieval evaluation exchange: Preliminary overview. In J.D. Reiss and G.A.Wiggins, editors, *Proceedings of the 2005 International Symposium on Music Information Retreival*, pages 320–323, 2005.

[48] Kenji Doya, Shin Ishii, Alexandre Pouget, and Rajesh P. N. Rao, editors. *Bayesian Brain*. MIT Press, 2007.

[49] Christoph Durr and Peter Hoyer. A quantum algorithm for finding the minimum, 1996.

[50] Jay Earley. An efficient context-free parsing algorithm. *Communications of the ACM*, 13(2):94–102, 1970.

[51] Lee Erman, Fredrick Hayes-Roth, Victor Lesser, and Raj Reddy. The Hearsay-II speech understanding system: Integrating knowledge to resolve uncertainty. *ACM Computing Surveys*, 12(2), June 1980.

[52] Edward Farhi, Jeffrey Goldstone, Sam Gutmann, and Michael Sipser. Quantum computation by adiabatic evolution, 2000.

[53] Richard Phillips Feynman. *Feynman Lectures on Computation*. Addison-Wesley Longman Publishing Co., Inc., Boston, MA, USA, 1996.

[54] Cordelia Fine. *A Mind of its Own: How your brain distorts and deceives*. Icon Books, 2005.

[55] Charles Fox. QCF: Quantum computing functions for Matlab. Technical Report PARG-03-02, Robotics Research Group, Oxford University, 2003.

[56] Charles Fox. Genetic hierarchical music structures. In *Proceedings of the International Florida Artificial Intelligence Society Conference*, 2006.

[57] Charles Fox. Review of 'Bayesian Brain'. *Connection Science*, 20(1):67–68, 2008.

[58] Charles Fox. ThomCat: A Bayesian blackboard model of hierarchical temporal perception. In *Proceedings of the 21st International Florida Artificial Intelligence Research Society Conference*, 2008.

[59] Charles Fox, Neil Girdhar, and Kevin Gurney. A causal Bayesian network view of reinforcement learning. In *Proceedings of the 21st International Florida Artificial Intelligence Research Society Conference*, 2008.

[60] Charles Fox and John Quinn. How to be lost: principled priming and pruning with particles in score following. In *Proceedings of the International Computer Music Conference*, 2007.

[61] Charles Fox and Chris Raphael. Music++ technical documentation. Technical report, Indiana University (Confidential), 2005.

[62] Charles Fox, Iead Rezek, and Stephen Roberts. Drum'n'bayes: Online variational inference for beat tracking and rhythm recognition. In *Proceedings of the International Computer Music Conference*, 2007.

[63] Charles Fox, Iead Rezek, and Stephen Roberts. Local quantum computing for fast probably map inference in graphical models. In *Proceedings of the Second AAAI Symposium on Quantum Interaction*, 2008.

[64] Bob French. *The Subtlety of Sameness: A Theory and Computer Model of Analogy-Making*. MIT Press, 1995.

[65] B.J. Frey and D.J.C.MacKay. A revolution: Belief propagation in graphs with cycles. In M.I.Jordan, M.S.Kearns, and S.A.Solla, editors, *Advances in Neural Information Processing Systems*, volume 10. MIT Press, 1998.

[66] Nir Friedman, Lise Gentoor, Daphne Koller, and Avi Pfeffer. Learning probabilistic relational models. In *Proceedings of the Sixteenth International Joint Conference on Artificial Intelligence*, 1999.

[67] Martin Gardner. The fantastic combinations of John Conway's new solitaire game 'life'. *Scientific American*, 223:120–123, 1970.

[68] Simon Godsill and Manuel Davy. Bayesian harmonic models for musical pitch estimation and analysis. In *Proceedings of the IEEE International Conference on Acoustics, Speech and Signal Processing*, 2002.

[69] R.P. Goldman and E. Charniak. A language for construction of belief networks. *IEEE Transactions on Pattern Analysis and Machine Intelligence*, 15(3):196–207, 1993.

[70] M. Goto. An audio-based real-time beat tracking system for music with or without drumsounds. *Journal of New Music Research*, 30(2):159–171, 2001.

[71] Lov K. Grover. A fast quantum mechanical algorithm for database search. In *Proceedings of the Twenty-Eighth Annual ACM Symposium on Theory of Computing*, pages 212–219, 1996.

[72] L. Grubb and R. Dannenberg. Enhanced vocal performance tracking using multiple information sources. *Proceedings of the International Computer Music Conference*, 1998.

[73] S. Hainsworth. *Techniques for the Analysis of Musical Audio.* PhD thesis, Unviersity of Cambridge, 2003.

[74] S. Hameroff. Anaesthesia, consciousness and hydrophobic pockets - a unitary quantum hypothesis an anaesthetic action. *Toxicology Letters*, 100-101, 1998.

[75] David J. Hand, Heikki Mannila, and Padhraic Smyth. *Principles of Data Mining.* MIT Press, 2001.

[76] Gavin Harrison. *Rhythmic Illusions.* Warner Bros. Publications, 1998.

[77] Jeff Hawkins and Sandra Blakeslee. *On Intelligence.* Times Books, 2004.

[78] G. E. Hinton and T. J. Sejnowski. Learning and relearning in Boltzmann machines. In *Parallel distributed processing: Explorations in the microstructure of cognition, vol. 1: foundations*, pages 282–317. MIT Press, Cambridge, MA, USA, 1986.

[79] Donald D. Hoffman. *Visual Intelligence: How we create what we see.* W.W. Norton and Company, 1998.

[80] Douglas Hofstadter. A non-deterministic approach to analogy, involving the Ising model of ferromagnetism. In E. Caianiello, editor, *The Physics of Cognitive Processes*. World Scientific, 1987.

[81] D.R. Hofstadter and the Fluid Analogies Research Group. *Fluid Concepts and Creative Analogies*. Basic Books, 1995.

[82] Tad Hogg and Mehmet Yanik. Local search methods for quantum computers, 1998.

[83] T. Jaakkola and M. Jordan. Variational methods and the QMR-DT database. *Journal of Artificial Intelligence Research*, 10:291–322, 1999.

[84] William James. *Pragmatism: A New Name for Some Old Ways of Thinking.* Reprinted Dover, 1995, 1907.

[85] William James. *Principles of Psychology.* New York: Holt, 1980.

[86] M.I. Jordan and C. Bishop. *An Introduction to Graphical Models.* Unpublished book, forthcoming.

[87] I. Kant. *Critique of Pure Reason.* Reprinted by Project Guttenberg, 1781.

[88] K. Kashino, K. Nakadai, T. Kinoshita, and H. Tanaka. Organization of hierachical perceptual sounds. *Proceedings of the International Joint Conference on Artificial Intelligence*, 1995.

[89] Kunio Kashino and Norihiro Hagati. A music scene analysis system with the mrf-based information integration scheme. *Proceedings of the IEEE International Conference on Pattern Recognition*, 1996.

[90] Katayose. Unknown publications, in Japanese only, 1989.

[91] S. Kirkpatrick, C.D Gellat, and M.C. Vecchi. Optimization by simulated annealing. *Science*, 220:671–680, 1983.

[92] Will Knight. Entangled photons secure money transfer. http://www.newscientist.com/channel/fundamentals/quantum-world/dn4914.

[93] D. Koller and A. Pfeffer. Object-oriented Bayesian networks. In *Proceedings of Uncertainty in Artificial Intelligence*, 1997.

[94] Steve Larson. Seek well: A creative microdomain for studying expressive meaning in music. Technical Report CRCC-77, Center for Research on Concepts and Cognition, University of Indiana, 1993.

[95] K. B. Laskey. MEBN: A language for first-order Bayesian knowledge bases. *Artificial Intelligence*, 172(2-3):140–178, 2007.

[96] Kathryn Blackmond Laskey. Quantum causal networks. In *Proceedings of the 2007 AAAI Spring Symposium on Quantum Interaction*, 2007.

[97] Steffen L. Lauritzen and Dennis Nilsson. Representing and solving decision problems with limited information. *Management Science*, 47(9):1235–1251, 2001.

[98] Peter M. Lee. *Bayesian Statistics: An introduction.* Arnold Publishers, third edition, 2003.

[99] Tai Sing Lee and Alan L. Yuille. Efficient coding of visual scenes by grouping and segmentation. In Doya et al. [48].

[100] Tod Levitt, Thomas Binford, and Gil Ettinger. Utility-based control for computer vision. In *Uncertainty in Artificial Intelligence 4*, 1990.

[101] David G. Lowe. Object recognition from local scale-invariant features. In *International Conference on Computer Vision*, 1999.

[102] Per-Olov Lwdin, editor. *Quantum Biology and Quantum Pharmacology - Quantum Biology Symposium Proceedings No. 17.* Wiley, 1991.

[103] Stephane Mallat. *A Wavelet Tour of Signal Processing.* Academic Press, 1999.

[104] E. Mariani and G. Parsi. Simulated tempering: A new monte carlo scheme. *Europhysics Letters*, 19:451–468, 1992.

[105] D. Marr. *Vision.* MIT, 1985.

[106] K.D. Martin. A blackboard system for automated transcription of polyphonic music. *MIT Media Lab Tech. Report 385*, 1995.

[107] K.D. Martin. Automatic transcription of simple polyphonic music. *Third Joint Meeting of the Acoustical Societies of America and Japan*, 1996.

[108] David McAllester, Michael Collins, and Fernando Pereira. Case-factor diagrams for structured probabalistic modelling. In *Proceedings of the Annual Conference on Uncertainty in Artificial Intelligence*, 2004.

[109] T. McInerey and D. Terzopoulos. *Deformable Models in Medical Image Analysis: A Survey.* Medical Image Analysis, 1996.

[110] Brian Milch. *Probabilisitic Models with Unknown Objects.* PhD thesis, UC Berkeley, 2006.

[111] Melanie Mitchell. *Analogy-Making as Perception.* MIT, 1993.

[112] Melanie Mitchell. Copycat source code. http://web.cecs.pdx.edu/ mm/ccat-src/, 1993.

[113] Samuel K. Moore. Prototype quantum computer demo'ed. http://www.spectrum.ieee.org/feb07/comments/1710.

[114] K. Murphy, A. Torralba, and W. Freeman. Using the forrest to see the trees: A graphical model relating features, object, and scenes. In *Advances in Neural Information Processing Systems*, 2003.

[115] Kevin Murphy. *Dynamic Bayesian Networks: Representation, Inference and Learning.* PhD thesis, UC Berkeley, 2002.

[116] Kevin Murphy, Yair Weiss, and Michael I. Jordan. Loopy belief propagation for approximate inference: an empirical study. In *Proceedings of the Annual Conference on Uncertainty in Artificial Intelligence*, pages 467–475, Stockholm, 1999.

[117] P. Myllymaki and H. Tirri. Massively parallel case-based reasoning with probabilistic similarity metrics. In K. Althoff, M. Richter, and S. Wess, editors, *Proceedings of the First European Workshop on Case-Based Reasoning*, 1993.

[118] R. Neal. Suppressing random walks in Markov Chain Monte Carlo using ordered overrelaxation. Technical report, Dept. of Statistics, University of Toronto, 1995.

[119] M. Neilsen and I. Chuang. *Quantum Computing and Quantum Information.* Cambridge University Press, 2000.

[120] P. Newman and Kin Ho. SLAM loop closing with visually salient features. In *Proceedings of the 2005 IEEE International Conference on Robotics and Automation*, pages 635–642, 2005.

[121] Eric P. Nichols. Modeling melodic expectation and preference: A pilot study based on Larson's musical forces. Technical Report CRCC-124, Center for Research into Concepts and Cognition, Indiana University, 2007.

[122] Eric Nicols. Dynamic melodic expectation in the creative microdomain seek well. Technical Report CRCC-138, Center for Research on Concepts and Cognition, University of Indiana, 2005.

[123] N. Orio and F. Dechelle. Score following using spectral analysis and hidden Markov models. *Proceedings of the International Computer Music Conference*, 2001.

[124] J. Pearl. *Intelligient Reasoning with Probabalistic Networks*. Morgan Kaufmann, 1988.

[125] J. Pearl. *Causality*. Cambridge University Press, 2000.

[126] Roger Penrose. *Shadows of the Mind*. Oxford University Press, 1994.

[127] Avi Pfeffer, Daphne Koller, Brian Milch, and Ken T. Takusagawa. SPOOK: A system for probabilistic object-oriented knowledge representation. In *Uncertainty in Artificial Intelligence*, 1999.

[128] J. Pickens, J.B. Bello, T. Crawford, M. Dovey, G. Monti, and M. Sandler. Polyphonic score retreival using polyphonic qudio queries: A harmonic modelling approach. *ISMIR*, 2002.

[129] L. Rabiner. A tutorial on hidden Markov models. *Proceedings of the IEEE*, 77:257–286, 1989.

[130] L. Rabiner and B. Juang. *Fundamentals of Speech Recognition*. Prentice Hall, 1993.

[131] C. Raphael. Automatic segmentation of acoustic musical signals using hidden markov models. *IEEE PAMI*, 1999.

[132] C Raphael. A probabalistic system for automatic musical accompaniment. *J. Comp. Graph. Stats.*, 1999.

[133] C. Raphael. Automated rhythm transcription. *Ann.Symp.Mus.Res.*, 2001.

[134] C. Raphael. A Bayesian network for real-time musical accompaniment. In *Advances in Neural Information Processing Systems*. MIT Press, 2001.

[135] C. Raphael. Can the computer learn to play music expressively? In *Proc. of Eighth Int. Workshop on Artif. Intel. and Stats.*, 2001.

[136] C Raphael. Coarse-to-fine dynamic programming. *IEEE Transactions on Pattern Analysis and Machine Intelligence*, 2001.

[137] C. Raphael. Music plus one: A system for expressive and flexible musical accompaniment. In *Proceedings of the International Computer Music Conference*, 2001.

[138] C. Raphael. Harmonic analysis with probabalistic graphical models. In *Proceedings of the International Symposium on Music Information Retreival*, 2003.

[139] C Raphael. Orchestra in a box: A system for real-time musical accompaniment. In *Proceedings of the International Joint Conference on Artificial Intelligence*, 2003.

[140] C. Raphael. Orchestral musical accompaniment from synthesized audio. In *Proceedings of the International Computer Music Conference*, 2003.

[141] C. Raphael. Aligning musical scores with audio using hybrid graphical models. *Machine Learning*, 65(2-3), 2006.

[142] Ben Y. Reis. A multi-agent system for on-line modeling, parsing and prediction of discrete time series data. In *Intelligent Image Processing, Data Analysis and Information Retrieval*, pages pp. 164–169. IOS Press Holland, 1999.

[143] Iead Rezek and Stephen Roberts. An operator interpretation of message passing. Technical Report PARG-03-01, Robotics Research Group, University of Oxford, 2003.

[144] Elaine Rich and Kevin Knight. *Artificial Intelligence*. McGraw-Hill, 1990.

[145] Bob Ricks and Dan Ventura. Training a quantum neural network. In Sebastian Thrun, Lawrence Saul, and Bernhard Schölkopf, editors, *Advances in Neural Information Processing Systems 16*. MIT Press, Cambridge, MA, 2004.

[146] Jérémie Roland and Nicolas J. Cerf. Quantum search by local adiabatic evolution. *Phys. Rev. A*, 65(4):042308, 2002.

[147] S. Russell and P. Norvig. *Artificial Intelligience: A Modern Approach*. Prentice Hall, 2002.

[148] Solomon E. Shimony. Finding MAPs for belief networks is NP-hard. *Artificial Intelligence*, 68(2):399–410, 1994.

[149] J Siskind, J Sherman, I Pollak, and C Bouman. Hierarchical perceptual organization with the center-surround algorithm. In *Proceedings of the International Conference on Computer Vision*, 2003.

[150] Squarepusher. Ultravisitor. Audio CD: Warp records, 2004.

[151] Amos Storkey and Chris Williams. Image modelling with position-encoded dynamic trees. *IEEE Transactions of Pattern Analysis and Machine Intelligence*, 25(7):859–871, 2003.

[152] R.S. Sutton and A. G. Barto. *Reinforcement Learning*. MIT, 1998.

[153] Sebastian Thrun, Wolfram Burgard, and Dieter Fox. *Probabilistic Robotics*. MIT Press, 2006.

[154] Robert R. Tucci. Quantum Bayesian networks. *International Journal of Modern Physics B*, 9(3):295–337, 1995.

[155] Shimon Ullman. *High-level vision: Object recognition and visual cognition*. MIT Press, 1996.

[156] L. Van Noorden and D. Moelants. Resonance in the perception of musical pulse. *Journal of New Music Research*, 28(1):43–66, 1999.

[157] Lieven M. K. Vandersypen, Matthias Steffen, Gregory Breyta, Costantino S. Yannoni, Mark H. Sherwood, and Isaac L. Chuang. Experimental realization of shor's quantum factoring algorithm using nuclear magnetic resonance. *Nature*, 414:883, 2001.

[158] Herman von Helmholtz. *On the sensations of tone*. Dover (reprint), 1888.

[159] C. Wiggs and A. Martin. Properties and mechanisms of perceptual priming. *Current Opinion in Neurobiology (CNS)*, 8:227–233, 1998.

[160] J. Winn and C. Bishop. Variational message passing. *Journal of Machine Learning Research*, 6:661–694, 2005.

[161] John Winn. *Variational message passing and its applications*. PhD thesis, University of Cambridge, 2003.

[162] J.S. Yedidia, W.T.Freeman, and Y.Weiss. Understanding belief propagation and its generalisations. In Gerhard Lakenmeyer and Bernhard Nebel, editors, *Exploring Artificial Intelligence in the New Millenium*. Morgan Kaufmann, 2003.

[163] Daniel H. Younger. Recognition and parsing of context-free languages in time n^3. *Information and Control*, 10(2):189–208, 1967.

[164] Alan L. Yuille. A double-loop algorithm to minimize the Bethe free energy. In *Proceedings of the Third Energy Minimization Methods in Computer Vision and Pattern Recognition*, Sophia-Antipolis. France, 2001.

[165] Christof Zalka. Grover's quantum searching algorithm is optimal. *Phys. Rev. A*, 60:2746, 1999.

[166] N.L. Zhang and David Poole. Exploiting causal independence in Bayesian network inference. *Journal of Artificial Intelligence Research*, 5:301–328, 1996.